CONCEPTUAL DESIGN AND MODELING OF A FUEL CELL SCOOTER FOR URBAN ASIA

by

Bruce Lin

Princeton University
School of Engineering and Applied Sciences
Department of Mechanical and Aerospace Engineering

Submitted in partial fulfillment of the requirements for the degree of Master of Science in Engineering from Princeton University, 1999

Prepared by:

_____
(Author's signature)

Approved by:

_____	_____
Professor Robert H. Socolow	Professor Enoch Durbin
Thesis Advisor	Thesis Reader

November, 1999

abstract

Air pollution is of serious concern in many Asian countries, especially in densely-populated cities with many highly-polluting two-stroke engine vehicles.The present value of health effects have been estimated at hundreds of dollars or more, over each vehicle's lifetime, for a reasonably wealthy country like Taiwan. Four-stroke engines and electric battery-powered scooters are often proposed as alternatives, but a fuel cell scooter would be superior to both by offering both zero tailpipe emissions and combustion-scooter class range (200 km).

Unlike 50 kW automobile-sized fuel cell stacks, the vehicular 5 kW fuel cell needed here has not received much attention. This niche is examined here with a conceptual design and consideration of the issues of water, heat, and gas management. The application is extremely sensitive to size, weight, and cost, so a proton exchange membrane fuel cell using hydrogen stored in a metal hydride is best. Hydrides also act as sinks for waste heat due to the endothermic hydrogen desorption process. Pressurized operation is found to be ineffective due to high parasitic power demands and low efficiencies at the low powers involved.

A computer simulation is developed to examine overall vehicle design. Vehicle characteristics (weight, drag, rolling resistance), fuel cell polarization curves, and a Taiwanese urban driving cycle are specified as inputs. Transient power requirements reach 5.9 kW due to the rapid accelerations, suggesting a large fuel cell. However, average power is only 600 W: a hybrid vehicle with a small fuel cell and peaking batteries could also handle the load. Results show that hybrid vehicles do not significantly improve mileage, but are certain to precede pure fuel cell scooters while fuel cells are still more expensive than peaking batteries.

System size is approximately the same as current electric scooters, at 43 L and 61 kg for the fuel cell, hydrogen storage, and electric motor / controller. Manufacturing costs of fuel cell scooters are expected to decrease to under $1,300 in the long term, with per-km fuel costs half of those for gasoline scooters. Hybrid zinc-air scooters offer similar performance at slightly lower vehicle price, but the fuel infrastructure costs may be prohibitive.

acknowledgments

With periods of hard acceleration, rapid decelerations, and occasional stalls in the course of writing this thesis, sometimes I felt that I was on the Taipei Motorcycle Driving Cycle myself. Thanks to everyone who had a part in this effort.

Thanks to my advisors Robert Socolow, Bob Williams, and Joan Ogden, and my thesis reader Enoch Durbin.

Thanks to the many people from various research groups, companies, and academic institutions who helped with guidance, hard data, and advice.

Thanks also to my family and friends and colleagues who supported me in the past twelve months, and for many, much longer than that.

Support for this research came from the Center for Energy and Environmental Studies, the Mechanical and Aerospace Engineering Department (including a Daniel and Florence Guggenheim Fellowship and a Sayre Prize), the United States Department of Energy, and the Energy Foundation.

This thesis carries 3055-T in the records of the Department of Mechanical and Aerospace Engineering.

table of contents

Abstract i

Table of contents iv

List of tables xi

List of figures xiv

1 Introduction 1

1.1 Transportation Background 6

1.1.1 Why Taiwan? 6

1.1.2 Taiwan vehicle fleet 8

1.1.3 Taiwan Energy 11

1.2 Air pollution 12

1.2.1 The internal combustion engine 12

1.2.1.1 The four-stroke spark-ignition cycle 13

1.2.1.2 The two-stroke spark-ignition cycle 17

1.2.1.3 Advantages and disadvantages 20

1.2.2 Pollutants 21

1.2.3 Vehicle emissions standards and the reality 23

1.2.4 Air pollution sources in Taiwan 27

1.2.5 Cleaner combustion technology 31

1.2.5.1 Exhaust gas recirculation 31

1.2.5.2 Superchargers 31

1.2.5.3 Fuel injection 32

1.2.5.4 Catalysis of exhaust gases 33

1.2.5.5 Replacement by four-stroke engines 34

1.2.5.6 Relative costs and benefits of various technologies 34
1.2.6 Assessing the damage 35
1.2.6.1 Reduction estimate 36
1.2.6.2 Externality damage estimate 38
1.2.7 Government Policy Approaches 40
1.2.7.1 Taiwan policy history: tighter emissions standards 40
1.2.7.2 Later years: inspection and maintenance 41
1.2.7.3 Future direction: zero-emission vehicles 42
1.2.7.4 Research interest in fuel cell scooters 44
1.2.8 Conclusion 45
References for Chapter 1 46

2 Electric Vehicles 51
2.1 Drive Systems 53
2.1.1 Electric drive systems: introduction 54
2.1.2 Electric motor theory 55
2.1.2.1 DC motors 56
2.1.2.2 AC motors 57
2.1.2.3 Hub motors 58
2.1.3 Converters and controllers 59
2.1.4 Choice 60
2.2 Chemical batteries 63
2.2.1 Theory 64
2.2.2 Technology 65

2.2.2.1 Existing scooter battery systems 65
2.2.2.2 Technology predictions 66
2.2.2.3 Lead-acid batteries 68
2.2.2.4 NiMH and NiCd batteries 69
2.2.2.5 Lithium variants 70
2.2.2.6 Zinc-air “regenerative” batteries 70
2.2.2.7 Summary 73
2.2.3 Peaking power and batteries for hybrids 74
2.2.3.1 Peaking battery modeling 76
2.2.3.2 Charge and discharge 78
2.2.3.3 Hybrid battery conclusion 79
References for Chapter 2 80

3 The hydrogen fuel cell power system 83
3.1 Fuel Cell Science 85
3.1.1 Fundamentals 85
3.1.1.1 Thermodynamics 86
3.1.1.2 Kinetics 91
3.1.1.3 A note on efficiency 94
3.1.2 Types of fuel cells 95
3.1.2.1 Phosphoric Acid Fuel Cell: well-developed, low density 96
3.1.2.2 Proton Exchange Membrane Fuel Cell: for mobile applications, the best 97
3.1.2.3 Alkaline Fuel Cell: poisoned by carbon dioxide 101
3.1.2.4 Solid Oxide and Molten Carbonate Fuel Cells: higher temperature 102

3.1.2.5 Direct Methanol Fuel Cells: long-term promise 102
3.1.3 Stack characteristics 104
3.1.3.1 Fuel cell stack specifications 105
3.1.3.2 Published results for automobile fuel cell stacks 105
3.1.3.3 Detailed construction 106
3.1.3.4 Detailed construction results 110
3.1.4 Gas flow management 111
3.1.4.1 Blowers 112
3.1.4.2 Compressors 113
3.1.5 Water management 114
3.1.6 Heat 116
3.1.6.1 Active cooling 118
3.1.6.2 Passive cooling 118
3.1.6.3 Boiling refrigerant 119
3.2 Fuel for the fuel cell 120
3.2.1 Reformed fuels 120
3.2.1.1 Hydrocarbon reforming 120
3.2.1.2 Methanol reforming example 125
3.2.1.3 Ammonia 126
3.2.1.4 Chemical hydride energy storage 128
3.2.2 Direct hydrogen storage 131
3.2.2.1 Safety 131
3.2.3 Metal hydride energy storage 133
3.2.3.1 Thermodynamics 134

3.2.3.2 Kinetics 137
3.2.3.3 Classification 138
3.2.3.4 Metal hydride performance 139
3.2.4 Compressed gas storage 142
3.2.4.1 Cylinder performance 143
3.2.4.2 Cylinder safety 145
3.2.5 Liquid hydrogen storage 146
3.2.6 Selection 147
References for Chapter 3 149

4 Modeling and design 154
4.1 Performance requirements 156
4.2 Vehicle modeling 160
4.2.1 Physical model 160
4.2.2 Modeling parameter selection 164
4.2.3 Relative importance of various factors 165
4.2.4 Validation 168
4.3 Driving Cycle 170
4.3.1 TMDC 172
4.3.2 Modification of TMDC 176
4.3.3 Torque vs. rpm requirements 180
4.3.4 Modeling results 183
4.3.4.1 Battery powered scooter 184
4.4 Fuel Cell System Design and Integration 186

4.4.1 Design tradeoffs 186
4.4.1.1 Maximum power and the polarization curve 187
4.4.1.2 Power density 188
4.4.1.3 Number of cells 189
4.4.1.4 Flow rate parameters 190
4.4.2 Gas subsystem 191
4.4.3 Water subsystem 192
4.4.4 Cooling subsystem 192
4.4.4.1 Cooling from storage system 194
4.4.4.2 Active cooling 196
4.4.4.3 Heat generation under the TMDC 198
4.4.4.4 Selection 202
4.5.4 Overall parasitics 203
4.5 Integrated Model 206
4.5.1 System performance 206
4.5.2 Size and weight of power system 208
4.5.3 Evaluation 211
4.6 Pressurized fuel cell option 213
4.7 Hybrid option designs 215
4.7.1 Types of hybrids 216
4.7.2 Fuel cell sizing 218
4.7.3 Peaking battery and operation policy 221
4.7.4 Simulation results 222
4.7.5 Hybrid power system designs 228

4.7.5.1 Design for 3.2 kW fuel cell 229
4.7.5.2 Design for 1.1 kW fuel cell 231
4.7.5.3 Hybrid zinc-air scooters 232
4.7.6 Hybrid results 234
4.7.7 Near-term possibilities 237
References for Chapter 4 239

5 Implementation and Conclusions 242
5.1 Scooter cost 243
5.1.1 Base cost by subtraction 244
5.1.2 Cost of hydrogen storage system 245
5.1.3 Fuel cell system cost based on parts predictions 246
5.1.3.1 The short term 249
5.2 Wells-to-wheels efficiency 250
5.3 Fuel cost and infrastructure 251
5.3.1 Zinc-air battery “fuel” costs 253
5.3.2 Hydrogen costs and infrastructure 255
5.3.3 Combustion scooter gasoline costs 257
5.3.4 Fuel cost summary 257
5.4 Final conclusions 259
5.4.1 Background 260
5.4.2 Modeling results 261
5.4.3 Design 262
5.4.4 Costs and infrastructure 263

5.4.5 Parting words 265

References for Chapter 5 267

Appendices 268

A. Electric scooters 268

B. Detailed stack cost/size analysis 269

C. Radiator performance curves 284

D. Conversion factors 286

E. Acronyms and abbreviations 286

F. MATLAB simulation 288

G. A prototype scooter 300

list of tables

Chapter 1

1.1	Motorcycle populations in selected countries, 1993	6
1.2	VMT data for Taipei, 1987	11
1.3	A comparison of vehicle emissions standards	24
1.4	Data on motorcycle emissions: four-strokes and catalysts	26
1.5	Simulated emissions from more realistic driving cycle	26
1.6	PSI subindex pollutants in Taiwan	29
1.7	Cleanup technology, effects and prices	35
1.8	ITRI prediction of effects of scooter replacement on pollution	37
1.9	Estimate of externality damages from air pollutants	38
1.10	Electric Motorcycle Development Action Plan	43

Chapter 2

2.1	Comparison of power systems	54
2.2	Motor specifications: UQM brushless and NGM hub motors	61
2.3	ZES-2000 electric scooter performance	66
2.4	Battery goals for various time frames	67
2.5	Peaking power battery characteristics	76

Chapter 3

3.1	Stack size, weight, cost summary	110
3.2	Fuel gravimetric and volumetric energy densities, lower heating value basis	121
3.3	Steam reforming versus partial oxidation	122
3.4	Hydrogen output from reformed hydrocarbon fuels	124
3.5	Reformer performance	126
3.6	Chemical hydride comparison	129
3.7	Theoretical performance of various metal hydrides	138
3.8	Metal hydride systems comparison	141
3.9	Compressed gas options	145
3.10	Storage technology comparison	148

Chapter 4

4.1	Performance of various vehicles of about 5 kW power	157
4.2	Fuel cell scooter performance requirements	159
4.3	Typical modeling parameters	164
4.4	Validation of physical model	168
4.5	Driving cycle comparison	174
4.6	Effects of “jitter”	175

4.7	Results of different algorithms applied to TMDC; comparison to FTP	178
4.8	Taiwan battery-powered scooter	185
4.9	Various battery-powered designs for Taiwan scooter	185
4.10	Fuel cell design parameters at maximum power	190
4.11	Flow rate parameters at maximum power	191
4.12	Stack temperature model parameters	200
4.13	System performance under TMDC and at cruising speed	208
4.14	Subcomponent summary	208
4.15	Size of various storage designs	209
4.16	Hybrid 1.1 kW scooter inadequacies	219
4.17	Hybrid fuel cell stack designs	221
4.18	Peaking power battery characteristics	221
4.19	Hybrid performance at 30 km/h	223
4.20	Hybrid performance under TMDC	223
4.21	Hybrid system design	229
4.22	Component breakdown for 3.2 kW scooter	230
4.23	Component breakdown for 1.1 kW scooter	232
4.24	Hybrid battery configuration for Taiwan scooter model	233
4.25	Hybrid power system summary	235
4.26	Performance metrics	236
4.27	Near term 1 kW fuel cell hybrid designs	238

Chapter 5

5.1	Internal combustion engine scooter parts	244
5.2	Battery-powered electric scooter parts	245
5.3	Metal hydride storage costs	245
5.4	Long-term scooter cost to manufacture	247

5.5	Summary of cost estimates	248
5.6	Short term bridging to the future	249
5.7	Taiwan vs. USA energy prices, 1997 USD	252
5.8	Fuel costs of Taiwan in $/GJ LHV	252
5.9	Comparison of assumptions for zinc-air electrowinning costs	253
5.10	Fuel cost summary	258
5.11	Fuel cell scooter performance requirements	261
5.12	System design results	263
5.13	Long-term cost of hybrid fuel cell scooters	264
5.14	Fuel cost summary	264

list of figures

Chapter 1

1.1	A scooter	3
1.2	Taiwan vehicle mix 1991-1998	9
1.3	Scooter distribution in Taiwan 1991-1998	9
1.4	Four-stroke cycle	15
1.5	Two-stroke cycle	18
1.6	Carbon monoxide emissions by source	28
1.7	Hydrocarbon emissions by source	28
1.8	PSI in Taiwan, 1994-1996	50

Chapter 2

2.1	Axial-gap pancake motor	59
2.2	Typical torque vs. rpm curve for DC motor	63

2.3 Voltage and internal resistance of Bolder peaking battery 78

Chapter 3

3.1 Fuel cell schematic 87

3.2 Tafel plot 92

3.3 Effects of pressurization on polarization curves 94

3.4 Nafion chemical structure 98

3.5 Stack diagram 100

3.6 Active cell 109

3.7 Ignition energy of hydrogen 132

3.8 Metal hydride adsorption curve 136

Chapter 4

4.1 Free body diagram of scooter 161

4.2 Cruising power required at various speeds 166

4.3 Power required to climb various slopes at 15 km/h 166

4.4 Power required for various accelerations from 30 km/h 167

4.5 Validation of physical model 169

4.6 mFTP: modified Federal Test Procedure 171

4.7 ECE-40 172

4.8 Taipei Motorcycle Driving Cycle (TMDC) 173

4.9 Smoothed TMDC 180

4.10 Torque vs. rpm during TMDC 182

4.11 Power required in TMDC 183

4.12 Polarization curve 187

4.13 Metal hydride cooling vs. power 195

4.14 Heat generation as a function of time in TMDC 198

4.15	Stack temperature as a function of time in TMDC	201
4.16	Parasitics as a function of power	204
4.17	Parasitics as a percentage of power	205
4.18	Effect of parasitics on efficiency	206
4.19	Weights of subsystems	212
4.20	Volumes of subsystems	212
4.21	Atmospheric power versus 3 atm power	214
4.22	Division of power between fuel cell and battery during TMDC, 3.2 kW stack	225
4.23	State of charge of battery over TMDC, 3.2 kW stack	226
4.24	Division of power between fuel cell and battery during TMDC, 1.1 kW stack	227
4.25	State of charge of battery over TMDC, 1.1 kW stack	228

~

Chapter One

Introduction

~

The hydrogen fuel cell has received extensive attention in the scientific community and the public at large since about 1990. The first experimental fuel cell was developed in the nineteenth century, and a 6 kW alkaline fuel cell in conjunction with a battery bank was used to power a small car as early as 1966, but it would not be until major improvements in power density were made in the 1990's that major car companies took serious interest in fuel cells.[1] Although the technology is currently quite expensive, fuel cells offer significant benefits including high overall efficiency, quiet operation due to few moving parts, and good efficiency over a wide range of operating points. Predicted cost reductions mean that in the near future, fuel cells could power everything from homes to vehicles to cell phones.

Although extensive research has been done into fuel cells for stationary power and for automobiles, and some research has been done for portable power applications like soldier power and devices like telephones and computers, virtually no work has been done in the field of small vehicles requiring under 10 kW of power.[2] This is an interesting option for small vehicles because the market – and governments – are beginning to put a high value on options offering low or zero emissions. Moreover, the challenge of putting fuel cells in scooters is an interesting technical problem because, due to weight and cost restrictions, power systems in these vehicles cannot be as complex as those found in cars. Yet, there is a high value on clean power. Subsystems like air compressors, reformers, and hydrogen storage tanks are all reduced in size and complexity, so production is made easier. On the other hand, efficiencies do not remain constant at small size so performance in this type of application will be poorer than in automobile fuel cell power systems.

The purpose of this study is to examine a particular application of fuel cell technology: the electric scooter. Scooters are small two-wheeled vehicles that can carry one or two people. They are unlike motorcycles in that they are ridden in a seated position with feet forward on a platform. Although

in North America they are most associated with 1950's Vespas and the mod scene of later decades, these small and cheap vehicles remain a major mode of transportation in Asia and Europe today.

(Note that the distinction between “scooters” and “motorcycles” is not always made in the literature, especially by Asian researchers. Here it is assumed that “motorcycles” refers to scooters; this assumption is almost certain when it comes to vehicles less than 50 cc in displacement.)

Figure 1.1 A Scooter

Honda CUV-ES electric scooter[3]

Due to their small size and low price point, scooters have traditionally been powered by high power density two-stroke internal combustion engines, (although some of the larger models use four-stroke engines). Two-stroke engines produce a great deal of pollution and are an object of concern in many Asian countries.

Severe pollution from two-stroke engines is a significant driver for cleaner technology. Thus, the target market for this study is the Asian urban commuter, since scooter use is so heavy in many Asian cities, and air pollution is a major problem in the crowded cities of the Far East. Specifically, Taiwan (i.e. the Republic of China) is a prime example, with twenty million people sharing an area the size of Vancouver Island with ten million scooters. Compared to the battery-powered scooters currently being promoted by the Taiwan government, fuel cell engines offer the advantages of extended range and quick refueling.

Some countries in Europe, like Italy, also have extensive scooter populations and might also be able to afford expensive new technology more readily. Poorer countries like China and India are facing dramatic growth rates in two-stroke vehicle population as rickshaws and bicycles are being replaced, and low-powered but clean scooters would be a major step in providing mobility without compromising urban air quality.

Five chapters comprise the thesis.

The first outlines the pollution situation, includes a description of the two-stroke engine's pollution characteristics, and outlines Taiwan air pollution policy. A possible method for valuing reductions in air pollution is presented.

The second chapter discusses electric scooters and battery power for them. Hybrid vehicles and peaking power batteries are explained. The new zinc-air batteries, with their excellent energy storage densities, are examined as some scooter researchers and manufacturers are carefully looking at them for second generation zero emission scooters.

The third chapter describes in detail the engineering issues and science behind fuel cell technology and hydrogen storage. Both advantages and disadvantages of this type of power are examined. Hydrogen storage in the form of metal hydrides, and a proton exchange membrane fuel cell running at low temperatures, are chosen for the reasons of ease of manufacture and operation, low cost, and minimal volume.

The fourth chapter is the simulation and conceptual design core of the thesis. It explains the physical vehicle simulation used to simulate vehicle power requirements during typical urban driving. Using the specifications produced by the driving simulation, a fuel cell power system is designed. The fuel cell components are selected along with the hydrogen storage subsystem. The possibility of "hybridizing" the system by using a battery energy storage system is treated; this idea offers possible energy savings from regenerative braking and reduces the maximum size of the fuel cell, reducing cost. The performance of such a vehicle is examined in terms of technical performance metrics: total weight, fuel economy. (Note that this thesis did not involve construction of a physical prototype construction; the interested reader is referred to Appendix G for more information on that topic.)

The final chapter describes how these scooters might be brought to market. How much would a prototype cost? Could a fully-developed scooter be competitive with electric or two-stroke scooters? How would fuel costs compare to battery-powered scooters and gasoline-powered scooters? Infrastructure issues are briefly discussed. With the cost information finishing off the body the study, a final summary is presented that recapitulates the findings.

1.1 Transportation Background

1.1.1 Why Taiwan?

There are approximately 100 million motorcycles in the world. The greatest numbers are concentrated in Asia, and it is here that alternative scooters could have a major impact. Some illustrative countries are listed below:

Table 1.1. Motorcycle populations in selected countries, 1993

Country	Motorcycles	% of total vehicles	Country	Motorcycles	% of total vehicles
Argentina	882,000	15.5%	Switzerland	834,900	20.7%
Brazil	1,371,800	9.6%	Spain	2,655,900	17.1%
Canada	434,200	7.0%	UK	913,600	3.6%
Chile	37,120	3.9%			
Mexico	661,230	7.8%	Bangladesh	119,790	50.0%
Peru	86,940	12.4%	China	3,047,520	41.2%
USA (1991)	6,830,000	3.7%	Hong Kong	17,100	5.0%
Venezuela	580,920	25.3%	India	7,666,640	69.6%
			Indonesia	5,890,760	74.6%
Austria	601,160	14.9%	Japan	18,451,300	26.0%
Belgium	131,670	3.2%	Korea	1,066,800	34.4%
France	3,661,450	12.6%	Malaysia	2,460,640	59.0%
Germany	2,427,480	7.3%	Pakistan	627,170	48.8%
Italy	7,938,420	23.8%	Philippines	281,530	27.2%
Norway	202,860	9.5%	Taiwan (1991)	9,232,889	73.4%
Portugal	51,500	2.9%	Thailand	6,343,558	66.1%

Data from Weaver and Chan [4]

Numbers of scooters in use are high in Asia, and growth rates are also high. The People's Republic of China, for instance, had 500,000 motorcycles in 1980, and 10 million in 1994 - an annualized growth rate of 24%, faster than the 15-20% of Chinese urban vehicles in general.[5] India had an average annual growth rate of 16% for two-wheeled vehicles from 1981 to 1998.[6]

Worldwide scooter production is estimated at 17 million per year.[7] In 1994, Taiwan's motorcycle industry included 418 assemblers and manufacturers of parts and 16,000 employees. Revenues totaled $2.4 billion that year while total domestic production reached $3.2 billion (all figures US dollars unless otherwise noted.) [8]

As one of the "Five Tigers", Taiwan experienced rapid growth in the latter half of this century and became a manufacturing power; its vast foreign reserves helped it weather the Asian economic problems of the summer of 1998. Average household income in 1995 was $36,470 for an average household size (1996) of 3.6; transportation costs were estimated at $4,000 per year, behind household expenditures for food; rent, fuel, and power; and education.[9] Household income is fairly large compared to Taiwan's poorer neighbours, so adoption here is (i) easier than elsewhere and (ii) may ease development of advanced scooters elsewhere.

(In 1998, the U.S. dollar was equal to approximately 30 New Taiwan Dollars).

Air pollution is a major problem on this 400-km long island with an area of 35,873 km^2. Industry, diesel-powered vehicles, and the omnipresent two-wheeled, two-stroke scooters all contribute to the extremely dirty air. In 1997, the overall population was 21.7 million and the population density was 601 persons per square kilometer. In the same year, the city of Taipei's population density was 9560 persons per square kilometer while the second largest city, Kaohsiung, had a population

density of 9350 persons per square kilometer. Urban centres with population over 1 million contained 67.8% of Taiwan's population.[10]

Taiwan is focused on here, because of the high fraction of scooters in its vehicle fleet, its poor air quality, and because it is one of the top six producers of scooters in the world. Being wealthier than many of the other countries with high scooter densities, Taiwan can afford to spend money on novel vehicle designs; on the other hand, it should be noted that any improved scooters that were developed would be of great benefit in reducing high air pollution levels in other developing countries.

1.1.2 Taiwan vehicle fleet

Taiwan's transportation split is interesting. Historically, the lack of an automotive industry in the critical growth period meant that people rapidly adopted scooters and then did not switch to automobiles as they became more wealthy. The crowded cities, warm weather, dense population and limited land continue to make scooters popular. Car use is increasing, but scooters have the advantage of being able to swarm through the congested car traffic in cities. This explains the over ten million scooters currently in Taiwan, of which approximately 60% are low-power scooters under 50 cc (cubic centimeters) in cylinder displacement.[11] The largest cylinder size (i.e. most powerful engine) allowed in Taiwanese scooters is 150 cc. Especially high-polluting two-stroke vehicles made up 40% of all vehicles in Taipei in 1996.[12]

Figure 1.2. Taiwan vehicle mix 1991-1998

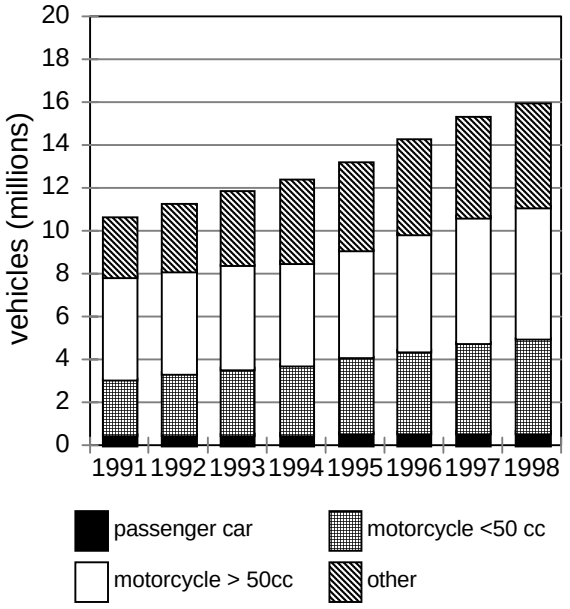

Data from the Monthly Bulletin of Statistics of the Republic of China, February 1999.[13]

Figure 1.3. Scooter distribution in Taiwan 1991-1998

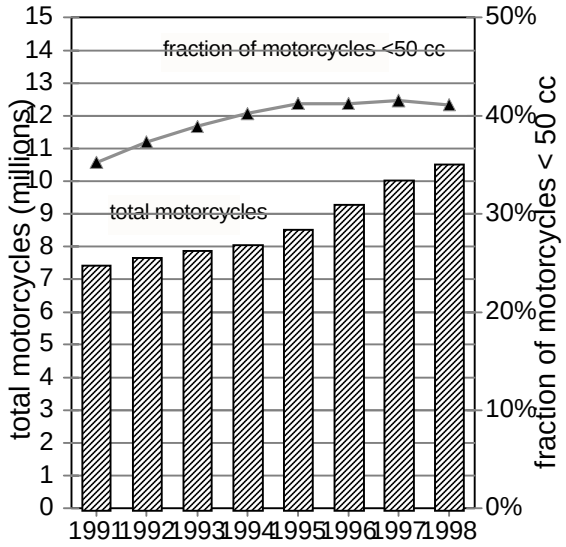

Data from the Monthly Bulletin of Statistics of the Republic of China, February 1999.[14]

The fraction of two-stroke scooters appears to have peaked, due to the cleaner and more powerful four-stroke scooters becoming cheaper and pollution standards becoming tighter.

A large number of vehicles are concentrated in the largest city, Taipei. According to the city's Department of Budget, Accounting, and Statistics, the Taipei motor vehicle population was approximately 1,532,000 in 1997, with 660,000 automobiles and 870,000 motorcycles.[15] Total Taipei vehicle density was 0.25 automobiles and 0.34 motorcycles per person, and the annual motorcycle growth rate was 7.3% between 1987 and 1997.

The 1991 percentage of motor vehicle air pollution that was produced by motorcycles and scooters was reported at: carbon monoxide, 37.7%; total hydrocarbons, 60.8%; nitrogen oxides, 2.9%. At this time, 73.4% of vehicles were motorcycles and scooters.[16] So the total amount of pollution contributed by motorcycles is less than their fraction of the vehicle population. Is their reputation for pollution undeserved, then?

Vehicle-mile-traveled (VMT) data for Taipei (1987) show the rest of the story. While more trips are made by scooters than by private car, the average car trip is farther and consequently more total miles are traveled by car. Scooters produce more pollution *per mile* than other vehicles:

Table 1.2. VMT data for Taipei, 1987

mode	% of trips	average length	fraction of total VMT
city bus	39%	6.5 km	38.1%
motorcycle	20%	7.8 km	23.5%
walking	17%	1.4 km	3.6%
private car	14%	13.5 km	28.4%
bicycle	6%	2.3 km	2.1%
taxi	3%	7.0 km	3.2%
train	1%	7.4 km	1.1%

Data from Price and Probert[17]

Although scooters only make up about 25% of VMT (when considering only engine-powered vehicles), they produce 38% of the carbon monoxide and 61% of the total hydrocarbons.

1.1.3 Taiwan Energy

Taiwan has virtually no energy resources of its own and imports the vast majority of its fuel. Its primary energy consumption is over 50% oil, approximately 25% coal, 10% nuclear, 5% natural gas, and under 5% hydroelectricity. In 1997, 3 million tons of LNG were imported (mainly from Indonesia), and the government expects to expand natural gas use to 13 million tons by 2010 and 16 million by 2020.[18] Oil is imported almost entirely from the Middle East, but coal is used for electric power generation, with imports mainly coming from Australia (35%), Indonesia (21%), South Africa (17%), and mainland China (15%).[19]

The US Energy Information Agency summarized the electric production situation as follows:

> At the end of 1997, Taipower [the government utility monopoly] operated 57 power plants (35 hydropower, 19 thermal, 3 nuclear) with total capacity of 23,763 megawatts (MW) (32% coal-fired, 23% oil-fired, 22% nuclear, 18% hydro, 5% gas-fired). In addition, cogenerators had 2,356 MW of capacity in place, which they used to generate about 10% of Taiwan's total electric power in 1996.[20]

Eight more coal-fired plants are to be built by 2001, with two nuclear reactors totaling 2.7 GW to be added at the Lungmen facility in Yenliao by 2004.

In terms of pollution, electricity is produced by relatively polluting coal plants, although this can be improved with different coals and power plants with advanced cleanup technology. For reasons of national security caused by the island's extreme dependence on a possibly unstable oil supply, energy efficiency is a major focus of the Taiwan government. This is an added incentive to move away from gasoline powered scooters or at least to improve fuel economy.

1.2. Air Pollution

Why are these two-stroke scooters so polluting, and what can be done about it?

1.2.1. The internal combustion engine

After an initial flowering of radically different ideas and concepts, including electric vehicles, cars since the nineteenth century have almost universally burned gasoline and run on the *four-stroke Otto cycle*. The majority use spark plugs for ignition. However, the *two-stroke Otto cycle* is still widely used for applications like lawnmowers, outboard motors, and scooters, where simplicity, low cost, and high power per weight are more important than fuel efficiency or minimized air

pollution. However, as more and more attention is paid to emissions, these two-stroke cycle engines (heretofore abbreviated “two-stroke engines”) are becoming less and less acceptable.

Why are two-stroke engines so polluting, and what can be done to improve them? The answer will be clear after a brief tour through the workings of a four-stroke car internal combustion engine.

1.2.1.1 The four-stroke spark-ignition cycle

The typical car contains four to eight cylinders which are connected by pistons to a crankshaft. Each cylinder is stopped at one end by a movable piston; the other end is closed but contains valves to allow air, fuel, and exhaust gases to enter and exit. The space in the cylinder is called the combustion chamber, and its volume is determined by the position of the piston head as it slides up and down the chamber.

The process by which combustion turns the crankshaft (and, through the transmission, the axles and the wheels) is relatively straightforward. A “charge” of fuel and air is sucked into the combustion chamber by a downwards motion of the piston, compressed by an upwards thrust of the piston, and then ignited by a spark plug; the resulting expanding gases drive the piston towards the crankshaft; and the hinge at the end of the piston transforms the piston's linear motion to rotational motion, turning the crankshaft and providing power. The crankshaft rotates, bringing the piston back up, the combustion product gases are squeezed out, and a fresh batch of air/fuel is drawn down into the combustion chamber. Since there are multiple cylinders firing at different points in the turning of the crankshaft, the motor remains in fairly steady rotation. A flywheel smooths out any remaining irregularities.

In reality the situation is more complicated, with auxiliary systems. In a four-stroke spark-ignition engine with carburetor, the fuel is first thoroughly pre-mixed with the air prior to intake in the carburetor before it is introduced to the combustion chamber. The alternative is fuel injection, where the fuel is sprayed by a controlled injector either into the compressed air stream at the inlet tract (just before the inlet valve opens), or directly into the combustion chamber. The former is more common. These both require high-pressure injection, and the fuel also has less time to vaporize before being burned.

Note that in diesel (compression-ignition) engines, the fuel is injected into high-pressure air toward the end of the compression stroke.

Figure 1.4 Four-stroke cycle

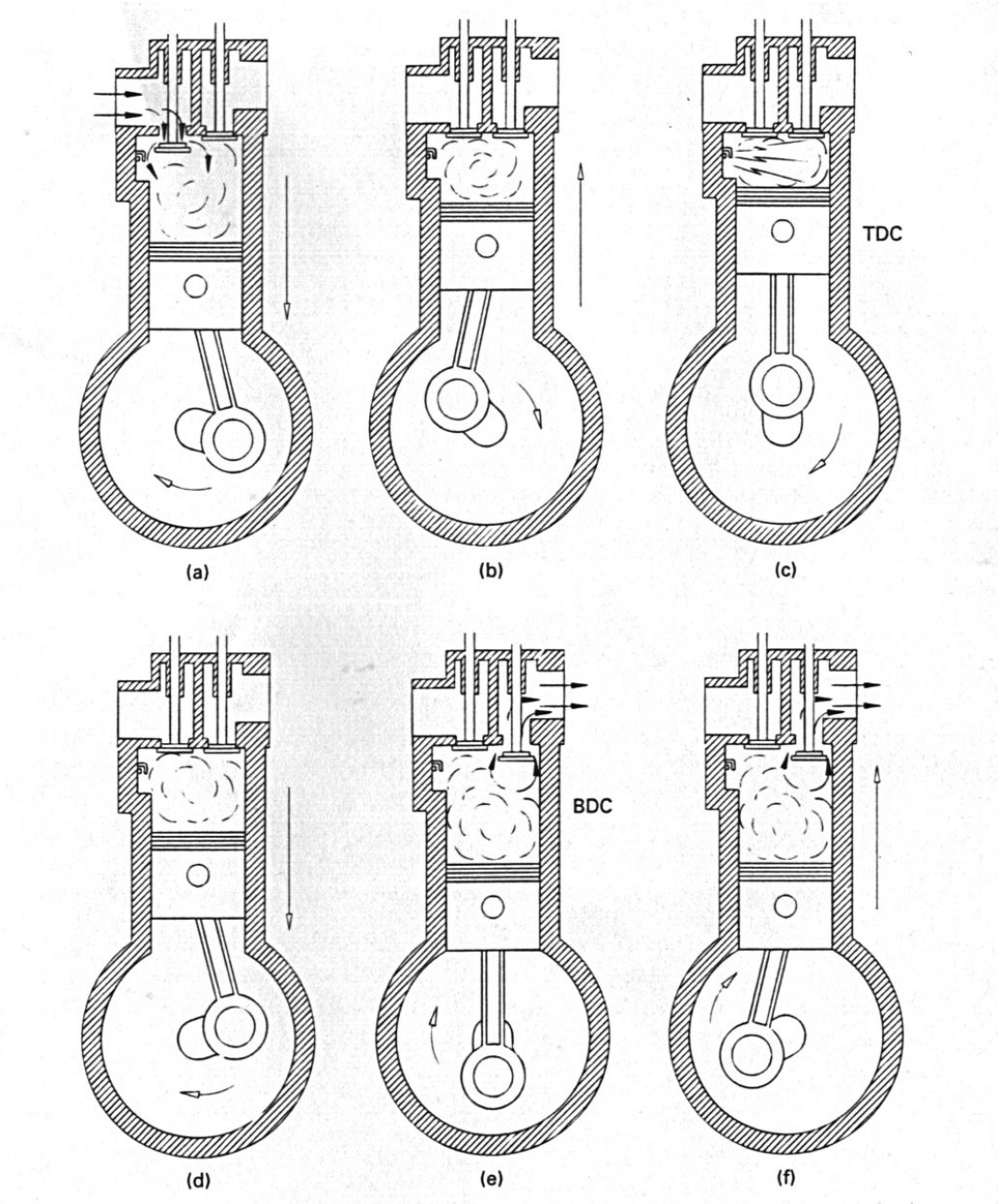

The four-stroke cycle moves from (a) the intake stroke to (b) compression stroke (c) ignition and combustion (d) power stroke (e) exhaust valve opens (f) exhaust stroke. The diagram is from Pulkrabek.[21]

The four strokes are:

Intake / Induction stroke. The piston draws down from the closed position (TDC, or "Top Dead Center") to BDC ("Bottom Dead Center"), and the intake valves are opened. A fresh charge of the pre-mixed air/fuel mixture is sucked into the chamber.

Compression stroke. At approximately BDC, the intake valves close. The turning of the crankshaft then begins to push the piston back up, compressing and heating up the air/fuel mix. Once the piston reaches approximately TDC, the spark plug fires, igniting the mixture. (If the heat causes the mixture to ignite before the spark plug fires, premature and unstable ignition occurs: "engine knock"). As the air/fuel mix burns, it releases heat and is transformed into combustion products: carbon dioxide, water, and various other compounds. The pressure and temperature increase dramatically.

Expansion / Power stroke. The piston is pushed downwards by the expanding gases and this push provides the power to rotate the crankshaft. At the end of the power stroke, the exhaust valve located at the top of the cylinder opens. The phenomenon known as "exhaust blowdown" begins: the gases in the combustion chamber, still at a higher pressure than the external atmosphere, escape out the exhaust valve.

Exhaust stroke. However, some gases remain after the pressure in the combustion chamber has dropped to atmospheric. The next stroke is an upwards motion; the piston moves from BDC to TDC, pushing out the remaining gas. The exhaust valve closes at the end of this stroke, and the cycle begins again.

Note that the valves open once per cycle, but each cycle consists of two strokes. Thus, lobes on a camshaft are needed to regulate this action. Lubrication is by oil pumped up from an oil sump at the bottom of the crankcase.

1.2.1.2 The two-stroke cycle

The key mechanical difference between the two-stroke cycle and the four-stroke cycle is that the two-stroke engine draws air/fuel in at the same time as it pushes out exhaust. However, it is this seemingly minor difference that produces all the major disadvantages and advantages: higher power, lower complexity, and increased hydrocarbon emissions.

Figure 1.5 Two-stroke cycle

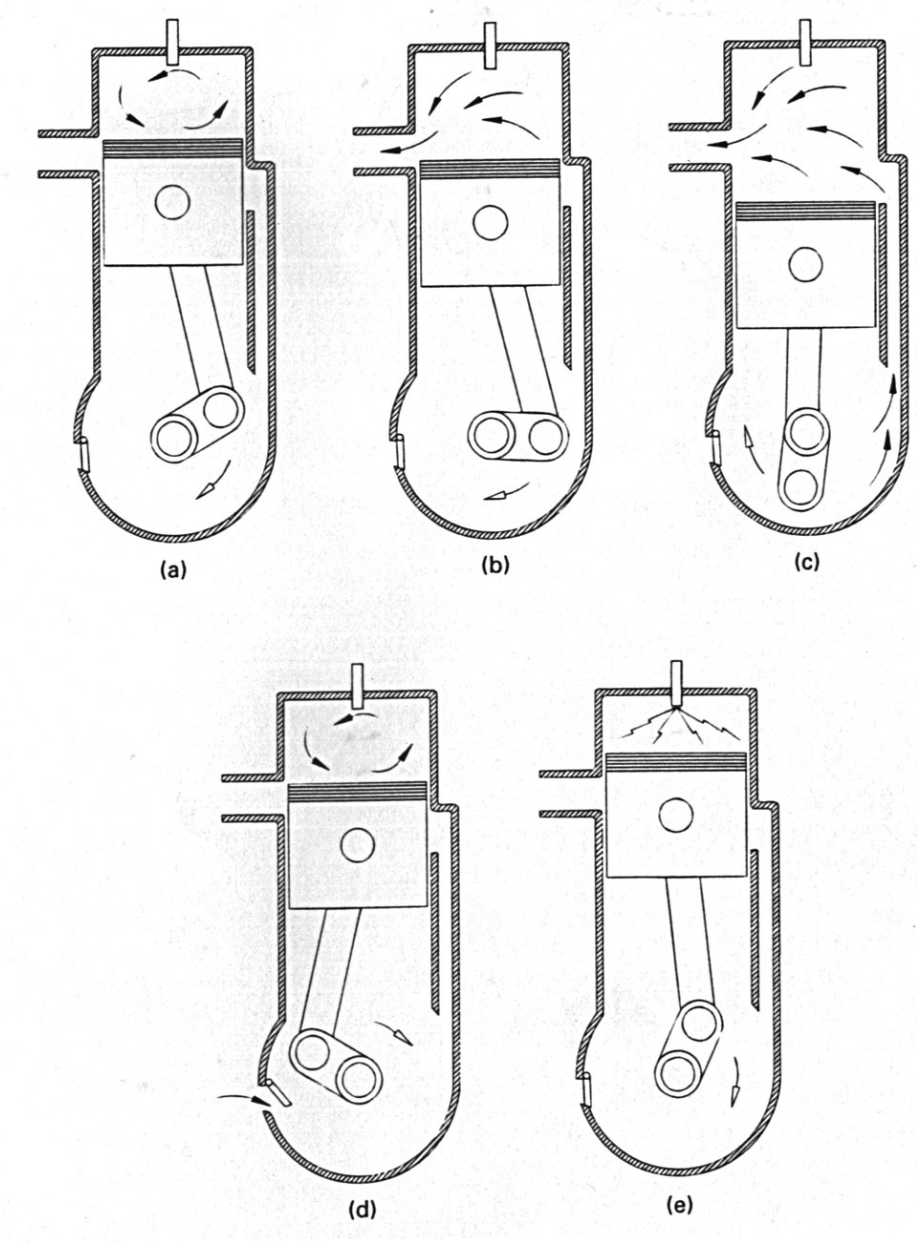

Here, (a) is the power stroke, (b) is exhaust blowdown, (c) is cylinder scavenging, (d) is the compression stroke and combustion occurs at (e). The diagram is from Pulkrabek.[22]

Expansion / Power stroke. In the two-stroke engine, as in the four-stroke engine, the expanding combustion products force the piston down to provide the power. Pressure and temperature start to

decrease from their maximum values. As the piston moves downwards - but before it reaches BDC - exhaust blowdown is begun. This is done by opening an exhaust valve at the cylinder head or by having the descending piston uncover ports at the sides of the cylinder, allowing the gases to escape.

Intake / Scavenging stroke As the pressure drops and atmospheric pressure is nearly reached inside the cylinder, intake slots at the side of the cylinder are uncovered and pressurized air/fuel is allowed to enter the cylinder. This mix pushes out remaining exhaust gases and fills the cylinder - a process known as "scavenging." The piston descends to BDC and switches direction. On its way up, the piston quickly covers the intake port and exhaust ports (or, exhaust valves are closed with a separate mechanism). With all valves/ports closed, the piston finishes compressing the air/fuel as it moves back up to TDC. A spark plug fires as the piston reaches TDC, ignition occurs, and the cycle repeats

Note that in the two-stroke cycle, the air/fuel mixture must enter under pressure, in order to force out the exhaust gases. This is done in one of two ways: with a supercharger (compressor) that compresses the air/fuel before it enters the cylinder, or more commonly, by redesigning the crankcase so that it acts as a compressor during the power stroke (in other words, as the piston descends, it turns the crankshaft *and* compresses the air in the crankcase) This crankcase compression replaced earlier designs which used blowers to push in the air/fuel mixture.

In the case of crankcase compression, the crankcase is no longer filled with lubricating oil as it is with four-stroke engines, since it needs to hold the air as well. In practice, what this means is that lubricating oil must be mixed with the fuel in a predetermined proportion; when the carburetor introduces the oil/fuel/air mix into the crankcase, the gasoline vaporizes and the oil turns into a

mist of liquid droplets. These droplets lubricate the crankshaft, piston pin, and cylinder walls, while the gasoline is compressed with air and eventually enters the cylinder. However, much of the oil that enters the cylinder is burned along with the fuel, and produces severe emissions problems. Small oil particulates may form. Finally, the oil also reduces the efficiency of the fuel combustion, because it is heavier and less reactive and thus does not completely burn.

1.2.1.3 Advantages and disadvantages

Due to the fact that both intake and exhaust valves are open at some point during the two-stroke cycle, it is possible for as much as 20-40% of the air/fuel to flow directly out of the cylinder.[23] This "short-circuiting" produces the blue smoke characteristic of unburned hydrocarbons, and reduces fuel economy. (Using direct fuel injection rather than carburetion can reduce this effect because air/fuel injection timing is better controlled, but this technology is only now beginning to be adopted for two-stroke engines, as environmental standards tighten and the extra cost thus becomes both bearable and necessary). Short-circuiting is an especially serious problem at high power, where the engine is turning at high rpm and there is very little time per stroke for scavenging to take place. The durability of two-stroke engines is also less than that of four-stroke engines.[24]

Incomplete combustion of the fuel is also a problem, especially at low loads. The residual gas left in the cylinder after scavenging increases if blowdown is too weak, and this high-heat capacity gas reduces flame temperatures. The result is unstable combustion, especially at the fringes of the fuel cloud where the mixture is lean, and the flame is extinguished before all the fuel is burned. The air/fuel mixture is kept rich to avoid this problem.[25,26] (A "lean" air/fuel mix has more air than is necessary for complete combustion; a "rich" mix, less)

On the other hand, a major advantage of two-stroke engines is that they offer far higher power per weight and per volume. Various components (oil pumps, distributor drives, valves) may be omitted because valves are replaced by ports, and because oil is included in the fuel. But most importantly, the two-stroke engine has a power stroke twice as frequent (per revolution) as the four-stroke engine of the same cylinder displacement, resulting in almost double the specific power. Related to this is the fact that the camshaft and relating mechanical timing devices required in a four-stroke engine are not needed. The high power density and simple construction make two-stroke engines attractive for scooters, outboard motors, and power tools like chainsaws and hedge trimmers.

Absolute maximum thermal efficiency is on the order of 14% for a typical 1 kW two-stroke engine, up to 21% for a modified lean-burn two-stroke engine.[27]

The size of scooter studied here is the 50 cc scooter - or rather, electric scooters with power and performance comparable to two-stroke internal combustion engine scooters with cylinder volumes of 50 cc. This translates to a gross power output of about 5 kW. Low-end 50 cc scooters are sold for approximately $1,000 in Taiwan.

1.2.2 Pollutants

The major vehicle pollutants are carbon monoxide (CO), nitrogen oxides (NO_x), sulfur oxides (SO_x), particulate matter (PM) and various hydrocarbons (HC). Combustion also produces carbon dioxide, a greenhouse gas. Two-stroke engines produce significant amounts of unburned hydrocarbons, atomized lubricating oil, and CO due to their design, but little NO_x

Carbon monoxide is generally a product of incomplete combustion, and is frequently found in rich

mixtures. Carbon monoxide binds with hemoglobin in the blood, reducing the blood's capacity to carry oxygen. This can result in heart strain and pulmonary problems.

NO_x is a collective name for nitrogen oxide (NO) and nitrogen dioxide (NO_2). Its production is largely thermally controlled in the combustion process from nitrogen in the air, which reacts with oxygen at high temperatures to form NO_2 and NO. NO_x tends to peak at an air-fuel ratio approximately 1.1 times stoichiometric, where there is excess oxygen.[28] The low NO_x output characteristic of two-stroke engines is due to the lower temperature and pressure at the same speed and torque as matching four-stroke engines.[29] The lower pressure of a two-stroke engine is the result of the higher stroke frequency and thus lesser need for high pressure to provide power. The lower temperature is partially the result of the richer mix being off-stoichiometric and thus being farther from the temperature peak and reduced in oxygen, and partially due to "exhaust gas recycling" where the incompletely exhausted combustion products, with their high heat capacity, keep down the temperature in the cylinder.

NO_x combines with moisture to produce acid rain, and increases the risk of respiratory disease and causes pulmonary and respiratory problems. NO_x and volatile organic compounds are also precursors for photochemically-produced ozone (smog), which is an irritant that affects the eyes, upper respiratory tract, and causes asthma and headaches.

Hydrocarbon emissions from two-stroke engines mainly result from the "short-circuit" passage of unburned fuel straight through the cylinder to the exhaust previously described.[30] Hydrocarbons in the atmosphere react photochemically to produce smog, and this is a major problem. Also, certain hydrocarbons are directly toxic to the human body.

Particulate matter consists of fine solid particles (often soot or agglomerated hydrocarbons), or liquid droplets. TSP ("total suspended particulates") is a measure of particulates smaller than 70 µm in diameter, while PM_{10} is a category for particles less than 10 µm. PM can lodge in the lungs and act as an irritant or cause cancer. (Recent medical and policy attention has turned to $PM_{2.5}$, an even finer classification of particulates). PM emissions from tailpipes are often measured by proxy, using the opacity of the exhaust. Black smoke is associated with soot, and blue, gray, or white smoke with condensed hydrocarbons from lubricating oil or incomplete fuel combustion. In two-stroke engines, lubricating oil is mixed with fuel at a ratio of about 1:40 by volume, and these more viscous lubricating oils tend to pass through the engine unburnt and condense as particulates.[31]

Finally, note that a major source of emissions is evaporative emissions. This can account for as much as 30%-40% of total volatile organic compound mobile source emissions.[32] Sources include losses during refueling, direct evaporation from the tank as it heats up and expands in the morning, and "hot soak" losses: those due to the engine continuing to heat up parts of the fuel system even when the vehicle is shut off.

1.2.3 Vehicle emissions standards and the reality

Vehicle emissions standards are the instrument by which vehicular air pollution has been traditionally addressed; these maximum emissions are measured using well-documented procedures generally involving placing the vehicle on a rolling-drum dynamometer, and accelerating/decelerating the vehicle through a "driving cycle" of prescribed velocities over a certain time period. This simulates the effects of different power levels on pollution production. Total pollutants are collected in a bag, separated and weighed, and divided by total distance "traveled" to give a pollution rating in terms of grams per kilometer.

Listed below are data showing Taiwan's increasingly strict emissions policy, compared with U. S. motorcycle and automobile standards. Data is from the Weaver and Chan study and an ROC-EPA document titled "Emission Standards of Air Pollutants for Transportation Vehicles".[33,34]

The "test procedure" column describes the driving cycle used for the vehicle; the ECE-40 (Economic Commission for Europe) test driving cycle and the American Federal Test Procedure are different driving patterns used for testing motorcycle emissions. The two velocity *vs.* time traces are plotted and described in greater detail in section 4.3.

Table 1.3 A comparison of vehicle emissions standards

motorcycle standard and driving cycle	**year**	**test procedure**	**THC (g/km)**	**CO (g/km)**	**NO_X (g/km)**
Taiwan "first stage"	1988	ECE-40	5.5*	8.8	*
Taiwan "second stage"	1991	ECE-40	3.0*	4.5	*
Taiwan "third stage"	1998	ECE-40	2.0*	3.5	*
Taiwan "third stage" special low emission motorcycles	1999	ECE-40	0.58*	1.08	*
Taiwan fourth stage (proposed) two-stroke motorcycles	2003	ECE-40 (cold test)	1.0*	7.0	*
Taiwan fourth stage (proposed) four-stroke motorcycles,	2003	ECE-40 (cold test)	2.0*	7.0	*
California motorcycles <280 cc	1988	Modified FTP	1.0	12.0	–
US motorcycles, all types	1980	Modified FTP	5.0	12.0	–
US automobiles (Clean Air Act Amendment)	1990	FTP	0.16†	2.11	0.25

Notes follow on next page.

* Taiwan standards asterisked are for THC + NO_x *combined*.

† Before 1990, the standards were for total hydrocarbons; since the 1990 Clean Air Act Amendment, the figure of 0.16 grams/km is for non-methane hydrocarbons (NMHC). A more aggressive driving cycle

will be introduced for the 2000 model year, as part of the Supplemental Federal Test Procedure.

Note that the fourth-stage standards require a different procedure in that the engine is started from cold conditions; this is supposed to produce 2.5 times as many pollutants as the equivalent "warm test", so what appears to be a loosening of the standards is in fact a move towards stricter requirements.

Particulate matter emissions from motorcycles are not regulated anywhere, although Taiwan does require a maximum smoke opacity of 15%, which is often considered a crude proxy for total particulate matter.[35]

As the data below show, when tested in the lab under the same ECE-40 test driving cycle, emissions from actual in-service motorcycles tend to be higher than the current ("third stage") standards of 2.0 g/km from THC and NO_x and 1.1 g/km of CO. For example, a two-stroke 50 cc scooter without benefit of catalyst produces 3.8 g/km of THC and $NO_{x,}$ and 7.5 g/km of CO. Data for four-stroke scooters, catalyst-equipped scooters, and an automobile are also provided for comparison:

Table 1.4 Data on motorcycle emissions: four-strokes and catalysts

model or standard	model year	test cycle	THC (g/km)	CO (g/km)	NO_X (g/km)	fuel econ (mpg)
50 cc Sanyang 2-stroke motorcycle, no catalyst	1995	ECE-40	3.8	7.5	0.007	91-95
50 cc Sanyang 2-stroke motorcycle, oxidation catalyst	1995	ECE-40	2.1	2.9	0.000	91-99
125 cc Sanyang 4-stroke motorcycle, no catalyst	1992	ECE-40	0.64	4.0	0.19	85-88
Ford automobile, 3-way catalyst, fuel injection	1991	FTP	0.12	1.3	0.14	26-33

Source: mean results of National Taiwan University study on scooter and car emissions[36] The low NOx readings are due to several test producing readings "below the analyzer's detection limit"

The evidence shows that two-stroke motorcycles produce very high quantities of hydrocarbons, and low NO_x. The ECE-40 driving cycle is a simplified test pattern not intended to mimic road driving, and modeling results done by Taiwan's Environmental Protection Agency shown below in Table 1.4 using the more representative Taiwan Motorcycle Driving Cycle strongly suggest that real world emissions factors are higher by as much as a factor of ten: 13.7 g/km of THC and NO_x and 29.2 g/km of CO.

Table 1.5 Simulated emissions from more realistic driving cycle

model or standard	model year	test cycle	THC (g/km)	CO (g/km)	NO_X (g/km)	fuel econ (mpg)
2- stroke motorcycle, modeled using MOBILE-5	1996	TMDC	13.2	29.2	0.51	n/a
4- stroke motorcycle, modeled using MOBILE-5	1996	TMDC	5.4	26.8	0.51	n/a

Source: Republic of China Environmental Protection Agency vehicle

simulation [37] The THC figure includes evaporative and resting losses in addition to exhaust.

Due to the high-power spikes of the TMDC, more pollution is generated than during the ECE-40 cycle test.

1.2.4. Air pollution sources in Taiwan

Taiwan has an average population density higher than virtually all other developed countries, and more importantly, one of the largest average motor vehicle densities in the world at 425 per square kilometer in 1997.[38] This vehicle density is double that of Japan, four times that of Germany, and eighty times that of the USA.[39] It should be noted that the central mountain range of Taiwan is thinly populated, meaning that the relevant densities are even higher in the urbanized coastal areas.

In terms of emission of pollution, a study done at ITRI (the Industrial Technology Research Institute – a Taiwanese national laboratory for applied research) reported that, in 1994, the majority of carbon monoxide is emitted by vehicles, while two-stroke motorcycles specifically are a major producer of hydrocarbons. The figures below are total emissions for 1994.

Figure 1.6 Carbon monoxide emissions by source

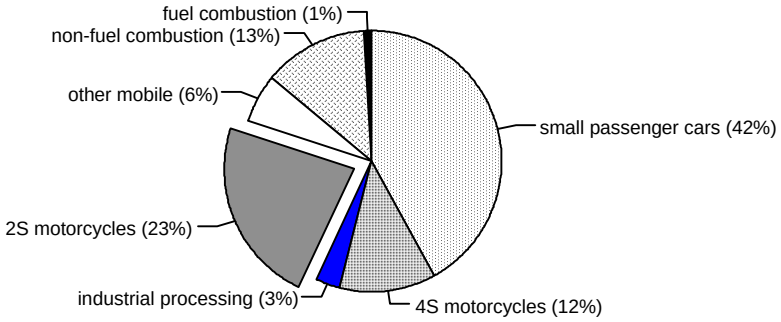

The total mass of CO emitted was 2.05 x 10^6 tonnes in 1994. Data from the Mechanical Industry Research Laboratories, Industrial Technology Research Institute, Taiwan[40]

Figure 1.7 Hydrocarbon emissions by source

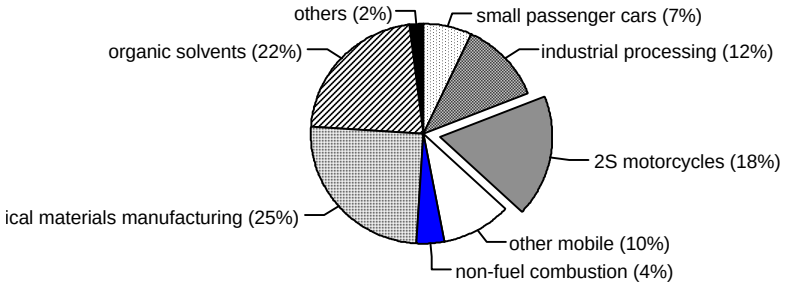

The total mass of THC - total hydrocarbons - emitted was 1.11 x 10^6 tonnes in 1994. Data from the Mechanical Industry Research Laboratories, Industrial Technology Research Institute, Taiwan.[41]

Two-stroke scooters produce 28% of carbon monoxide emissions, and 51% of hydrocarbon emissions. The relative unimportance emissions from power plants (included under either "nonfuel combustion" or "other") from this data is a little surprising.

Air conditions are poor. One yardstick of pollution, the Pollution Standards Index (PSI) common to many countries, illustrates this point. PSI, an artificial measure used to provide a single level of "pollution", is the maximum of the indices for five different pollutants: CO, ozone, NO_2, SO_2, and PM_{10}. These indices are segmented linear functions of concentration, as shown below. (Note that the original units of ppm and ppb were homogenized to $\mu g/m^3$).

Table 1.6 PSI subindex pollutants in Taiwan

PSI value of subindex	24-hr PM_{10}	24-hr SO_2	8-hr CO	1-hr O_3	1-hr NO_2
50	50	90	5600	130	n/s
100	150	400	11250	260	n/s
200	350	860	18750	430	1230
300	420	1710	37500	860	2460
400	500	2290	50000	1070	3290
500	600	2860	62500	1290	4110

n/s: no standard for short-term; the index merely measures exceedances in this case. Data is from the Republic of China EPA's web site[42]

Thus, an unhealthy condition (PSI>100) takes place when any of the five concentrations exceeds the "100" subindex value. For example, if the average PM10 concentration over 24 hours is higher than 150 $\mu g/m^3$, *or* if the average SO_2 concentration over 24 hours is higher than 400 $\mu g/m^3$, then the PSI itself is greater than 100. The same holds true for carbon monoxide, ozone, and NO_2.

The number of PSI exceedance days for each year from 1987 to 1991 was over 15% but for the years 1995-1997, this had reduced to 6%.[43,44] This is still three times higher in Taiwan than in many other countries.[45] As a comparison, some urban Southern California counties had years in which over 20% of days had PSI > 100 (data for years since 1993), but these were the extreme cases. For 5,690 county-years between 1993 to 1998 for counties across the United States, *fully 99.2%* had less than 6% exceedances per year.[46] In fact, 83.5% of the county-years had less than 1% PSI exceedances. In other words, Taiwan's *overall* pollution rate of 6% exceedances per year was worse than all but 0.8% of American individual county readings.

In addition, the *average* level of pollution has been decreasing over time, as indicated by various subsets of the seventy-one monitoring stations scattered across Taiwan:

Figure 1.8 PSI in Taiwan, 1994-1996

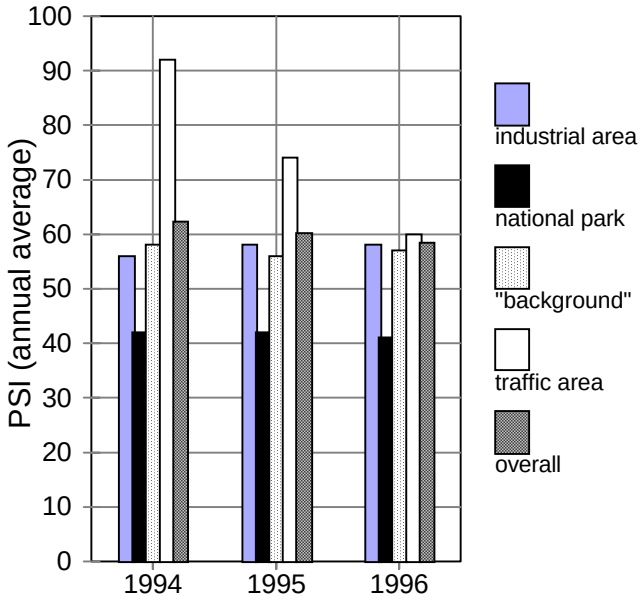

Data is from the Taiwan Environmental Protection Agency.[47]

1.2.5 Cleaner combustion technology

There are numerous options for reducing vehicle emissions. Over the years, four-stroke engines have received much more research attention than two-stroke engines, due to the overwhelming number of automobiles in the world, and this is part of the reason automobile technologies like catalysts and fuel injection have not been adapted for the two-stroke market. The most important reason, however, is that most of the pollution cleanup technologies add weight and cost, eroding the original benefits of two-stroke engines.

1.2.5.1 Exhaust gas recirculation

EGR is mainly used in automobiles to reduce NO_x production, but it is discussed here mainly to explain why two-stroke scooters produce low levels of that particular pollutant. Exhaust gas recirculation causes some of the burned gases to combine with the incoming air/fuel. This lowers the engine temperature because the relatively large heat capacity of triatomic species like CO_2 and H_2O in the recirculated exhaust gas dilute the contents and steal heat from the combustion process, and this means less NO_x production. In fact, due to the nature of two-stroke engines (with the incoming charge partially mixing with the outgoing gases), some EGR occurs automatically. EGR has the disadvantage of slowing combustion rate and thus making stable combustion more difficult; there is increased possibility of unburnt hydrocarbon emissions.[48]

1.2.5.2 Superchargers

Superchargers allow precompression of the air/fuel without requiring crankcase compression, and avoid mixing lubricating oil with the fuel, but add expense. Essentially, a supercharger is a

compressor or blower that increases the pressure of the intake air. It may be powered off the crankshaft (thus parasitically consuming some of the developed power), electrically, or by a turbine driven by the exhaust gas flow in which case it is called a turbocharger.

1.2.5.3 Fuel injection

As alluded to earlier, with fuel injection systems only air is compressed in the crankcase, not an air/fuel mixture. The fuel spray is then injected at high pressure into the compressed air stream just before intake or directly into the combustion chamber; such a system allows more precise, electronic control of the air-to-fuel ratio than a carburetor. Orbital Engineering in Australia is one company trying to combine the high power density of two-stroke engines with the efficiency of direct fuel injection; the company also modifies the combustion chamber to improve emissions.

Fuel injection is estimated to reduce fuel consumption by 25-35% due to the more complete combustion, and to reduce unburned hydrocarbon emissions by 75-85% and carbon monoxide by 50% for the same reason.[49]

However, the pumping system required to maintain injection pressure reduces the power density advantage of two-stroke engines.[50] A Piaggio study estimates the pump power at 300 W at maximum speed of 8000 rpm, for a test 4 kW engine; this amounts to a 7.5% parasitic power loss.[51]

1.2.5.4 Catalysis of exhaust gases

Three-way catalysts like those found in typical automobile engines are composed of alloys of expensive metals like platinum and/or palladium with rhodium. Three-way catalysts are so named because they simultaneously oxidize hydrocarbons and CO, and reduce NO to nitrogen. A rich air/fuel ratio is needed for the NO_x reduction; this richer condition increases exhaust pollutants and partially offsets the benefit of catalysis. These systems require fairly precise stoichiometry and typically electronic control using oxygen sensors in the exhaust pipe is needed to maintain this ratio.

Oxidation catalysts, on the other hand, use metals like platinum and/or palladium to increase the rate of oxidation of exhaust molecules like CO and hydrocarbons; essentially, this is catalytic combustion. Catalysts are "poisoned" by lead in the fuel, and sulfur or phosphorous compounds that may be found in the lubricating oil; active sites are taken up by these compounds and the catalysts must be thermally or chemically treated to restore their function.

The high proportion of scavenged unburnt air/fuel in the exhaust gas is problematic for catalytic converters. On the one hand, the heat capacity of the hydrocarbons reduce the temperature of the exhaust, delaying catalyst activation. On the other hand, catalyst oxidation of the unburned A/F may increase temperature to *too* high a level, causing catalyst durability problems. The solution is sometimes to use two-stage catalysts, with the rate of catalysis controlled by admitting "secondary air"[52]

In the National Taiwan University experiment described in Table 1.4, an oxidation catalyst attached to a two-stroke motorcycle was found to reduce 45.4% of total hydrocarbons, and 61.2%

of CO; emissions for NO_x were already extremely low. (In comparison, the same study found that car three-way catalysts achieved reductions of 90.5% of total hydrocarbons, 88.0% of CO, and 94.2% of NO_x of automobile exhaust).

1.2.5.5 Replacement by four-stroke engines

The more and more stringent emissions standards have made switching to four-strokes an increasingly attractive option. In fact, a researcher at ITRI wrote that the announced year 2003 fourth-stage standards would be "too tough for 2 stroke [engines] to survive. This is an understanding between Taiwan EPA and motorcycle makers to phase out 2-strokes by that time."[53] This is an easy solution because it leverages well-understood existing technology. Drawbacks include greater vehicle weight and larger engine sizes, and of course more expensive engines. Advanced four-strokes would follow the advances made on the automobile side, with three-way catalysts, engine timing optimization for reduced emissions rather than specific power, etc.

1.2.5.6 Relative costs and benefits of various technologies

A Piaggio study also estimated the costs for various clean two-stroke technologies that they considered for new high-efficiency and low-emissions two stroke engines. The relative costs are reproduced below, along with estimates of air pollution reduction. Note that the base cost to manufacture a two-stroke scooter engine is approximately $150.[54]

Table 1.7 Cleanup technology, effects and prices

Type of engine	relative cost	THC reduction	CO reduction
Two-stroke standard	1.0	baseline	baseline
Fuel injection with external scavenge (separate blower to scavenge cylinder)	1.5-1.7	75% - 85%	50%
FAST ("Fully Atomized Stratified Turbulence") - mechanical control	1.2-1.4	68% - 76%	65% - 80%
FAST - electronic control	1.4-1.6	68% - 76%	65% - 80%
catalytic converter	1.7	45% - 80%	61 - 95%
Equivalent four-stroke	1.5-1.7	83%	47%

Sources: for catalyst cost, Felton.[55] For other costs, Piaggio study.[56] For reductions in pollution, National Taiwan University study[57], Piaggio study for direct injection with electronic-control pollution reductions assumed to be the same as mechanical-control reductions.[58]

Improvements that may seem simple, technologically speaking, actually add about 50% to the engine cost. On the other hand, the standard engines cost only about $150 to manufacture, so the difference in dollars is not great - perhaps $150 once manufacturing and markups are included.

So significant reductions are possible using relatively inexpensive improved combustion techniques, the easiest of which is a transition to only four-stroke vehicles. Are electric vehicles necessary, then? Or in other words, is it worth spending additional money on "zero-emission"vehicles to reduce emissions further?

1.2.6. Assessing the damage

The process of establishing - and quantifying - a causal link between scooter tailpipe emissions and health and environmental damages is a long one with many steps. In general, researchers have

proceeded through the following stages:

1. Measurement of pollutant emissions by collecting tailpipe exhaust under various simulated driving cycles, as tested on a dynamometer.

2. Dispersion modeling, based on local wind patterns and atmospheric models, to proceed from pollution emitted per kilometer on the streets to ambient concentrations in the local environment.

3. Estimation of individual exposure to various pollutants by studying population distributions

4. Dose-response modeling of health effects resulting from exposure. Epidemiological studies are generally used to try to correlate incidences of high pollution with acute and chronic negative health effects, which are measured in terms of deaths (mortality) and loss of useful function (morbidity).

5. Estimates of the cost of health damages, either by calculating the value of lost work-days or by contingent-valuation surveys that aim to capture the value of health externalities.

Similar processes are applied to damage caused to buildings and other material objects. The literature contains little data quantifying specific Taiwan conditions, although studies have been done to estimate valuation of health episodes (i.e. the fifth step).

1.2.6.1 Reduction estimate

Also, a previous ITRI study estimated reductions in CO and THC levels in the air assuming

current emission rates and increasing vehicle populations after 1991 (steps 1 and 2 of the cost-benefit analysis process enumerated above). The CALINE-4 line source and dispersion model was used to estimate ambient pollution concentrations near roads. Three situations were studied and the following results were obtained for the 1991-1996 time period:

Table 1.8 ITRI prediction of effects of scooter replacement on pollution

Scenario	*CO*	*HC*
Baseline: no change in scooter pollution levels	0%	0%
All motorcycles after 1991 meet second-stage standards	-17.4%	-5.8%
As above but with 20% of scooters replaced by electric	-24.8%	-12.2%
As above, but with 50% of scooters replaced by electric	-35.1%	-17.2%

Data from ITRI study [59]

These reductions are almost equal to the fractions of carbon monoxide and hydrocarbons emitted by scooters overall, but it should be kept in mind that these measurements are for roadside ambient concentrations, not overall emissions.

It is not clear whether it is old, highly polluting scooters or a random sample of scooters that are being replaced with battery-powered scooters. However, the results clearly demonstrate how important scooter pollution reductions are in improving localized air quality; scooters clearly were predicted to produce *at least* 35% of roadside CO and 17% of roadside HC.

1.2.6.2 Externality damage estimate

A systematic study of the health and environmental benefits of reduced air pollution is not within the scope of this study. However, as a rough estimate of the benefits of cleaner air, the particulate ($PM_{2.5}$) pollution emitted by four-stroke scooters was calculated as if it were an automobile, but factored by the greater fuel economy of the scooter. Next, the externality cost of air pollutants was obtained from a recent study by Spadaro and Rabl.[60] They calculated the following externality costs of various vehicle air pollutants:

Table 1.9 Estimate of externality damages from air pollutants

Pollutant	***Euros / tonne***	***$ / gram***
Urban nitrate	1.6×10^4	$0.0200
Ozone from NOx	1.45×10^3	$0.0018
Fine particles ($PM_{2.5}$)	2.2×10^6	$2.75

Note: at the time the study was done (October 1998), 1 ecu was equal to 1.25 US dollars. The ecu has since been replaced by the euro.

The authors used a fine particulate ($PM_{2.5}$) emission rate of 0.75 grams for a 43.3 km Paris trip in a three-way-catalyst-equipped automobile, or 0.017 g/km. This is based on Heywood, which specifically quotes a figure of 0.020 g/km for particulates for a car running on unleaded fuel with no catalyst.[61] Using the authors' figure and their implied fuel economy of 9.14 km/L (21.5 mpg) gives an emission rate of 0.155 grams of fine particulates per liter of fuel. An equal emission rate was assumed for scooters running on the same four-stroke cycle as the automobiles. With a 100 mpg fuel economy (4.6 times better than the car), the per-kilometer emission rate is only 0.0037 g/km. Annual health costs for 12,000 km/y driving means annual health externalities of $120 per

year per four-stroke scooter.

The figure of 0.51 g/km of NO_x from Table 1.5 for simulated urban scooter driving, when taken through similar calculations, yields externalities of $133 per year, for a total pollutant damage of $253 per year. Damages from other pollutants are not included.

The health cost is scaled by a factor proportional to the ratio of Taiwan GNP per capita to French GNP per capita, taken to the power of the elasticity of willingness to pay for health with respect to GNP:

$$\text{damage in Taiwan} = \text{damage in France} \times \left(\frac{\textit{Taiwan GNP per capita}}{\textit{France GNP per capita}} \right)^{\textit{elasticity}}$$

In 1998, French GNP per capita was $23,789 in 1997 US dollars, and the Taiwan GNP per capita was $13,819 in 1997 dollars.[62,63] The elasticity of willingness to pay with respect to income was estimated at 0.4 for Taiwan by an Alberini, Cropper, *et al*. study.[64] Note, however, that the original damages were obtained for a uniform distribution of population around emission sources, and a population density of 7500 persons per km^2 was used. Average density in Taipei is 1.27 times greater, for a final ratio of 1.022 for Taipei damages to Paris damages in terms of g/km.

Assuming a ten year vehicle lifetime and 10% discount rate means a final present value cost of emissions of $1,590. Spadaro and Rabl quote a very broad uncertainty in terms of a geometric mean standard deviation of 4.0, so that a 68% confidence level corresponds to $400 to $6,355. If elasticity is 1.0 rather than 0.4 (i.e. damage scales linearly with GNP), then the equivalent interval is $290 to $4,590.

This is a large amount and suggests that improvements in air quality would produce a significant

benefit; a complete elimination of tailpipe emissions from the use of electric scooters could be a significant benefit over even four-stroke engines, the expected replacement for two-stroke engines. Of course, as the large geometric standard deviation suggests, this is only an attempt to broadly quantify the problem and is subject to the large uncertainties involved in any cost-benefit analysis.

1.2.7 Government policy approaches

Due to the problem of air pollution, several Asian governments have implemented measures to control two-stroke vehicles. For example, Thailand motorcycles have been restricted to 150 cc, "presumably ... to limit the maximum engine power, and thus the acceleration rates, top speed, and fuel consumption"[65]. In practice, the policy encourages use of *more* polluting two-stroke engines for their higher power at the same 150 cc displacement. Similarly, the city of Shanghai currently tightly restricts the supply of motorcycle licenses, although as previously discussed, all predictions point to vastly increasing Chinese vehicle usage. Taiwan's policy towards scooters, which is more advanced than virtually all of its neighbours, is discussed below.

1.2.7.1 Taiwan policy history: tighter emissions standards

Taiwan's 1991 ("second stage") standards were the strictest in the world, and essentially forced two-stroke motorcycles to be equipped with oxidation catalytic converters to meet these requirements. These catalytic converters cost approximately $80 for the manufacturer. To meet the 1991 standards, four-stroke motorcycles required modification to allow exhaust air injection (estimated cost $40-$60).[66]

Most Taiwanese motorcycle manufacturers depend on foreign (Japanese) parent companies for advanced technology, and catalytic converters are all imported. Naturally, Taiwanese manufacturers would like to produce them domestically.[67]

1.2.7.2 Later years: inspection and maintenance

In addition to tightening standards for new motorcycles and scooters, the Taiwanese government has acted to control emissions from highly polluting existing motorcycles. This is an effective method of cleaning up the worst offenders, which can account for the majority of the pollution. Originally, this consisted solely of roadside testing of emissions from randomly selected vehicles. Annual stationary emissions testing was begun in several counties. Testing was voluntary and there were no fines; incentive was provided by a system where drivers who brought in their vehicles for testing were given ballots to enter in a cash lottery.[68]

Later, a sticker system was implemented and as of 1998, motorcycle and scooter licenses can be revoked if the owner fails to bring in the vehicle for annual emissions testing. Vehicles that fail the test must be tuned up and brought in a month later for retesting; a second failure also means license revocation. By tackling the most errant vehicles, significant gains can be made; statistics report an average 48% reduction in CO emissions and 35% reduction in total hydrocarbons in offending vehicles after rechecking[69]. Currently, there are 456 inspection and maintenance (I&M) stations across the island, and approximately 400,000 scooters were inspected in 1996. Remote sensing is employed to measure CO and hydrocarbon emissions. [70]

1.2.7.3 Future direction: zero-emission vehicles

In 1991, ITRI researchers estimated that by 1996, up to 50% of scooters would have to be replaced by electric scooters to prevent continued degradation of air quality. This was in addition to the adoption of second stage emission standards and gradual replacement of the existing fleet by more advanced vehicles. No 50% replacement occurred, but a government policy was defined that required 2% of the scooter fleet to be zero-emission scooters by the year 2000.[71] This is almost as aggressive as California's clean air policy requiring zero emission automobiles, but whether either will succeed is uncertain.

The objective appears to be to convert small engine (50 cc) scooters to electric power, while keeping clean four-stroke engines for the larger (100 cc and up) scooters.[72] By 1997, there were approximately 300 electric scooters in use in Taiwan.[73] There is currently a $5,000 New Taiwan Dollar (USD $150) subsidy for each electric vehicle purchased.

This "Electric Motorcycle Development Action Plan" will be funded by the government at a cost of NTD $3.8 billion (USD $115 million) from 1999 to 2002. This money is to go to research funding and subsidizes for electric scooter purchases. Details of the plan are listed below.

Table 1.10 Electric Motorcycle Development Action Plan

Year	*Number of electric vehicles to be sold*	*Notes*
1999	10,000	Republic of China EPA to select specially designated locations for initial promotion The Kwang Yang Motor Co. (Kymco) plans to begin mass production in March, 1999 5% of annual motorcycle sales by manufacturers producing more than 50,000 motorcycles per year must meet special "low emission motorcycle" standards (see Table 1.3)
2000	40,000	Electric motorcycle sales required to comprise 2% of all motorcycle sales
2001	80,000	Electric motorcycle operating environment [recharging infrastructure, etc.] to be gradually put in place; sales to increase
2002	150,000	50% of two-stroke motorcycle sales anticipated to be replaced by electric motorcycle sales; four-stroke motorcycles will absorb the other half.
2003	200,000	Electric motorcycle technology to become mature; production of nickel [metal] hydrogen batteries to begin Introduction of fourth stage emissions standards; improvements in battery-powered scooter technology to reduce price below that of (not necessarily equivalent) four-stroke motorcycles.
2006	400,000	Continued growth of electric motorcycle sales; annual sales of electric motorcycles to reach 40% of *total* motorcycle sales.

The description of this plan is paraphrased from an Engine, Fuel, and Emissions Engineering, Inc. study and the March 1998 issue of the Taiwan EPA's *Environmental Policy Monthly.*[74,75] The latter source writes that

> Current trends indicate that by 2010 annual sales of motorcycles will reach 9 million units. It is estimated that electric motorcycles will make up one-third of this total, or three million units sold. If this sales rate is achieved, the EPA has calculated that carbon monoxide (CO) emissions can be reduced by 42,000 metric tons annually . . . Hydrocarbon and nitrogen oxide (NOX) emissions can be reduced by 23,400 tons, and carbon dioxide (CO2) can be reduced by 62,800 tons annually. As for energy savings, each year 2.2 million megawatt hours can be saved and off-peak electricity use rates can be raised.[76]

The “three million electric scooters” target seems extremely high, consider that only 400,000 are expected to be sold by 2006. A TTVMA (Taiwan Transportation Vehicle Manufacturers’ Association) study was also not as optimistic, estimating that by 2010 only 150,000 electric motorcycles will be produced, for an average unit price of $909 and a sales value of $136 million.[77]

For comparison, current electric scooters like the SWAP (Shang Wei Air Preserver) cost approximately $2,000[78], while ordinary two-stroke scooters cost on the order of $1,000.[79] Scooters currently have very low range and recharging is inconvenient due to the times involved and the fact that not all scooter owners have access to an electric outlet (for example, they may not have enclosed garages or parking off the street).

1.2.7.4 Research interest in fuel cell scooters

As of July 1999, several Taiwanese scooter manufacturers have explored the possibility of fuel cell scooters with North American research groups, hydride supplies, and fuel cell companies. Projects begun in the past two years include the following:

- A Department of Energy - funded contract awarded in 1998 to Energy Conversion Devices, a Michigan metal hydride manufacturer, to study hydrogen fuel for transportation (especially scooters) in developing countries.[80]

- A 1998 feasibility study of fuel-cell powered scooters performed by Sanyang Industry Company, the Taiwan Institute of Economic Research, the Desert Research Institute, and Texas A&M's Engineering Experiment Station. Partial funding supplied by the W. Alton

Jones foundation; one of the projects was to build a prototype scooter.[81] Please see Appendix G for more information on this prototype scooter.

- A collaborative fuel cell scooter development project spearheaded by the Taiwan Institute for Economic Research and including other Taiwan scooter concerns, announced in July 1999, and growing out of the previous study. The power system is to be based on a 3 kW fuel cell stack developed by fuel cell scientist John Appleby of Texas A&M, and hydrogen is expected to be produced by the China Petroleum Corporation, the Taiwan government's gasoline monopoly.[82]

Interest in fuel cell scooters has been growing rapidly in 1998 and 1999. The first step in understanding the technological issues, then, is the next chapter which describes electric scooters, and how they can be powered by either batteries or fuel cells.

1.2.8 Conclusion

Historically, two-stroke engines have been used for their high power density and low cost. Two stroke scooters have become a major cause of concern in many Asian countries due primarily to hydrocarbons short-circuiting through the chamber and escaping, unburned, in the exhaust.

Tightening government air pollution standards are squeezing out two-stroke engines in the policy leader, Taiwan. Four-stroke engines are a cheap and effective replacement. However, an additional benefit of several hundred, or even a thousand dollars could be realized by switching to electric scooters with their zero tailpipe emissions.

The target vehicle in this study is thus an electric replacement for the small 5 kW two-stroke scooter. A detailed comparison will be made between fuel cell scooters and battery-powered scooters using both conventional and advanced technologies

References for Chapter 1

1. A. John Appleby and F. R. Foulkes. *Fuel Cell Handbook* (Van Nostrand Reinhold: 1989) pp.193-196. The vehicle described was an Austin A-40 developed by Karl Kordesch at Union Carbide and run off compressed hydrogen tanks. It was driven by Kordesch on public roads from 1971-1975.

2. Although relatively little work has been done, the interest is there from several parties as of September 1999. Vehicle manufacturers from Taiwan, which has more scooters than any other country in the world, have explored the possibility of fuel cell scooters with several North American fuel cell companies. The Desert Research Institute in Nevada had run a program to produce a prototype fuel cell scooter, while Energy Conversion Devices, a Michigan metal hydride and battery manufacturer, has analyzed the market possibilities for both combustion and fuel cell scooters run on hydrogen. Yamaha of Japan has studied the prospects for fuel cell motorcycles. So far, no results have yet been published aside from this work.

3. Yoshihiro Nakazawa, Chiaki Kumagai, Mikio Kato. "Development of an electric scooter for practical use" *JSAE Review* **15** (1994) pp. 373-377

4. Christopher S. Weaver, Lit-Mian Chan."Motorcycle Emission Standards and Emission Control Technology" Revised Final Report, submitted to The World Bank. (Engine, Fuel, and Emissions Engineering, Inc.: August 1994), p.3

5. Xiannuan James Lin, Karen R. Polenske. "Energy Use and Air Pollution Impacts of China's Transportation Growth" in *Energizing China: Reconciling Environmental Protection and Economic Growth*. Editors Michael B. McElroy, Chris P. Nielsen, Peter Lydon. Harvard University Press, 1998. p. 211

6. Dr. Pradeep Monga. United Nations Development Programme. "Discussion on Better Environment & Natural Resource Management". http://rrmeet.undp.org.in/_disc2/00000008.htm Accessed July 11, 1999

7. Taiwan Transportation Vehicle Manufacturers' Association web page. "Taiwan Transportation Vehicle Manufacturers' Association - Industry Updates" http://ttvma.asiansources.com/INDUSTRY/IUPDAUTO.HTM. Accessed May 16, 1999

8. Industrial Technology Information Service, Industrial Technology Research Institute."ROC: Republic of Computers -- Taiwan" *1997 Taiwan Industrial Outlook* http://www.itis.itri.org.tw/eng/rep9712.html Accessed March 26, 1999. Updated January 20, 1998.

9. Encyclopædia Britannica Online. "Encyclopaedia Britannica: Taiwan" http://www.eb.com:180/bol/topic?tmap_id=205530000&tmap_typ=gd. Accessed April 1999

10. Government Information Office of Taiwan web page. The Republic of China Yearbook 1997. "Chapter 2 - People" http://www.gio.gov.tw/info/yb97/html/ch2.htm. Accessed March 9, 1999

11. Directorate-General of Budget, Accounting and Statistics, Executive Yuan, the Republic of China. Monthly Bulletin of Statistics of the Republic of China, February 1999. "Table K-5 Number of Registered Motor Vehicles" http://www.dgbasey.gov.tw/dgbas03/english/bulletin/k5.htm. Accessed March 25, 1999

12. Laurie Underwood. "Airborne Menace" in *Free China Review* September 1, 1996

13. Directorate-General of Budget, Accounting and Statistics.

14. Directorate-General of Budget, Accounting and Statistics.

15. Department of Budget, Accounting, and Statistics - Taipei City Government. Summary of Statistics Taipei City for 1998. "Vehicle Registration". http://www.dbas.taipei.gov.tw/stat/summeng/sume19.htm Accessed March 25, 1999

16. Hsiung-Wen Chen, Hui-Chuan Hsaio, Sheng-Jonh Wu. Environmental Protection Agency, Republic of China (EPA ROC). "Current Situation and Prospects of Motorcycle Pollution Control in Taiwan, Republic of China" 1992. Society of Automotive Engineers (SAE) 922176.

17. T. J. Price and S. D. Probert. "Taiwan's Energy and Environmental Policies: Past, Present and Future" *Applied Energy* **50** (1) (Elsevier:1995), p. 56

18. United States Energy Information Administration (EIA). "Taiwan" http://www.eia.doe.gov/emeu/cabs/taiwan.html. Accessed May 8, 1999. Page updated December 1998.

19. United States Energy Information Administration (EIA). "Taiwan"

20. United States Energy Information Administration (EIA). "Taiwan"

21. Willard W. Pulkrabek. *Engineering Fundamentals of the Internal Combustion Engine*. Prentice Hall (Upper Saddle River: 1997), p. 26

22. Pulkrabek, p. 28

23. Weaver and Chan, Appendix p. 16

24. Mark L. Poulton. *Alternative Engines for Road Vehicles* (Computational Mechanics Publications: 1994), p.54

25. Toshiharu Sawada, Minoru Wada, Masanori Noguchi, Buhei Kobayashi. "Development of a Low Emission Two-Stroke Cycle Engine". Society of Automotive Engineers (SAE) 980761. 1998. p. 81

26. Todd D. Fansler, Donald T. French, Michael C. Drak. General Motors Global Research and Development Operations. "Individual-Cycle Measurements of Exhaust-Hydrocarbon Mass from a Direct-Injection Two-Stroke Engine". SAE T980758. 1998. p. 50

27. Sawada, Wada, Noguchi, Kobayashi p. 89

28. Weaver and Chan, Appendix p. 7

29. Mark L. Poulton. *Alternative Engines for Road Vehicles* (Computational Mechanics Publications: 1994), p. 50

30. Note that methane is often excluded from the category of hydrocarbon air pollutants because it is not reactive in forming secondary air pollutants; the category then becomes non-methane hydrocarbons (NMHCs).

31. TVS Suzuki Limited. TVS Scooty KS specifications. http://www.tvssuzuki.com/html/sco_ks.html. Accessed May 12, 1999

32. OECD. *Motor Vehicle Pollution: Reduction strategies beyond 2010* OECD, 1995. p. 57

33. Weaver and Chan, p. 47

34. Republic of China EPA document. "Emission Standards of Air Pollutants for Transportation Vehicles" (no author or date)

35. Weaver and Chan, p. 62

36. Chang-Chuan Chan, Chiu-Kuei Nien, Cheng-Yuan Tsai and Guor-Rong Her, "Comparison of Tail-Pipe Emissions from Motorcycles and Passenger Cars" in *J. Air & Waste Management Association* **45** (2) February 1995, pp. 116-124

37. H-W Chen, S. Lu, Y-P Yu, Y-W Lin. Environmental Protection Agency ROC. "The study of driving cyclye [sic] and emission factors estimation of vehicle in Taipei Metropolitan ROC". Presented at International Symposium on Automotive Technology & Automation (ISATA) 1997, paper number 97EN026

38. Government Information Office of Taiwan web page. The Republic of China Yearbook 1997. "Chapter 13 - Environmental Protection" http://www.gio.gov.tw/info/yb97/html/ch13.htm. Accessed March 9, 1999

39. ROC EPA web page. "Air Pollution Control Approach in Taiwan". http://www.epa.gov.tw/english/Offices/taiwan.htm. Accessed May 16, 1999 .

40. P. H. Jet Shu, Wei-Li Chiang, Bing-Ming Lin, Ming-Chou Cheng. Mechanical Industry Research Laboratories, Industrial Technology Research. "The Development of the Electric Propulsion System for the Zero Emission Scooter in Taiwan" SAE 972107, JSAE 9734403. 1997

41. Shu, Chiang, Lin, Cheng

42. ROC EPA web page. "Air Quality Monitoring Network In Taiwan". http://www.epa.gov.tw/english/Offices/aqmnit.htm Accessed May 16, 1999.

43. Shu-Hwei Fang, Hsiung-Wen Chen. "Air Quality and Pollution Control in Taiwan". *Atmospheric Environment* **30** (5) pp. 735-741, Elsevier 1996

44. ROC EPA web site. "Air Pollution Control Approach in Taiwan"

45. ROC EPA web page. "Air Pollution Control Approach in Taiwan"

46. EPA Office of Air Quality Planning And Standards. "AIRSData - Monitor PSI Report" http://www.epa.gov/airprogm/airs/data/monpsi.htm Accessed June 23, 1999

47. ROC EPA web page. “Air Pollution Control Approach in Taiwan”

48. John B. Heywood. *Internal Combustion Engine Fundamentals*. McGraw-Hill 1988. p. 837

49. Marco Nuti and Roberto Pardini. Piaggio V.E. S.p.A. “Twenty Years of Piaggio Direct Injection Research to Mass Produced Solution for Small 2T SI Engines” SAE 980760. 1998

50. Weaver and Chan, Appendix p. 17

51. Marco Nuti, Roberto Pardini, David Caponi. Piaggio V.E. S.p.A. “FAST Injection System: PIAGGIO Solution for ULEV 2T SI Engines” SAE 970362. 1997.

52. Mark L. Poulton, p. 53

53. Wei-Li Chiang, Mechanical Industry Research Laboratories, ITRI. Personal communication, July 16 1999

54. $150 estimate of cost from Dr. Philip G. Felton, Princeton University Department of Mechanical and Aerospace Engineering, personal communication July 26 1999

55. Dr. Felton from Princeton University’s Mechanical and Aerospace Engineering department estimated catalytic converter costs at approximately $100 and engine costs at $150, both manufacturing prices. Personal communication, July 26 1999.

56. Nuti and Pardini, p. 73

57. Chan, Nien, Tsai, Her.

58. Nuti, Pardini, Caponi

59. Chien-Tung Liu, C. C. Kuo, Jyh-Sheng Pan, Bing-Ming Lin. “Development of electric motor cycle technologies in Taiwan” *J. Power Sources* **48** (1994) p. 244

60. Joseph V. Spadaro and Ari Rabl. Ecole des Mines de Paris, Centre d’Energetique, Paris. “Social Costs and Environmental Burdens of Transport: An Analysis using Two Case Studies in France”. October 1998

61. Heywood, p. 626

62. OECD web site. February 1999. “GDP per capita based on exchange rates and on PPP”, http://www.oecd.org/std/gdpperca.htm. Accessed March 16 1999.

63. Encyclopædia Britannica Online. “Encyclopaedia Britannica: Taiwan”

64. Anna Alberini, Maureen Cropper *et al*. “Valuing Health Effects of Air Pollution in Developing Countries: The Case of Taiwan” *J. Environmental Economics and Management* **34**, 1997. p. 123

65. Weaver and Chan, p. 69

66. Weaver and Chan, p. 45

67. Chen, Hsaio, Wu.

68. In much the same way, a Taiwan government lottery based on numbers automatically printed on cash register receipts is used to encourage customers to get receipts from legitimate businesses rather than deal with the black market.

69. Republic of China EPA, "Periodic Motorcycle Inspections fully implemented" *Environmental Policy Monthly*, Volume 1, Issue 4. November 1997

70. ROC EPA web page, "Air Pollution Control Approach in Taiwan"

71. ROC EPA, "Electric Motorcycles Targeted as Key Industry for Development" *Environmental Policy Monthly*, Volume 1 Issue 9. March 1998. http://www.epa.gov.tw/english/Epm/issue9803.htm. Accessed May 7, 1999

72. Chen, Hsaio, Wu

73. ROC EPA web page. "Air Pollution Control Approach in Taiwan"

74. Weaver and Chan, p. 42

75. ROC EPA, "Electric Motorcycles Targeted as Key Industry for Development"

76. ROC EPA, "Electric Motorcycles Targeted as Key Industry for Development"

77. Industrial Technology Information Service, Industrial Technology Research Institute."ROC: Republic of Computers -- Taiwan" *1997 Taiwan Industrial Outlook* http://www.itis.itri.org.tw/eng/rep9712.html Accessed March 26, 1999. Updated January 20, 1998.

78. T. Chi Kung, Shang Wei EV Tech Inc. Personal communication, May 3 1999.

79. Chien-Liang Lin, Energy and Resources Lab. Industrial Technology Research Institute. Personal communication, April 29 1999.

80. Energy Conversion Devices, Inc. press release. "ECD AWARDED $3.5 MILLION IN NEW DOE COST-SHARED CONTRACTS" http://www.ovonic.com/news/Oct8_1998.html Published October 8, 1998.

81. "Desert Research Institute Designs Prototype Fuel Cell Scooter for Taiwan Manufacturer" Hydrogen and Fuel Cell Letter, October 1998.

82. "Taiwan Group Launches PEM Scooter Project With Help from Texas A&M, DRI" Hydrogen and Fuel Cell Letter, July 1999. http://mhv.net/~hfcletter/letter/july99/JulyFeature.html

~

Chapter Two

Electric Vehicles

~

The purpose of this chapter is to discuss various electric drive and battery possibilities and obtain data for these options. Electric scooters require drive systems (motor, controller, transmission) and power sources (batteries or fuel cells). Since a fuel cell scooter is essentially a battery-powered scooter with battery replaced by fuel cell plus hydrogen storage, the basic electric scooter is described first.

Components are chosen for the electric scooter on the basis of technical qualifications and economic considerations. The resulting electric battery-powered vehicle is used as a base platform to develop the fuel cell scooter design.

The chapter also includes a section on high-power batteries that would supply transient bursts of peaking power for hybrid scooters.

It should be noted that battery-powered scooters are currently commercially available in North America, Asia, and Europe, although they have met with only limited success.

2.1 Drive systems

The speed of a vehicle is determined by the output of its engine. This is more accurately characterized in terms of the motor's torque and angular velocity, but often measured in terms of the product: power.

Torque is measured in lbf-in, ft-lb, or N-m, power in hp or kW, force in lbf or N, and motor speed in rpm or rad/s. Essentially, an internal combustion engine or electric motor generates rotation at a specific speed and torque; this rotation drives a transmission of which changes the speed of the rotation through gearing, and transmits the force to the slower-turning wheel axle.

A transmission decreases engine speed by the same factor it increases engine torque. Its influence is measured by the gear ratio, the ratio of engine revolution speed to driveshaft revolution speed; the slower the output speed, the greater the output torque. Car linear speed v is the wheel circumference ($2\pi r$) times the engine speed ωdivided by the gear ratio u:

$$v = 2\pi \, r \, \omega/u$$

Typical passenger cars use engine speeds between 2000 and 3500 rpm. Transmissions allow the construction of a smaller motor and allow operation closer to the motor's optimum efficiency at all speeds by changing the gear ratio as a function of output desired. As the car accelerates, the maximum desirable engine speed is reached and the gear ratio is reduced to the next level to stay within an efficient zone; engine speed is allowed to drop again, but with the reduction in gear ratio, velocity increases continuously (at the expense of torque). Essentially, torque translates to force at

the wheel, and large torques are required for steep hill climbing and fast acceleration.

Scooters are single-wheel drive devices; the engine powers the rear wheel, while the unpowered front wheel is used for steering.

2.1.1 Electric drive systems: introduction

An electric drive system replaces the internal combustion engine and assorted transmission systems with an electric system. The various differences are listed below.

Table 2.1. Comparison of power systems

Internal combustion system	Electric battery system	Electric fuel cell system
• engine including cylinders, air intake • fuel tank, carburetor, air filter • pump for lubricating oil, oil tank • exhaust system • transmission and chain • starter battery	• battery • electric motor(s) • motor controller • transmission and chain	• fuel cell stack • fuel cell subsystems including cooling system, air intake, hydrogen intake, humidification system if any • hydrogen storage device • electric motor(s) • motor controller • transmission and chain • battery for startup

A small internal combustion scooter engine of 50-80 cc weighs about 32 kg and occupies under 50 L of space.[1] Note that current 50 cc scooters require a 12 V starting battery on the order of 1.3 kg and 0.7 L.[2] The cost is on the order of $20 retail. In a fuel cell scooter this extra battery, or something similar, would likely be necessary to start the intake blower, open valves, activate electronic controls, and perhaps even warm up the fuel cell. It would not be necessary at all in a battery-powered scooter.

Three different groupings are defined here for the advanced scooters presented here: “fuel cell stack”, “power system”, and “drive system”. “Fuel cell stack” refers to the series-connected electrochemical cells that make up the core power source of the system, and includes manifolding and a plastic insulating housing around the stack. “Power system” includes not only the stack, but also subsystems like the blower to supply air to the fuel cell, the radiator to cool down the stack, and the coolant pump. The most inclusive term, “drive system,” includes the power system and peaking power battery (if any), hydrogen fuel storage, and the electric motor and controller. For an equivalent battery-powered scooter, “drive system” includes the storage batteries, any peaking power batteries, and the motor and controller pair.

2.1.2 Electric motor theory

Electrical motors operate on the basic principle that a current-carrying wire in a magnetic field will experience a force. The magnetic field can be generated by permanent magnets or by a current in an electromagnet. The *stator* is stationary and produces the magnetic flux, while the rotating armature or *rotor* contains the coils that carry the armature current. In general, motor speed is controlled by increasing the armature voltage, while torque is controlled by increasing the current flowing through the armature.

In a combustion engine, the explosions of the air/fuel mix directly produce rotation with a fixed velocity-torque relation. More flexibility can be achieved in an electric motor, where the ratio between torque and speed can be controlled independently and electronically within the motor/controller. For example, in a pulse-width-modulated system the frequency of rotation of the magnetic field governs the speed output, while the phase difference between the rotor and stator

fields determines torque. Transmissions are often not be necessary at all; where used, they offer optimum efficiency (since the output mechanical power can be remapped by the transmission to the higher efficiency portions of the electric motor output) for both driving and regenerative braking.[3] In this study, no transmission was assumed - only a fixed final gearing between the motor output and the wheel.

2.1.2.1. DC motors

DC motors employ a fixed current that causes the rotor to "want" to turn to line up with the poles in the stator. However, the current in the stator is *commutated*, often by a split-ring brush system, so that the direction of the current in the poles switches as the rotor passes by. This ensures that the rotor stays in continual motion. Multiple sets of poles are used to smooth out the rotation. In general, controllers are cheaper than for AC motors; on the other hand, the motors themselves tend to be bulkier and heavier and more expensive.[4]

In the basic *field-wound motor* described above, the stator field is provided by an electromagnet. Speed and torque are controlled by changing the current in the stator field and/or rotor windings.

In a variant, *permanent magnet motors* use permanent magnets rather than electromagnetic windings in the stator. The presence of brushes means relatively high maintenance, but these motors tend to have higher efficiencies than other DC motors due to the lack of stator field windings.[5] They have a narrow peak efficiency, so transmissions are required.

With *brushless DC motors*, it is the rotor that is a permanent magnet. The stator electromagnet

current is switched on and off at the correct frequency (instead of commutated to reverse current direction), creating a rotating magnetic field in the stator and causing rotation in the rotor. Changing the speed of the rotating magnetic field effects rotor speed control. Torque is controlled here by varying the magnitude of the magnetic flux of the stator. (The flux, in turn, is controlled by changing stator current). These motors are relatively efficient due to the absence of brushes and can achieve average efficiencies of about 84% for both motor and controller together.[6] Control, however, is more complex.[7]

2.1.2.2 AC motors

Alternating current motors are inexpensive, simple, and reliable. They operate by take advantage of the changing phase of the stator current. AC motor control is expensive, however, and implemented by changing input frequency ("dragging" the actual rotor frequency ahead to match the input frequency) or by changing voltage. Also, an inverter is needed to produce AC from the fuel cell or battery's DC output.

Induction (asynchronous) motors apply alternating current to the stator winding, creating a rotating magnetic field. There is no current in the rotor windings; the stator *induces* a current in the rotor which creates torque. Efficiencies are greater than those of DC motors, on the order of 85%-91%.[8]

An *AC synchronous motor* is identical to an asynchronous motor, but with a magnet (permanent or electromagnet) in the rotor. In other words, the permanent magnet AC synchronous motor is identical to a brushless DC motor except that the frequency of the supplied alternating current

controls the rotation speed of the magnetic field, not the on-off switching of a pulsed DC current.

2.1.2.3 Hub motors

Hub motors, included as a separate section, are an interesting development which could offer benefits for electric vehicles. These motors have stators fixed at the axle, with the permanent magnet rotor embedded in the wheel. By directly driving the wheel, they eliminate the inefficiency of a transmission and chain connecting the motor to the axle. Other advantages include higher efficiencies, less space, and often easier servicing.

The more traditional “exterior rotor” design has the rotor in a hollow cylinder shape and spinning around a stator axle. The rotor consists of permanent magnets, and this is a “radial gap” motor because the air gap between the stator and rotor extends in the radial direction. In a slightly different option known as the pancake or disc-type brushless motor, the rotor is not around the stator, but rather a flat disc of permanent magnets sitting on top of another flat disc which contains the stator coils. These are “axial gap” motors because the space between stator and rotor is in the direction of the axis. The stator can be a Mylar plate, stack of silicon steel plates with wound coils, or even a printed circuit for small, flat applications.

Figure 2.1 Axial-gap pancake motor

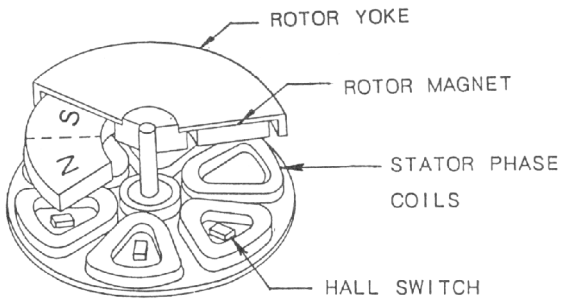

Source: Hendershot Jr. and Miller, p. 2-11.[9]

Pulse width modulated (PWM) current is used to supply current to the stator, so in essence the system is a DC brushless motor. Hub motors must run at relatively low speed – equal to the actual rotation of wheel if there is no final gearing stage. The benefit is about a 10% increase in efficiency due to the lack of transmission.

2.1.3 Converters and controllers

The controller connects the power source - fuel cell or battery - to the actual motor. It controls speed and direction, and optimizes energy conversion. While batteries produce fairly constant voltages which decrease as they are used up, the voltage output by fuel cells varies as a function of power. Some controllers require a DC-to-DC converter to step down this changeable voltage to the motor's expected constant operating voltage, but other controllers incorporate a DC-to-DC converter and can accept a varying voltage. In either case, DC-to-DC conversion losses are minimized if the fuel cell output voltage is near the operating voltage. Converter efficiencies are typically greater than 90%.

The controller varies the speed and torque of the motor. Today voltage control is almost always achieved by "chopping" the source current - the voltage is switched on and off, with the ratio of on-to-off determining the *average* voltage. The number of constant-width "on" pulses per unit time can be varied, or the width (duration) of the pulses can be varied. Chopping is performed by power electronics circuitry - diodes and thyristors and silicon control rectifiers (SCRs)

Controllers also effect regenerative braking, which is the process of driving the motor as a generator to recharge the batteries. In practice, about a third of total energy is discarded in ordinary friction braking (the other two-thirds is lost to rolling resistance and drag and auxiliary power). Due to inefficiencies in the regeneration process, only about 70% of this third can be recovered in regenerative braking.[10] (In the Taipei driving cycle studied later, approximately 20% rather than one third of the total mechanical energy output is lost as friction in braking).

2.1.4 Choice

Standard DC electric motors run at 24 or 48 V; The Taiwan scooter industry appears to be moving towards a de facto standard of 48 V and this was the chosen operating point.[11] For the fuel cell design developed for this thesis and described in later sections, voltage varies from 56 V at minimum power to 34 V at maximum power (5.6 kW). Current varies from zero to a maximum of 163 A over this range.

Most electric scooter motors surveyed use DC motors, the majority brushless rather than brushed (see Appendix A). For the reason of good DC efficiency and the lack of need for an AC inverter,

this is the type chosen here. Two systems are examined: a New Generation Motors (NGM) hub motor, and a Unique Mobility (UQM) axial gap DC brushless motor.

Table 2.2 Motor specifications: UQM brushless and NGM hub motors

spec	UQM motor	NGM motor
Model	SR121/1.5 L	SC-M150-04
Maximum power output	3.6 kW	2.5 kW
Peak torque (geared)	115 N•m at 2000 rpm	105 N•m at up to 300 rpm
Speed	0-800 rpm	0-1300 rpm
Controller voltage	40-60 VDC	30-68 VDC
Maximum controller current	95 A	260 A
Efficiency	up to 87%	up to 95%
Motor cost	$250 (estimated)	$7,000 (retail)
Motor diameter	20 cm	31.5 cm
Motor volume	5.0 L	unk.
Motor weight	11.4 kg	20 kg
Controller volume	4.1 L	7 L
Controller weight	4.1 kg	5 kg
Controller cost	$300 (projected)	$3,000 (current)

The Unique Mobility SR121/1.5L brushless, permanent magnet design has a maximum output of 3.56 kW. The CD 05-100A controller system includes a battery charger that can rectify AC voltage to battery charging voltage and allows regeneration. A final gearing ratio of 7.24 increases torque and reduces speed.[12] Current prices(May 1999) were estimated by Unique Mobility representatives at $250 for the motor plus $300 for the controller if the motor were to be mass produced immediately.[13] In comparison, a Lynch Motors brushed DC motor with 3 kW continuous output (6 kW peak output), weighing approximately 9 kg, has a retail price of $1,000, suggesting

that current prices are higher than Unique Mobility's estimates.

Hub motors offer higher efficiency, but can cost thousands of dollars due almost entirely to their relative newness and lack of development. For example, the New Generation Motors SC-M150-04 motor described above costs almost $7,000, plus $3,000 for the controller, and is used in solar cars - a very small market.[14]

The arrival of cheap electric bicycles run on hub motors and made in the People's Republic of China promise to reduce hub motor prices, though, and the New Generation Motors president stated a high-volume price target of $500 in the future for scooter-sized hub motors.[15] For now, the UQM motor was chosen due to the more established nature of its technology. Hub motors will play a greater role in the future for electric scooters. A 77% efficiency was chosen for the electric drivetrain system, consisting of the DC motor efficiency, fuel cell DC-to-DC conversion, and gear chain / transmission losses. This is at the low end of the motor map, and performance might in reality be slightly greater. The figure was based on previous research in electric vehicles.[16] The variation in efficiency over a DC motor "efficiency map" (plot of iso-efficiency contours on a torque/speed graph) is only 3% so a single value is justified.

The following curve gives an example of how maximum torque decreases as a function of speed; the space of possible torque/speed combinations lies under this curve. For the most part, the curve follows a hyperbola since the product of torque and angular speed is equal to a fixed maximum power. However, the torque is capped at low speeds by the maximum current the electric motor can handle.

Figure 2.2 Typical torque vs. rpm curve for DC motor

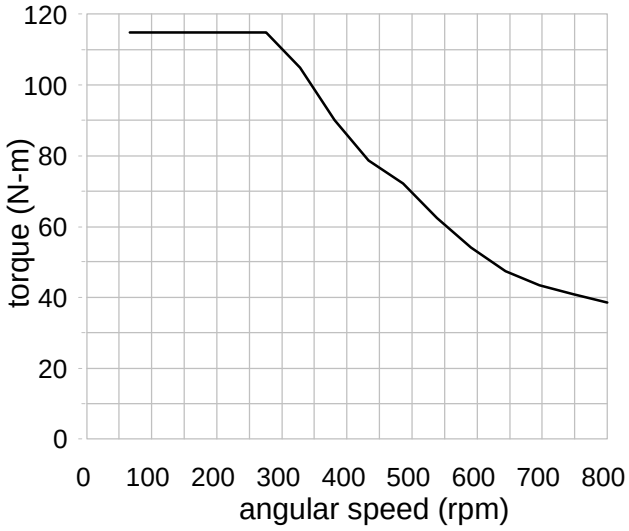

The data presented is from a Unique Mobility data sheet for the SR121/1.5 L brushless motor.[17]

2.2. Chemical batteries

Rechargeable chemical batteries are the traditional option for electric vehicles. They tend to be heavy and expensive to replace over their limited lifetimes. In this section, the theory behind battery operation is laid out with some discussion of various battery energy storage options for electric vehicles. A final section deals with the use of specialized high-power batteries to provide surge peaking power during moments of high energy demand, and thereby allow design with a smaller primary power source.

2.2.1. Theory

A battery pairs reduction and oxidation half-reactions to generate electricity. At the anode, one substance is oxidized. The electrons flow through the external circuit (power load) and arrive at the cathode, where a different substance is reduced. Electrochemical equilibrium is maintained by cations in the solution flowing across an ion bridge.

Batteries are divided into primary and secondary cells. Primary cells are those that are used once and cannot be restored by reversing the current flow, because the half-reactions are irreversible. Voltage decreases over time as the reactants are depleted and the concentrations decrease, and eventually the cell becomes useless and must be disposed of, ideally after the chemicals inside are recycled .

Secondary (sometimes termed “storage”) batteries can recover the original reactants by reversing the current flow. For example, in the common lead-acid secondary battery, the following half-reactions take place: at the anode, lead metal is oxidized to lead sulfate ($PbSO_4$); at the cathode, lead oxide (PbO_2) is reduced to $PbSO_4$. The electrolyte is a sulfuric acid (H_2SO_4) solution.

$$\text{oxidation: } Pb_{(s)} + SO_4^{2-}{}_{(aq)} \rightleftharpoons PbSO_{4\,(s)} + 2\,e^-$$

$$\text{reduction: } PbO_2 + SO_4^{2-}{}_{(aq)} + 2\,e^- + 4\,H^+ \rightleftharpoons PbSO_{4\,(s)} + 2\,H_2O$$

The overall reaction is:

$$Pb_{(s)} + PbO_{2(s)} + 4\,H^+_{(aq)} + 2\,SO_4^{2-}{}_{(aq)} \rightleftharpoons 2\,PbSO_{4(s)} + 2\,H_2O$$

The reversible electrochemical potential E_r^o in this case is approximately 2.04 V, and driving the cell in reverse (i.e. as an electrolytic reaction) regenerates the lead metal and lead oxide. However, there is a ceiling to the number of times any battery can be "cycled" in this way: when recharged the metals tend to precipitate in low-energy configurations like metallic needles or dendrites that eventually grow close to each other, and internal short circuits make the battery useless. After this point, reprocessing is needed if the chemicals inside are to be reused. This accounts for the limited lifetime of rechargeable batteries.

2.2.2. Technology

2.2.2.1 Existing scooter battery systems

As an example of current electric vehicle battery technology, the prototype Taiwan ZES-2000 battery-powered electric scooter developed by ITRI runs on a 24 VDC power system with two configurations: sealed lead-acid batteries, or the more advanced nickel metal-hydride (NiMH) batteries. Each configuration is designed to store the same amount of energy, but the more expensive NiMH batteries do so in about 60% of the lead-acid batteries' weight.

Table 2.3 ZES-2000 electric scooter performance

	sealed lead-acid	**nickel metal-hydride**
Total stored energy (output)	1.34 kWh	1.34 kWh
Total weight	44.0 kg	26.1 kg
Total volume	14.5 L	12.8 L
Specific energy density (Wh/kg)	31	51
Volumetric energy density (Wh/L)	92	105
Range at 30 km/hr	65 km	78 km
Range under ECE 40 driving cycle	35 km	46 km

Data from the ITRI ZES 2000 project[18]

The NiMH batteries a much smaller package but, as discussed in more detail later, are very expensive: $900 or more. Due to the lower weight of the NiMH vehicle, it uses less energy in driving and obtains higher fuel economy. This accounts for the improved range for the same energy storage.

Note that current battery specific energy is very low; to compare, gasoline has an energy density on the order of 920 Wh/L (although conversion to propulsion energy is on the order of 15%, more than five times worse than the round-trip efficiency of battery-powered scooters at about 80%).

2.2.2.2. Technology predictions

The United States Advanced Battery Consortium (USABC) was formed by Chrysler, Ford, and GM in 1991 to accelerate development of electric vehicle batteries. In 1992, goals were set for "mid-term" and "long-term" battery performance. The table of goals is reproduced below.

Table 2.4 Battery goals for various time frames

	1992 lead-acid	Mid-term prediction	Long-term prediction
Specific power (W/kg) 80% DoD, 30 seconds	67-138	150	400
Energy density (Wh/L) C/3 discharge rate	50-82	135	300
Specific energy (Wh/kg) C/3 discharge rate	18-56	80	200
Life (years)	2-3	5	10
Cycle life at 80% DoD	450-1000	600	1000
mass-produced target cost ($/kWh) set by USABC	$70- $100	<$150	<$100

Data is from the *Transportation Energy Data Book: Edition 12* and Hunt (1998).[19,20]

"DoD" stands for depth of discharge, and the nomenclature "C/3" means a discharge rate where the entire battery is expended in three hours. Due to the nonlinear nature of battery capacity, the total energy available is a function of how quickly the battery is discharged; the faster power is drawn, the less total energy is available.

In addition to traditional batteries like lead-acid, nickel metal-hydride and nickel-cadmium (NiCd), there are advanced technologies like lithium-polymer and lithium-ion. Despite the explosion in popularity of notebook computers and their rapid progress from nickel-cadmium batteries to nickel-metal hydride batteries to lithium-ion batteries, electric vehicle battery technology has not kept pace. Most practical electric battery automobiles still use lead-acid batteries, with the more sophisticated using NiMH batteries. The faster adoption of battery technology in notebook computers is due partly to their small size and energy requirements, and the fact that consumers are willing to pay significantly more for improved technology.[21] However, a telling point about how electric vehicle battery technology has not progressed is revealed in USABC's definitions of "mid-

term" and "long-term": the mid-term was originally defined as 1994, and the long-term goals had a target date of 1995 [19], but by 1998 the mid-term was redefined as "1995-1998" and the long term goals were not fixed to a date, but rather defined in terms of performance: "competitive with today's internal combustion vehicles"[22].

Some of the different types of chemical battery are listed in the sections below.

2.2.2.3 Lead-acid batteries

Lead-acid batteries have been used for a century due to their high power density, reliability, and ability to satisfy widely varying loads. However, their energy densities are far too poor to act as "storage" batteries for electric vehicles; to store enough energy for decent range requires a massive battery bank. On the other hand, lead-acid batteries specifically designed to provide repeated burst of high power have proven to be useful peaking power devices. Novel spiral-wound designs offer specific powers of over 500 W/kg, at the cost of compromised specific *energy*.[23]

Lead-acid batteries are often classified as either "flooded" or "sealed". In flooded (also "wet") batteries, measuring the density of the liquid offers a method of measuring the state of charge of the battery since as the reaction proceeds, $PbSO_4$ precipitates out and the density of the electrolyte decreases. Note that electrolysis of water can be a side reaction in a lead-acid battery, so hydrogen and oxygen must be vented (electrolysis is favoured when the battery is overcharged). Water vapour also escapes, so that water needs to be occasionally replaced.

Sealed (sometimes called "VRLA", valve-regulated lead-acid) batteries have the electrolyte in a gel

rather than liquid form, and valves that release gas only when pressure is too high; otherwise, the battery remains sealed and oxygen is transferred through the gel membrane to the hydrogen side and allowed to recombine with hydrogen into water before levels become high enough to be dangerous.

Lead-acid storage batteries currently cost approximately $60-$80 per kWh retail.[24]

2.2.2.4 NiMH and NiCd batteries

Nickel metal-hydride is currently the advanced technology of choice for electric vehicles, including both automobiles and scooters. Existing Ovonic NiMH batteries for electric vehicles have superior energy and power densities, on the order of 70 Wh/kg, 170 Wh/L, 200 W/kg, and 485 W/L. This is better than USABC's mid-term projections.

However, the predicted "ultimate" commercialized cost is $200-$250/kWh.[25] For 4.1 kWh of storage (the amount of energy needed to drive a 130 kg scooter approximately 200 km at 30 km/h, as discussed later in Chapter 4), this is $820 – $1025 for the batteries alone. This matches the results of a 1998 paper, which estimated that the cost of a NiMH battery for electric scooters "rivals the cost of the entire IC (internal combustion) motorcycle"[26].

NiCd batteries offer fairly high power density for peaking power applications, up to 300 to 660 W/kg possible, but may fall out of favour in the United States due to the toxicity of the cadmium they contain. For peaking power, specially designed lead-acid batteries serve just as well.

2.2.2.5 Lithium variants

Li-ion batteries, like those currently used in notebook computers, transfer Li^+ ions from the anode to cathode through an electrolyte, with "insertion compounds" accepting the cations without significant structural change. This lengthens overall lifetime.

The more recent Li-polymer batteries use a metallic lithium anode, polymer electrolyte, a cathode, and a current collector in a flat sandwich. Although predicted energy densities are on the order of 200 Wh/kg, and the system is theoretically cheap to manufacture, there are drawbacks: metallic lithium tends to experience dendritic growth that reduces charge transfer, and the battery must operate at 70°C.[27]

The high cost of lithium batteries has prevented their use in electric vehicles. Only the Nissan Altra electric vehicle has demonstrated lithium-ion technology in that application.[28]

2.2.2.6. Zinc-air "regenerative" batteries

The zinc-air battery is an interesting primary battery alternative that offers high energy density - up to 200 Wh/kg, four times the specific energy of lead-acid batteries. The paired reduction and oxidation half-reactions are listed below.

anode reactions:

$$2\ Zn + 8\ OH^- \rightarrow 2\ Zn(OH)_4^{2-} + 4\ e^-$$

$$2\ Zn(OH)_4^{2-} \rightarrow 2\ ZnO + 4\ OH^- + 2\ H_2O$$

net anode half-reaction (oxidation):

$$2\ Zn + 4\ OH^- \rightarrow 2\ ZnO + 2\ H_2O + 4\ e^-$$

cathode half-reaction (reduction)

$$O_2 + 2\ H_2O + 4\ e^- \rightarrow 4\ OH^-$$

The overall reaction is thus the oxidation of zinc metal to zinc oxide:

$$2\ Zn + O_2 \rightarrow 2\ ZnO$$

$$(\Delta G = 318.3\ kJ \bullet mol^{-1},\ \Delta H = -348.3\ kJ \bullet mol^{-1})$$

The theoretical voltage available from this reaction is $E_r^\circ = 1.65$ V but in practice, only 1.16 V are available at a C/5 rate (full discharge in five hours) due to kinetics, competing reactions, and other inefficiencies.[29] The quoted figure of 200 Wh/kg includes this inefficiency.

The system has the advantage of using oxygen as one of its reactants. Oxygen can be taken in from the ambient air, so the amount of mass in the battery is lessened and energy and power density are improved. (Of course, as the zinc oxide product accumulates, the total mass increases.) The “air electrode” cathode consists of a polymer-bonded carbon layer, humidified and loaded with electrocatalysts to reduce overpotential and make it easy for the oxygen atoms to adsorb, dissociate, and ionize to O^{2-} anions. In this way, it is much like a fuel cell cathode. It is necessary to keep the oxygen away from the anode to prevent direct oxidation of the zinc.[30] Also, the catalyst on the cathode can be poisoned by other species in the air.

The zinc-air battery is actually a primary battery, since it is not recharged electrically. However,

an interesting concept being developed by Electric Fuel, Ltd. of Jerusalem, Israel is that of "regenerative" zinc-air batteries, batteries that are replenished mechanically. These systems run on potassium hydroxide electrolyte, have zinc anodes, and catalyzed oxygen reduction electrodes. Although the specific power is relatively low at less than 90 W/kg, the specific energy of the zinc-air battery is a very good 200 Wh/kg, and the company predicts a price of $80/kWh after full mass production.[31,32] (Zinc recovery and regeneration costs do not appear to be included in this sum.)

The batteries are not recharged by reversing the reaction to restore the initial reactant zinc. Rather, the anode (now mainly converted to zinc oxide) is physically removed and replaced with a fresh zinc anode assembly. The spent anode is returned to a factory for chemical reprocessing – the zinc oxide is reacted with KOH, and the resulting potassium zincate is electrolyzed to restore the original zinc. In some sense these are fuel cells since the system is recharged by replacing reactants, rather than by reversing electric flow. The lifetime of the system is thus not restricted by changes in anode morphology, but by cathode poisoning and contamination. The zinc oxide dissolving process is:

$$ZnO_{(s)} + 2\ KOH_{(aq)} + H_2O_{(l)} \rightarrow K_2Zn(OH)_{4\ (aq)}$$

The electrolytic metal recovery process ("electrowinning") for zinc electrode reprocessing follows:

$$K_2Zn(OH)_{4\ (aq)} \rightarrow Zn + 2\ KOH_{(aq)} + H_2O_{(l)} + \tfrac{1}{2}\ O_{2\ (g)}$$

The voltage of this reaction is 2.2 V if electrocatalysts are used to reduce oxygen evolution overpotential. Considering only electrowinning losses, the maximum possible round-trip efficiency from power plant electricity to battery output electricity is (1.16 V / 2.2 V) = 52.7%. Additional energy is needed to reprocess the zinc and to complete the potassium zincate process and this could

be not only energy-intensive but expensive as well.[31] The technical performance of the battery is good, but the difficulties and costs in exchanging and regenerating the anodes are not well known at this time.[33]

Note that the zinc-air batteries have a self-discharge rate of 1-2% per week.[34]

As alluded to earlier, there is a second replacement cost. Since this is an alkaline electrolyte system, carbon dioxide in the air forms carbonates that accumulates in the potassium hydroxide solution and the air cathode. After 10-30 replacements of the anode (in this application, after about one and a half to four months of travel), the entire battery must be replaced or remanufactured for this reason.[35] On a per-km basis, this could be three times the electricity cost of electrowinning the zinc; as well, beyond the cost of the electricity are the infrastructure costs for stations to process the zinc "fuel" and to remanufacture the batteries.[36]

2.2.2.7 Summary

Ordinary rechargeable batteries are currently a practical technology, and may be adequate for limited-use scooters and "neighbourhood vehicles," but energy densities are far from good enough to compare with current low-end scooters. On the other hand, regenerative zinc-air batteries offer high energy density - six times those of current lead-acid batteries used in the ZES-2000. Power density is not very high, though, and to design a zinc-air battery with the maximum driving cycle *power* as the target would be to create a very heavy battery with an overdesigned range, since power and energy are inextricably bound in a battery-powered system.

One way of decoupling power from energy is to use a hybrid system, with a high-energy battery providing the energy, and a high-power battery supplying extra power for peaking purposes. This is discussed in the next section.

2.2.3 Peaking power and batteries for hybrids

One concept proposed for automobiles is the "hybrid" vehicle. This type of design combines a reduced-size main power source (combustion engine, fuel cell, or even a storage battery) with a peaking power device (flywheel, ultracapacitor, battery). The peaking power device kicks in in moments of high power need to supplement the output of the main power source, and is recharge during periods of low overall power demand.

This allows the main power source to be sized smaller, saving money if it is expensive (fuel cell), saving weight if it is particularly heavy (battery). A hybrid in conjunction with a small combustion engine allows the engine to run at a fixed, well-tuned constant power output for greater efficiency and lower emissions. Transients in all three cases are completely or partially handled by the peaking power device. The important qualities required for the peaking power device: high power density, not necessarily high energy density, and the ability to respond quickly to transients.

A detailed discussion of different hybridization policies, and modeling of various fuel cell hybrid options, is deferred to section 4.7. However, some peaking power options are discussed in this section because the most promising are high-power batteries.

Flywheels offer high power density but low energy density. They have the advantages of long

lifetime, linear behaviour, and high round-trip efficiency. On the other hand, they can be perceived as unsafe (although they are not as dangerous as some claim), are expensive, and unless designed carefully produce gyroscopic forces that can be serious in a vehicle as light as a scooter.

High-density capacitors ("ultracapacitors" or "supercapacitors") like those used in the Mazda Demio fuel cell vehicle can supply a great deal of power for many cycles. The energy stored can be measured in a linear fashion, unlike batteries, and power densities can be as high as 4.2 kW/kg for a very brief surge, or 560 W/kg for a six second discharge.[37] Energy densities are low, on the order of 5-10 Wh/kg,[38] but this is not a significant concern for the irregularly peaked scooter driving pattern. They are currently too expensive for practical use, at hundreds to thousands of dollars per kilowatt, but in a few years could offer an ideal alternative to peaking batteries.

A high-power battery like the Bolder Technologies advanced lead-acid offers high power density at relatively low cost. Bolder cells are used in the Chrysler Intrepid ESX series hybrid vehicle. However, with all batteries, chemical changes limit the number of cycles before the battery must be replaced, and current/voltage behaviour is extremely nonlinear, making it difficult to make sure that the battery lifetime is not shortened by overcharging or overdischarging. The power density of this type of high-power lead-acid cell is dependent on discharge rate, and is estimated at about 500-900 W/kg[39]. Cost is much more difficult to estimate, with most data being for storage batteries and not peaking power.

Current PNGV research is focused on batteries, and that group recently dropped research into ultracapacitors and flywheels for reasons of low energy density and safety, respectively.[40]

Thus, a high-power lead-acid battery is selected for the peaking power unit here. The peaking power unit is modeled as a scaled up version of current Bolder "Rebel" thin metal film battery packs, with six cells and a total output of 12 V and capacity of 1 Ah (600 W over 43 seconds). Power density is an impressive 840 W/kg. At an estimated cost of under $100 per pack for volume ordering, this is $167/kW which is halved to $83/kW for pre-installed cost in the scooter.[41]

2.2.3.1. Peaking battery modeling

The Bolder lead-acid battery studied here has the following properties.

Table 2.5 Peaking power battery characteristics

Retail cost based on today's "Rebel" pack	$167/kW
Power density at 43 second discharge	836 W/kg
Energy density by weight	17 Wh/kg
Density	1.02 kg/L
Power density by volume	853 W/L
Energy density by volume	17 Wh/L
Voltage per cell	2.0 V
Capacity per cell	1 Ah
Lifetime for full-discharge and recharge	400 cycles

Data is from a Bolder product sheet for the "Rebel" battery pack

These figures are close to the 1.2 kW/L, 1.2 kW/kg, 59 Wh/kg and 57 Wh/L reported for the 100 kW Bolder peaking power battery used in the Chrysler Intrepid ESX series hybrid (note that the discharge time for the Intrepid performance statistics was not given).[42]

Batteries designed specifically for peaking power (unlike the "Rebel") should sustain many more cycles than the 600 or so for lead acid batteries used for base power, due to the shallower discharge patterns. (Base power batteries are almost fully depleted and recharged to the maximum each cycle). Peaking power batteries might last for 3-5 years, although lifetimes are highly dependent on usage patterns.

The battery is modeled in terms of its state of charge (fraction of total energy capacity), based on an empirical model developed by Tom Kreutz at the Center for Energy and Environmental Studies at Princeton University.[43] Specifically, voltage and internal resistance at any time are a function of the state of charge, while the total cell output is a function of the voltage, internal resistance, and current. The cells in the battery are connected in series. Voltages are in volts and resistances in milliohms.

$$V_{cell} = V_o\,(SOC) + IR\,(SOC)$$

$$V_o(SOC) = 1.88 + 0.375\ SOC - 0.176\ SOC^2$$

$$R(SOC) = 2.09 - 1.28\ SOC + 1.07\ SOC^2 \text{ if } SOC < 0.4$$

$$R(SOC) = 1.75 \text{ if } SOC > 0.4$$

So the voltage output is a function of the state of charge, as is the internal resistance, as illustrated graphically:

Figure 2.3 Voltage and internal resistance of Bolder peaking battery

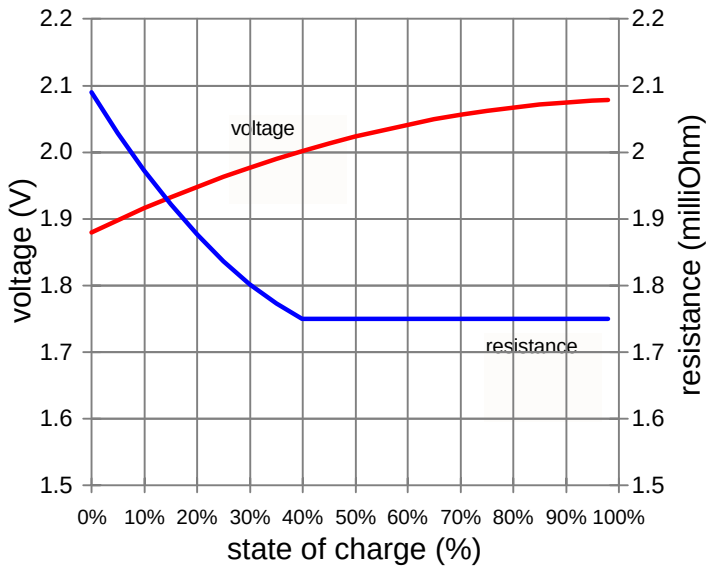

2.2.3.2. Charge and discharge

Assume that a certain power $P_{kinetic}$ is available to recover from the wheels from a calculation of *mav*. 30% of this energy is simply unavailable, as reported by an NREL paper, due to frictional and other losses.[44] For the generation of electricity from this kinetic energy by driving the electric motor in reverse, a 77% efficiency is assumed - approximately the same as the efficiency of driving the motor in a forward direction.

A final efficiency factor is incurred by the charging of the battery, and is calculated as $(\sqrt{\eta}_{coloumbic})V_o/V_{cell}$. The coulombic efficiency is 95%. The result is an efficiency of 90-95%, comparable to PNGV goals and data for current lithium-ion batteries.[45] So at any point, the power of charging is calculated, and I is solved such that the power into the battery, as given

below, is reached

$$P_{charge} = N_{cells} \bullet V_{cell} \bullet I$$

After charging inefficiency, the actual energy entering the battery is $\sqrt{\eta_{coloumbic}} \bullet N \bullet V_o \bullet I$. The battery can only charge at a given maximum rate that is a function of the state of charge; the rate is higher when the battery is near empty. This maximum current limits the amount of energy that can be recovered during periods of heavy braking, and is given by:

$$I_{max} = I_o (SOC^{-\alpha} - 1)$$

$I_o = 0.979$ A, and $\alpha = 4.44$, fitting parameters to experimentally-observed curves.[46]. Even if the braking "power" needed is greater than the battery's ability to accept power, braking can still be effected by dissipating the surplus power through resistors (as in dynamic braking for diesel-electric or pure-electric locomotives). An ordinary set of brakes may be used at low speeds where generator-type braking is weak.

The discharge rate for the Bolder cell is 80 A over extended (20-second) periods.[47] With a maximum voltage of approximately 2 V per cell, this is 160 W per cell. Higher powers, up to 1000 A, are possible for short-circuit discharge; in this model, a maximum of 250 W per cell is set.

2.2.3.3 Hybrid battery conclusion

Detailed modeling will describe more precisely how many of the above cells will be needed, and how the power supplied will be divided between the peaking power and base power batteries. The

combined fuel cell and hydrogen storage systems, both of which are discussed in the next chapter, have to beat not only four-stroke technology and current batteries, but future hybrid battery systems as well.

References for Chapter 2

1. She Lung Electric Engineering Company. “Scooter Engine Series” http://www.she-lung.com.tw/p2.htm. Accessed May 12, 1999.

2. Yuasa, Inc. “Battery Search: Maintenance Free (GRT) 12 Volt” http://www.yuasabatteries.com/grt.asp?BatteryFamily=GRT Accessed May 20, 1999

3. L. E. Unnewehr, S. A. Nasar. *Electric Vehicle Technology*. (John Wiley & Sons, Inc, New York: 1982). p. 168

4. Unnewehr and Nasar, p. 126

5. Margaret M. Steinbugler, Princeton University. “Electric Drive Systems for Electric Vehicles”. Unpublished draft. August 6, 1998.

6. Unnewehr and Nasar. pp. 129-130.

7. Steinbugler

8. Steinbugler

9. J. R. Hendershot Jr. and T. J. E. Miller. “Design of Brushless Permanent-Magnet Motors” (Magna Physics Publishing and Clarendon Press, Oxford: 1994), p. 2-11

10. Daniel Sperling. *Future Drive: Electric Vehicles and Sustainable Transportation*. (Island Press, Washington, DC: 1995) p. 47

11. Ling-Yuan Tseng, I-Ho Li. “Hub motor development of electric vehicles”. Presented at EVS-15 at Brussels, Belgium, October 1998.

12. Unique Mobility, Inc. Product data sheet. *Brushless PM Motor/Controller SR121/1.5L and CD05-100A* Received May 7, 1999

13. Jeffrey Ho. Deputy Manager, Taiwan UQM. Personal communication, May 24 1999

14. New Generation Motors Corporation. “Announcement for Sunrayce ‘99 Teams” http://www.ngmcorp.com/docs/solarcar.pdf. Accessed April 26 1999

15. Nabih Bedewi, New Generation Motors president. Personal communication, August 12 1999.

16. Joan M. Ogden, Margaret M. Steinbugler, Thomas G. Kreutz. “A comparison of hydrogen, methanol and gasoline as fuels for fuel cell vehicles: implications for vehicle design and infrastructure development.” *Journal of Power Sources* **79** (Elsevier: 1999) pp. 143-168

17. Unique Mobility, Inc. Product data sheet. *Brushless PM Motor/Controller SR121/1.5L and CD05-100A*

18. Jet P. H. Shu, Wei-Li Chiang, Bing-Ming Lin, Ming-Chou Cheng. Mechanical Industry Research Laboratories, Industrial Technology Research Institute. “The Development of the Electric Propulsion System for the ZES2000 in Taiwan” Internal paper

19. Stacy C. David and M.D. Morris. “Transportation Energy Data Book: Edition 12" ORNL-6710 (Oak Ridge National Laboratory: 1992), p. 5-6. Referenced in James J. MacKenzie, “The Keys To The Car” pp. 44-45.

20. Gary L. Hunt. Idaho National Engineering and Environmental Laboratory. “The great battery search”. *IEEE Spectrum.* **35** (11) November 1998. p.24

21. Laptop batteries last about two hours and provide power at about 15 W, depending on the performance of the computer. The energy stored in a battery costing $100-$300 is thus 30 Wh: a very high cost per watt-hour.

22. Stacy C. David and Philip D. Patterson. “Transportation Energy Data Book: Edition 17", ORNL-6919, (Oak Ridge National Laboratory: 1998), Table 5-8

23. Gary L. Hunt., p. 23

24. Suntrek Alternative Energy Systems. “Lead Acid Batterys [sic]” http://www.suntrekenergy.com/leadacid.htm Accessed August 1, 1999

25. S. K. Dhar, S. R. Ovshinsky, P. R. Gifford, D. A. Corrigan, M. A. Fetcenko, S. Venkatesan, “Nickel/metal hydride technology for consumer and electric vehicle batteries – a review and up-date” *Journal of Power Sources* **65** (1997) p. 1

26. Jenn-Shing Chen, L. F. Wang. “Effect of curing on positive-plate behaviour in electric scooter lead/acid cells” *J. Power Sources* **70** (1998) p. 269

27. Gary L. Hunt, p. 24

28. Electric Power Research Institute. “Nissan Altra EV” http://www.epri.com/csg/trans/evrn/nissan.html. Accessed May 28, 1999

29. Yehuda Harats, Binyamin Koretz, Jonathan R Goldstein, Menachem Korall. Electric Fuel. "The Electric Fuel System Solution for an Electric Vehicle" presented at "Batterien und Batteriemanagement" Conference Essen, Germany, February 22-23, 1995

30. Encyclopædia Britannica Online. "Battery" http://www.eb.com:180/bol/topic?eu=108543&sctn=6> Accessed March 1999.

31. Jonathan R. Goldstein, Ina Getkin, Binyamin Koretz. Electric Fuel Ltd. "Electric Fuel™ Zinc-Air Battery Regeneration Technology" presented at 1995 Annual Meeting of the Applied Electrochemistry Division of the German Chemical Society at Duisburg, Germany. September 27-29, 1995. http://www.electric-fuel.com/techno/duisburg.doc

32. Jonathan Goldstein, Ian Brown, Binyamin Koretz. "New developments in the Electric Fuel Ltd. zinc / air system" *Journal of Power Sources* **80** (1999) pp. 171-179

33. Michael J. Riezenman and Willie D. Jones."EV watch". IEEE Spectrum, June 1998.

34. Jonathan R. Goldstein, Ina Getkin, Binyamin Koretz. Electric Fuel Ltd. "Electric Fuel™ Zinc-Air Battery Regeneration Technology" presented at 1995 Annual Meeting of the Applied Electrochemistry Division of the German Chemical Society at Duisburg, Germany. September 27-29, 1995. http://www.electric-fuel.com/techno/duisburg.doc

35. chemTEK representative, personal communication August 18 1999.

36. China Steel Corporation study for chemTEK. Received August 21, 1999 from chemTEK.

37. Maxwell Technologies. "Energy Products: PowerCache Ultracapacitors" at http://www.powercache.com/products/product_main.html Accessed May 27, 1999

38. National Renewable Energy Laboratory. "Hybrid Electric Vehicle Program - Ultracapacitors". http://hevdev.nrel.gov/components/ultra.html. Accessed May 27, 1999

39. Thomas G. Kreutz, Margaret M. Steinbugler, Joan M. Ogden, Sivan Kartha. Center for Energy and Environmental Studies, Princeton University. "System Modeling of Fuel Cell Hybrid Electric Vehicles with Onboard Fuel Reformers" 1998. Unpublished paper.

40. National Research Council. Review of the Research Program of the Partnership for a New Generation of Vehicles. Fifth Report. (National Academy Press, Washington DC: 1999) p. 36

41. Walter Woodley, Engineering Assemblies Corporation. Personal communication, June 8 1999

42. Chrysler web site. "ESX/Hybrid Technology Release Material" http://www.media.chrysler.com/wwwprkt/23a6.htm Accessed June 30, 1999

43. Kreutz, Steinbugler, Ogden, Kartha.

44. Keith Wipke, Matt Cuddy, David Rausen. Center for Transportation Technologies and Systems, National Renewable Energy Laboratory. "Using Systems Modeling to Facilitate the PNGV Technology Selection Process" Presentation October 28, 1997 to 1997 Automotive Technology Development Customers' Coordination Meeting

45. National Research Council, p. 37

46. Kreutz, Steinbugler, Ogden, Kartha.

47. Bolder Technologies Corporation data sheet, "Power Full Solutions"

~

Chapter Three

The hydrogen fuel cell power system

~

This chapter discusses two major issues: (i) fuel cell theory and engineering, and (ii) providing fuel for the fuel cell.

The first section thoroughly discusses the science behind fuel cells in general. Of the different kinds of fuel cells, the proton exchange membrane type is identified as the unquestioned best candidate for the small vehicle application. Engineering issues like how to cool the fuel cell stack and whether to pressurize the fuel cell are discussed in general terms and the feasibility of certain design options is determined. (On the other hand, more complete, quantitative analyses of cooling and pressurization require more detailed information about steady-state and transient power requirements that are not calculated until Chapter 4, and are thus properly analyzed within that chapter). The size and weight of the fuel cell are discussed with reference to previous researchers' results.

The second half of this chapter concerns fueling of hydrogen fuel cells, which is considerably more complex than filling a tank with gasoline. It explains why reformed fossil fuels cannot yet be used to power a fuel cell vehicle, and describes various options for storing pure hydrogen on board the vehicle. The issue of safety is discussed.

3.1. Fuel Cell Science

3.1.1. Fundamentals

Fuel cells are electrochemical engines that produce electricity from paired oxidation / reduction reactions. One can think of them as batteries with flows of reactants in and products out. In contrast, the battery has a fixed supply of reactants that transform into products without being steadily replaced. The distinction is a nice one as zinc-air “batteries” have replaceable zinc electrodes, making them very like fuel cells.

A standard high school chemistry demonstration involves passing an electric current from a battery through a jar of water (with dissolved salts) by way of two metal electrodes suspended in the water. Hydrogen evolves at the cathode and oxygen at the anode as the water is broken into its constituent elements by electrolysis. Essentially, a fuel cell uses the reverse process: hydrogen and oxygen are combined to form water, and electricity is produced.

Technically, the two chemicals do not have to be hydrogen and oxygen; the redox reaction requires only a reducer and an oxidizer, but since oxygen is easy to obtain from the air and hydrogen has suitably fast reaction kinetics, these are the two most often chosen. All further examples will use hydrogen and oxygen unless otherwise noted.

Specifically, the hydrogen and oxygen diffuse into their respective electrodes, ionize, and one type of ion migrates through an electrolyte and recombines at the other side with the other ion to form water. At any given temperature there is an equilibrium ratio of ions to molecules. Coatings of

noble metal catalyst on the electrodes lower the activation energy of the ionization / recombination process, accelerating the restoration of equilibrium as the ions are consumed by the fuel cell.

The principle behind fuel cells was discovered as early as 1839 by Welsh physicist and judge Sir William Grove. However, due to high costs, the technology was not significantly used until the American Gemini space missions of the 1960's. For this and subsequent space missions, fuel cells were thought to be safer than nuclear electric generation and cheaper than solar. They have been thrust to the forefront of energy technology in the 1990's, however, as high power densities have made them feasible for both stationary and portable applications. ONSI corporation, a subsidiary of United Technologies, has produced over 170 of its PC25 stationary 200 kW fuel cell systems since their introduction in 1992.

Fuel cells have the advantages of high efficiency, low or even zero pollution, quiet operation, and fewer moving parts – only pumps and fans to circulate coolant and reactant gases, respectively – for greater reliability than internal combustion engines (once fuel cell systems are well-developed).

3.1.1.1 Thermodynamics

An electrolyte physically separates the two reactants and also prevents electronic conduction, while allowing ions to pass through; the electrons travel through an external loop to supply the load. Electrodes are attached to either side of the electrolyte. At the anode, the hydrogen is oxidized:

$$H_{2\,(g)} \rightarrow 2\,H^{+} + 2\,e^{-}$$

The electrons pass through the load to provide the desired current and end up at the cathode, where the matching reduction reaction occurs:

$$2\ e^- + \tfrac{1}{2}\ O_{2\,(g)} \rightarrow O^{2-}$$

Electrostatic balance is reached as the hydrogen ions diffuse through the electrolyte to get to the cathode:

$$2\ H^+ + O^{2-} \rightarrow H_2O_{\,(l)}$$

Figure 3.1 Fuel cell schematic

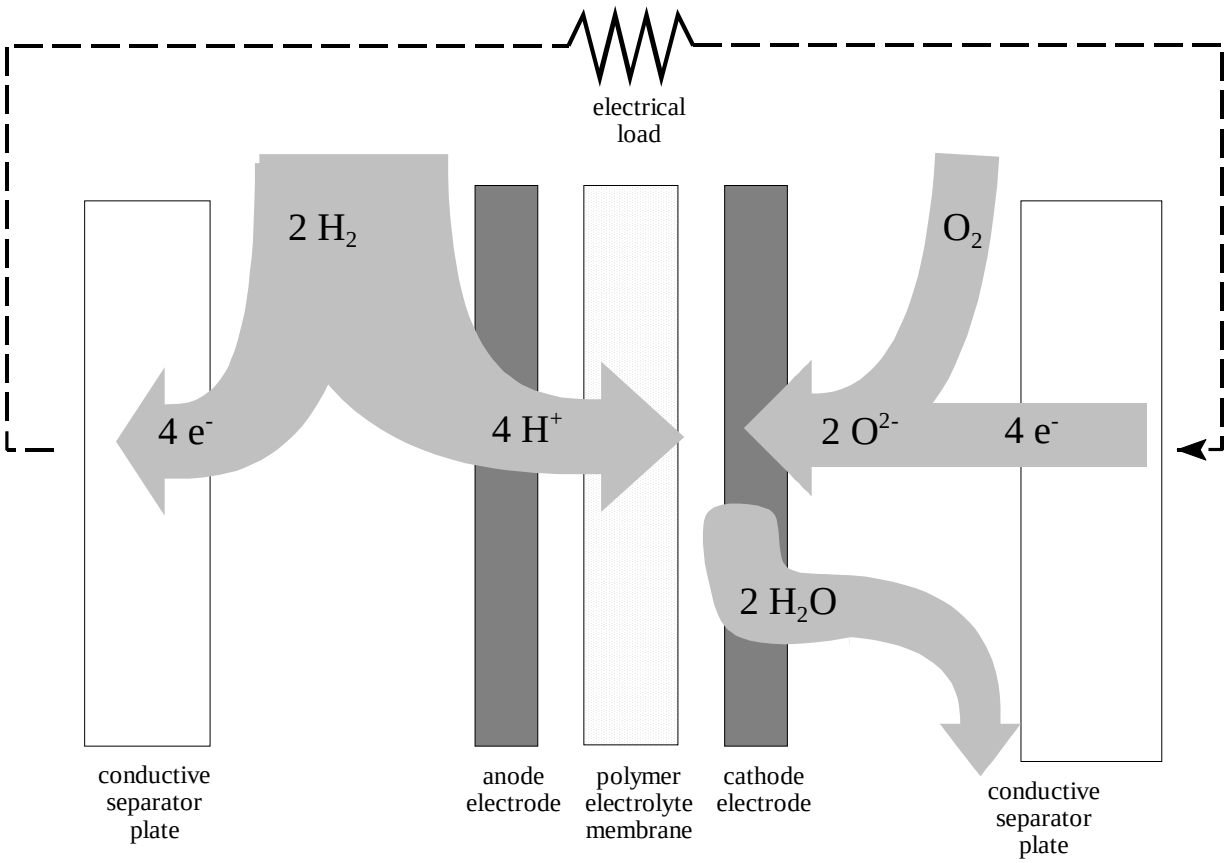

The theoretical energy release of the overall reaction is determined by the enthalpy change ΔH in the overall (isothermal) reaction,

$$H_{2\,(g)} + \tfrac{1}{2}\, O_{2\,(g)} \rightarrow H_2O_{\,(l)}$$

$$(\Delta H^\circ = -285.8 \text{ kJ/mol}; \Delta G^\circ = -237.2 \text{ kJ/mol};)$$

ΔG is the Gibbs free energy and standard conditions, as indicated by the nought superscript, are T=25°C, partial pressures of 1 atm for each of the gases, and water in the liquid state. This last distinction is important. For high temperature fuel cells, water emerges in the gaseous state, so the "lower heating value" would be used. In this (non-standard) case, ΔH = -241.8 kJ/mol and ΔG = -228.6 kJ/mol. The higher heating value is used in the remaining calculations since most fuel cells operate below the boiling point of water.

The next step is to determine fuel cell efficiency.

$$\Delta G^\circ = \Delta H^\circ - T\Delta S^\circ$$

so the standard change in entropy is -0.163 kJ • mol^{-1} • K^{-1}. An energy balance on a fuel cell shows that

$$d/dt\,(dQ + dW_{elec}) = d/dt\,(dH + dKE + d\,PE)$$

Kinetic energy (KE) and potential energy (PE) changes are assumed to be negligible, and steady state operation is assumed. A "perfect" fuel cell operating irreversibly means dQ = T dS. Thus, W_{elec}, the electrical power output, is

$$W_{elec} = \Delta H - T\Delta S = \Delta G$$

Efficiency at any given point is usually defined here by dividing the maximum work out by the enthalpy input, so fuel cell efficiency is:

$$\eta_{FC} = \Delta G / \Delta H$$

Using the standard free energy and enthalpy given previously (ΔG° = -237.2 kJ/mol, ΔH° = -285.8 kJ/mol) shows the maximum thermodynamic efficiency under standard conditions is 83%. The change in standard free energy can be used to calculate the maximum reversible voltage provided by the cell:

$$\Delta G^\circ = -nFE_r^\circ$$

where n is the number of electrons in the reaction as written, F is Faraday's constant (96,487 coulombs per mole of electrons), and E_r° is the *standard* reversible potential. Since n=2 here, E_r° = 1.229 V. This reversible potential changes with changing pressure as the Nernst equation:

$$E_r = E_r^o + \frac{RT}{nF}\ln\left(\frac{A_{H_2} A_{O_2}^{1/2}}{A_{H_2O}}\right)$$

Again, n=2, and the "A"s are the activities of the various species – the partial pressures for hydrogen and oxygen, and 1 for water since it is in the liquid form. (Activity measures the concentration relative to standard conditions, so for the gases this becomes the partial pressure relative to 1 atm, and for solutes it is relative to a 1-molality solution in solvent. Water *is* the solvent, so its activity is 1) The voltage increase derived from an increase in pressure by a factor λ (assuming that the hydrogen intake pressure is increased by the same factor as the oxygen intake), is given below.

$$\Delta E_r = \frac{RT}{nF} \ln\left(\frac{P^*_{H_2(2)} P^{*1/2}_{O_2(2)}}{P^*_{H_2(1)} P^{*1/2}_{O_2(1)}} \right) = \frac{RT}{nF} \ln \lambda^{1.5} = 1.5 \frac{RT}{nF} \ln \lambda$$

The "(2)" subscripts refer to the pressurized states of the reactant gases and the "(1)" to the unpressurized partial pressures. At 80°C and 2 moles of electrons in the reaction as written, the theoretical voltage change is 16 mV for a doubling of the intake pressures from the default 1 atm to 2 atm. For an increase in pressure to 300 kPa, a typical figure used for fuel cells, a voltage increase of 25 mV could be realized. However, as the next section on kinetics shows, the improvement ΔE_r is actually much larger.

(Some researchers have considered variable-pressure systems where greater compression is used when higher power is demanded. This produces higher efficiencies at high power, and lower parasitic compressor losses at low power. On the other hand, a constant-pressure fuel cell is cheaper and simpler to manufacture.)

The relationship between voltage and temperature is derived by taking the free energy, linearizing about the standard condition of 25°C, and assuming that the enthalpy change ΔH does not change with temperature:

$$E_r = -\frac{\Delta G}{nF} = -\frac{\Delta H - T\Delta S}{nF}$$

$$\Delta E_r = \left.\frac{dE_r}{dT}\right|_P \Delta T$$

$$\Delta E_r = \left.\frac{dE}{dT}\right|_P \left(T - 25^o C\right) = \frac{\Delta S}{nF}\left(T - 25^o C\right)$$

Because the change in entropy is negative, the open-circuit voltage output decreases with increasing temperature; the fuel cell is theoretically more efficient at low temperatures. However, other effects like mass transport and ionic conduction are faster at higher temperatures and this more than offsets the drop in open-circuit voltage.

In theory, the power generated by a single fuel cell is simply the reversible potential times the number of electrons generated per second (i.e. the current). The fuel cells are connected in a "stack" to multiply the power.

3.1.1.2 Kinetics

The cell potential, however, is also limited by the kinetics of the reaction. These losses are most often shown in what is known as a Tafel plot or polarization curve; cell potential in volts is graphed against the cell current density in amperes per square centimeter of cell area. The current density basically represents how fast the reaction is taking place (it is the number of electrons per second, divided by the surface area of the fuel cell electrolyte face); measured voltage divided by reversible voltage is equal to the efficiency defined previously. The power curve as a function of current (V*i versus i) shows a peak at high current density.

Figure 3.2 Tafel plot

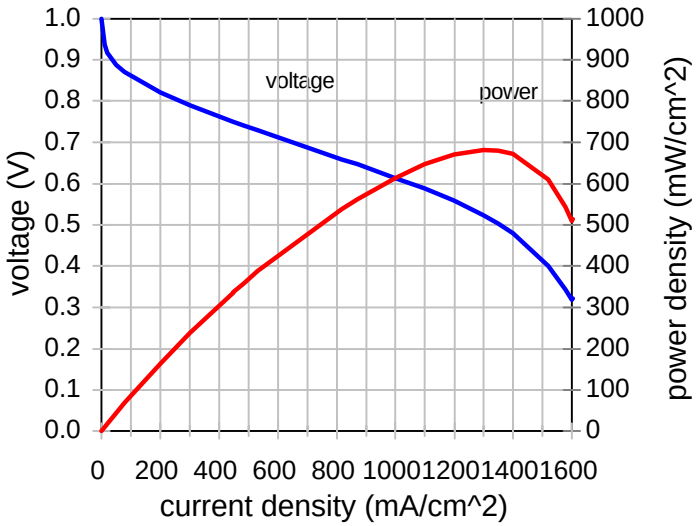

At non-zero current densities, there is what is known as an "activation overpotential": to drive the dissociation of the oxygen and hydrogen molecules quickly, a certain activation energy must be exceeded. Essentially, the oxygen and hydrogen molecules must diffuse in through pores in the metal catalyst and adsorb. This is a "three phase interface problem," since gaseous fuel, solid metal catalyst, and liquid electrolyte must all contact. The catalyst reduces the height of the activation barrier but a loss in voltage remains due to the still-slow oxygen reaction. (Note that the hydrogen activation overpotential is negligible compared to the oxygen overpotential; the oxygen reaction is five to six orders of magnitude slower.[1]) Also, competing reactions occur at the oxygen electrode: oxidation of the platinum, corrosion of carbon support, and oxidation of organic impurities on the electrode. The total overpotential is 0.1 to 0.2 V, reducing the maximum potential to less than 1.0 V even under open-circuit conditions.[2]

There is also a continuous drop in voltage as current increases, and this is due to linear, ohmic losses (i.e. resistance) in the ionic conduction through the electrolyte. The thinner the membrane,

the lower this loss. Thinner membranes are also advantageous because they keep the anode electrode wet by "back" diffusion of water from the cathode, where it is generated, towards the anode.

Finally, at very high current densities (fast fluid flows), mass transport causes a rapid drop-off in the voltage, because oxygen and hydrogen simply cannot diffuse through the electrode and ionize fast enough, and products cannot be moved out quickly enough.

The Tafel plot is often modeled semi-empirically with an equation of the form

$$E = E_o - b\ln(i) - Ri - m\,e^{ni}$$

where the voltage E is a function of current density i.

Higher pressure improves kinetics as well as thermodynamics due to the higher concentration of reactants; the Nernst equation does not tell the whole story. For an increase in pressure to 300 kPa, a voltage increase of 25 mV is expected from the Nernst equation. The additional voltage derived from the kinetics of the reaction is estimated at 29 mV for 3 atm operation by one researcher.[3] This doubles the voltage increase to 54 mV. The gain in voltage in a Ballard Mk IV single cell operating at 400 mA•cm^{-2} was experimentally determined to be 2.7 times greater than predicted by the Nernst equation for - in the example of pressurizing to 3 atm, this is an increase of 67.5 mV.[4]

In terms of the overall effect of pressurization, significantly larger increases in voltage are often realized at 300 kPa, as the following Energy Partners polarization curves below show. Here, the difference in voltages widens to as much as 0.150 V (25%) at 1400 mA•cm^2. At 1000 mA•cm^{-2}, the improvement is 14%.

Figure 3.3 Effects of pressurization on polarization curves

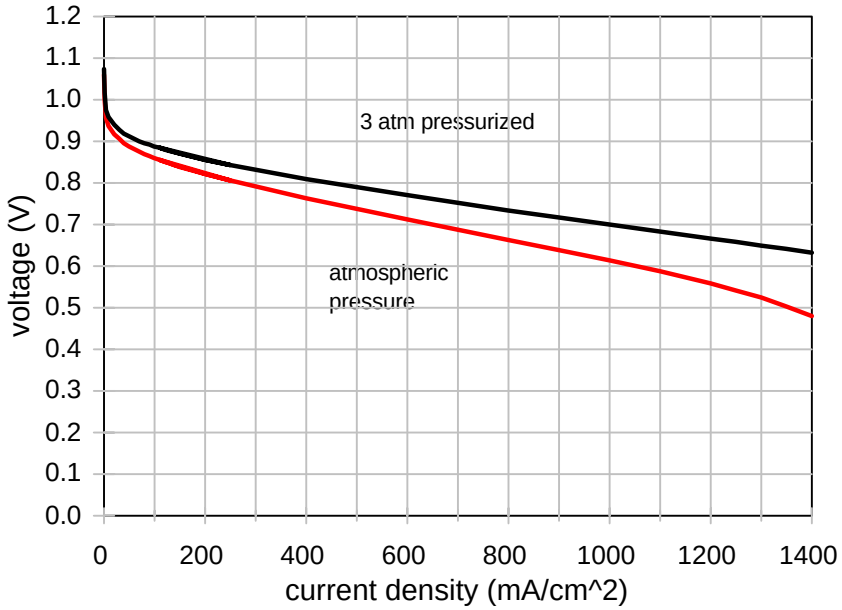

Data from Barbir is for a single cell running on hydrogen/air, with a Gore MEA and operating temperature of 60°C. Air-side stoichiometry is 2.5, meaning that 2.5 times as much oxygen is supplied than the minimum needed for stoichiometry.[5]

3.1.1.3 A note on efficiency

Since efficiency will later be used to calculate waste heat generation, the method here is to divide electrical power output by the rate of energy consumed. As alluded to earlier, "energy consumed" is measured in terms of the higher heating value of the hydrogen used.

In other words,

$$Efficiency\ \eta = \frac{power_{out}}{power_{in}} = \frac{\dot{n}_{electrons}\, F\, V_{output}}{\dot{n}_{hydrogen}\, \Delta H_{HHV}} = \frac{2\, F\, V_{output}}{\Delta H_{HHV}}$$

where $\dot{n}$ are flow rates in moles per second, F is the Faraday constant, V is the voltage of the cell output, and ΔH_{HHV} is -285.8 kJ/mol. In practice, the higher heating value enthalpy can be converted to an equivalent voltage of 1.481 V, so that

$$\eta = \frac{V_{output}}{1.481V}$$

This equivalent voltage concept is very useful in calculating efficiency and waste heat; with the efficiency defined in this way, the waste heat generated is simply

$$\dot{Q} = \dot{n}\, \Delta H_{HHV}\, (1 - \eta)$$

and the maximum efficiency is a thermodynamically-limited 83%.

(If the assumption that water stays in the liquid form is incorrect, the waste heat that must be rejected decreases because the vaporization of the water cools the stack).

3.1.2 Types of fuel cells

The classification of fuel cells is generally by type of electrolyte used. The electrolyte can be a

solid polymer, liquid acid or base, ceramic, or molten ionic salt. For reasons that will be detailed below, proton exchange membrane fuel cells (PEMFCs) are the type most suited for scooter applications.

3.1.2.1 Phosphoric Acid Fuel Cell: well-developed, low density

The fuel cell technology that has been in commercial (non-military) use for the longest time uses phosphoric acid, often in silicon carbide ceramic matrices, as the electrolyte. The phosphoric acid fuel cell runs at over 150°C, which increases catalyst activity. The higher temperatures are also necessary because phosphate anions adsorb on to the oxygen (reduction) electrode below 100°C, reducing catalytic performance.[6]

Phosphoric acid fuel cells accept either direct hydrogen or "reformate", a mixture of hydrogen, carbon dioxide, water, carbon monoxide and possibly nitrogen and trace gases produced from the conversion of fossil fuels into hydrogen and carbon monoxide. Carbon monoxide mixed with the fuel (anode) flow is dangerous, because it can "poison" the catalyst. Basically, this means that active sites on the metal structure become filled with carbon monoxide molecules, making them unavailable for hydrogen catalysis; this is a problem with hydrogen fuel reformed from hydrocarbons, where the hydrogen is mixed with carbon monoxide. Carbon monoxide pollution in the air reaching the cathode is less of a problem, because here the concentration of oxygen and the oxidation potential are high; the oxidation of carbon monoxide to carbon dioxide proceeds rapidly and the catalyst is not poisoned although there is a slight drop in voltage. Depending on temperature, phosphoric acid fuel cells (PAFCs) are able to tolerate concentrations of CO in the fuel stream of up to 1-3%.[7] The output of a steam reformer is roughly double this value which is why an additional carbon dioxide cleanup step is needed.

For 5 kW applications, passive cooling (heat sinks and fins) may be sufficient to cool the system. The high temperatures also have the advantage of transporting the product water as steam instead of as liquid. The temperatures are low enough that noble metal alloy catalysts are required, on the order of 0.2 mg•cm^{-2} on the hydrogen electrode and 0.4 mg•cm^{-2} on the oxygen electrode.[8]

PAFCs have about a third of the performance of modern polymer electrolyte membrane fuel cells (PEMFCs), in terms of power per membrane area in W•cm^{-2}, because PEMFCs have stronger acids in their electrolytes and because the thinner polymer membranes have much lower ohmic losses. Power densities are lower in PAFCs for another reason: the silicon carbide matrix that holds the phosphoric acid electrolyte must be a minimum of 0.1-0.2 mm thick for mechanical stability, increasing total stack size. Finally, PAFCs must be kept above 45°C even when not in use because below this temperature the acid solidifies and expands, risking damage to electrodes or silicon carbide matrix.[9] These two reasons of low power density and finicky temperature conditions explain why, after a few bus demonstrations, PAFCs have been relegated to stationary applications.

3.1.2.2 Proton Exchange Membrane Fuel Cell: for mobile applications, the best

The type of fuel cell currently receiving the most attention is the PEM fuel cell; PEM stands variously for “proton exchange membrane” or “polymer electrolyte membrane”. The membrane is usually a perfluorosulfonic acid polymer. This is a polytetrafluoroethylene (PTFE, trade name Teflon) chain with side chains terminating in an SO_3H group. It is the hydrogen on this sulfonate group that dissociates from the polymer when wet and appears as protons in the solution; polymer acids have the advantage that the anion ($–SO_3^-$ tail) is fixed in the electrolyte rather than dissolved..

One common PEM is Nafion, a polymer developed by DuPont in the 1960's for use as a separator in the chlor-alkali industry and now used for other industrial electrochemical purposes. It is sometimes classified with the compounds known as "superacids" because they are stronger than pure sulfuric acid. Nafion and similar "ionomers" are currently produced at the rate of 100,000 m^2 a year, and sell for about 600 $/$m^2$. [10,11] This is predicted to decrease to 50 $/$m^2$ if production expands to 1 million m^2 per year (150,000 PEMFC automobile engines each year)[12]

Figure 3.4 Nafion chemical structure

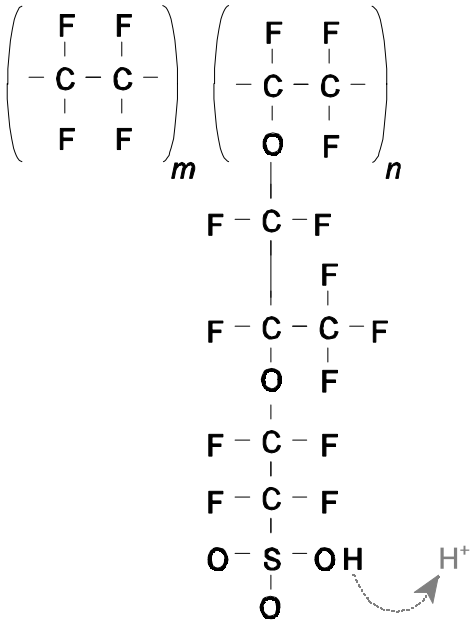

The ratio of *n* to *m* (i.e. active sites to inactive chain monomers) determines the acidity of the electrolyte.

Polymer electrolyte membranes can be made extremely thin, less than 50 µm, making for densely packed stacks and, consequently, high power densities. The thinness of the polymer electrolyte also means high conductance and low ohmic resistance losses, for about three times the performance (in

W•cm^{-2}) of PAFCs. The moderate conditions that the fuel cell runs under are also a benefit when compared to the alternatives - highly corrosive acids, or high temperature ceramics and molten salts.

On the other hand, PEMFCs are especially vulnerable to "flooding": the membrane becomes over-wet due to production of water at the cathode and diffusion of reactants is blocked. Also, platinum is required, less than 0.4 mg•cm^{-2} for each of anode and cathode, mainly to resist the effects of carbon monoxide poisoning from impure hydrogen. Part of the reason is that PEMFCs operate at a relatively low temperature, under 100°C, because higher temperatures remove water from the membrane and damage it. At these low temperature catalysts are simply not as active. More catalyst is required at the cathode than at the anode due to the much lower activity of oxygen ionization.

Pt/Ru alloys are often used at the anode alloy in order to prevent carbon monoxide poisoning, because the presence of Ru changes the lattice constant of the resulting catalyst and makes carbon monoxide adsorption more difficult. PEMFCs significantly degrade in performance when operating on reformate of more than 50 ppm.

With maximum power densities of about 600 mW•cm^{-2} and platinum costing about $450 per ounce, this is a catalyst cost of 10.6 $/kW.

In the stack, the fuel cells are arranged so that ions (protons) pass through the membrane, while electrons are conducted through the separating graphite plates in the opposite direction.

Figure 3.5 Stack diagram

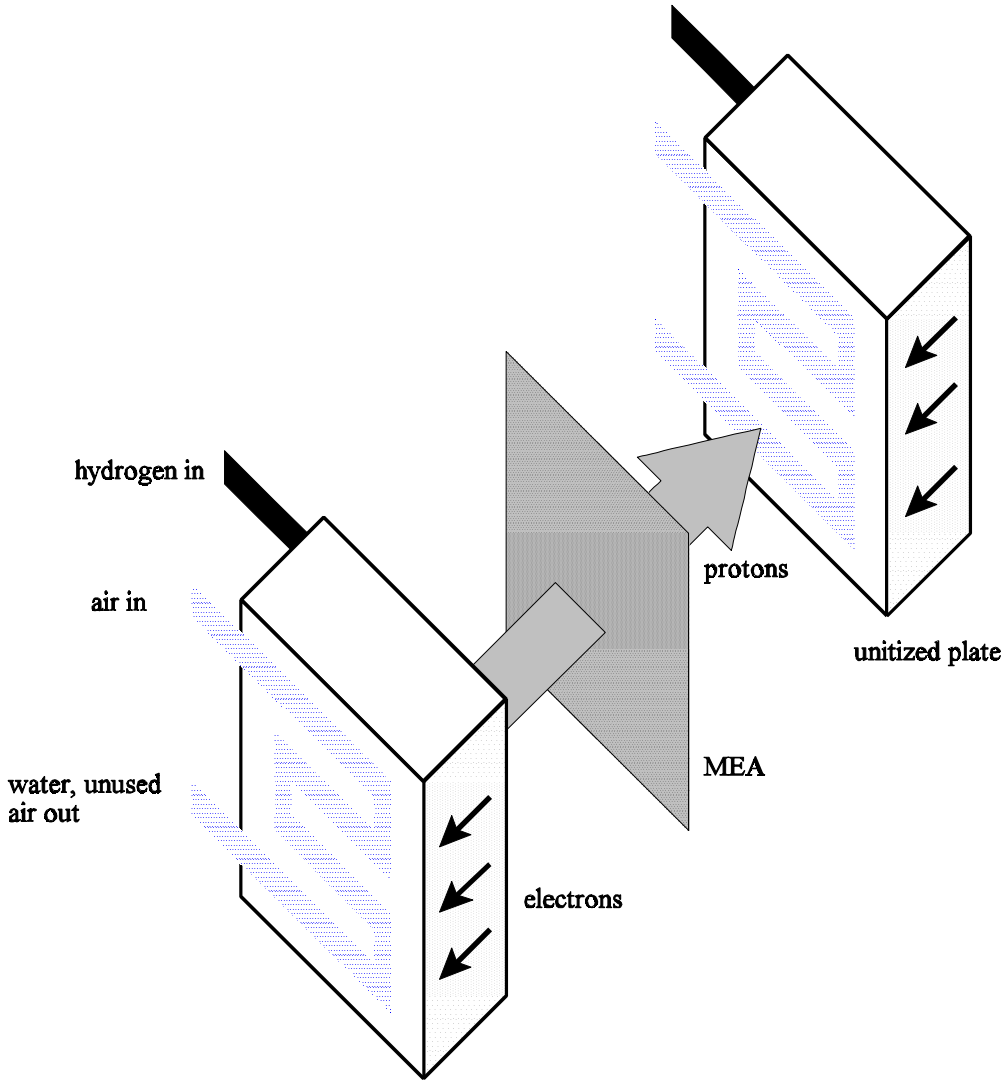

3.1.2.3 Alkaline Fuel Cells: poisoned by carbon dioxide

Alkaline fuel cells, which work at a temperature of about 100 °C, are among the most efficient, and allow the use of less expensive catalyst materials like nickel because the use of an alkaline electrolyte and consequent high pH shifts the electrochemical potential to reduce activation overpotential. They have fairly high power densities. The anode reaction is:

$$H_2 + 2\ OH^- \rightarrow 2\ H_2O + 2\ e^-$$

The cathode reaction is:

$$½\ O_2 + H_2O + 2e^- \rightarrow 2\ OH^-$$

The net reaction is the same as the PEMFC: the combination of hydrogen and oxygen molecules to form water. However, the ionic conductor here is the hydroxide anion rather than H^+. The electrolyte (typically potassium hydroxide, KOH) is either fixed in an asbestos matrix or pumped and circulated as a liquid. Power density is not as high as in a PEM fuel cell.

Another serious deficiency is that alkaline fuel cells cannot withstand carbon *dioxide*; carbon dioxide in the air or fuel streams reacts with the electrolyte to form potassium carbonates which can precipitate out. The content of CO_2 in air was 353 ppm in 1990[13], but modern AFCs can only tolerate 50 ppm[14]. This is fine for space applications where oxygen can be supplied in its pure form, but in ground vehicles powered by AFCs, scrubbers are needed to reduce the carbon dioxide level to acceptable levels. This is not practical for scooters, although Zevco, a British company, is working on a taxi fleet running on alkaline fuel cells equipped with chemical carbon dioxide scrubbers.[15]

3.1.2.4 Solid Oxide and Molten Carbonate Fuel Cells: higher temperature

For applications above 600°C, more exotic materials can and must be used for the electrolyte. With a solid oxide fuel cell (SOFC), the electrolyte is a ceramic oxide and conduction takes place by oxygen ion (O^{2-}) hopping through the electrolyte. Molten carbonate fuel cells use molten ionic salts (e.g. Li_2CO_3, K_2CO_3, and mixtures thereof).

Both of these fuel cells find their utility in stationary power applications, where efficiency gains can be realized by using the exhaust stream and its high grade waste heat to drive a gas turbine bottoming cycle or provide cogenerated heat. These additional outflows would be wasted in a scooter which lack the room for additional "bottoming" cycles.

The high temperatures of these fuel cells offer the possibility of "internal reforming," where natural gas and steam are introduced directly into the fuel cell and steam-reforming and water-gas cleanup occur automatically. SOFCs can even use carbon monoxide as fuel without reforming. The high temperatures mean that noble metal catalysts are not needed, but also bring with them their own materials problems.

Neither of these fuel cells has the high power density needed for vehicle power.

3.1.2.5 Direct Methanol Fuel Cells: long-term promise

A direct methanol fuel cell is an exception to the rule that fuel cells are categorized by their electrolytes; in this case, it is the fuel that defines the fuel cell. (Typically, the electrolyte used in conjunction with DMFCs is a PEM). Dilute methanol is flowed through the anode as the fuel and

broken down to protons and electrons and water. Methanol is chosen because it is one of the few widely-available fuels that is electroactive enough to use in a fuel cell; ethanol can also be used but with poorer efficacy, due to its poorer electrical activity.

Much research is being done on direct methanol fuel cells, because a fuel cell run directly on liquid fuel would offer dramatic advantages in overall system density since neither low-density hydrogen nor bulky reformers would be needed. Methanol can be made relatively easily from gasoline or biomass, and although it only has a fifth the energy density of hydrogen by weight, as a liquid it offers more than four times the energy per volume when compared to hydrogen at 250 atmospheres.

For a DMFC, the overall anode reaction is:

$$CH_3OH_{(l)} + H_2O_{(l)} \rightarrow CO_2 + 6\ H^+ + 6\ e^-$$

At the cathode,

$$6\ H^+ + 3/2\ O_2 + 6\ e^- \rightarrow 3\ H_2O_{(l)}$$

The net reaction is the oxidation of methanol:

$$CH_3OH_{(l)} + 3/2\ O_{2\ (g)} \rightarrow CO_{2\ (g)} + 2\ H_2O_{(l)}\ \ (E_r° = 1.214\ V)$$

For the lower heating value reaction, E_r is 1.170 V, slightly less than hydrogen at 1.185 V. For each mole of methanol, six electrons are transferred, and this would seem far superior to the two electrons of a hydrogen PEMFC, but the comparison is properly with not one mole of hydrogen,

but one mole of methanol reformed into hydrogen. In the theoretical maximum case, three moles of hydrogen molecules can be reformed, so the total number of electrons are equal in each case.

Note that the presence of carbon dioxide means that an acid electrolyte must be used. Since the ion being exchanged is a proton, the DMFC can operate with a polymer electrolyte membrane.

One major problem is that the oxidation of methanol produces intermediate hydrocarbon species which poison the electrode. The other major problem is that the exchange current for methanol is much lower than that for hydrogen - by as much as six orders of magnitude.[16] This means that the oxidation of methanol at the anode becomes as slow as the oxygen electrode reaction, and large overpotentials are required for high power output. Also, there is high crossover of the methanol through the electrolyte, meaning that the fuel molecules diffuse directly through the electrolyte to the oxygen electrode. As much as 30% of the methanol can be lost this way, severely compromising power.[16]

As a result, maximum demonstrated power densities in 1998 were on the order of 200 $mW \cdot cm^{-2}$ with air at 2.5 atm in a 2" x 2" cell, insufficient for current applications except very small portable fuel cells.[17] Platinum loadings were 4 $mg \cdot cm^{-2}$, almost a factor of ten greater than hydrogen-air fuel cells. Future improvements in catalyst and membrane design are expected to change this situation, with year 2000 goals of 300 $mW \cdot cm^{-2}$ at 1 $mg \cdot cm^{-2}$.[18]

3.1.3 Stack characteristics

The PEM fuel cell is the best for this, and many other, vehicle applications. The next step is to characterize how large a fuel cell would be needed to supply the demanded power. This is done

first by a comparison with published overviews of automobile fuel cell power, and second with a more detailed, ground-up model based on a Directed Technologies, Inc. (DTI) study.

3.1.3.1 Fuel cell stack specifications

The fuel cell stack is sized here by determining a standard motor voltage and connecting many fuel cells in series to create the desired voltage. Maximum current *density* is fixed by the properties of the membrane, but the total current can be increased by choosing cells with larger surface area. For a given nominal power output, a fuel cell that is oversized for that nominal power means that the power system is more often operating at a smaller fraction of maximum power - and thus at higher voltages and higher efficiency. On the other hand, it is expensive and often inefficient from an overall systems perspective to build such a heavy and expensive stack, especially since in road vehicles the maximum power is so infrequently required.

The process described above is carried out in section 4.4.1, after detailed power and performance requirements are derived in sections 4.1, 4.2, and 4.3. However, to give away the ending, the maximum gross power output is 5.9 kW for standard urban driving (5.6 kW net of parasitic power).

3.1.3.2 Published results for automobile fuel cell stacks

First, PEM fuel cell stack characteristics are estimated based on previous top-down studies for automobiles.

The PNGV (Partnership for a New Generation of Vehicles government/industry collaboration)

goals for fuel cell stack mass and weight are 0.35 kW/kg and 0.35 kW/L, by approximately the year 2000.[19] This is exclusive of auxiliary systems like radiators and blowers. The same source sets goals of 0.5 kW/L and 0.5 kW/kg by 2004. (For the 5.9 kW system studied here, that translates into 12 kg and 12 L). However, it should be noted that Ballard achieved 1 kW/L as early as 1996.[20]

The PNGV also defined year 2004 goals of 50 $/kW net power for the fuel cell system (stack and auxiliaries) and an intermediate price target of 150 $/kW by 2000.[21] Thus, for a 5.6 kW system, in five years the cost could be as low as $280 if automotive-sized system costs scale down to the scooter size. This depends on significant cost reductions from current prices, which are on the order of $1000/kW.

Ogden *et al* surveyed price estimates in the literature and found a price range of $33 to $100 per net kW for the fuel cell stack, and $10 to $20 per kW for the peaking power battery. The range cost estimates is thus $185-$560 for the 5.6 kW fuel cell-only scooter.[22]

3.1.3.3 Detailed construction

The fuel cell engine itself is made of several cells electrically and physically connected in a box-shaped "stack". Oxygen and hydrogen must be brought to the membranes where they can react, while the membranes themselves must be kept wet so that they can conduct the hydrogen ions (protons). Surplus water must be pushed out of the stack, and waste heat must be rejected from the stack to avoid overheating and membrane damage. The cells, which are made of electrically conductive graphite or metal, are constructed in series so voltages from each cell add up; the same current flows through the entire stack. The hydrogen and oxygen flow in molded manifolds

typically built off the side of the stack, and are divided into parallel feeds into the individual cells; water and exhaust gas are collected in another manifold and rejected to the atmosphere (the water may be recycled to humidify the incoming gases).

Essentially, each fuel cell in the stack contains an MEA, or membrane electrode assembly, which consists of the polymer ion-conduction membrane with flat electrode sheets attached to either side. Oxygen and hydrogen are channeled to the cathode and anode sides respectively in flow fields carved or pressed into plates that are next to the electrodes. These can be two separate plates, each serving a single electrode ("unipolar" design), or a single plate carved on both sides with flowfields can be used for two adjacent electrodes ("bipolar design"). The membrane must pass hydrogen ions but not electricity; the plates must conduct electricity, but not allow water, hydrogen, or oxygen to permeate through.

The DTI study examined a number of options with membranes of active area 116 cm^2 to 697 cm^2, and calculated costs and weights for each of the sub components using design for manufacture and assembly ("DFMA") techniques. Four possible cell designs were studied in the DTI report: unitized stainless steel; three-piece stainless steel; amorphous carbon; and carbon-polymer composite. The three-piece stainless steel cells were chosen here to estimate long-term, mass-produced cost estimates for the fuel cell stacks.

A detailed description of the stack size, weight, and cost analysis is provided in Appendix B. Essentially, the model was built from the bottom up, rather than simply extrapolating from the automotive-sized vehicles, although some of the figures are still based on the automotive model.

The MEA from DTI's model is 70 µm thick in total. It consists of a 5 µm composite membrane, sandwiched between 28 µm thick layers of electrode (these electrodes consist of platinum deposited on carbon black which sits on an inert ionomer carrier, and then 25 µm of electrically conductive porous backing, made of carbon paper impregnated with fluoropolymer like Teflon to repel accumulated water).[23]

Right now, typical membrane thicknesses are on the order of 50 µm - 127 µm for Nafion, and as low as 25 µm for a newer Gore membrane. A prediction of 5 µm is aggressive although it should be noted that, in DTI's model, the thinness of the membrane mainly reduces costs, not stack size.

Today's separator plates are made from graphite, which has low electrical conductivity but resists the corrosion caused by the electrochemical potentials in the cell. However, it is extremely expensive to machine flow field patterns into the graphite surfaces, and graphite itself is not inexpensive. (Machined graphite separator plates currently cost "as much as 200 $/kW"[24]). Future prices are predicted to be as low as 5 $/kW, and cheaper material options include conductive polymers, impregnated amorphous carbon, and metal treated with anticorrosive coatings.

The three-piece cell design is chosen: in each active cell, one metal separator plate is matched with two separate, unipolar plates etched with flow fields.

51 µm separator plate

76 µm anode flow field

1000 µm anode gasket

70 µm MEA

76 µm cathode flow field

1000 µm cathode gasket

[repeat with next separator plate; total thickness 2.3 mm]

Figure 3.6 Active Cell

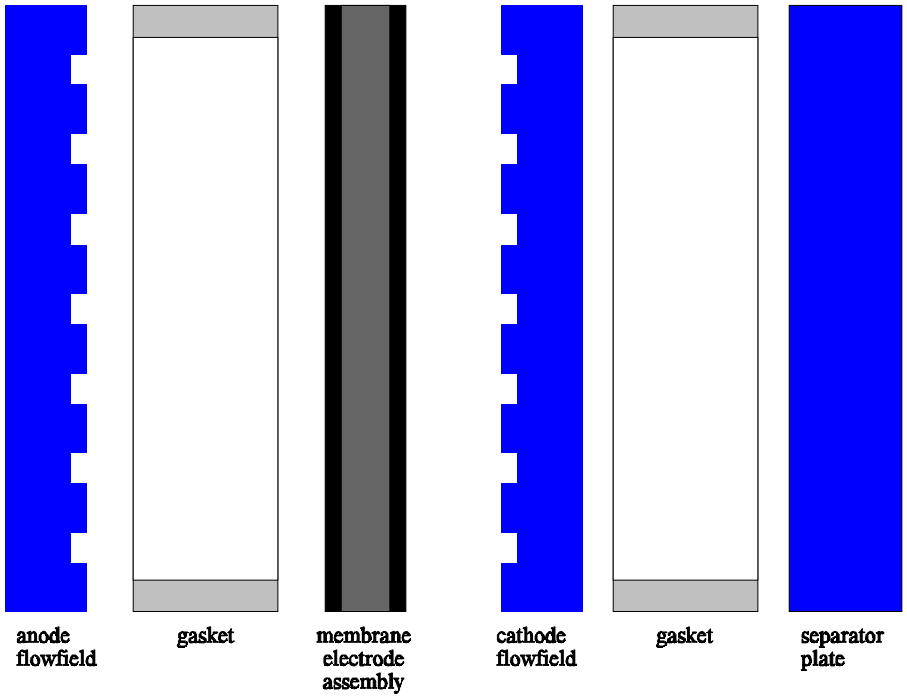

Each system requires cooling plates periodically interspersed between the active cells described above. The cooler cells allow flow of coolant within the stack, and are essentially flow fields through which only water flows. The cells are made of the same electrically-conductive stainless steel to allow bulk conduction of current. The reason for using cooler cells of the same design as the ordinary ("active") cells is to increase the number of identical components and, again, decrease manufacturing costs. A cooler cell to active cell ratio of 1:2 is defined here.

A three-piece metallic cooler cell consists of:

51 µm separator plate

76 µm coolant flow field

1000 µm gasket

[repeat with next separator plate; total thickness 1.1 mm]

In addition to the repeating cells, the stack requires an electrically insulating plastic housing; tie rods to hold the cells together; current collectors at the ends of the stack to conduct electricity to the power system; and insulators and endplates over the current collectors.

3.1.3.4 Detailed construction results

The results are summarized below for three different fuel cell stack sizes, each 56 cells long for a total voltage close to 48 V.

Table 3.1 Stack size, weight, cost summary

	5.9 kW	**3.3 kW**	**1.1 kW**
membrane active area	170 cm^2	100 cm^2	35 cm^2
total mass of non-repeat units	5.1 kg	3.6 kg	3.3 kg
total mass of repeat units	2.8 kg	1.8 kg	0.8 kg
total stack mass	7.6 kg	5.4 kg	4.0 kg
total stack volume	7.8 L	5.3 L	3.2 L
stack power density by weight	0.78 kW/kg	0.62 kW/kg	0.27 kW/kg
stack power density by volume	0.76 kW/L	0.62 kW/L	0.34 kW/L
total stack cost	$244	$161	$124
cost of power	42 $/kW	47 $/kW	103 $/kW

These are long-term mass-produced prices. In comparison, a Ballard 37 kW stack available today has power densities of 1.1 kW/L and 0.8 kW/kg, so the results above are not overly ambitious.[25]

For comparison purposes: a simplistic curve-fitting to the DTI model's results for automotive fuel cell engines gives lower costs of $176, $125, and $96 - about 20% to 30% lower. See Appendix B for more details.

3.1.4 Gas flow management

In addition to the stack itself, several subsystems are needed in a fuel cell power plant. One of the most important ones is the gas flow subsystem. Oxygen and hydrogen are introduced into the fuel cell system at the appropriate flow rate required for the current at any given moment; this requires a variable-flow system if the stoichiometry is to be kept constant. Even in an "atmospheric-pressure" system, some pressure over atmospheric is needed in order to push the gases through the often-serpentine passages carved into the flow plates, and to force liquid water out of the same passages. This additional pressure is on the order of 0.1 to 2.0 psi (0.7 to 13.8 kPa) above atmospheric; IFC (International Fuel Cells) quotes 0.8 psi.[26,27]

A minimum flow speed of 0.35 m/s is needed to eliminate product water, and a Schatz Energy Research Center patent estimates flow velocities at up to 7 m/s.[28, 31,28] Due to the fact that the cathode reaction is much slower than the anode reaction, oxygen is often supplied at a higher-than-stoichiometric flow rate. The ratio of air flow rate to the minimum flow rate required for stoichiometric oxygen-hydrogen reaction is often 2.0 or higher in order that the concentration of oxygen in the air not drop too much as it passes through the flow field, and the excess air also helps to push product water generated at the cathode out of the fuel cell.

An air filter is needed to prevent foreign objects from being taken into the fuel cell.

Hydrogen is supplied dead-ended in the design proposed here. This means that there is no outlet to the anode side; the pressure is simply allowed to equilibrate in the stack to match the pressure regulator output. Electrochemical consumption is matched by replacement from the hydrogen store. The result is 100% hydrogen utilization. This technique can only be used for pure hydrogen vehicles because the anode stream from reformed hydrocarbons or ammonia would contain inerts (N_2, CO_2, H_2O) and poisons (CO) that would build up at the anode dead end. Dead-ended fuel cells still need to vent occasionally in order to purge impurities that may have entered the fuel cell; this involves opening the anode exhaust valves for a brief period and allowing the hydrogen to flow directly into the atmosphere for a very brief time. Effective utilization is slightly less than 100% for this reason, although in this study this loss is assumed to be negligible. (Stacks running open-ended have hydrogen utilizations of approximately 85% unless pure hydrogen is recycled.)

To manage the air flow, blowers are briefly discussed below. Then, the utility of pressurized operation is analyzed.

3.1.4.1 Blowers

Blowers are used in atmospheric systems to draw air into the fuel cell; no corresponding device is needed for the hydrogen side, because in all current designs the hydrogen is kept under pressure higher than the operating pressure of the fuel cell, and expands as it is released from the storage container or produced above atmospheric pressure in a reformer. The blower is typically powered electrically from the fuel cell output, with a battery required for startup.

The blower power required is:

$$\dot{W} = \frac{\Delta P \dot{V}}{\eta}$$

where η is the blower efficiency. For the power requirements of a 5 kW fuel cell (2.0 psi pressure drop and a flow rate of 15.6 cubic feet per minute) and a 50% blower efficiency the power consumption is 200 W.

An industrial heavy-duty blower that could be used to provide the required output is the Ametek 5.7" BLDC three-stage blower, model 116638-08, with a catalog sale price of $430.[29]

3.1.4.2 Compressors

Compressing the air input increases the concentration of oxygen per volume per time – its effective partial pressure – and thus increases the fuel cell efficiency. This means that a smaller and lighter fuel cell stack can be used, at the price of parasitic power required by the compressor and increased cost. In addition, the drop-off in voltage caused by mass transport problems is delayed until higher current densities. Another benefit of higher pressures is that, for the same molar flow rate, a lower volumetric flow rate can be used. Thus, humidification is easier because less water is needed for saturation (per mole of air). Finally, flow-field design is less restrictive because larger pressure drops can be tolerated in the flowfield.

Since most of the hydrogen storage techniques involve pressurized hydrogen, it is not be difficult to obtain a matching pressurized hydrogen stream; in any case, a typical PEM can tolerate a pressure difference of about 0.5 bar for Nafion-115.[30]

In a tightly-integrated system, the compressor can be powered mechanically as a turbocharger, using a shaft attached to a turbine running off the exhaust from the fuel cell. This allows recovery of some of the expansion work. On the other hand, the system may be simpler if the compressor is powered only by an electric motor, with separate battery for startup purposes.

Compressors on the order of 0.5-10 kW are difficult to find and generally inefficient.[31] The Department of Energy has a goal of 3 kg, 4 L, 68% efficiency, and $200 at 70-80 grams/second for a turbocompressor/expander for a 50 kW fuel cell system.[32,33] Note that this is ten times the flow rate required for a 5-6 kW scooter, and efficiency decreases dramatically with "turn-down" (operating below the design point), so actual efficiency will likely be lower. Also, for the low flow rates involved, variable speed positive-displacement compressors (rather than turbomachines) are typically used and efficiency may be lower for that reason as well. The DOE target size and weight are quite low for the benefit in voltage, but cost would be significant when compared to the cost of the total system.

The net benefit of compression for the scooter system is analyzed in section 4.6 in the system modeling chaoter.

3.1.5 Water management

Water is vital to fuel cells in that the electrodes and the electrolyte must be kept wet in order to allow proton conduction through the acid medium. Water enters the system from externally humidified hydrogen and/or air streams and generation at the cathode by the electrochemical reaction. Due to hydrogen bonding, on average 1 to 2.5 water molecules are dragged along with each proton as it migrates from the anode to the cathode; this is known as "electro-osmotic drag."

Water also flows in the other direction due to back-diffusion, since the concentration of water in the cathode electrode is much higher than at the anode electrode. Water exits the system with the cathode exhaust as blown-out liquid or vapour.

The greatest danger posed by water is that of drying out. Loss of water can dry out the electrodes or the membrane, leading to a runaway in overheating and current loss and damage to the membrane. On the other hand, if too much liquid water accumulates at an electrode, it can block the diffusion of gas into that electrode, preventing dissociation and slowing down the overall conversion to electricity. Drops in current density are often the symptoms of flooding.

Voltage (efficiency) is higher with humidified flow than with unhumidified reactant streams. In test stations, “external” humidification is typically achieved by bubbling the reactants through a reservoir of water. IFC has demonstrated “internal humidification” by absorbing water into porous bipolar separator plates, and using this reservoir of water to replenish the water in the electrodes and electrolyte.

Various methods have been proposed to remove water from the cathode. If the temperature and flow rate are high enough, the warmed oxidant can vaporize the product water and carry it away as water vapor. If the oxidant pressure and flow rate are high enough, the liquid water is physically pushed out, although flow rates that are too high will dry out the membrane and anode. Finally, a separate path of hydrophilic polymer can be used to “wick” (draw by capillary action) the water from the cathode back to the anode side, which tends to dry out faster.

Fuel cells running with a dead-ended fuel supply cannot humidify the anode flow, because water would accumulate in the hydrogen dead end. So, to prevent the anode from drying out, the

incoming *air* flow is humidified by passing it over a wetted polymer wicking water from a reservoir, or through a water bottle. Back-diffusion is allowed to carry the moisture through the membrane back to the anode, and the thinner the membrane, the more quickly back-diffusion can operate. If temperatures are low, this diffusion can be enough to remove the need for external humidification.

Water in the fuel cell has to be deionized; this can be done by forcing the water through a filter or by supplying the vehicle with deionized water only. In the case where all water needs are supplied by condensation and then recirculation of the product water, deionization is not a concern. In the scooter system, without room for a condenser and second cooling fan, the water may just be exhausted.

3.1.6 Heat

The designed operating temperature of the fuel cell affects various factors. A higher operating temperature means that more of the product water is vaporized, so that more waste heat goes into the latent heat of vaporization and less liquid water is left to be pushed out of the fuel cell. Higher temperatures also mean faster kinetics and a voltage gain that in general exceeds the voltage loss from the negative *thermodynamic* relationship between open-circuit voltage and temperature. Heat rejection is also abetted at higher temperatures due to the larger difference between the fuel cell temperature and ambient temperature. On the other hand, lower stack temperatures mean shorter warmup times for the system as a whole, and lower thermomechanical stresses. Corrosion and other time- and temperature-dependent processes are retarded, and much less water is required for saturation of input gases.

The upper limit of operation for PEMFCs is about 90°C because water evaporates from the membrane and performance drops quickly; permanent damage can occur to the membrane. At Princeton and various other places, membranes are being developed that can handle higher temperatures while retaining the high power density of PEMFCs. This is being attempted by making novel electrolyte that are composites of Nafion with materials that hold water more tightly and prevent evaporation: proton-conducting glasses and hydrated oxides of silicon. Another technique is to replace water in Nafion with different chemicals that have higher boiling points.[34] The primary objective is higher CO tolerance (since the catalysts are more effective at higher temperatures) without drastic loss of performance.

Another heat-related issue is preheating of the inlet air and hydrogen. This is advantageous to prevent flooding at the inlet at the part of the stack closest to the air entry. This is the point at which the air is coolest, having not yet warmed up to the full stack temperature, and has the highest concentration of oxygen since the air has not yet been depleted of oxidant. Cathode water production is highest here, and the cool air saturates with water easily if not preheated.[35]

Preventing overheating is described in greater detail. Under the most strenuous conditions, a 5.9 kW fuel cell operating at 50% efficiency produces 5.9 kW of waste heat - a significant instantaneous load to manage. However, as will be shown later, the *average* fuel cell load for a scooter in a city driving cycle is one-tenth of the maximum, and at this power level efficiencies are higher than at maximum load. The thermal mass in the system damps out the peaks when the transient heat generations are converted to temperature rises, as analysis in section 4.4.4.3 shows.

Cooling can be achieved through a number of means. First, the evaporation of some of the product water at the cathode absorbs some heat. Second, active cooling with air or liquid coolants can be

used to transfer heat to radiators. Third, passive cooling of the fuel cell can be performed with cooling fins and heat sinks. Finally, the fuel cell might be coupled with subsystems that absorb heat like turbine reheaters and metal hydride containers.

3.1.6.1 Active cooling

Pumping a coolant fluid (either air or water) through cooling passages within the fuel cell stack would allow much heat to be removed. This heat would have to be dissipated at a radiator, so in addition to the pumping energy, a fan would be needed to increase convection over the radiator.

Requirements include noncorrosive coolant fluid; a pump to circulate the fluid; seals; a radiator and radiator cooling fan; a deionizing filter; and a surge tank. Researchers at the Institute of Integrated Energy Systems at the University of Victoria estimated the power required by the fan blowing over the radiator at 83 W for a 5 kW Ballard Mark V stack.[36]

Radiator and fan size, weight, and cost are described in more detail in section 4.4.4.4, after the radiator cooling capability requirements are calculated.

3.1.6.2 Passive cooling

Cooling using fins *without* a powered fan blowing over them is virtually impossible to achieve at sizes greater than 50 W because of the limited surface area and the low temperature difference between the maximum ~80°C temperature of PEMFCs and the ambient temperature, which in Taiwan can be as high as 40°C. However, forced air ventilation over fins attached to the fuel cell stack is possible for cells of the proper narrow aspect ratio, as H Power fuel cell stacks have

demonstrated. Less total cooling air flow is required than for water cooling because the intermediate (water circulation) step is eliminated, and stack weight and volume are saved by not having to interpose cooler cells between active cells. On the other hand, some kind of heat conduction path is needed to get from the stack to the environment. Also, the heat capacity of air is far lower than water, and when coupled with the small change in temperature from fuel cell to ambient environment, the result is poor heat transfer.

3.1.6.3 Boiling refrigerant

Using a closed-loop refrigerant that boils at the fuel cell operating temperature (50°C - 80°C) would allow a great deal of thermal energy to be withdrawn from the stack. In addition, the pressure of the vaporized coolant (in conjunction with a check valve) could be used to drive the coolant cycle without requiring a pump, minimizing parasitic losses. A fan would likely still be needed on the condensation (radiator) side, but otherwise the system would feature automatic control without electronics.

Active cooling with a liquid coolant loop is chosen here, to be certain of sufficient cooling. Air cooling is unlikely to be successful in a stack as large as 5.9 kW, as the available surface area is low. Heat issues are discussed in more detail in section 4.4.4.

3.2. Fuel for the fuel cell

The PEMFC must be supplied with hydrogen. This hydrogen can be stored as hydrogen, but it can also be "reformed" from other chemicals using an onboard chemical processor. The advantages of the latter are that liquid fuels, with their high energy density (as a function of volume) and easier distribution, can be used. However, reforming requires additional equipment which comes at a premium on a small vehicle. Also, reformers usually produce some pollution on their own but this is trivial compared to combustion engines.

Modeling results from sections 4.5.1 and 4.4.1.4 will show that the fuel requirement for the scooter to travel 200 km at 30 km/h is 250 grams of hydrogen, and a maximum flow rate of approximately 0.05 moles $H_2 \bullet s^{-1}$ is needed at the upper limit of 5.9 kW of gross power.

3.2.1. Reformed fuels

The standard technology predicted for the first commercial fuel cell cars is hydrogen reformed onboard from liquid fossil fuels like methanol or gasoline, because these fuels are widely available and have excellent energy densities. Some interesting other technologies, like producing hydrogen from dissolving certain chemicals in water, and reforming ammonia into hydrogen, are mentioned here because they might find use in the smaller scooter application.

3.2.1.1. Hydrocarbon reforming.

Liquid hydrocarbon fuels contain a great deal of energy per unit volume, far more than hydrogen,

and are cheaply available. The two major candidates for fuel cell vehicles are methanol and gasoline. Methanol produces less carbon dioxide and reduces long-term oil dependence, and is easier to reform; gasoline has extensive existing production and distribution infrastructure. Natural gas is another possibility.

Table 3.2 Fuel gravimetric and volumetric energy densities, lower heating value basis

	by mass	**by volume**
Hydrogen gas, atmospheric pressure	120 MJ/kg	11 kJ/L at STP
Compressed hydrogen gas, 3600 psi	120 MJ/kg	2,700 kJ/L at 3600 psi
Gasoline (approximate)	44 MJ/kg	31,800 kJ/L liquid
Methanol	20 MJ/kg	15,900 kJ/L liquid
Natural gas (pure methane)	50 MJ/kg	36 kJ/L at STP
Compressed methane, 3600 psi	50 MJ/kg	8,700 kJ/L at 3600 psi

Data from Electric Vehicle Technology, CARB report [37,38]

There are two major methods of reforming hydrocarbon fuels: partial oxidation ("POX") and steam reforming. Partial oxidation is partial burning of the fuel to produce carbon monoxide and hydrogen. It is exothermic. To pick a sample fuel, if methane is partially oxidized:

$$CH_4 + \tfrac{1}{2}\, O_2 \rightarrow CO + 2\, H_2 \quad (\Delta H = -35.7 \text{ kJ/mol})$$

Gasoline partial oxidation proceeds in essentially the same way. Partial oxidation requires high temperatures, 900°C - 1500°C, but can handle a wider variety of fuels than steam reforming.

Steam reforming combines the fuel with steam to produce the same products, and is endothermic. The steam reforming equivalent of the reaction above would be

$$CH_4 + H_2O \rightarrow CO + 3\ H_2\ (\Delta H = +206.2\ kJ/mol)$$

A steam reforming system is more efficient because waste heat from the later processes can be recycled as input into the endothermic steam reforming process (for example, if unused hydrogen in the anode exhaust is burnt). Steam reformers also produce more hydrogen because some comes from the water.

In general, partial oxidation is the simpler system because of the fewer heat integration and water management issues; it has lower capital costs for this reason. Partial oxidation reformers also have superior startup times, fuel flexibility, and may have faster response times.However, partial oxidizers for vehicles run on air so much intert nitrogen flows through; flow rates are higher and thus the downstream reactors like the water-gas shift and the PROX must be larger; also, the concentration of hydrogen in the reformate is lower in POX reactors than it is for steam reformers.

Table 3.3 Steam reforming versus partial oxidation

	Partial Oxidation	**Steam Reforming**
PROS	• Simpler system • Fast response time • Greater fuel flexibility	• Theoretically more efficient • More hydrogen in reformate (higher fuel cell efficiencies)
CONS	• Air intake means greater flow rates, larger components • Less efficient	• Slow response time (several seconds) • Catalysts needed • Cannot handle gasoline • Capital-intensive heat exchangers necessary • H_2 burners, if needed, add complexity

The next step in either process is the water-gas shift reaction. Here, most of the remaining carbon monoxide is reacted with water to produce additional hydrogen. A typical conversion is from 7.1% CO in a steam reformer's output (or 46.1% in from a partial oxidation reactor), to 0.5% coming out of the water-gas shift reactor.[39] Essentially,

$$CO + H_2O \rightarrow CO_2 + H_2 \ (\Delta H = -41.2 \text{ kJ/mol})$$

There is one other important issue: the fuel cell must be optimized to accept an anode fuel stream that can be as low as 40% hydrogen for POX, or 75% hydrogen for steam reforming. The lower amount of hydrogen in either case means that fuel cell efficiency is lowered. Also, water must be either carried to supply the water-gas shift reaction (and any steam reformer), or recirculated from the exhaust. The total water needed is on the order of 3 grams per gram of H_2 for partial oxidation, and 4.5 grams per gram of H_2 for steam reforming.

CO poisoning is an important issue for polymer electrolyte membrane fuel cells, because the CO poisons the platinum (or other) catalyst on the electrode, reducing voltage at a given current density. Thus, for the same power output, a fuel cell running off reformed hydrogen must be sized larger. It is difficult to completely eliminate CO from the reformer exhaust, and fuel cells can only tolerate at most 50 ppm CO before efficiency drops dramatically, so a final "cleanup" step is required even after the water-gas shift. A preferential oxidizer ("PROX") or similar cleanup device is needed to perform CO removal. (A PROX is so named because it, due to the catalyst microdesign, it "prefers" to oxidize carbon monoxide rather than hydrogen; PROX efficiencies are often measured in terms of how much hydrogen is must be sacrificed to reduce CO down to acceptable levels.)

The amount of hydrogen that can be produced by reforming various hydrocarbons is listed below for both steam reforming and partial oxidation; as modeled, both processes include a water gas shift reaction to create more hydrogen from shifting carbon monoxide. The results are listed as effective hydrogen concentrations in the fuel; due to inefficiencies not all of the hydrogen can be recovered, but on the other hand, some of the weight fractions are greater than the fraction of hydrogen in the fuel molecules themselves because much hydrogen comes from the water.

Table 3.4 Hydrogen output from reformed hydrocarbon fuels

		Steam reforming			**Partial oxidation**		
Fuel	**Formula**	**wt% H_2**	**g H_2 per L_{fuel}**	**mols H_2O per mol fuel**	**wt% H_2**	**g H_2 per L_{fuel}**	**mols H_2O per mol fuel**
Methanol	CH_3OH	19%	150	1.0	13%	100	0.0
Ethanol	C_2H_5OH	26%	209	3.0	22%	168	2.0
Methane (LNG)	CH_4	50%	205	2.0	38%	151	1.0
Gasoline	$C_8H_{15.4}$ (approx.)	43%	301	16.3	28%	200	8.1
Diesel fuel	$C_{14}H_{25.5}$ (approx.)	42%	357	28.3	28%	231	14.2

Data from CARB study.[40]

Excellent overall weight fractions and hydrogen densities can be achieved in the fuel, but note that this does not include the additional weight of reformer equipment required, nor the extra water that is needed. Reformers for automobiles are predicted to cost 16-25 $/kW for 50 kW sized stacks, but there is little data on pricing so far.[41]

The fuel cell industry is split on whether reformed methanol or gasoline will succeed first; methanol reforms with greater efficiency, but gasoline is perhaps easier to distribute (although it should be

noted that only gasoline free of detergents, sulfur, and other additives should be run through reformers. Sulfur would poison the reformer, PROX, or fuel cell catalysts and the effects of elements other than carbon, hydrogen, nitrogen, and oxygen passing through the reformer may be negative. Gasoline is likely to be reformulated for fuel cell cars running on reformed gasoline.)

The scooter design is extremely volume- and weight- sensitive, and bulky and complex heat exchangers are to be avoided, so if reformers make sense at all, a less efficient POX is superior.

3.2.1.2 Methanol reforming example

Methanol reforming is discussed as an example of hydrocarbon reforming for the scooter. This most simple alcohol (CH_3OH) is often cited as a leading candidate for fuel cell vehicles, because as a liquid it has high energy density, and because it is easier to reform than gasoline. It contains 12.5% hydrogen by weight.

The figures for a HotSpot POX reformer are given below. Johnson Matthey predicts an additional 20% volume for a PROX on top of that required by the POX, and 95% efficiency for this second stage, with overall efficiencies of 89%.[42] Fuel cells running on reformate cannot be operated dead-ended, so hydrogen utilization at the anode decreases to about 85%, for a total efficiency of 76%. The reduced hydrogen content in the reformate output (when compared to pure hydrogen) reduces the voltage of the fuel cell by approximately 0.128 volts per $A \bullet cm^{-2}$, or roughly 20% at maximum power output.[43]

Table 3.5 Reformer performance

reformer volume	7.2 L
reformer weight	9.5 kg + cleanup unit weight
hydrogen output after cleanup	1.36 L/s
hydrogen output	0.061 mol•s^{-1}
fraction of hydrogen in output	43%
fraction of CO in output	8 ± 5 ppm
overall efficiency	76%
output per mole of methanol	2.3 mol H_2

At this production rate, 55 moles of methanol would be needed for the required 250 grams of hydrogen gas output. This corresponds to 1.8 kg of methanol, and a volume of 2.2 L, much less than a compressed gas cylinder or a metal hydride hydrogen adsorption device. The total volume is only 9.4 L, for POX and PROX and fuel tank; the total weight of the system is 11.3 kg plus the weight of the PROX. Assuming an 8 kg preferential oxidizer, and considering the reformer and PROX and fuel tank as a single "hydrogen storage system" produces densities of 1.3 wt% and 26 g/L, measured in terms of hydrogen output.

3.2.1.3. Ammonia

Ammonia reforming is an interesting option that is somewhat different from the standard fossil-fuel reforming ideas, since it offers clean combustion from a chemical feedstock that is commercially available as a fertilizer. Fuel cell companies like Analytic Power and H-Power have developed prototypes running on liquefied ammonia.

Ammonia contains 17.6% hydrogen atoms by weight. This is as good as POX-reformed methanol

and with the advantage that the only products of ammonia reforming are hydrogen and nitrogen gas, ammonia would seem to be an excellent carrier for hydrogen. Also, ammonia is easily liquefied under pressure, and at a liquid density of 601 g/L at 300 K, equivalent to an H_2 volumetric density of 55 g / L. This liquefaction requires a pressure of only 10 bar at 300 K.

In principle, the ammonia cracking reaction is

$$NH_3 \rightarrow \frac{1}{2} N_2 + 3/2\ H_2 \quad (\Delta H = +46.4\ kJ/mol\ NH_3)$$

The reaction takes place at over 400°C, which requires an external heat source since the exhaust from a typical proton exchange membrane exits at only 80°C. Traditionally, some of the hydrogen in the reformer's output stream is burned to provide the working temperature for the reformer and to provide the heat needed for cracking, although it is possible to tune the anode utilization of the fuel cell so that the exhaust stream from the fuel cell has enough heating value from the unconsumed hydrogen to supply the required heat if burned. The reformer efficiency, measured as the fraction of product hydrogen that does not need to be burned, is at most 70% and the system cannot be run dead-ended, so that there is a 15% anode utilization penalty.[44]

Fuel cell company Analytic Power has created an ammonia reforming system called the "A-Cracker". The system weighs 6 lbs, and has dimensions of 4" x 2.5" x 12", and operates at 60% efficiency (overall anode utilization efficiency of 51% due to incomplete consumption of hydrogen at the anode). The system consists of a dissociator, hydrogen burner, and regenerator for recycling heat. The maximum flow rate is 6 standard liters of ammonia per minute, which translates to 0.0040 net moles/s of hydrogen (enough hydrogen for a 500 W_e alkaline fuel cell).[45]

For 5.9 kW, and assuming a lack of economies of scale, the reformer would require 33 kg of equipment with a volume of 22 L in addition to storage of the ammonia. The ammonia itself would take up about 2.2 kg and 3.7 L not including the tank itself. The system mass would be 35 kg and 26 L, for quite poor system hydrogen densities of 0.57 wt% and 7.7 g/L.

A major problem is the undissociated ammonia concentration in the product gas. Although the concentration is less than 50 ppm, this is still enough to damage fuel cells with acid electrolytes, so an acid scrubber is needed to remove the final traces of ammonia gas from the cracker. Also, ammonia is toxic; spills and evaporative emissions could be dangerous in a different way than gasoline or hydrogen spills, as inhaled ammonia damages the lungs.

Ammonia infrastructure exists for agricultural (fertilizer) use in many areas of the world. Ammonia sells for roughly $1 per pound.[46] As a fuel, this makes is extremely expensive: at 120 MJ/kg of hydrogen lower heating value and 50% reforming efficiency, this is equivalent to a cost of 205 $/GJ of hydrogen lower heating value, about ten times the cost predicted for hydrogen reformed from hydrocarbons in large centralized plants. This expense means that ammonia cannot be considered a viable option for scooters.

3.2.1.4 Chemical hydride energy storage

Hydrogen fuel can also be produced by chemical reaction with solid “chemical hydrides”. This technique lies somewhere between the metal hydrides and reforming, but is included here in the reforming section.

Chemicals like lithium hydride, lithium aluminum hydride, and sodium borohydride can be

combined with water to evolve hydrogen gas (exothermically):

$$LiH + H_2O \rightarrow LiOH + H_2$$

$$(\Delta H = -312\ kJ \bullet mol^{-1}\ LiH)$$

$$LiAlH_4 + 4\ H_2O \rightarrow LiOH + Al(OH)_3 + 4\ H_2$$

$$(\Delta H = -727\ kJ \bullet mol^{-1}\ LiAlH_4)$$

$$NaBH_4 + 4\ H_2O \rightarrow NaOH + H_3BO_3 + 4\ H_2$$

These compounds are lighter than the reversible metal hydrides, and release more hydrogen because hydrogen is liberated from the water reactant. The three example chemical hydrides and their hydrogen storage capabilities are reproduced below.

Table 3.6 Chemical hydride comparison

	LiH	**$LiAlH_4$**	**$NaBH_4$**
hydrogen-to-hydride ratio (wt%)	25.2%	21.1%	21.3%
hydrogen-to-hydride plus stoichiometric water ratio (wt%)	7.7%	7.3%	7.3%
hydrogen-to-system ratio (wt%), assuming 20% additional weight	6.4%	6.1%	6.1%
mass of hydride powder needed for 250 g hydrogen output	980 g	1177 g	1173 g
cost for mass of hydride given above (laboratory-scale pricing)	$268	$503	$178

Data is from Browning *et al*,[47] with the exception of cost information which is from laboratory catalogs: Aldrich for the $LiAlH_4$ and Alfa Aesar for the others.[48,49]

The weight fraction is much higher, and the system requirements for containment are much less since the partial pressure of hydrogen over the hydride is low (1-10 atm). Browning *et al* estimate an extra 20% "for the weight of the hydrogen and water cylinders, mixing device and control valves." For example, for the LiH to produce 250 grams of hydrogen, 0.98 kg of powdered hydride and a 2.2 kg tank of water would be needed. An additional 200 g of control and mixing systems would be needed.

Packaging the chemical hydrides in small subunits would make fuel distribution easy; if properly and safely contained, they could even be sold in convenience stores. Containment is not a trivial problem; the hydrides must be protected from water in liquid or vapour form that might cause an extremely exothermic reaction and ignite the released hydrogen. One other issues is that the scooter accumulates hydroxides which must be collected and safely disposed of, or better, reprocessed. Finally, the *less* exothermic of the two reactions, that for $LiAlH_4$, produces 182 kJ of heat per mole of H_2 released. At maximum fuel cell power, when 0.05 moles of hydrogen are consumed every second, over 9 kilowatts of heat are generated! This is an enormous amount which exceeds that produced by the fuel cell itself, and makes for a large heat rejection problem.

As for cost, the prices are currently for small quantities of chemicals (2 kg maximum) produced at high (>95%) purity for experimental purposes. If chemical hydrides were actually to be used for vehicles, this price would have to decrease significantly. Also, the waste solution left after the reaction would be reprocessed and the cost would be expected to be lower than that for manufacturing a fresh batch of chemical hydride powder.

This type of technology is not well developed and tall barriers of cost and safety must be overcome if chemical hydrides are to be seriously considered for hydrogen vehicles. The exothermicity of the

reaction appears to be wasted in the scooter, where the primary purpose of heat management is to get *rid* of heat. They do offer the tempting possibilities of extremely high energy densities and easy distribution in convenient units.

3.2.2 Direct hydrogen storage

An alternative to reformers and chemical hydrides is to store fuel directly in the form of hydrogen. This is easier in terms of system complexity, and the expense of producing the hydrogen is offloaded to central processing plants where hydrogen can be produced from chemical reforming of natural gas or other fossil fuels.

3.2.2.1 Safety

Hydrogen is often thought of as dangerous fuel. This is partly true; unlike gasoline and most hydrocarbons, which only ignite over a narrow range of fuel-to-air ratios (for example, about 1.3 - 7.1% for gasoline), hydrogen can ignite over a wide range of concentrations (4% - 75% in air).[50] Also, hydrogen has a relatively low ignition energy; a low-energy spark can begin an almost invisible flame (0.2 mJ at stoichiometric conditions in air, less than 10% of the ignition energy of methane, propane, or isooctane.[51])

Figure 3.7 Ignition energy of hydrogen

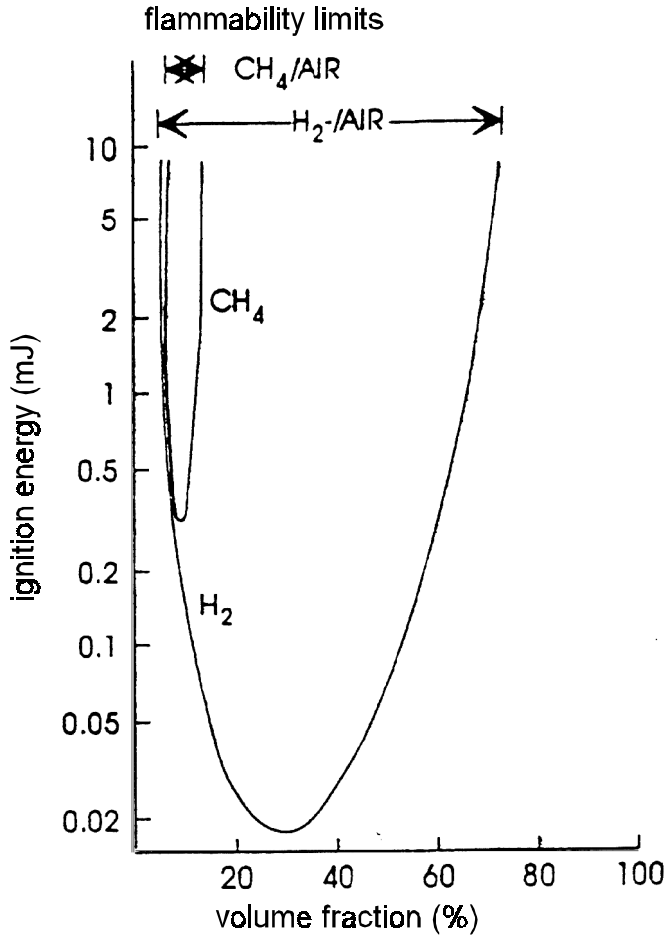

Data from Fischer[52]

On the other hand, hydrogen is a very light atom, and leaks tend to disperse quickly. Being lighter than air, hydrogen also tends to diffuse upwards rather than accumulate near the ground. (This benefit could be a problem in indoor situations where the ceiling traps hydrogen). The lower limit of flammability is higher for hydrogen than it is for gasoline, so greater concentrations of hydrogen have to build up before ignition is reached.

Slow leaks in enclosed areas were defined as the greatest risk by a thorough hydrogen safety study done by DTI for Ford and the Department of Energy.[53] Odorants could be added to hydrogen in the same way that they are added to natural gas, except that most sulfur-containing compounds poison platinum catalysts; also, only pure hydrogen can be used in dead-ended systems, because other substances would accumulate in the blocked supply channel.

Scooters in Asia are often driven in a fashion that would be considered reckless in North America. As with gasoline scooters, there is some risk of fire or explosion from a collision; neither gasoline nor hydrogen scooters would be as safe as battery-powered scooters. Safety devices can be designed to shut down power to the battery and cut off hydrogen flow in the case of a collision. Fortunately, the risks are far lower than for automobiles which, due to a combination of their lower fuel economy and greater range, carry about fifteen to twenty times as much fuel. Also, as later modeling will show, fuel cell scooter economy is three or four times that of the equivalent gasoline-powered scooter, so the total energy carried onboard is reduced by 66%-75%.

The following sections describe metal hydride storage and compressed gas cylinders, two forms of easily refillable direct hydrogen storage.

3.2.3 Metal hydride energy storage

Metal hydrides, which are formed when metal atoms bond with hydrogen to form stable compounds are a good option. Although metals are rather heavy for hydrogen storage, they can uptake a large amount of hydrogen per unit volume so storage density is good. They are typically used as powders in order to maximize the surface area to mass ratio; these metal powders are stored in (low) pressure vessels. Metal hydrides suffer from the problems of high alloy cost,

sensitivity to gaseous impurities, and low gravimetric hydrogen density.

Hydrides have the inherent advantage of being endothermic when releasing hydrogen, increasing safety; in addition, the hydrogen is kept at a relatively low pressure of 1-10 atm within the metal hydride containment cylinder. If the containment vessel is not properly designed, hydrogen embrittlement of the vessel itself is a factor, though, and certain metal hydrides are pyrophoric: they can burn.

3.2.3.1 Thermodynamics

The metal hydride adsorption reaction is:

$$M + (x/2)\ H_2 \rightarrow MH_x \quad \text{(exothermic; } \Delta H<0)$$

where the number of hydrogen atoms "x" per metal atom "M" is a function of the chemistry of the metal. The exothermicity of the reaction means that more heat causes the equilibrium to shift towards free hydrogen gas, and higher partial pressure of H_2 causes a shift towards adsorption and metal hydride formation. The law of mass action shows that the equilibrium constant is $K_{eq} = [H_2]^{(-x/2)}$, and substituting this into the free energy equation illustrates how hydrides are classified.

$$\Delta G = -RT \ln K_{eq} = (x/2)\ RT \ln (P_{H2}).$$

A hydride with a high heat of reaction ΔG has a lower equilibrium pressure of hydrogen over the metal / metal hydride system at a given temperature, and a stronger metal-hydrogen bond. For a metal to be a useful storage medium for hydrogen, it must easily (strongly) bond to hydrogen so that it can be charged up, but the bond cannot be too strong or else the metal will not give up its hydrogen under depressurization/heating.

Hydrogen uptake shows a characteristic plateaued curve when plotted for isothermal conditions. At low pressures, hydrogen fills the metal structure in interstitial sites as a solid solution. As more hydrogen is injected, the metal begins a phase transition from the α (metal) phase to the β (metal hydride compound) phase. This is the constant-pressure plateau phase of the isotherm. Above the plateau, the hydrogen concentration can still increase as other compounds begin to form with more hydrogen than the nominal ratio; also, more and more hydrogen molecules compress into the macropores.

Figure 3.8 Metal hydride adsorption curve

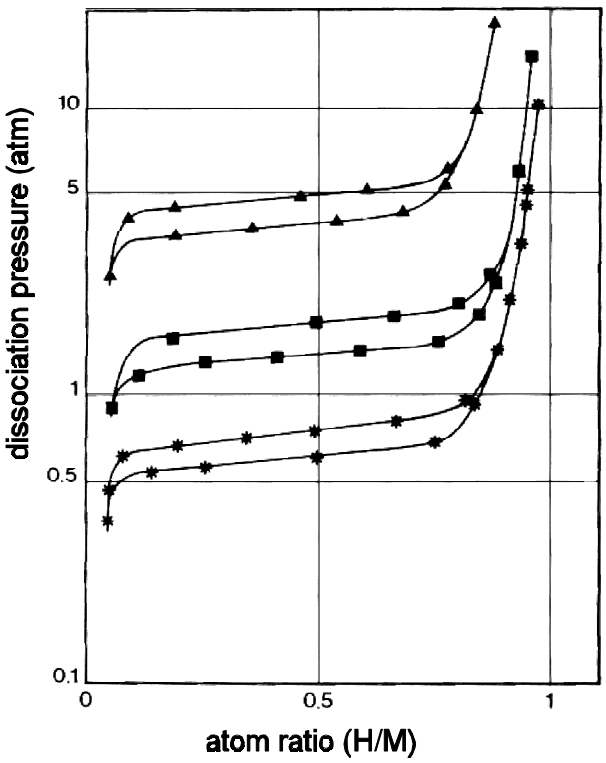

Typical metal hydride isotherms for a single metal hydride compound ($LaNi_{4.7}Al_{0.3}$) at various temperatures: (✳) at 30°C, (■) at 50°C, (▲) at 80°C. Data from Percheron-Guégan and Welter.[54]

Since the desorption process is endothermic, raising a given hydride to a high temperature at a fixed pressure shifts the equilibrium towards more gaseous H_2, while a low temperature means that more gaseous H_2 is adsorbed. At a constant temperature, the removal of gaseous hydrogen will causes the equilibrium to shift to release more hydrogen from hydride form. This latter situation essentially describes how metal hydrides are used in practice.

Hydrides are also sensitive to contaminants (some are poisoned by oxygen or water vapour) so care must be taken to only introduce pure hydrogen to the hydride.

3.2.3.2 Kinetics

The use of metal hydrides as a storage medium for hydrogen is dependent not only on thermodynamics but on kinetics. Fortunately, the intrinsic kinetics of hydrogen dissociation are fast; the rate determining step in general is heat transport into the powder. Powders generally do not conduct heat well, and metal hydride powders are no exception with a thermal conductivity in the range of 1-2 $W \bullet m^{-1} \bullet K^{-1}$.[55] For comparison, copper, one of the best thermal conductors, has a conductivity of 401 $W \bullet m^{-1} \bullet K^{-1}$, window glass is at 1.0 $W \bullet m^{-1} \bullet K^{-1}$; and fiberglass, a thermal insulator, has a thermal conductivity of 0.05 $W \bullet m^{-1} \bullet K^{-1}$.[56]

Heat typically needs to be transferred between the walls of the pressure vessel and the powder. While high surface area means fast hydrogen adsorption and desorption, it also means smaller powder particles, which conduct heat more poorly. Schemes thought of to improve conduction include embedding the metal hydride in aluminum foam with high-porosity arteries, or running channels holding hot liquid through the powder. This can increase net thermal conductivity to as much as 7-9 $W \bullet m^{-1} \bullet K^{-1}$.[57]

Also, hydrogen tends to embrittle the particles and cause them to crack into smaller pieces. This increases the total surface area of the powder, increasing the hydrogen desorption/adsorption rate, but the smaller hydride particles can be entrained in the gas flow, requiring filtering to keep the particles out of the hydrogen output. This leads to concerns about metal hydrides' long term usage.

It might be useful to have some kind of hydrogen storage reservoir between the metal hydride and the fuel cell, in order to damp out peaks and valleys in the hydrogen consumption rate that are lagged by heat transfer into the metal hydride. Fortunately, the gas above the metal hydride in the container can serve this purpose. Transient response time is thus fast, although extended flow rate will depend on the hydrogen desorption rate which in turn is controlled by heat input into the powder.

3.2.3.3. Classification

Metal hydrides are classified by the temperature at which the plateau partial pressure of hydrogen (H_2) above the metal hydride is greater than 1 atm. The two broad divisions are low-temperature metal hydrides, which have partial pressures of more than 1 bar below 100°C, and high-temperature metal hydrides, which generally require temperatures of over 200°C to exceed 1 bar of partial pressure. Some sample specifications are presented below. The data were taken from Browning *et al*,[58] and a DTI report on hydrogen storage.[59]

Table 3.7: Theoretical performance of various metal hydrides

	low-temperature		**high-temperature**
	$FeTiH_{1.9}$	**$LaNi_5H_{6.7}$**	**MgH_2**
H_2 storage by weight	1.75%	1.43%	7.60%
Density of metal hydride	5.47 $g \cdot cm^{-3}$	6.59 $g \cdot cm^{-3}$	1.40 $g \cdot cm^{-3}$
H_2 storage by volume	101 g/L	93 g/L	106 g/L
Heat of desorption ΔH ($kJ \cdot mol\ H_2^{-1}$)	-28.0	-8.9	-74.0
Dissociation temperature	50°C	50°C	290°C
Desorption pressure at given temp.	10 atm	4 atm	1 atm
DTI estimates of cost	8.80 $/kg	–	6.60 $/kg

The chart demonstrates hydrides' excellent volumetric densities but only average weight densities. For vehicle applications, the low temperature hydrides are favoured because the hot exhaust gas from a fuel cell (80°C) can be coupled to the fuel storage system to supply the heat input required for hydrogen evolution; alternately, the fuel cell coolant can be circulated through the metal hydride to dissociate hydrogen from the hydride. High temperature hydrides have perhaps four times the hydrogen weight fractions of low temperature hydrides, but would require the use of burners or other heating devices to reach the 300° needed for 1 atm of hydrogen partial pressure.

For scooters, weight, volume, and safety are the most important concerns. Note that Browning *et al*[?] estimate that the hydride storage container and heat exchange equipment will halve the storage density of metal hydrides; Michael Le of NASA estimates the extra equipment at an extra 50% weight[60]. The latter assumption is used here.

3.2.3.4. Metal hydride performance

To compare practically achievable systems, three estimates are made based on existing hydride systems and projections of future performance.

First, Mazda's 20 kW fuel cell electric vehicle, the Demio, runs on an unspecified metal hydride divided into eight modular units. It carries approximately 1.1% hydrogen by weight in the metal hydride (1.4% in the hydride itself, but an extra factor of 1.25 is needed to account for the pressure vessel and attachments), with a volumetric density of 40 g/L. The discharge rate of 0.48 grams per second is enabled by heat transfer from fuel cell cooling water. At 120 MJ/kg LHV for hydrogen, this is a LHV power rate of 57.2 kW, and with an estimated 50% fuel cell efficiency the maximum

electricity output rate is 28.5 kW: the quoted 20 kW plus some margin. Total storage is 1.3 kg of hydrogen, for a range of 170 km.[61,62,63,64]

The second estimate is made from characteristics of the metal hydride and cost predictions. If the raw alloy has the storage properties of TiFe as listed in Table 3.7, then to carry 250 grams of hydrogen would require 14.3 kg of hydride and 2.5 L. For raw TiFe alloy, DTI estimates a mass-produced cost of 9 $/kg[65], for a total alloy cost of $100. Assuming that the container and subsystems add 50% to cost, weight, and volume yields final results of 3.7 L, 21.4 kg, and $190. For "retail" pricing this is doubled to $380.

For the third comparison, Ergenics offers today a metal hydride hydrogen supply called the ST-90. By default, this system can supply hydrogen at 30 psig at room temperature at a rate of 28 standard liters/minute (0.019 g/s). The system uses "Hy-Stor 208" alloy, with formula $MmNi_{4.5}Al_{0.5}$ (Mm stands for *mischmetal*, a slightly variable mixture of a number of rare earth elements: approximately, 50% cerium; 32-34% lanthanum; 13-14% neodymium; 4-5% praesodymium; 1.5% other rare earths.[66]) The system is made of stainless steel and is generally sold as one-off units for test and research purposes at a cost of approximately $10,000.[67] (It should be noted that Ergenics sells the raw Hy-Stor 208 alloy at a cost of 204 $/kg, accounting for a significant portion of the ST-90 cost.[68] In fact, a Ergenics representative estimated that with a switch from small-scale processing for research purposes to factory manufacturing, costs would be as low as 30 $/kg.[69]) If designed for custom applications, the transfer rate can be increased to 0.04 g/s by raising the desorption temperature to 45°C (by a warm water bath, for example), and the weight can be reduced to 27 kg by switching to an aluminum design. Costs on the order of $3,500-$4,000 for production in the hundreds is estimated by Ergenics representatives.[70] For true mass production, the costs would drop dramatically, but prediction of costs becomes difficult.

The three predictions are compared below, for predicted system capable of carrying 250 grams of hydrogen and a currently-available hydride system sized at 204 grams.

Table 3.8 Metal hydride systems comparison

	Ergenics ST-90 (aluminum)	**scaled-down Demio hydride**	**DTI prediction: scaled-up FeTi**
Status	available for sale and use in labs	for vehicle demonstration	projection of future performance
H_2 storage capacity	204 g	250 g	250 g
system weight	27 kg	22.6 kg	21.4 kg
system volume	14 L (2' x 1' x 3")	6.2 L	3.7 L
system H_2 storage by weight	0.76%	1.11%	1.17%
system H_2 storage by volume	15 g/L	40 g/L	67 g/L
cost	$3,500 (short term)	data not released	$380 (long term)

Extrapolating the Demio hydride down to 250 grams should not bring up nonlinear scaling issues, since the system is already designed in eight modular containers. The DTI prediction estimates long term cost, while the Ergenics ST-90 represents currently available technology at lab bench scale prices.

Metal hydrides were used in some demonstration fuel cell vehicles but due to their weight and expense are not being considered for the first wave of fuel cell vehicles. On the other hand, small, highly fuel-efficient vehicle like a scooter may be able to take advantage of the safety and low-volume benefits of metal hydrides.

3.2.4 Compressed gas storage

One of the less exotic but most practical of the methods of storing hydrogen is to simply compress it as a gas. This increases its density. The major concerns are the large volume required to store the gas even when compressed, and the ability of the container to resist impact.

Storage conditions are set at 3600 psi (standard for natural gas cylinders) at ambient temperature (300° K). 5000 psi cylinders have been suggested for greater storage density, but a more conservative option was chosen here. The Redlich-Kwong equation of state below predicts a molar volume of 0.117 L/mol under these conditions, 16% worse than the 0.101 L/mol calculated by the ideal gas law.

$$\left(P + \frac{a}{V_m (V_m + b) T^{\frac{1}{2}}} \right) (V_m - b) = RT$$

V_m is the volume per mole, R is the ideal gas constant, and P is the pressure. a and b are empirical constants that can be estimated by the formulas

$$a = 0.42748 \bullet R^2 \bullet T_c^{2.5} / P_c$$

$$b = 0.08664 \bullet R \bullet T_c / P_c$$

where T_c is the critical temperature, P_c is the critical pressure, and R is the ideal gas constant.

The amount of work required to compress the hydrogen gas into the cylinder means that there is an energy penalty of approximately 5-10%. The temperature increases when the hydrogen cylinder is

filled with compressed hydrogen, and the pressure is higher than the nominal operating pressure until the cylinder has a chance to cool; care must be taken not to overpressurize the cylinder. The decrease in temperature during usage due to expansion of hydrogen is not as great a concern, because the release rate is much slower.

Current hydrogen gas storage containers are made from steel alloys that are resistant to hydrogen embrittlement; more advanced cylinders made from aluminum and wrapped with carbon fibre laminate for stiffness are lighter and currently used to contain both natural gas and hydrogen. Less well developed are fully-composite cylinders made solely from carbon fibre impregnated with resin or some other binder; these can have hydrogen gravimetric densities of as much as 9.5% due to their light weight. However, they are more fragile and currently expensive.

3.2.4.1 Cylinder performance

Dynetek of Calgary currently produces a range of aluminum/carbon cylinders for hydrogen storage. Although the smallest size they manufacture holds 50 L "water volume" (i.e. internal volume), a representative from Dynetek estimated that a cylinder 380 mm long, with 325 mm outside diameter and an internal volume of 20 L could be made Such a system would weigh 11 kg and have an external volume of 31.5 L. Price would be very dependent on quantities but a Dynetek representative estimated 18-20 $/L.[70] This system would contain 344 grams of H_2 at the 0.117 L/mol discussed previously. The results are a mass fraction of 3.1%, volumetric density of 10.9 grams $H_2/L_{external}$, and a cost of $360. This is a good hydrogen mass fraction, and low-priced for something available today, but poor in terms of volume.

An aerospace-quality gas sphere made by Lincoln Composites weighs 2.4 kg and takes up about

15 L, and holds 8.0 L of internal volume at 3600 psi for a storage density of 5.4 wt%. Two spheres would hold 270 grams of hydrogen at a total weight of 4.8 kg and a volume density of 14.0 g H_2/L. This is an exceptionally low weight, but 30 L is relatively bulky and fitting two ten-inch spheres in a scooter chassis might be difficult; worse, costs for this aerospace-standard pressure vessel begin at $5,500 per sphere.[71,72] Where this information is most important is in showing what technical performance is possible.

The smallest natural gas vehicle tank supplied by Lincoln Composites is listed in the table below; it has poorer gravimetric density but is much cheaper at an estimated cost of $900.[73] Also considered is a pair of carbon composite cylinders from Luxfer Composites.

A final comparison product is an all-metal cylinder. Air Products' size "C" aluminum cylinder weighs 15 kg and holds 15.8 L of internal volume. The cylinder is 84 cm long and 18 cm in diameter (21.4 L external volume) - rather long for a scooter.[74] At its (low) maximum design pressure of 2216 psi, 177 grams of hydrogen can be stored. Hydrogen storage is thus at 1.2 wt% and volumetric density is 8.3 $g/L_{external}$.

The technologies are summarized below. Note that D. Browning *et. al*[75] calculate that pressure regulators add an additional 200 grams to the listed weights.

Table 3.9 Compressed gas options

manufacturer	**Air Products**	**Dynetek**	**Lincoln Composites**	**Lincoln Composites**	**Luxfer Composites**
model number	"C" model	custom	#220088-1	natural gas 23 L tank	L58C
material	aluminum	carbon w/ aluminum liner	carbon w/ aluminum liner	carbon-polymer	full carbon wrap
storage pressure	2213 psi	3600 psi	3600 psi	3600 psi	3600 psi
radius per unit	9 cm	16 cm	13.1 cm	11.7 cm	7.8 cm
length per unit	84 cm	38 cm	(sphere)	88.9 cm	47.0 cm
external volume	21.4 L	31.5 L	15 L	38.1 L	9.1 L
internal volume	15.8 L	20 L	8.0 L	23.0 L	6.0 L
number of units	1	1	2	1	2
total hydrogen storage	177 g	345 g	280 g	395 g	206 g
total filled weight	15.2 kg	11.3 kg	5.3 kg	17.2 kg	3.7 kg
wt%	1.2%	3.1%	5.5%	2.3%	2.7%
volumetric density (external volume)	8.3 g/L	11.0 g/L	9.4 g/L	10.4 g/L	11.4 g/L
current price per unit	$250-$300	$360	$5,500	$900	unknown

In terms of technological feasibility, 5.4% storage is possible, although not practical from a cost perspective. Volumetric densities on the order of 9-12 g/L define the range of possible cylinders, while the Dynetek cylinder is an example of the current commercially available, affordable state-of-the-art. Metal cylinders will likely be too heavy.

3.2.4.2. Cylinder safety

Natural gas cylinders are typically designed with pressure release devices (PRDs) to discharge the contents of the cylinder in case of fire. Because failure occurs by composite material degradation

rather than by pressure increase, most are eutectic switches designed to release when a certain temperature is reached. The concept of a rapid discharge of hydrogen (under five minutes) is somewhat disturbing, especially considering the fact that these devices are designed to operate when engulfed in flame. On the other hand, a controlled release of flammable hydrogen could very well be better than an abrupt cylinder failure and explosion.

A maximum cylinder lifetime of 15,000 cycles was defined in the standard proposed to the Canadian government by EDO Canada.[76] This would be enough for over 120 years of usage at 45 km per day and one recycle every three days. Thus, the problem of invisible fatigue flaws and microcracks is thus not as much of a concern as abrupt failure due to a collision.

Hydrogen cylinders are likely useful for short term fuel cell scooters, but metal hydrides offer advantages of compact volume and heat removal that are extremely valuable if metal hydride costs can be reduced.

3.2.5. Liquid hydrogen storage

Cryogenic technology and expensive well-insulated cylinders are required if the high volumetric density of liquid hydrogen is to be used. At 20 K and 0.1 MPa vapour pressure, 5.3 wt% H_2 is achievable. Even better, at this temperature liquid hydrogen density is 70 g/L, so carrying 240 grams of hydrogen would only require 3.4 L of liquid hydrogen. However, maintaining the hydrogen at such low temperatures is extremely difficult, with very good insulation, vacuum gaps, and liquid-nitrogen-cooled heat shields typically required. As well, the energy of reducing hydrogen to 20 K and then liquefying it is an important factor when considering liquid hydrogen storage. This energy can amount to an extra 33-40% of the total energy content of the hydrogen.[77]

Another problem is that as heat leaks slowly warm up the liquid hydrogen, more and more is converted into gas over the liquid. Unless this gas is allowed to escape, hydrogen buildup would eventually create leaks in the tank, so a minimum boiloff rate is required and to do this a pressure release valve is needed. A car left unattended for a long period of time would eventually lose all its hydrogen to this safety requirement.

Cryogenic storage for a small scale application like fueling a scooter is not feasible

3.2.6 Selection

The few practical options for storing hydrogen are summarized and considered below. First of all, liquid hydrogen storage is eliminated as being too expensive, difficult to handle, and inefficient for the low storage requirements of scooters, and chemical hydride storage is postponed until future developments demonstrate their practicality. This leaves methanol reforming, metal hydrides, and compressed gas cylinders.

The following table is a comparison of dimensions and weight of storage system required to carry 250 grams of hydrogen. For comparison, a gasoline tank in a scooter is about 5 L, contains approximately 3.7 kg of gasoline, and allows a range of 240 km at 30 km/h, while the battery used in the ZES 2000 scooter is 3.7 L and weighs 38 kg, but only provides 65 km of range at 30 km/h.

Table 3.10 Storage technology comparison

	HotSpot reformer + methanol	**Dynetek gas cylinder**	**DTI hydride (includes 50% system factor)**
dimensions	–	16 cm radius, 38 cm long cylinder	–
external volume (including tank)	9.4 L	31.5 L	3.7 L
total filled weight	11.1 kg + PROX	11.4 kg	21.4 kg
weight of fuel	1.75 kg CH_3OH (250 g H_2)	400 g H_2	250 g H_2
wt% of hydrogen in system	< 1.8%	3.6%	1.17%
system volumetric density	22 g/L	12.7 g / L	67 g/ L
estimated price	unknown	$360 (as of 1999)	$190 (long-term)

Due to their inherent safety, decent hydrogen gravimetric density, and excellent volumetric density, metal hydrides are a good choice for electric scooters. They offer an important side benefit, that of acting as a heat sink for waste fuel cell heat. One difficulty is refueling; since metal hydride tanks are likely to cost over a hundred dollars, swapping fresh packs for old is not likely to be a viable distribution model unless modular units can be made that satisfy a fraction of the refueling need. Refueling at hydrogen pumping stations, an inferior distribution option, is likely necessary but not impossible. On the order of five to fifteen minutes would be required to fill a small metal hydride container, with the fill rate dependent upon pressure and the rate at which at which the adsorption heat can be removed.[78]

Compressed gas cylinders at 3600 psi are a more well-established technology, but they have the drawbacks of lower safety and poor perception of safety. 31.5 L is likely extremely bulky for a scooter. Refueling would be done from hydrogen filling stations at much higher pressure than for

metal hydrides.

As for reforming, the technology for partial oxidation is well-established, but the final cleanup step required to reduce carbon monoxide from 0.5% to the few ppm required for fuel cell intake is not sufficiently developed to install in a scooter. Reformer technology is quite complex in terms of integrating the various heat and chemical flows, but if hydrogen distribution turns out to be a major stumbling block, reformers would be a fallback option.

References for Chapter 3

1. Supramaniam Srinivasan, personal communication, July 1998

2. Supramaniam Srinivasan, B. B. Davé, K. A. Murugesamoorthi, A. Parthasarathy, and A. J. Appleby "Overview of Fuel Cell Technology". Chapter 2 in *Fuel Cell Systems*, Eds. Leo J. M. J. Blomen and Michael N. Mugerwa. (Plenum Press: 1993), p. 39

3. Supramaniam Srinivasan, personal communication, June 17 1999

4. J. C. Amphlett, M. Farahani, R. F. Mann, B. A. Peppley, P. R. Roberge. "The operation of a solid polymer fuel cell: a parametric model" *Proceedings of the 26th Intersociety Energy Conversion Engineering Conference* 1991 (Boston) pp. 624-629

5. Frano Barbir. Energy Partners. "Operating Pressure and Efficiency of Automotive Fuel Cell Systems" No date. 1997 or later.

6. Arvind Parthasarathy *et al*., p. 103

7. Embrecht Barendrecht, "Electrochemistry of Fuel Cells", Chapter 3 in *Fuel Cell Systems*, Eds. Leo J. M. J. Blomen and Michael N. Mugerwa. (Plenum Press: 1993) p. 94

8. Supramaniam Srinivasan, Fuel Cell Tutorial, August 13 1998.

9. Rioji Anahara. "Phosphoric Acid Fuel Cell Systems", Chapter 8 in *Fuel Cell Systems*, Eds. Leo J. M. J. Blomen and Michael N. Mugerwa. (Plenum Press: 1993) p. 306-307

10. Fritz R. Kalhammer, Paul R. Prokopius, Vernon P. Roan, Gerald E. Voecks. State of California Air Resources Board. *Status and prospects of fuel cells as automobile engines: a report of the fuel cell technical advisory panel*. July 1998. p. III-17

11. *ibid*, p. III-6

12. *ibid,* p. III-17

13. Michael N. Mugerwa and Leo J. M. J. Blomen. "System Design and Optimization", Chapter 6 in *Fuel Cell Systems*, Eds. Leo J. M. J. Blomen and Michael N. Mugerwa. (Plenum Press: 1993) p. 215

14. Hugo Van den Broeck, "Research, Development, and Demonstration of Alkaline Fuel Cell Systems", Chapter 7 in *Fuel Cell Systems*, Eds. Leo J. M. J. Blomen and Michael N. Mugerwa. (Plenum Press: 1993) p. 245

15. Zevco web site. "Zevco News - The Millenium [sic] Taxi" http://www.zevco.com/news/taxi1.html. Accessed June 14, 1999

16. Srinivasan Supramaniam, personal communication August 1998

17. S. R. Narayanan, Jet Propulsion Laboratory - Electrochemical Technologies. "Factors Affecting Design and Performance of Direct Methanol Fuel Cell Systems" Presentation at *Fuel Cells for Transportation TOPTEC* March 18-19, 1998 Cambridge, MA

18. *ibid (Narayanan)*

19. Kalhammer, Prokopius, Roan, Voecks. p. II-24

20. *ibid,* p. III-7

21. *ibid,* p. II-24

22. Joan M. Ogden, Margaret Steinbugler, Thomas G. Kreutz. "Hydrogen as a fuel for fuel cell vehicles: a technical and economic comparison" Presentation at National Hydrogen Association 8th Annual Conference, Arlington, VA March 11-13, 1997

23. Franklin Lomax, Jr., Brian D. James, George N. Baum, C. E.. (Sandy) Thomas. Directed Technologies, Inc. "Detailed Manufacturing Cost Estimates for Polymer Electrolyte Membrane (PEM) Fuel Cells for Light Duty Vehicles". Prepared for The Ford Motor Company under Prime Contract No. DE-AC02-94CE50389 to the U. S. Department of Energy, Office of Transportation Technologies. August 1998, p. 2-2

24. Kalhammer, Prokopius, Roan, Voecks, p. III-23

25. Ballard Power Systems. "Ballard Fuel Cell Stack: Mark 700 Series" product data sheet. August 1998.

26. Peter A. Lehman, Charles E. Chamberlin, Ronald M. Reid, Thomas G. Herron. "Proton Exchange Membrane Fuel Cell". United States Patent number 5,879,826. March 9, 1999

27. Notes of Tom Kreutz from Alfred P. Meyer, International Fuel Cells. "Ambient Pressure PEM Systems" Talk during Fuel Cells for Transportation TOPTEC (SAE), March 18-19, 1998, Cambridge, MA.

28. Peter Lehman *et al.*, U. S. Patent 5,879,826

29. Lisa Fawcett, AMETEK. Personal communication, April 26 1999.

30. D. Picot, R. Metkemeijer, J. J. Bezian, L. Rouveyre. "Impact of the water symmetry factor on humidification and cooling strategies for PEM fuel stacks" in *Journal of Power Sources* **75** (1998) 251-

260

31. Peter Lehman *et al.*, U. S. Patent 5,879,826

32. Frano Barbir, Energy Partners, Inc. “Operating Pressure and Efficiency of Automotive Fuel Cell Systems”

33. Kalhammer, Prokopius, Roan, Voecks, p. E-3

34. Chris Yang, Princeton University Center for Energy and Environmental Studies, personal communication July 22 1999. The Department of Energy-sponsored research project is operated in conjunction with the Princeton University Chemistry Department.

35. Franklin Lomax Jr., personal communication April 9 1999

36. Ryan Cownden, Meyer Nahon. “Performance Modeling and Improvements of a Solid Polymer Fuel Cell System”. Proceedings, The Second International Fuel Cell Conference, February 5-8, 1996. Kobe, Japan.

37. L. E. Unnewehr, S. A. Nasar. *Electric Vehicle Technology*. (John Wiley & Sons, Inc: 1982) p. 52

38. Kalhammer, Prokopius, Roan, Voecks. p. II-11

39. J. H. Hirschenhofer, D. B. Stauffer, R. R. Engleman, M. G. Klett. Parsons Corporation. “Fuel Cell Systems”, Chapter 7 of *Fuel Cell Handbook* Fourth Edition. November 1998. p. 7-3

40. Kalhammer, Prokopius, Roan, Voecks. p. II-11

41. Kalhammer, Prokopius, Roan, Voecks p. III-39

42. Neil Edwards, Suzanne R. Ellis, Jonathan C. Frost, Stanislaw E. Golunski, Arjan N. J. van Keulen, Nicklas G. Lindewald, Jessica G. Reinkingh. Johnson Matthey Technology Centre. “On-board hydrogen generation for transport applications: the HotSpot™ methanol processor”. *Journal of Power Sources* **71** (Elsevier: 1998) pp. 123-128

43. Joan M. Ogden, Margaret M. Steinbugler, Thomas G. Kreutz. “A comparison of hydrogen, methanol and gasoline as fuels for fuel cell vehicles: implications for vehicle design and infrastructure development” *Journal of Power Sources* **79** (Elsevier: 1999) pp. 143-168

44. R. Metkemeijer, P. Achard “Comparison of Ammonia and Methanol Applied Indirectly in a Hydrogen Fuel Cell” in *International J. Hydrogen Energy* **19** (6) 1994, p. 535

45. Luyu Yang, David P. Bloomfield .Analytic Power Corporation. “Ammonia Cracker for Fuel Cells” *Fuel Cell Seminar 1998 Abstracts*, p. 296

46. Analytic Power web page, “Ammonia Cracker” http://www.analyticpower.com/NH3CRACK.html

47. D. Browning, P. Jones, K. Packer. “An investigation of hydrogen storage methods for fuel cell operation with man-portable equipment” *J. Power Sources* **65** (1-2) March-April 1997, pp. 187-195

48. Aldrich. *1998-1999 Catalog Handbook of Fine Chemicals.* $LiAlH_4$, p. 1010

49. Alfa Aesar. *Research Chemicals, Metals and Materials 1997-1998.* LiH, p. 317; $NaBH_4$, p. 512

50. Ed. Yuda Yurum. *Hydrogen Energy System: production and utilization of hydrogen and future aspects*. Proceedings of the NATO Advanced Study Institute on Hydrogen Energy System, Utilization of Hydrogen and Future Aspects, Akcay, Turkey, August 21 - September 3 1994. (Kluwer: 1994), p. 222

51. Irvin Glassman. Appendix G: Minimum Spark Ignition Energies and Quenching Distances, *Combustion*. Third Edition. (Academic Press: 1996)

52. M. Fischer. "Safety Aspects of Hydrogen Combustion in Hydrogen Energy Systems" *International Journal of Hydrogen Energy* Vol. 11 No. 9, pp. 593-601 quoted in C. E. Thomas, Directed Technologies, Inc. *Direct-Hydrogen Proton-Exchange-Membrane Fuel Cell System for Transportation Applications: Hydrogen Vehicle Safety Report*. Prepared for U. S. Department of Energy, Office of Transportation Technologies. Prepared by Ford Motor Company. May 1997

53. C. E. Thomas. Directed Technologies, Inc. *Direct-Hydrogen Proton-Exchange-Membrane Fuel Cell System for Transportation Applications: Hydrogen Vehicle Safety Report.* Prepared for U. S. Department of Energy, Office of Transportation Technologies. Prepared by Ford Motor Company. May 1997.

54. Annick Percheron-Guégan and Jean-Marie Welter. "Preparation of Intermetallics and Hydrides. Chapter 2 of *Hydrogen in Intermetallic Compounds I: Electronic, Thermodynamic, and Crystallographic Properties, Preparation.* Ed. Louis Schlapbach Topics in Applied Physics Volume 63 (Springer-Verlag, 1988) p. 35

55. G. Sandrock, S. Suda, Louis Schlapbach. "Applications", Chapter 5 in *Topics in Applied Physics Volume 67, Hydrogen in Intermetallic Compounds II: Surface and Dynamic Properties, Applications*. Ed. Louis Schlapbach (Springer-Verlag:: 1992), p. 204

56. David Halliday, Robert Resnick, Jearl Walker. *Fundamentals of Physics*. Fifth Edition. (John Wiley & Sons, Inc. New York: 1997). p. 470

57. Sandrock, Suda, Schlapbach. p. 205

58. Browning, Jones, Packer.

59. Brian D. James, George N. Baum, Franklin D. Lomax, Jr., C. E. (Sandy) Thomas, Ira F. Kuhn, Jr. Directed Technologies, Inc. "Comparison of Onboard Hydrogen Storage for Fuel Cell Vehicles" Task 4.2 Final Report. Prepared for Ford Motor Company under Prime Contract DE-AC02-94CE50389 "Direct Hydrogen Proton-Exchange-Membrane (PEM) Fuel Cell System for Transportation Applications" to the U. S. Department of Energy, pp. 4-56, 4-63, 4-52

60. Michael Le, NASA. Personal communication August 1998

61. Shinichi Hirano, Kenichiro Egusa, Chikara Iname. Technical Research Center (Yokohama), Mazda Motor Corporation. "Development of Electric Vehicle Powered by Polymer Electrolyte Fuel Cell System" Fuel Cell Seminar Abstracts 1998. pp. 730-733

62. Mazda Australia web site. "Mazda" http://www.mazda.com.au/corpora/460.htm Accessed June 17, 1999

63. Mazda Japan web page. 'Mazda Develops Fuel Cell Electric Vehicle, "Demio FCEV"' http://www.e.mazda.co.jp/Publicity/Public/9712/971203.html Accessed June 17, 1999

64. Mazda Japan web page. "From exiting [sic] engines to next generation vehicles" http://www.e.mazda.co.jp/Action/engine/main3.html Accessed June 28, 1999

65. James *et al*, p. 4-62

66. Y. Osumi, H. Suzuki, A. Kato, K. Oguro, M. Nakane. *J. Less-Common Met.* **74** (1980) pp. 271-277 in Annick Percheron-Guégan and Jean-Marie Welter, "Preparation of Intermetallics and Hydrides", Chapter 2 in *Topics in Applied Physics Volume 63, Hydrogen in Intermetallic Compounds I: Electronic, Thermodynamic, and Crystallographic Properties, Preparation.* Ed. Louis Schlapbach (Springer-Verlag:: 1988), p. 19

67. Ergenics web site. "ST-90 Metal Hydride Storage Unit" http://www.ergenics.com/st90.htm Accessed July 1, 1999

68. Ergenics web site. "Price List" http://www.ergenics.com/alloyPL.htm Accessed July 1, 1999

69. Dave Tragna, Ergenics. Personal communication, March 3 1999

70. Colin Armstrong, Dynetek. personal communication, October 5 1998

71. Lincoln Composites web page. "Pressure Vessels for Aircraft and Missile Applications" http://www.lincolncomposites.com/products/pv_details/space.html. Accessed June 1, 1999

72. Jack Schimenti, Aerospace/Defense business manager. Lincoln Composites. Personal communication June 1, 1999

73. Christine Simetich, Natural Gas Vehicle Tanks. Lincoln Composites. Personal communication June 1, 1999

74. Air Products web site, "Specialty Gas Cylinder Information" http://www.airproducts.com/specgas/cylind/cylind.htm

75. Browning, Jones, Packer.

76. EDO Canada Limited. *Compressed Hydrogen gas vehicle cylinder development* Transport Canada document TP 13023E. April 1997

77. Joan Ogden, Princeton University. Personal communication July 22 1999

78. *ibid.*

~

Chapter Four

Modeling and Design

~

This chapter describes how, utilizing the technology described in previous chapters, a fuel cell scooter may be designed. It leads from an analysis of performance requirements to a vehicle model to a systems design of the fuel cell stack and auxiliary systems. The model uses basic assumptions to obtain an overall measure of performance; parasitic power is a linear function of gross power, and conservative assumptions are made where data is poorly known.

Two additional options for improved performance and reduced cost, respectively, are considered: operation of the fuel cell at 3 atm pressure, and hybridization with peaking power batteries.

A different kind of scooter – a zinc-air battery-powered alternative – is considered as well because electric scooter manufacturers and researchers in Taiwan are extremely interested in this technology

4.1 Performance requirements

Despite the attraction they offer in the form of zero emissions, battery-powered electric vehicles have failed to capture significant market shares because they are inconvenient to recharge, and because they simply do not match the performance of existing alternatives. The important performance criteria are vehicle range before refueling, power, cost, and to a lesser extent vehicle weight.

The performance characteristics of a few sample vehicles with similar power needs are summarized here as a baseline for the fuel cell scooter; they range from ordinary gasoline scooters to prototype electric scooters to a much heavier demonstration fuel cell - powered golf cart which is included because it is virtually the only PEM fuel cell vehicle designed at the 4-6 kW power output level.

Note that the motor power quoted here is the mechanical power generated; battery or fuel cell output will typically be larger by a factor of 30% due to drivetrain losses.

Table 4.1. Performance of various vehicles of about 5 kW power

Vehicle	Fuel cell electric golf cart	Battery-powered electric scooter (NiCd battery)	Medium-sized two-stroke scooter	Battery-powered electric scooter (lead-acid)
name	Schatz "Personal Utility Vehicle"	Honda CUV ES	Honda Dio	Taiwan ITRI ZES-2000
maximum motor power	1.5 kW (4.0 kW fuel cell)	3.2 kW	5 kW	3.4 kW
range at 30 km/h cruise	24 km	35 km	240 km (5 L tank)	60 km
fuel efficiency at 30 km/h cruise	96 mpge	1000 mpge (46.2 km/kWh)	116 mpg	1300 mpge (60 km/kWh)
acceleration	–	0-200 m in 17.3 seconds	~0-50 m in 6 seconds	0-30 m in 4.5 seconds
maximum speed	20 km/h	60 km/h	~70 km/h	50 km/h
charging time	2 minute cylinder refilling	8 hours full recharge	5 minute gasoline refill	8 hours full recharge
hill climbing	–	–	–	15 km/h at 10° slope
curb weight	380 kg	130 kg	68 kg	105 kg

Taiwan data is from reports published by the Industrial Technology Research Institute[1]. Honda vehicle data are from a Society of Automotive Engineers of Japan paper and a paper published by the ITRI.[2,3] The Schatz Energy Research Center's Personal Utility Vehicle was documented in a 1998 Fuel Cell Seminar abstract, and the weight was from a data sheet for that E-Z Go 4Caddy electric golf cart.[4,5]

Performance measurements marked with tildes were for 50 cc scooters similar to the Dio as data were not directly available.

"curb weight" is the mass of the vehicle without passengers or cargo.

The unusual acceleration measurement (time required to cover a given distance) is a standard for scooters in Asia.

Note that the Dio's 5 kW engine is at the high end of 50 cc vehicles. Many 50 cc scooters have powers of 2-4 kW, while 125 cc scooters produce 6-9 kW of power.

"mpge" (miles per gallon equivalent) fuel economies for the non-combustion vehicles were

calculated by taking the total energy stored – whether as chemical energy in a battery or in terms of hydrogen lower heating value – and calculating how many gallons of gasoline would have to be burned to produce the same amount of heating value energy. This "on-vehicle" fuel economy is slightly misleading in that hydrogen and batteries tend to be higher grade carriers of energy; that is, it would take a large amount of energy from burned petroleum to store the same energy in hydrogen or battery form. Later wells-to-wheels fuel efficiency calculations will take into account the conversion losses.

Nakazawa *et al* claim that the Honda CUV-ES's 35 km range under an urban driving cycle is "sufficient for practical use."[2] Researchers from Taiwan's ITRI (Industrial Technology Research Institute) also claim that daily driving ranges are less than 25 km 68% of the time, and 70% of the daily driving *time* is less than one and a half hours.[6] But, as a point of comparison, a gasoline scooter of similar power (i.e. one with 50 cc displacement) achieves quadruple the range of even the best electric scooters when being driven at a steady speed of 30 km/h. A 35 km range may be enough for use, but electric scooters will never replace a third of two-stroke scooters if their competitors have four times the range with quicker refueling. A more reasonable set of requirements would be to preserve the same minimum acceleration characteristics, but to require that the range be at least 200 km. A range of over 240 km like the Dio is optimal, but probably not necessary and expensive in terms of dollars and volume.

The power of 4-6 kW is relatively high for a lightweight and small vehicle like the scooter, but this is due to the way in which scooters are driven under typical urban conditions. Bursts of rapid acceleration are used to dodge in between larger vehicles in congested traffic, and quick starts are often required when red lights turn green. Frequent decelerations and stops are needed in the city, and scooters are not often taken out on the highway for prolonged high-speed driving. Basically,

average speeds and average power are low, but peak power is high.

Mass is an important consideration too; a curb weight of approximately 130 kg approaches the limits of manageability for parking and unpowered handling.[7] Thus, the minimum requirements for the fuel cell scooter should be:

Table 4.2. Fuel cell scooter performance requirements

Specification	Fuel cell scooter
max motor power output	4-6 kW
range before refueling at 30 km/h cruising speed	200 km
fuel efficiency	> 100 mpge
acceleration	0-30 m in less than 5 seconds
speed on 15° slope	10 km/h
speed on 12° slope	18 km/h
maximum speed	60 km/h
maximum curb weight	140 kg

The slope climbing, acceleration, and maximum speed requirements are based on a Taiwan research lab electric scooter proposal, which in turn was based on surveys of scooter users.[8] (As a comparison point for the speed on inclines, San Francisco's Lombard Street wends up a hill with a 40°slope, although the twisting road itself is limited to 21°).

A broader list of electric scooters that are being developed now is included in Appendix A.

4.2 Vehicle modeling

Essentially, the purpose of vehicle modeling is to convert input parameters (performance measurements like desired range, driving cycle that must be sustained, and types of power and storage components) into the output parameters of curb weight, size of engine required, heating system design, cost, and convenience. The process is iterative; for example, the size of the cooling system is a function of the average vehicle power, but larger cooling system itself requires more power to drive the fans and pumps, increasing the power load, which necessitates more cooling.

4.2.1 Physical model

To properly simulate the performance of a fuel cell scooter, a computer model was created based on the physical properties of the scooter. This model calculates the instantaneous power required from a scooter's engine as it travels through various driving patterns, and derives various numerical performance characteristics: fuel consumed per kilometer of travel, maximum power during the driving cycle, average power during the driving cycle, amount of energy recovered in regenerative braking, and overall hydrogen-to-mechanical-work conversion efficiency.

For the MATLAB program listing, please see Appendix F.

This power is calculated as the dot product of the current velocity of the vehicle and the various forces acting upon it, divided by the motor and controller efficiency, plus the auxiliary power demanded by various lighting and control systems, plus "parasitic" power required by the fuel cell blowers and coolant pumps. The road is assumed to be level. There are several different physical

forces to consider: air resistance (drag); the rolling resistance of the wheels; the force of gravity, which is not necessarily perpendicular to the velocity if the vehicle is traveling uphill or downhill; and the normal force of the ground acting upon the vehicle. These forces must sum to zero if the vehicle is to be held at a constant velocity, or to a net forward acceleration times mass if the vehicle is to accelerate.

Figure 4.1 Free-body diagram of scooter

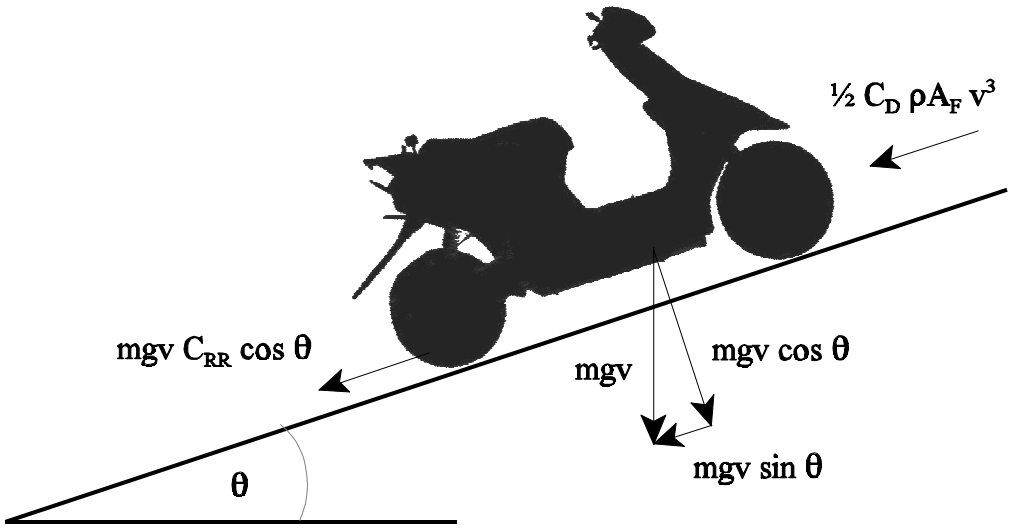

In the computer model used to simulate vehicle performance, the various power demands are summed to a total mechanical power P_{wheels} demanded "at the wheels" by the motion of the vehicle.

$$P_{wheels} = (ma v) +(mgv\sin\theta) + (mgvC_{RR} \cos\theta) + (½ \rho_{air} C_D A_F v^3)$$

The variables are listed below.

m = total mass of vehicle, passengers and cargo

θ = angle of slope

a = acceleration of vehicle

v = velocity of vehicle

C_{RR} = coefficient of tire rolling resistance.

ρ_{air} = density of air, approximately 1.23 kg•m^{-3}

C_D = drag coefficient

A_F = frontal area

The terms are described one at a time:

Acceleration term. If the acceleration is negative - that is, the vehicle is decelerating - the first term can be negative. If the overall expression for P_{wheels} is still positive even though the first term is negative, it means that energy must still be supplied by the power source to the wheels to maintain the desired deceleration rate, because the drag and rolling resistances are so large. If P_{wheels} is negative, then the motor can be driven as a generator to regenerate some of the energy expended. A battery capable of reabsorbing this energy is needed, and less than 70% of the kinetic energy is recoverable. This figure is reduced if rapid deceleration is required, because the battery can only charge up at a certain maximum rate.

Slope term. The second term is the force of gravity resolved opposite to the direction of motion.

Rolling resistance term. The coefficient of rolling resistance is a function of tire pressure and deformation, and is the ratio of rolling resistance force to the load on the tires; it is fairly constant for a given tire.[9] A perfectly rigid wheel on a rigid, flat surface would have no rolling resistance,

but minor deformations in the wheel and properties of the road cause deviation from ideal geometry and thus irreversible losses.

Aerodynamic drag term. The drag coefficient C_D is a dimensionless constant that attempts to capture, in one term, an object's resistance to flow. C_D can vary from as high as 1.2 for a bicycle with erect rider to 0.47 for a sphere to 0.20 for a very aerodynamically-styled modern automobile.[10] Although the equation used to determine the drag power is a simplification, it avoids complex air flow simulation while preserving the general behaviour of the drag force with respect to velocity. The frontal area used here was measured for the scooter by projecting a bright light parallel to the front of the scooter and then measuring the area of the shadow on a wall behind.[11] Typical values are listed in Table 4.3.

The inefficiencies in the system are applied afterwards to determine how much power must be put out by the power source:

$$P_{output} = (P_{wheels})/\eta_{drivetrain} + P_{auxiliary} + P_{parasitics}$$

$P_{auxiliary}$ = power needed by auxiliary systems - headlights, signal lights, dashboard, etc.

$\eta_{drivetrain}$ = efficiency of the electric motor and controller subsystem - 77%

$P_{parasitics}$ = parasitic power needed by fuel cell system - blowers, fans, etc.

The parasitic and auxiliary powers are electric power requirements so they do not go through the 77% efficiency loss. A more sophisticated model would not use a single value of $\eta_{drivetrain}$ but rather employ an efficiency map to determine electric motor efficiency as a function of wheel speed and torque.

Factors not accounted for in this model include: turning, where the velocity is not parallel to the acceleration / deceleration direction; wind blowing at an angle to the direction of motion; resistances in other parts of the scooter. Friction in the transmission and similar losses are assumed to be captured by the drivetrain efficiency of 77% above, discussed in section 2.1.4.

4.2.2 Modeling parameter selection

Vehicle modeling parameters for a typical scooter are listed below with data for other vehicles for comparison. Although most two-stroke scooters weigh about 80 kg, the presence of lead-acid batteries and/or fuel cell plus hydrogen storage brings the mass of an electric scooter up to approximately 130 kg as in the case of the Honda CUV-ES with NiCd batteries.

Table 4.3. Typical modeling parameters

Vehicle	C_{RR}	C_D	A_F (m^2)	curb weight (kg)	auxiliary power (W)
Electric Scooter	0.014	0.9	0.6	130	60
Roadster Bicycle	0.008	1.2	0.5	10	0
Motorcycle	unknown	0.6	0.8	300	unknown
Ford AIV Sable	0.0092	0.33	2.13	1291	500
PNGV Automobile	0.007	0.20	2.0	920	400

The PNGV Automobile properties are targets set out by the Partnership for a New Generation of Vehicles,[12] except for the rolling resistance and auxiliary power which were obtained from separate studies.[13,14] The Ford AIV Sable is a light weight "aluminum intensive vehicle", a modern mid-sized sedan.[15] Motorcycle data was obtained for some of the parameters.[16] Finally, the bicycle data is for a"roadster" upright model.[10]

The scooter coefficient of tire rolling resistance was estimated to be 0.014, based on measurements done at the Desert Research Institute[17], while the drag coefficient and frontal area were obtained

from researchers at the ITRI Mechanical Industry Research Laboratory.[18] A slight mass dependence (less than 6%) in the drag coefficient reported by the MIRL researchers was ignored, and the largest measurement taken; the velocity dependence of the rolling resistance coefficient was likewise neglected. Note also that in scooters and bicycles the product of drag coefficient and frontal area can vary dramatically, depending on how the driver sits on the scooter. The values chosen were assumed to be for the rider in a typical position.

The curb weight was set at 130 kg, which was 30 kg more than the ZES-2000 but equal to that of the CUV-ES electric scooter. This choice was made to ensure that performance requirements would be met even if the lower ZES-2000 weight could not be reached, whether due to the extra structural weight needed to support the heavier power system, or due to the weight of the components themselves. The driver weight is defined as 75 kg.

Auxiliary power: in a typical scooter, the head lights, tail lights, and dashboard total about 50 W; assuming that these lights are always on, and that the 26.4 W turn lights are on 30% of the time, yields an average load estimate of 60 W.[19]

4.2.3 Relative importance of various factors

Now that the parameters are defined, power requirements are calculated for (i) a scooter traveling at constant velocity at various slopes, and (ii) a scooter traveling with constant velocity at various speeds, and finally (iii) power required for various accelerations starting from 30 km/h. The total power shown below is the electric output from the power source including auxiliary power, but not subsystem parasitic loads (blowers, pumps, etc.) which are calculated later.

Figure 4.2. Cruising power required at various speeds.

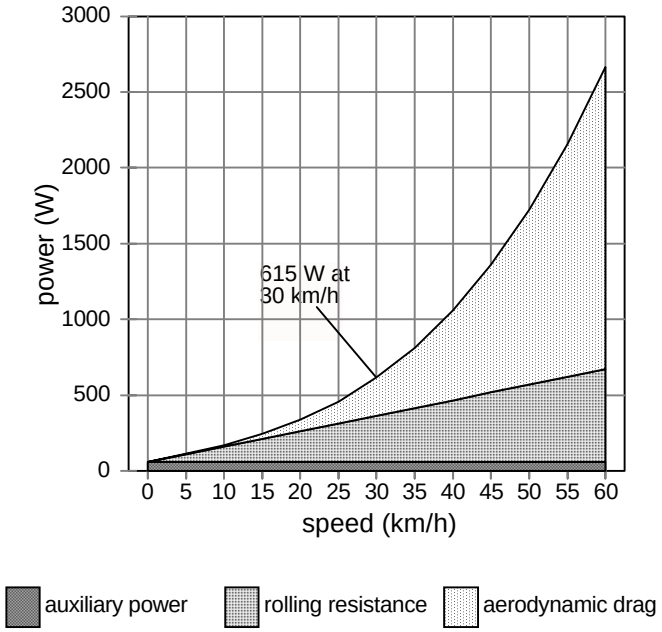

Figure 4.3. Power required to climb various slopes at 15 km/h

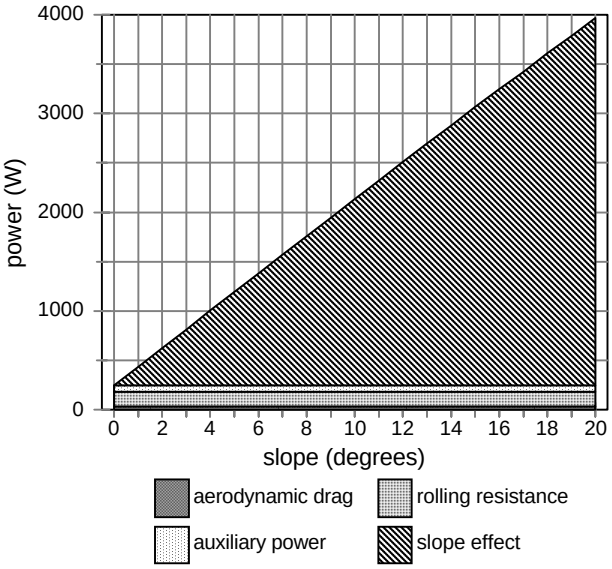

Figure 4.4 Power required for various accelerations from 30 km/h

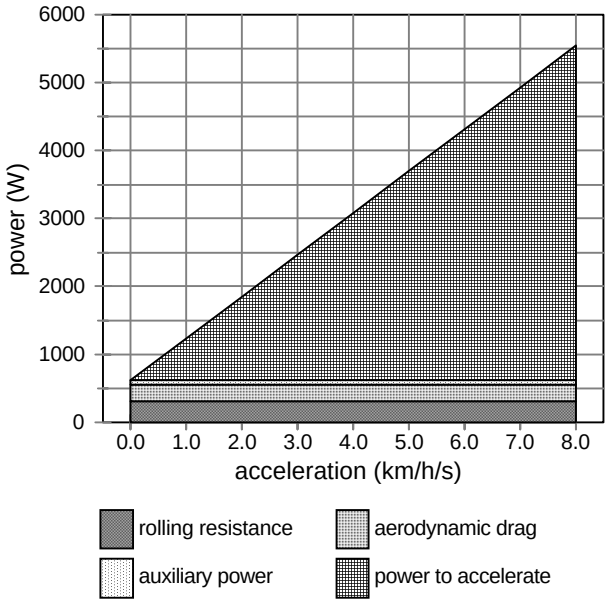

According to the model, continuous hill climbing as set out in the requirements (10 km/h at 15°, 18 km/h at 12°) require 2050 W and 3020 W out of the electric power source, respectively. Cruising at 30 km/h requires 615 W.

Due to the low speeds scooters are typically operated at, and the relative insignificance of the tire rolling resistance, the power needed for acceleration dominates the *maximum* power need. The effect of gravity on scooters traveling up a slope is also significant. In other words, for a scooter traveling on a level road and accelerating and decelerating in a typical stop-and-start urban driving cycle, the dominant term is *mav*, and the total power requirement is thus dominated by the mass of the scooter and the velocity/acceleration profile. Aerodynamic drag, which is not proportional to mass, tends to be a minor factor at the low speeds most scooters are driven at, especially in urbanized areas.

4.2.4 Validation

Some comparisons with others' results were provided to check the physical model. As in Figures 4.2 to 4.4, these results are for P_{output} *without* parasitic power, although they do include auxiliary power load and drivetrain efficiencies.

Table 4.4 Validation of physical model

	ITRI ZES-2000	DRI Sun Com	T. C. Pong requirements	This physical model
0 to 30 m in five seconds				2800 W
Maximum power (sustained for 5 seconds)	3800 W		3600 W	
Climbing a 15° hill at 10 km/h				2050 W
Climbing a 12° hill at 18 km/h	2160 W		2700 W	3020 W
Cruising at 50 km/h (sustained for 30 minutes)	1870 W		1800 W	1720 W
Cruising at 35.0 km/h		1200 W		810 W
Cruising at 30 km/h (sustained for 2 hours)	500 W		600 W	615 W
Cruising at 26.0 km/h		550 W		490 W
Cruising at 15.5 km/h		275 W		250 W
Cruising at 10.3 km/h		225 W		175 W

T. C. Pong, an electric scooter designer, listed a set of electric scooter power requirements for a 48 V motor system[20], while another set of data was measured from road tests of a Sun Com scooter by Arne LaVen of the Desert Research Institute.[21] The ITRI ZES-2000 results were from published papers.[22,2]

The physical properties of the other scooters were unknown but likely not more than 20% different from the drag coefficient, rolling resistance, and frontal area used in this study. A 77% drivetrain

efficiency was assumed for the ZES-2000, since these data were based on motor output; the other data points were from battery output measurements, and thus no drivetrain efficiency had to be assumed. The tabulated results are presented graphically below.

Figure 4.5 Validation of physical model

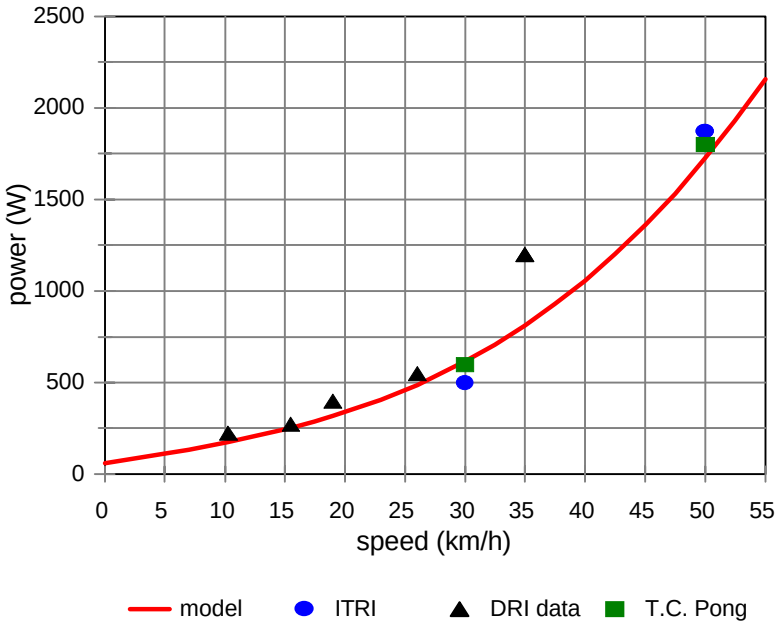

To verify the model in a different way, the cruising power of 615 W for 30 km/h was used to calculate average thermal efficiency if the drivetrain efficiency was also 77% for a mechanical system, and net fuel economy was 100 mpge as reported by various manufacturers. This means an average 9.5% thermal efficiency, a reasonable estimate for small two-stroke engines (As an example, a 34 cc engine designed for a blower, hedge trimmer, or chain saw has a peak thermal efficiency of 13.6%, or 20.6% for a prototype advanced stratified lean-burn design.[23])

If a 50% fuel cell conversion efficiency is assumed and parasitic losses are not included yet, then the equivalent fuel economy is 560 mpge; detailed analysis later will provide a more accurate result.

4.3 Driving Cycle

The main purpose of driving cycles, in the past, was to provide a schedule to put cars through to collect tailpipe emissions and, in the United States, to compute mileages for CAFE (Corporate Average Fuel Economy). Simulated driving patterns have high-power peaks that produce more emissions than a constant driving speed, and are more representative of actual driving behaviour. The typical procedure is to place the vehicle on a wheeled dynamometer and then to execute the driving cycle. Emissions are collected in a sampling bag and diluted with a predefined amount of air to obtain vehicle emissions in terms of grams per kilometer.

Typical automobile test cycles include the American FUDS (Federal Urban Driving Schedule), FHDS (Federal Highway Driving Schedule), and FTP (Federal Test Procedure 1975). American motorcycles are tested using a modified version of FTP ("mFTP"), with one part scaled down for motorcycle with engines less than 170 cc, so that the maximum speed is reduced from 91 km/h to 59 km/hr. Another method for testing motorcycles is the ECE-40 (Economic Commission for Europe) test procedure, which employs a much simpler and more abstracted driving cycle. Low acceleration rates and lack of transients mean that pollution is generally underestimated.

Figure 4.6 mFTP: modified Federal Test Procedure

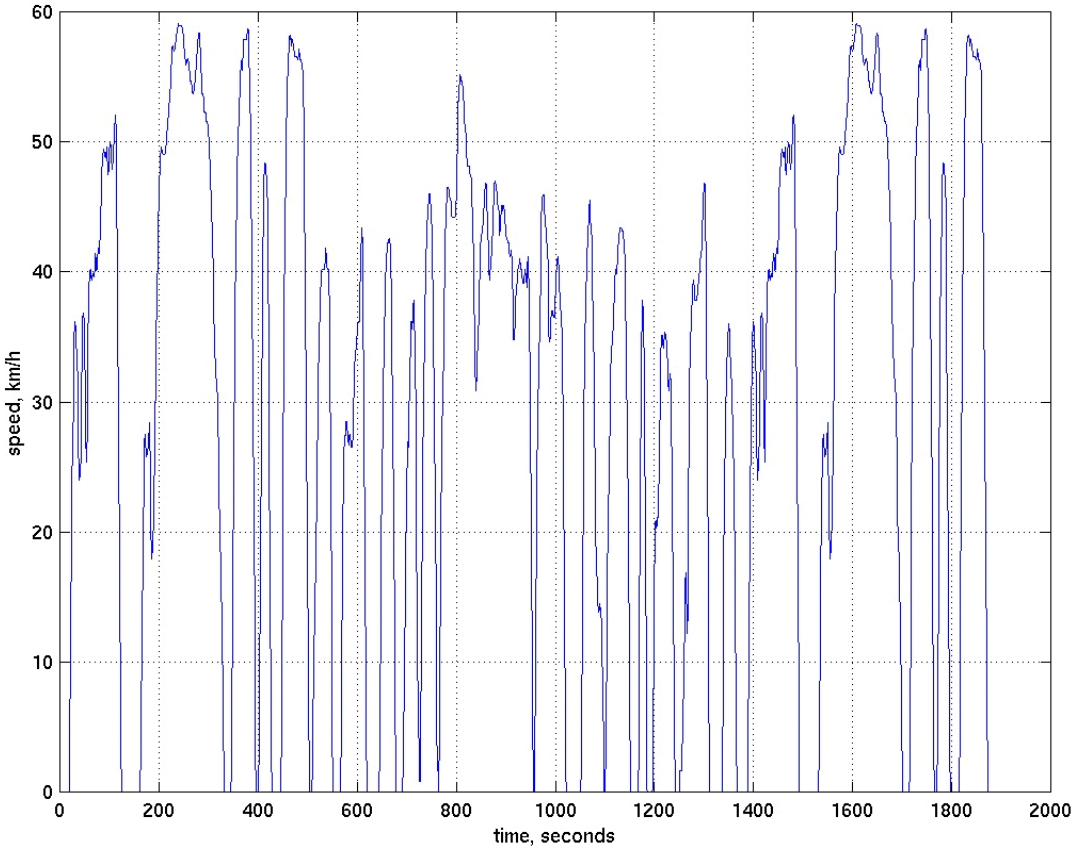

Figure 4.7 ECE-40

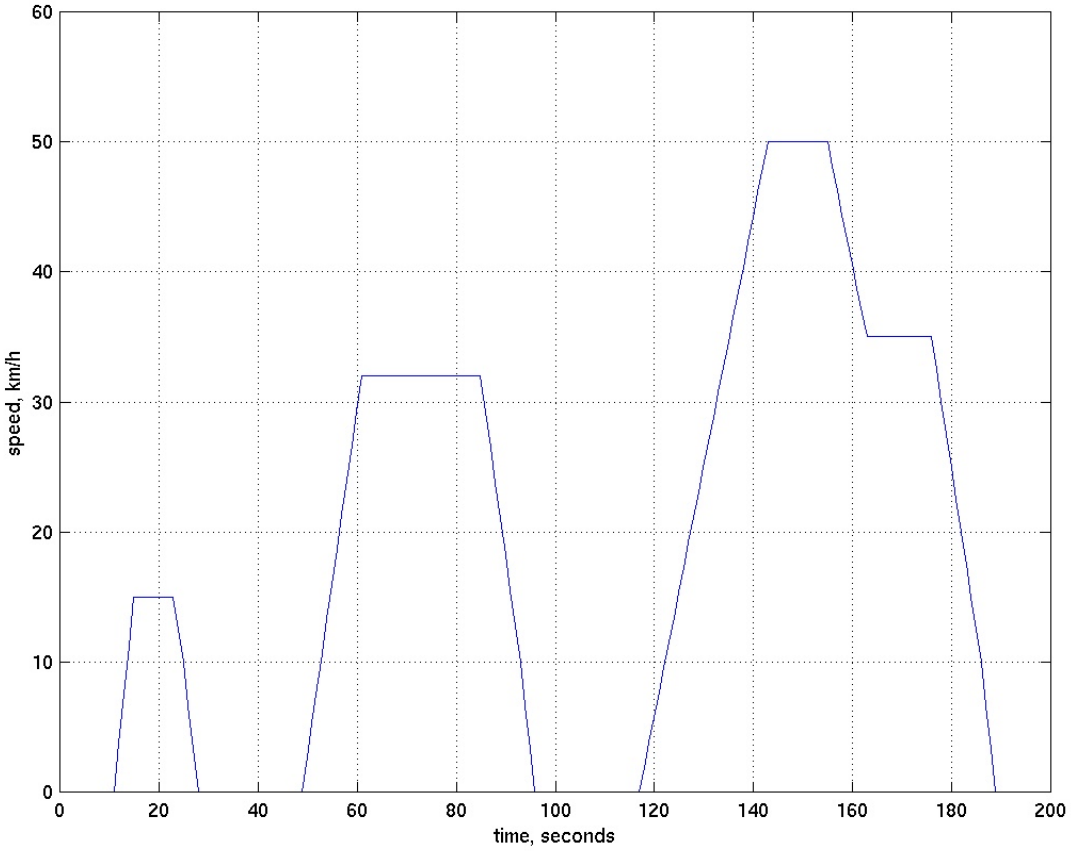

In recent years, driving cycles have been paired with computer models of road load, as described above, to predict and model vehicle performance.

4.3.1 TMDC

Driving patterns in Asian cities are significantly different from American highway driving, and even American city driving. For example, Taipei's congestion and frequent stops mean that average driving speed is less than 15 km•h^{-1}, and driving speed exceeds 40 km•h^{-1} only 10% of the time.[24]

The driving cycle used here, therefore, should be specifically targeted for the Asian driver. One

candidate is the Taipei Motorcycle Driving Cycle (TMDC), developed by researchers at the Institute of Traffic and Transportation at Taiwan's National Chiao Tong University. The TMDC is an actual velocity trace obtained by researchers who followed target vehicles on an instrumented "chase vehicle". The driving cycle consists of 950 velocity measurements (one per second) and each velocity measurement is rounded to the near $km \bullet h^{-1}$. An acceleration profile was derived by taking finite differences in temporally-adjacent velocity measurements.

Figure 4.8 Taipei Motorcycle Driving Cycle (TMDC)

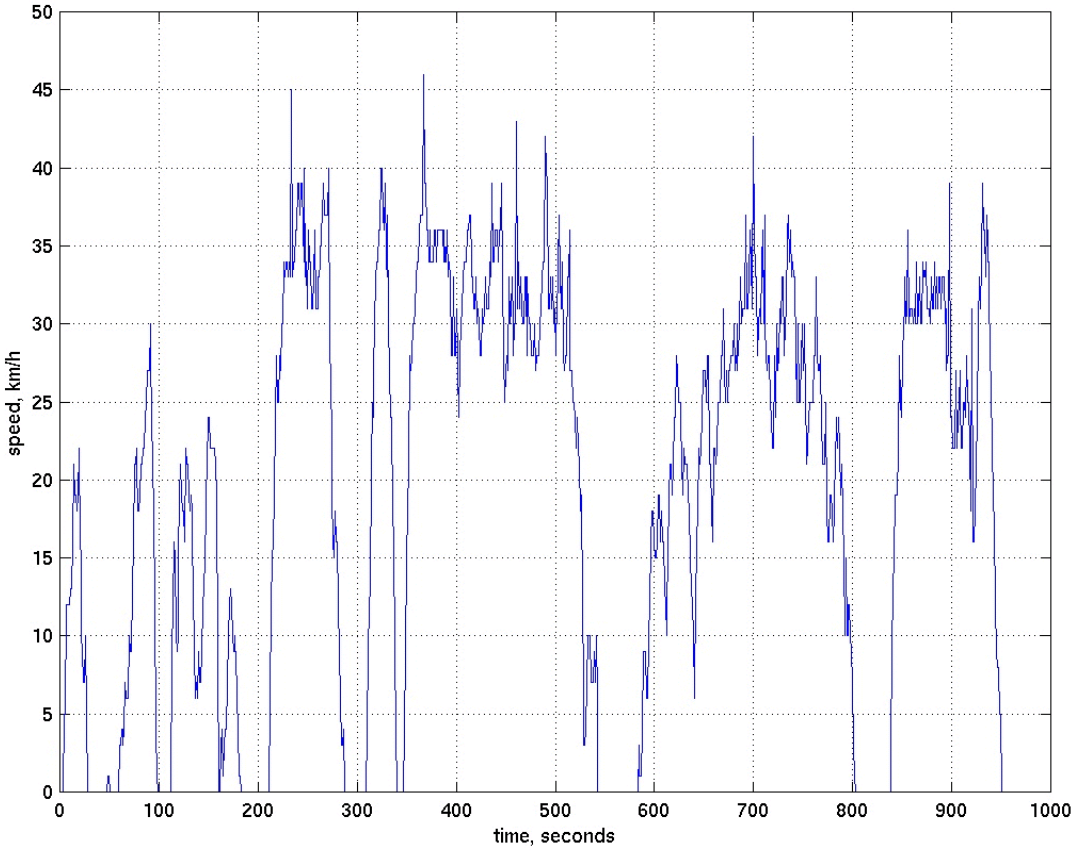

As a comparison of several characterizing parameters shows, the TMDC is different from FUDS and the motorcycle-modified FTP:

Table 4.5 Driving Cycle Comparison

	TMDC	modified FTP	FUDS
Total time	950 s	1873 s	1372 s
Total distance traveled	5109 m	15537 m	7450 m
Average speed	19.3 km/h	29.9 km/h	19.6 km/h
Maximum speed	46 km/h	59 km/h	57 km/h
Maximum acceleration	13.0 km/h/s	5.4 km/h/s	3.6 km/h/s
Maximum deceleration	-15.0 km/h/s	-5.4 km/h/s	-3.3 km/h/s
Fraction of time spent accelerating	31.5%	42.7%	39.7%
Fraction of time spent decelerating	30.3%	56.3%	34.6%
Fraction of time at steady non-zero speed	18.5%	1.0%	6.6%
Fraction of time at standstill (v = 0)	19.7%	15.2%	19.0%

The TMDC exhibits especially severe accelerations and decelerations - maximums of +13.0 km/h/s and -15.0 km/h/s, respectively. The maximum acceleration in the modified FTP cycle often used for testing vehicle emissions is 5.4 km/h/s, but the maximum acceleration observed in Bangkok motorcycle traffic is quoted as being 12 km/h/s.[25] (It is not clear what size of motorcycle the Bangkok number refers to). While it is true that scooters in Taiwan are driven in a more aggressive way than cars in American cities, these accelerations and their consequent power requirement of over 12 kW at the wheels significantly exceed the maximum performance capabilities of scooters 125 cc or less.

One important ramification of the high accelerations and decelerations is that a significant amount

of energy can theoretically be recovered by regenerative braking. Also, maximum power is much larger than average power.

Note also in Figure 4.8 “jitter” in the velocity reading. Errors due to rounding of the speedometer reading to the nearest km/h when the data was recorded create exaggerated accelerations and decelerations that did not reflect reality. For example, a speed that varied from 20.4 to 20.6 and back to 20.4 in two seconds would appear in the data as a one-second acceleration from 20 to 21 and back to 20. This jitter was analyzed below using the scooter model described previously. (The jitter starts from the base speed and oscillates up and down by 1 km/h)

Table 4.6 Effects of “jitter”

initial speed (km/h)	average power to accelerate 1 km/h faster in 1 second, then return to original speed (W)	power if speed was a constant 0.5 km/h faster (W)	jitter increases power by this fraction
5	179	117	53%
10	290	177	64%
15	416	252	65%
20	564	348	62%
25	740	472	57%
30	951	632	50%
35	1204	834	44%
40	1507	1085	39%
45	1866	1393	34%

The test shows that these oscillations produce significant variations in power required by the model that are not representative of actual driving.

4.3.2 Modification of TMDC

The TMDC is more representative of Taipei driving conditions than FTP or FUDS, but it has flaws that should be compensated for. As given, to achieve the performance of the TMDC simulation, a total power output of more than 12 kW is needed, significantly greater than the maximum power achieved by the internal combustion engines of even 125 cc scooters.

As a first attempt at improving the TMDC, the maximum speed was clipped to 40 km/h to more closely approximate reality. Accelerations were calculated from this less strenuous driving cycle; fortunately, these peaks were very brief and the integral under these parts of the velocity curve was small, so that there was very little difference in parameters of the driving cycle like total distance and fuel consumption. However, this first cut reduced maximum power only to 9.7 kW, so this technique was discarded.

Smoothing with a moving three-second box, as suggested by the researcher who developed the TMDC, was not adequate in attenuating the maximum peaks.

Another method of adjusting the driving cycle to reflect a more realistic assumption was to use a low-pass filter to get rid of the quantization jitter and to attenuate the very quick accelerations. Changing the characteristics of the low-pass filter would modify the final modeling results, so to choose an appropriate filter function, the results of the adjusted cycle were compared against reported data on scooter performance levels. (For example, the ZES-2000 was specified as being able to travel 30 m from a standstill in 4.5 seconds at maximum acceleration[1, 7], and the power required to achieve this acceleration was found to be 3.7 kW using the physical model. Similarly, a standard gasoline-powered scooter was quoted elsewhere as having a maximum power of 5.0 kW [2].

A maximum net electrical output power of about 5.0 kW seemed reasonable given these examples.)

The low pass filter was created as a transfer function defined to have a DC gain of 1 to not change the average value of the function acted upon (in this case the velocity as a function of time).

$$H(s) = \frac{1}{1 + \frac{2\pi s}{\tau_o}}$$

τ_o is the characteristic time, so that larger values of τ_o produce greater smoothing. This function was convolved with the velocity profile of the driving cycle to reduce high-frequency jitters and to attenuate accelerations and decelerations. The smoothing effect can be thought of as a multiplication (in the frequency domain) of the transfer function and the frequency spectrum of the driving cycle; due to the hyperbolic shape of the transfer functions, high-frequency components are attenuated while low-frequency components are increased.

The results of running the simulated scooter under the TMDC for various manipulations of the TMDC are presented below. The scooter parameters given in Table 4.3 were used. The FTP was compared to the smoothed driving cycles as a check to see if the results were close. The italicized choice was the one eventually selected.

Table 4.7 Results of different algorithms applied to TMDC; comparison to FTP

	original	**clip at 40 km/h**	**1/(s+4) smooth**	***1/(s+1.5) smooth***	**1/(s+1) smooth**	**mod. FTP**
average speed over cycle (km/h)	19.3	19.3	19.3	*19.3*	19.3	29.9
max net power from engine (includes drivetrain)	12.6 kW	9.8 kW	9.0 kW	*5.6 kW*	4.2 kW	5.5 kW
avg power from engine (no parasitics; includes drivetrain)	935 W	759 W	651 W	*566 W*	537 W	1254 W
max acceleration (km/h)	13.0	13.0	9.8	*6.4*	5.1	5.4
max deceleration (km/h)	-15.0	-15.0	-9.2	*-8.6*	-7.7	-5.4
std. dev of accelerations	0.79	0.76	0.61	*0.48*	0.44	0.58
avg. acceleration power (avg. of positive and negative)	63 W	59 W	38 W	*24 W*	20 W	34 W
avg. acceleration power (positive only)	370 W	355 W	285 W	*215 W*	188 W	289 W
avg. rolling resistance power	151 W	151 W	151W	*151 W*	151 W	234 W
avg. aerodynamic drag power	118 W	117 W	117 W	*117 W*	116 W	425 W
accel. power (when in motion)	1178 W	1129 W	678 W	*517 W*	446 W	674 W
rolling power (when in motion)	189 W	188 W	184 W	*179 W*	175 W	272 W
aerodynamic drag (when in motion)	147 W	146 W	143 W	*138 W*	134 W	495 W

Note that the average acceleration powers are very low because acceleration can be negative; the average acceleration power for positive results only is more indicative of how the energy is split between the various components. It should be noted, however, that negative acceleration power can be used to "cancel out" power demands from aerodynamic drag and rolling resistance. That is, when the vehicle is decelerating, the drag power and rolling resistance can be allowed to slow down the vehicle so negative accelerations are not entirely meaningless to the power calculation.

The mFTP results show much higher average power than the selected smoothed curve, due to rolling resistance and aerodynamic drag, which in turn are due to the average speed being 50% higher than the TMDC. On the other hand, the maximum power is very close to that of the smoothed curve, suggesting that a scooter designed for the TMDC will be capable of sustaining the FTP driving cycle which was originally designed for the more powerful motorcycles. The maximum mFTP power of only 5.5 kW is a telling indicator that the TMDC (unsmoothed) is too severe.

Smoothing dramatically decreases maximum accelerations and decelerations, and changes the acceleration characteristics of the driving cycle, but does not significantly change the other components; this is because acceleration is such a large component of maximum power but not such a strong determinant of average power.

The low-pass filter with a 3.1 second smoothing interval (italicized in Table 4.7) was chosen to smooth out jitter and reduce the maximum power required to on the order of 6 kW - specifically, 5.6 kW including auxiliaries but not including parasitics because parasitics are dependent on later calculations based on these results. This is comparable to modern 50 cc scooters, with maximum power closer to those of the mFTP.

Figure 4.9 Smoothed TMDC

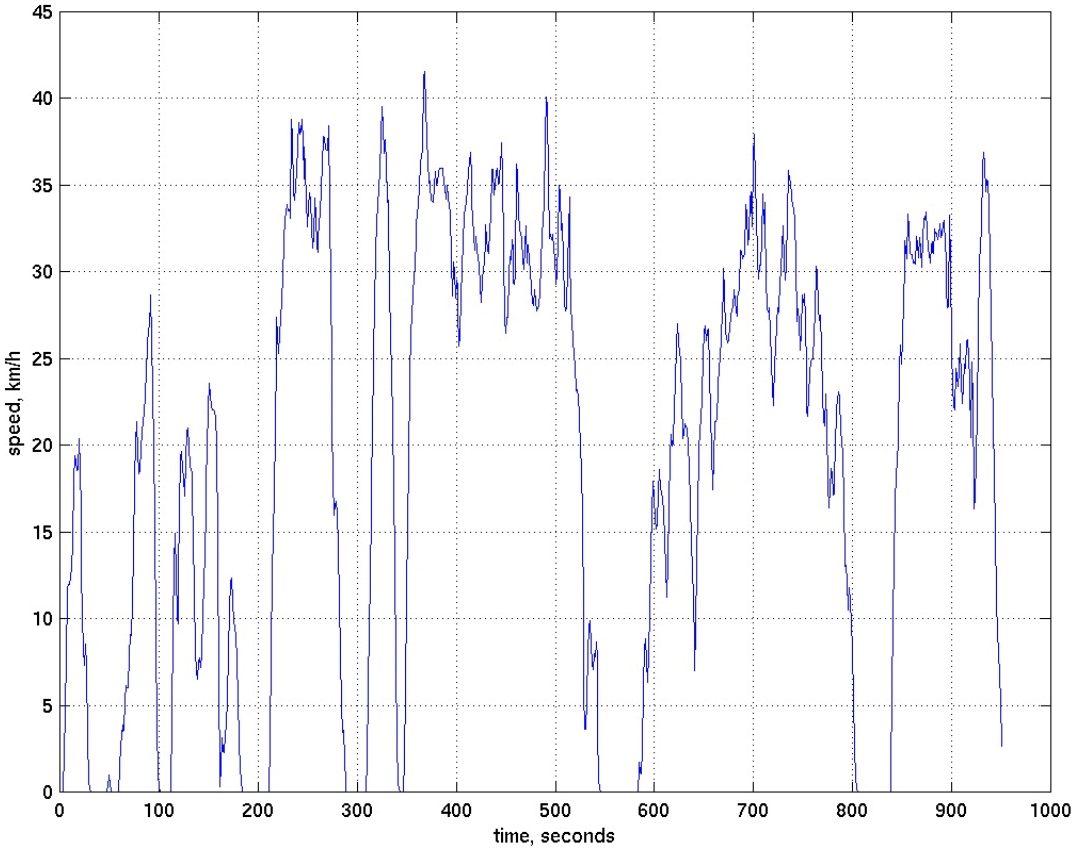

The "smoothed TMDC" driving cycle was used for all further calculations, and referred to as simply the TMDC. Note that the energy finally dissipated in braking (i.e. where deceleration "power" is greater than aerodynamic drag and rolling resistance powers) is 116 kJ over the 950 second cycle, or 122 W in the smoothed TMDC. This is about 20% of the 566 W engine output.

4.3.3 Torque vs. rpm requirements

Looking only at the maximum power produced by the electric motor and the maximum power produced from the fuel cell or battery is not sufficient to ensure that the power demands of everyday driving are met. This is because the total output is limited by the maximum power of the motor, but

also by other factors like the maximum current (which sets a maximum torque even when the speed might be low).

Torques are summed about the axle of the drive wheel; the rolling resistance and acceleration "torque" have moment arms equal to the radius of the wheel (15.8 cm), while the drag force is assumed to be act at the center of mass of the scooter, 20 cm above the axle. In order to ensure that the required torques could be produced, the model results were illustrated as a scatterplot of torque versus speed. Imposed on this graph was the maximum performance curves of the chosen Unique Mobility (UQM) brushless DC scooter motor rated at a nominal 3.6 kW.

Figure 4.10 Torque vs. rpm during TMDC

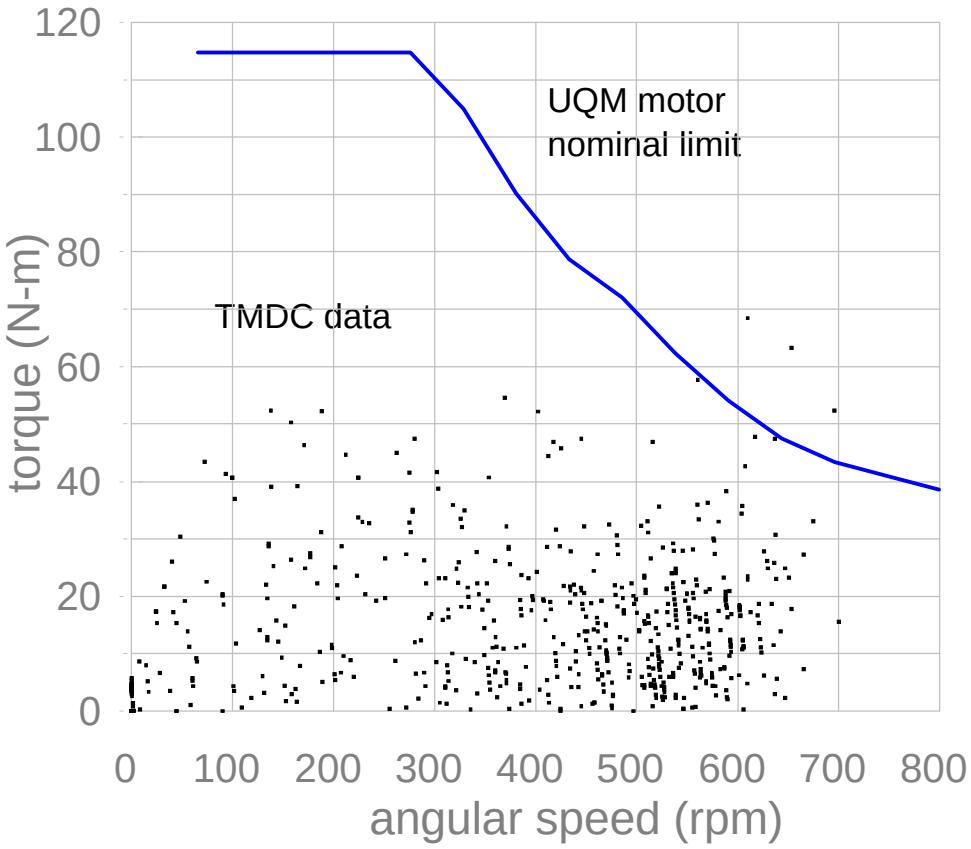

Note that at three one-second time intervals, torque required exceeds that available from the UQM motor. These peaks represent the maximum power of 5.6 kW of electrical output, which translates to 4.3 kW of mechanical power after the 77% drivetrain efficiency - greater than the 3.6 kW maximum output of the UQM motor. The assumption was made that the three outliers were sustainable for short periods of time.

4.3.4 Modeling results

The results of the TMDC driving cycle are shown below.

Figure 4.11 Power required in TMDC

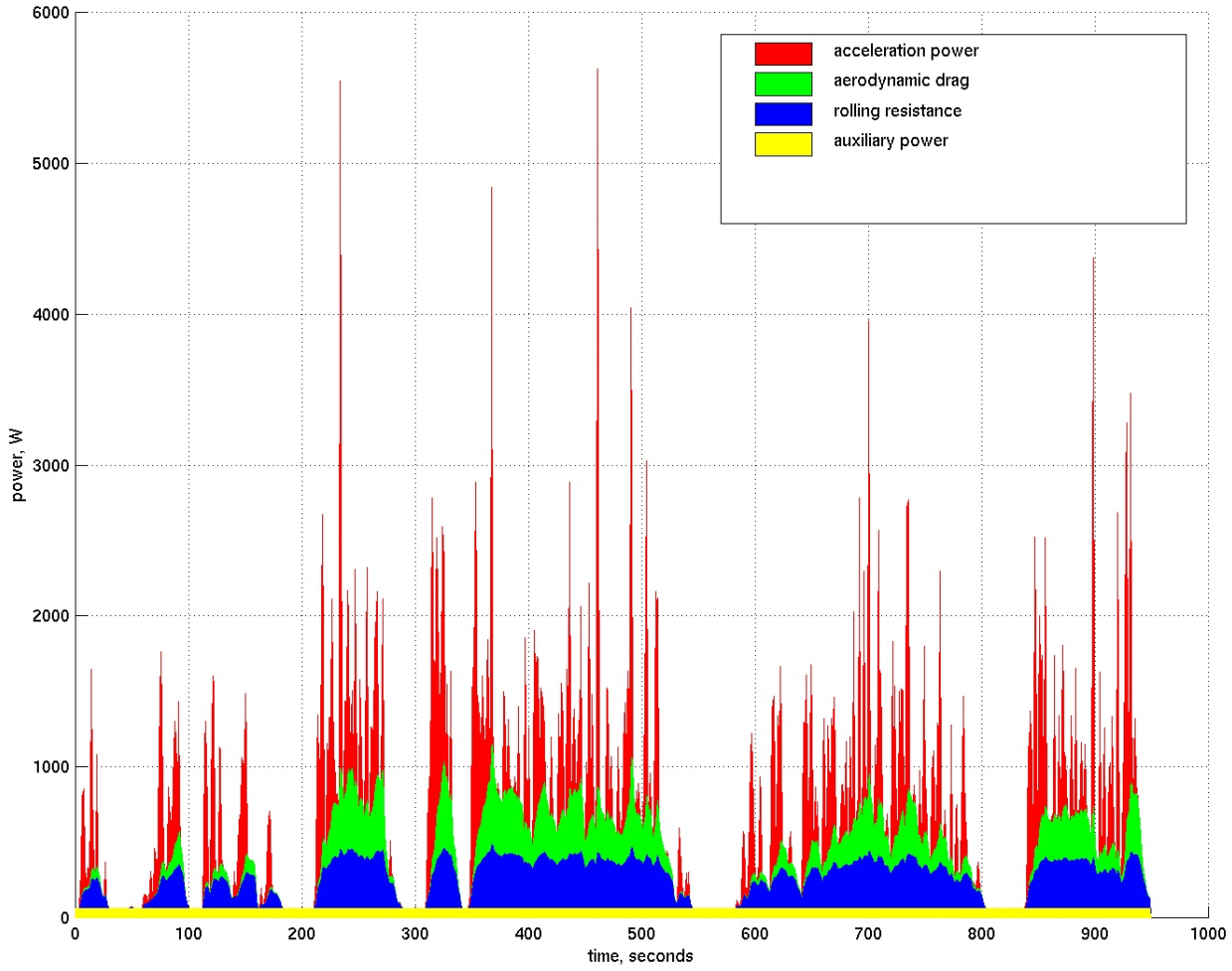

Acceleration power demands the greatest peaks in the cycle, and also accounts for most of the energy in the cycle (not including braking energy recovered from negative accelerations). Rolling resistance accounts for somewhat less energy, and aerodynamic drag even less. The 60 W of auxiliary power is at most 10% of the average power.

Interestingly, the average power is approximately one tenth of the maximum power. The extreme variability in the power demands suggests that hybridization would be useful, with a battery providing surges of extra power during bursts of acceleration and also the capability to store braking energy.

The physical model shows that the power needed, under the TMDC, is an average 566 W of electric power out of the fuel cell without parasitics. A complete analysis of fuel economy, however, requires a polarization curve of efficiency versus net power, and an understanding of the parasitic power. This is in section 4.5.

4.3.4.1 Battery powered scooter

The parasitic power requirements of the fuel cell have not yet been calculated but there is enough information here to calculate performance of a scooter running on just a single battery. The power output is the same as the fuel cell power output except without the parasitic requirement. A total of 4.1 kWh (output) are needed to store enough electricity for 200 km of range.

Table 4.8: Taiwan battery-powered scooter performance

	TMDC driving cycle	**30 km/h cruising**
Average speed	19.3 km/h	30 km/h
Average power (electric output)	566 W	615 W
Mileage in terms of electric output	35.5 km per kWh-output	48.8 km per kWh-output
Maximum power output	5.6 kW	615 W
Total energy storage for 200 km at 30 km/h		4.1 kWh

The battery requirements, given the different USABC battery technology predictions and a 4.1 kWh storage capacity, are compared to today's lead-acid batteries.

Table 4.9: Various battery-powered designs for Taiwan scooter

	Lead-acid: today's battery	**Mid-Term advanced battery**	**Long-Term advanced battery**
Weight	117 kg	62 kg	25 kg
Volume	58 L	36 L	16 L
Cost	$245-$735 (current)	$735 (mid-term)	$490 (long-term)

For the lead-acid battery, the critical assumptions were 35 Wh/kg and 70 Wh/L. Note that in the mid-term and long-term cases, the battery weight and volume are determined by the maximum energy requirement, not the *power* requirement. In fact, a mid-term battery of this size would offer 7.7 kW of maximum power, while the long-term battery would output a maximum of 8.2 kW! The limiting factor in battery size and weight for these batteries is energy storage, not power storage. Section 4.7 on hybrid design shows how decoupling the energy and power functions of the battery improve the system.

Today's ZES-2000 scooter with far shorter range than the systems described above gives an idea of how much room is available in the scooter: at least 44 kg and 15 L (not including the electric motor and controller). The next step is to design a fuel cell power system within these size and weight parameters that can output a continuous 610 W for 30 km/h cruising for 200 km (or 6.7 hours); produce a 5.6 kW maximum output; and generate 3.2 kW of continuous hill climbing power.

4.4 Fuel Cell System Design and Integration

4.4.1 Design tradeoffs

The fuel cell stack is specified by only two independent variables plus the polarization curve and the maximum power:

1. Maximum power
2. The polarization curve
3. Power density
4. Number of cells in the stack

(Note that, instead of power density and number of cells, we could have equivalently chosen area per cell and total active area of all cells)

4.4.1.1 Maximum power and the polarization curve

A maximum gross fuel cell power of 5.9 kW is assumed from parasitic requirements calculated in section 4.4.5. This is slightly over the sum of the maximum TMDC requirement of 5.6 kW net power plus an initial estimate of 300 W for parasitic power losses. The parasitic requirements are discussed in greater detail later on, but for now it is enough to say that they are approximately linear with gross power output so that maximum parasitic power occurs at maximum gross power.

The polarization curves used are those derived from Energy Partners for single atmospheric-pressure *cells*; these are extrapolated to be equal to future *stack* performance.

Figure 4.12 Polarization curve

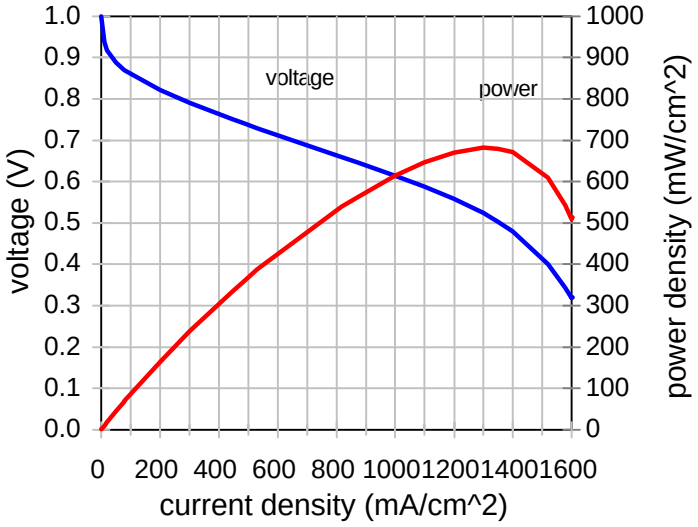

Data is from Barbir is for a single cell running on hydrogen/air, with a Gore MEA and operating temperature of 60°C. Air-side stoichiometry is 2.5.[26]

4.4.1.2 Power density

The first choice to make is to determine the power density to operate at, under conditions of maximum power. If maximum output is arranged to take place at low power density, the left portion of the polarization curve is used (since power density scales almost linearly with current density); voltage, and thus efficiency, are high in this portion of the curve. However, a large total active fuel cell area is needed and much electrolyte membrane and platinum will then be required. The stack size will be larger.

If a low total area is used, then power density per area is high. The power density curve peaks at high current densities, with correspondingly low voltages and low efficiencies. (The low total area can be achieved by a combination of low cell area and/or few cells). Total price is a monotonic function of total area, so the high power density approach results in a smaller stack and cheaper stack, although efficiency would suffer and consequently hydrogen storage requirements for a given range would be higher.

Power density also controls the flow rates of the air and hydrogen reactants. The flow rates are functions of the designed hydrogen utilization and oxygen stoichiometric ratio, and also of the efficiency of the fuel cell; low efficiency means that more reactants must be flowed for a given power output. Thus, for a given power level, high power densities mean higher flow rates because they operate in the low voltage (low efficiency) portion of the polarization curve. The sizes and costs of air management equipment are determined in part by flow rate, but it should be noted that the scooter application demands flow rates far below those normally available for vehicle systems so most systems for scooters based on automotive designs would be oversized anyway.

To maximize efficiency and produce a small, cheap fuel cell, a high power density is selected. According to the polarization curves presented, power is maximized at about 1300 mA•cm^{-2}; to be conservative and leave room for unusual bursts of speed, a point below this power peak is chosen: 1000 mA•cm^{-2}. At 1000 mA•cm^{-2}, voltage is 0.614 V, and power density is thus 614 mW•cm^{-2}. For 5.9 kW at this point, 9.6 x 10^{3} cm^{2} of active area are needed.

4.4.1.3 Number of cells

The number of cells is a function of the desired operating voltage. The electric scooter industry in Taiwan is standardizing on 48 V electric motors, so the number of cells is chosen so that the stack operates in the vicinity of 48 V at the most common power demand; note that in a fuel cell, as the total power output changes, the voltage varies as well.

The DC-to-DC conversion is assumed to be performed by the motor controller, and is included in the 77% drivetrain efficiency. (In comparison, standalone DC-to-DC converters from Vicor offer approximately 410 W/L and 381 W/kg, with efficiencies of 80%-90%; prices are on the order of 1 $/W.[27,28]) All parasitic power – fans, pumps, blowers, etc. – should be DC to avoid the large additional expense of a DC-to-AC inverter.

The average TMDC power demand is 566 W, and later modeling in shows that the final result including parasitic power (after iterative calculation) is 674 W. With a 9.6x10^{3} cm^{2} total membrane area, the power density is 70 mW•cm^{-2}. To obtain this power density on the polarization curve, 79 mA•cm^{-2} and 0.870 V are needed - only 8% of the maximum current density, and high up on the efficiency curve. The system is designed to run at 48 V at this point, and dividing 48 V by the 0.870 V per cell gives a minimum of 56 cells. Area per cell is then approximately 170 cm^{2}.

Table 4.10: Fuel cell design parameters at maximum power

	maximum power	hill climbing power	average TMDC power
Power with parasitic load	5.9 kW	3.2 kW	665 W
Current density	1000 mA•cm^{-2}	448 mA•cm^{-2}	79 mA•cm^{-2}
Stack current	172 A	76 A	13 A
Cell voltage	0.614 V	0.751 V	0.870 V
Power density	614 mW•cm^{-2}	336 mW•cm^{-2}	69 mW•cm^{-2}
Stack voltage	34.2 V	42.0 V	49.0 V
Open-circuit voltage (occurs at minimum power; parasitics not included)	56.0 V		
Total active area needed	9600 cm^2		
Total number of cells	56		
Active area per cell	170 cm^2		

(Note that this stack could also have been designed as two electrically parallel stacks of 56 cells each 85 cm^2 in area and with half the maximum current (86 A), or various other configurations).

4.4.1.4 Flow rate parameters

It is further assumed that the air flow rate is 2.5 times stoichiometric (to reproduce the performance of the Energy Partners polarization curve) and that the hydrogen consumption is 100% due to dead-ended operation. The surplus air lessens the effects of oxygen depletion in the cathode as oxygen is consumed by the fuel cells and also helps to push out product water. The exhaust gas flow rate was calculated by summing the input gas streams of air (21% oxygen) and hydrogen and then subtracting the hydrogen and oxygen consumed. The water is assumed to emerge as liquid so is not included in the exhaust flow rate. From this set of data, the following flow rate characteristics are

derived:

Table 4.11: Flow rate parameters at maximum power

	volumetric	molar	mass
hydrogen intake rate	2.6 CFM	0.05 mol•s^{-1}	0.1 g•s^{-1}
air intake rate	15.6 CFM	0.30 mol•s^{-1}	8.6 g•s^{-1}
total exhaust gas rate	16.9 CFM	0.27 mol•s^{-1}	7.8 g•s^{-1}
(liquid) water production rate	0.9 mL•s^{-1}	0.05 mol•s^{-1}	0.9 g•s^{-1}

4.4.2 Gas subsystem

As discussed previously, the pressure drop in fuel cell stacks has been estimated at 0.5 - 2 psi. With a 50% blower efficiency, worst-case 2 psi air drop, and the calculated 15.6 cfm of air flow, this is a maximum theoretical power consumption of 200 W. In theory, this scales down linearly with decreasing flow rate, but in practice the pressure drop also decreases as a function of flow rate so the decrease is somewhat sharper than linear. A heavy-duty blower that could be used to provide the required output is the Ametek 5.7" BLDC three-stage blower, model 116638-08. Its volume flow capacity is much higher than the 16 cfm required, but it is the smallest model capable of the relatively high 2 psi needed.[29] Retail cost is $430.

The blower power was modeled in the simulation as a linear 50-250 W load, for a gross power output of 50-5850 W. This is a conservative calculation based on comparison with a reported parasitic power draw of 105 W for a 24 VDC Ametek blower at 1.3 psi for a 4 kW nominal power fuel cell.[30]

On the hydrogen side, a pressure regulator expands the hydrogen from either the 1-10 atm partial

pressure of a metal hydride system, or a 3600 psi (260 atm) pressure of a compressed gas system.

4.4.3 Water subsystem

A low fuel cell operating temperature of 50°C is chosen to minimize evaporation losses and eliminate the need for external humidification (and complex control of that humidification). The maximum allowable fuel cell temperature is set to 65°C.

According to Mazda Demio documentation, external humidification requires an additional 15% in stack volume, but thin wicking polymer membranes can allow water to be backdiffused from the cathode to the anode to keep the membranes humidified without external humidification.[31] The wicking polymers could alternately transfer water from a reservoir to pre-humidify incoming air if humidification turns out to be necessary after all.

4.4.4 Cooling subsystem

There are several heat flows to consider in fuel cell systems.

1. Waste heat must be removed from the stack with a liquid coolant loop.
2. The liquid coolant must have heat removed at the cold side with a fan.
3. Air entering the system may be preheated in order to retain more water from any humidification
4. The humidification water, if any, can be preheated as well
5. Reformers, if present, require temperatures of at least 300°C to operate, and may produce net heat
6. Heat must be supplied to the metal hydride system, if one exists, in order to desorb the hydrogen.

To optimize the system, some of the flows can be combined. For example, the coolant loop is a convenient source of heat for a metal hydride storage system, while the blower could be designed to draw its input air from behind the coolant radiator.

All heat flows in the system are functions of the instantaneous power, since the waste heat, hydrogen demand, and air demand all scale according to the efficiency curve with respect to power in almost the same way. The maximum heating load occurs at maximum power in the driving cycle - at 5.9 kW of gross electric output, efficiency is 41.2% and heat output is 8.4 kW. However, the *average* heat load during typical TMDC driving is much lower, only 742 W. Given sufficient thermal mass, temperatures in the stack can be kept near the design point without the use of a large radiator. The ultimate concern is to keep the temperature low to avoid evaporating too much water from the membrane.

In comparison, a 20% efficient 5 kW internal combustion engine outputs 20 kW of waste heat. The difference is that this load is produced at high temperatures and thus is easily rejected to the environs by air blowing over cooling fins

There are two beneficial cooling effects that are not quantified here. First, fuel cell efficiency is calculated on a higher heating value basis, meaning that the product water is assumed to emerge solely as liquid water. In fact, some is vaporized and this removes heat from the system, making the cooling design somewhat conservative.[32]

Second, some heat is "used up" by the intake air. At a maximum flow rate of 8.6 g/s, an intake temperature of 30°C, and a heat capacity for air of approximately 1 $J \cdot g^{-1} \cdot K^{-1}$, 170 W of heat are required if the incoming air heats up to the stack temperature of 50°C. This small amount of cooling

is not included below but is noted for the sake of completeness.

4.4.4.1 Cooling from storage system

Here, cooling from metal hydride adsorption is discussed, along with more conventional cooling. The temperature of the fuel cell stack is modeled over the entire driving cycle to ensure that the fuel cell remains within its designed limits of 50°C and 65°C.

TiFe metal hydride systems consume 28 kJ of heat per mole of hydrogen desorbed. In the system, the maximum heat production is 8.4 kW and occurs at the maximum gross power of 5.9 kW. Here, hydrogen consumption is 0.05 moles•s^{-1}, so the hydride takes up 1.4 kW (16.7%) of the waste heat. This percentage increases as the fuel cell is turned down to lower powers, because the number of moles of hydrogen per heat output increases due to the greater efficiency; over the full range, the metal hydride system eliminates 16.7% - 30.2% of the waste heat. This reduces the size of the radiator and decreases the parasitic power required for cooling.

Figure 4.13 Metal hydride cooling vs. power

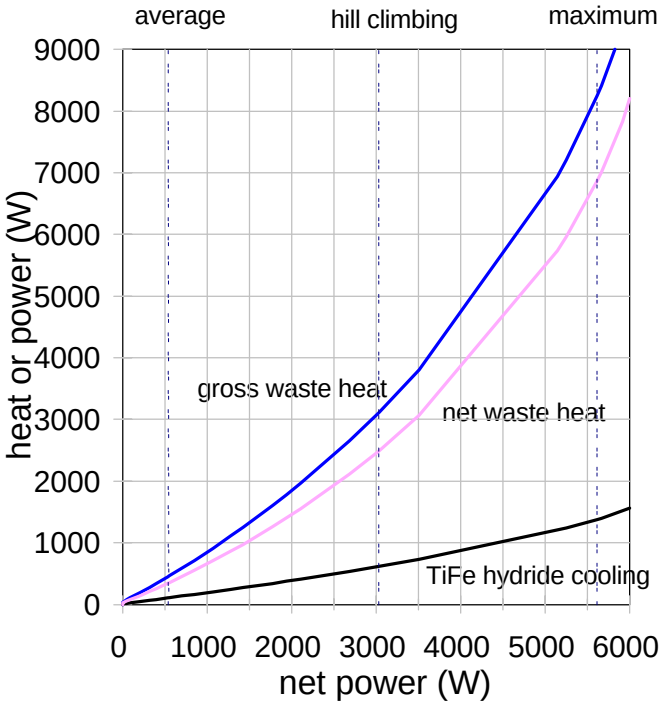

For this reason, metal hydrides have a significant advantage over gas cylinders. Combining a water cooling system for the fuel cell with the metal hydride allows the transfer of this heat, although a backup heating system might be necessary for startup heating and active control of the metal hydride temperature. This backup system could be a resistance heater wrapped around part of the metal hydride, connected to the startup battery. (The pressure of hydrogen gas over the hydride at room temperature would be greater than atmospheric, so there would be some hydrogen at startup. However, with waste heat slow to reach the hydride, an extra heater could provide a faster flow rate for immediate high power).

4.4.4.2. Active cooling

There are several possibilities for liquid cooling.

1. Cooling is provided by a closed loop water coolant circulated at constant flow rate through the stack by way of cooling plates. The hot water exiting the stack is circulated to a heat exchanger exposed to the atmosphere, where a fan enhances heat transfer. The fan speed can be increased to provide additional cooling. Alternately, a constant-speed fan can be used in a thermostat mode (allowed to switch on and off as needed), allowing the coolant temperature to fluctuate.

2. Variable coolant flow rate, fixed fan speed. As stack output power increases, the coolant circulation speed is increased. The change in temperature of coolant as a function of power is dependent on the heat exchanger properties. A variable-flow pump is needed.

3. Variable coolant flow rate, variable fan speed.

4. The pump is eliminated, reducing weight, cost, and parasitic power; instead, a refrigerant designed to boil at the fuel cell operating temperature is used in conjunction with a check valve, and the expanding gas drives circulation in the coolant loop.

In all cases, water circulation should be stopped altogether when the engine is warming up to operating temperature, so some kind of thermostat (if not variable) control should be employed for the coolant loop.

The heat exchanger cooling factor, in terms of watts of heat dissipated per degree of temperature

difference between the coolant and ambient temperature, provides an upper limit on how much heat can be removed from the stack at a constant output power. Charts of cooling factor (W/K) as a function of air flow rate and coolant water flow rate for various heat exchangers, in conjunction with charts of pressure drops, were used to determine parasitic loads for the radiator fan and coolant pump, respectively. This information was obtained from Lytron, a heat exchanger manufacturer (see Appendix C)

Continuous hill climbing determines maximum continuous power output (intermittent higher power output, like that of the TMDC, is interspersed with many periods of low power output). To satisfy the hill climbing requirement of 18 km/h at a 12° slope, 3200 W (gross output with parasitics) are required. Efficiency at this output point is 50.7%, waste heat is 3.1 kW and hydrogen consumption is 0.022 moles/s. The 28 kJ/mol of the hydrides eliminates 20% of the waste heat, leaving 2.5 kW, or 100 W/K that must be dissipated for a fuel cell at the design maximum of 65°C and a worst-case ambient temperature of 40°C (ΔT=25°C). An extra 10 W/K was added for a design specification of 110 W/K, which is met by an M14-120 radiator at a retail cost of $240.

Due to the lack of space at the front of the scooter, the radiator would likely have to be installed at the sides of the rear compartment, where flowing air would pass over the radiator pipes.

Here, the assumption is that the coolant pump and cooling fan draw power all the time. This is not a realistic assumption in that the power should be turned off when cooling is not needed (to ensure the fuel cell is above the minimum operating temperature). However, it is a safe assumption in that it overestimates (slightly) the power needed for parasitics, especially since pump and fan power draw needs are uncertain.

4.4.4.3. Heat generation under the TMDC

Maximum heat dissipation is determined by continuous hill climbing, but to ensure that the short spikes of high heat generation in the TMDC do not push the fuel cell temperature past 65°C, the temperature of the stack was simulated using a simple model. Heat generation under the TMDC simulation has the same general shape as the power output graph, but the peaks and valleys are exaggerated because efficiency decreases with increasing power output.

Figure 4.14 Heat generation as a function of time in TMDC

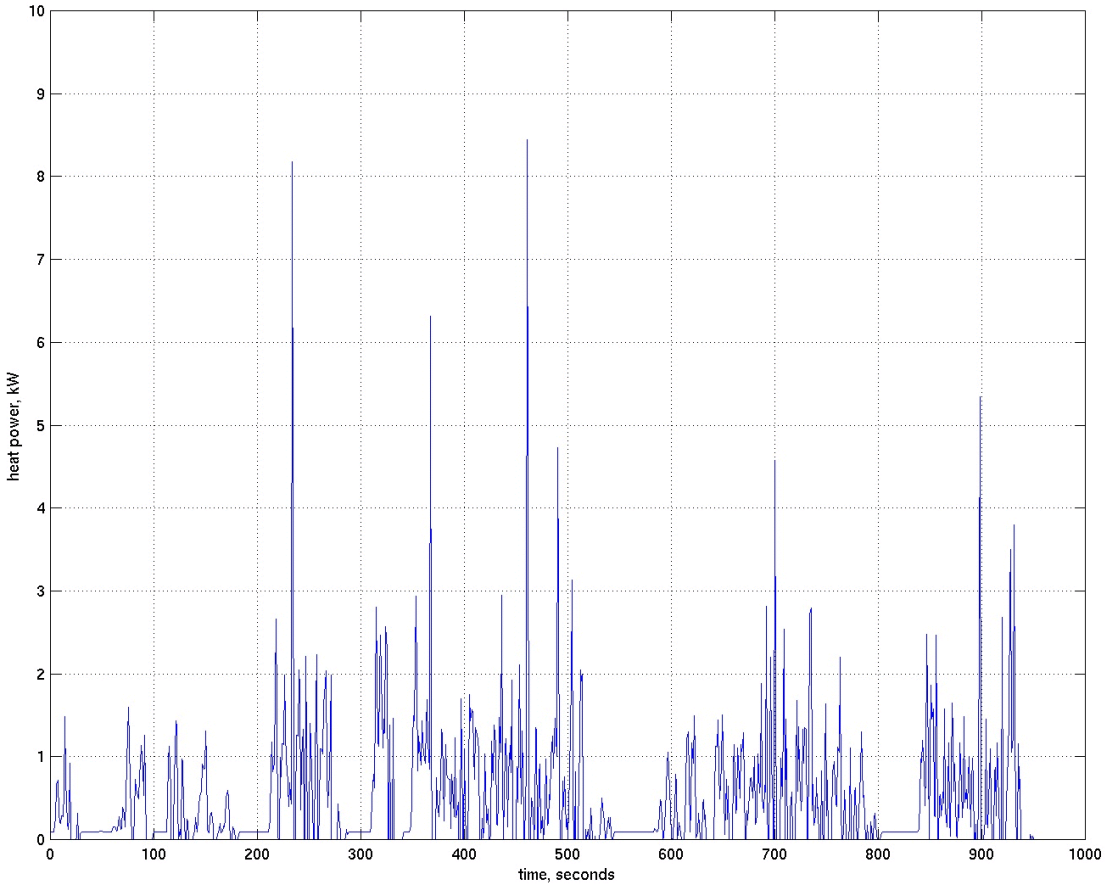

Note that average heat generated is 742 W for the 5.9 kW stack. After the metal hydride heat absorption is included, this decreases to an average load of only 393 W. The net heat generated was calculated for each step of the TMDC and used to calculate a change in temperature for the stack. The purpose of this further test was to make sure that the cooling factor (sized for continuous load) would be enough to keep stack temperature below the design limit of 65°C through the peaks and spikes of the TMDC.

The heat capacity equation used was

$$Q = M C \Delta T$$

for heat Q, stack mass M, average heat capacity T, and change in temperature ΔT. This was discretized for each time step, and the mass and heat capacity were separated into the different materials found in the stack, resulting in the following equation:

$$\frac{\Delta T}{\tau} = \frac{\dot{Q}}{M_1 C_1 + M_2 C_2}$$

$\dot{Q}$ is the heat power generated in a given time interval; M is the mass of the parts of the stack that make up the bulk of the total weight and are closest to the membranes (i.e. “1" for the stainless steel separator plates and “2" for the polypropylene gaskets); C is the heat capacity of the stack materials; and τ is the length of time of a single time step of the model.

Table 4.12 Stack temperature model parameters

parameter	value	note
Mass of 316 stainless steel separator plates	2.0 kg	0.5 $J \bullet g^{-1} \bullet {}^{\circ}C^{-1}$ specific heat capacity
Mass of polypropylene gaskets	0.8 kg	2 $J \bullet g^{-1} \bullet {}^{\circ}C^{-1}$ specific heat capacity
Heat capacity of stack as a unit	2.6 $kJ \bullet {}^{\circ}C^{-1}$	Weighted sum of steel and polypropylene
Specific heat capacity of stack	0.93 $J \bullet g^{-1} \bullet {}^{\circ}C^{-1}$	c.f. water at 4.2 $J \bullet g^{-1} \bullet K$
Heat exchanger cooling factor	150 $W \bullet K^{-1}$	maximum cooling
Ambient temperature	40°C	worst case
Heat removed by metal hydride	28 $kJ \bullet mol\ H_2^{-1}$	minimum 17% of waste heat

The assumption made was that most of the heat would be trapped inside the plastic housing (designed for electrical insulation), removed mainly by the active cooling system. The membrane itself is negligible because it is so light. This simple model does not include the effects of heat conductivity - just heat capacity.

The cooling system was designed to turn on only above a temperature of 50°C in the stack (as detected by thermistors in the stack), with a maximum allowable temperature of 65°C. The following temperature patterns were recorded for the TMDC for cooling factors of 110 W/K as designed, and 30 W/K for comparison.

Figure 4.15 Stack temperature as a function of time in TMDC

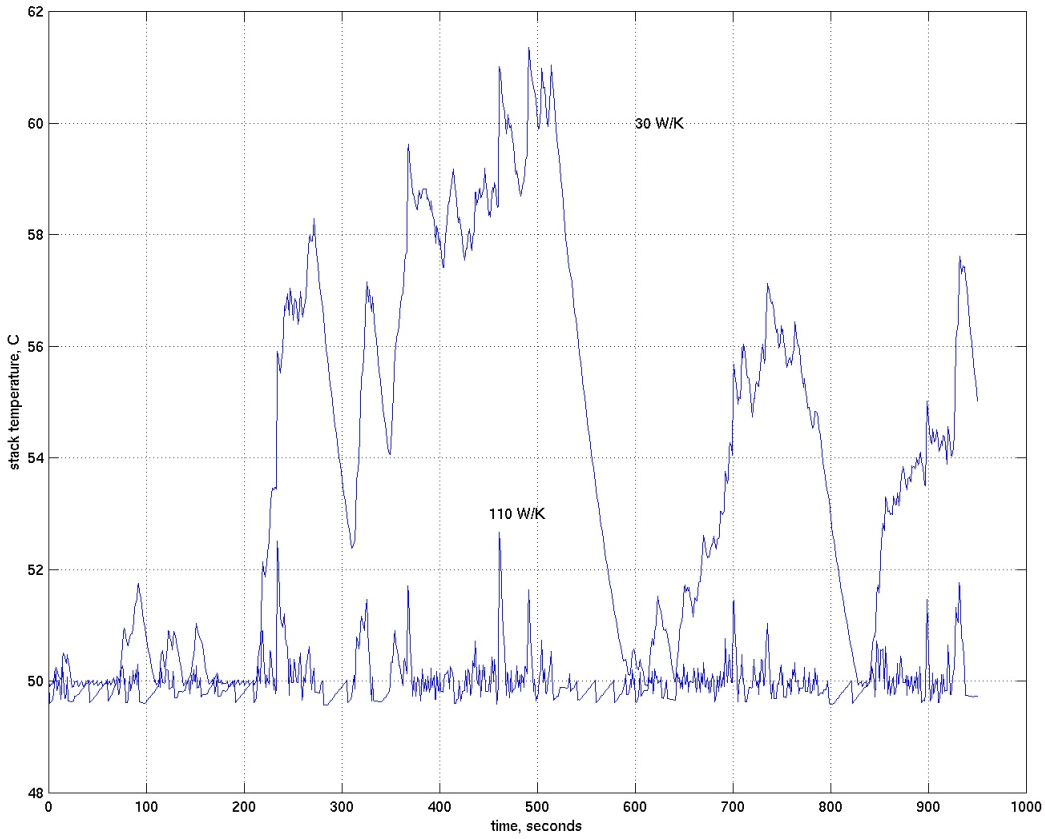

The smaller cooling factor is perfectly adequate to keep the maximum temperature below 65°C but, as calculated previously, the full 110 W/K is needed for sustained hill climbing.

As discussed, either the cooling fan or the pump could be switched on and off to produce cooling. In practice, the pump should be the unit controlled, because some cooling is still derived from pumping the water through the externally-exposed radiator, even if the fan blowing over the radiator is off. This seems like a benefit, except that excessive cooling would lower the fuel cell stack temperature below its designed operating point of 50°C; also, when the fuel cell is first started, it needs to warm up as quickly as possible.

A more sophisticated temperature simulation would include a time lag between the temperature measurement inside the stack and the control (turning the pump on or off). A more sophisticated *design* would vary the pump speed in order to reduce the power taken up by the pump, especially since adequate control could be maintained at just 20 W/K to achieve the result graphed above. This would decrease parasitic load and extend range, but, again, this was not assumed here due to the uncertainty in actual cooling power needs.

4.4.4.4 Selection

To achieve the upper limit of 110 $W \bullet K^{-1}$, a Lytron M14-120 radiator was selected. The cooling system includes a metal heat exchanger, pump operating at 1 gallon per minute (0.06 L/s), and fan blowing over the heat exchanger. For 110 $W \bullet K^{-1}$ of cooling, a fan speed of 375 cubic feet per minute (cfm) is necessary.[33]

According to performance charts (Appendix C), the coolant pressure drop in the radiator is 1.0 psi, while the fan-blown air decreases in pressure by 0.16 inches of water (40 Pa). Assuming a 50% pump efficiency and 50% fan efficiency, these translate into power demands of 25 W for the pump and 14 W for the fan. (Note that this takes the 1.0 psi coolant water pressure drop in the radiator and adds an estimated 2 psi drop from the fuel cell cooling cell flow fields)

It might seem that air supplied by ram-effect from the motion of the scooter would be enough to cool the exchanger. This is true in most cases, making the heat exchanger fan speed conservative, but false for the case of low-speed hill climbing, where power demands are high but air speed low. The design is also conservative because parasitic power is calculated as if the pump were on all the time, whereas this is actually not true as discussed previously.

This heat exchanger weighs 8.9 kg and takes up 15.2 L of space, including the fan, and accounts for a significant fraction of the total weight and volume.

4.4.5. Overall parasitics

Note that the specifications for pumps and blowers and radiators are for industrial, and often stationary, AC power components. This was done to get an idea of real world performance and cost without designing specifically for the scooter application. In practice, DC components would be needed to avoid an expensive DC-to-AC inverter, and components could likely be optimized for the application at hand. Prices, described in Chapter 5, are retail; cost to the scooter manufacturer would be as little as a quarter of retail.

The system requires a blower to push the air in, but omits the bulkier compressor and possibility of expander motor power recovery at the exhaust of the fuel cell.

The maximum parasitics estimated for the scooter system are 25 W for the coolant pump and 14 W for the fan blowing over the radiator, as discussed previously, plus a power draw from the Ametek blower power which is assumed to scale linearly with flow rate (i.e. power), from a minimum of 50 W of power at no load to 200 W at maximum fuel cell output of 6 kW. The power is calculated as if the pump and fan were on all the time, with the blower always requiring 50 W, for a total parasitic load of 89 W – 239 W over the output range of the fuel cell; in practice, power is saved by turning off – or slowing down – the fan and pump when not used.

The results are compared with those obtained by a study published by the Schatz Energy Research Center.[34] The Schatz report calculates the following total parasitic power requirements for a

nominal 4 kW vehicle (“Personal Utility Vehicle” - i.e. golf cart) fuel cell stack operating at atmospheric pressure.

In the Schatz system, the parasitic power comes from the water coolant pump, atmospheric-pressure blower, and the cooling fans. The system operates at approximately 40°C, and the air flow rate at 1.74 kW is 4.48 cfm (approximately 60% higher at the same power than the system presented here). So parasitic demands vary from 100% of gross power down to 5% above 2000 W, a fairly small fraction.

Figure 4.16 Parasitics as a function of power

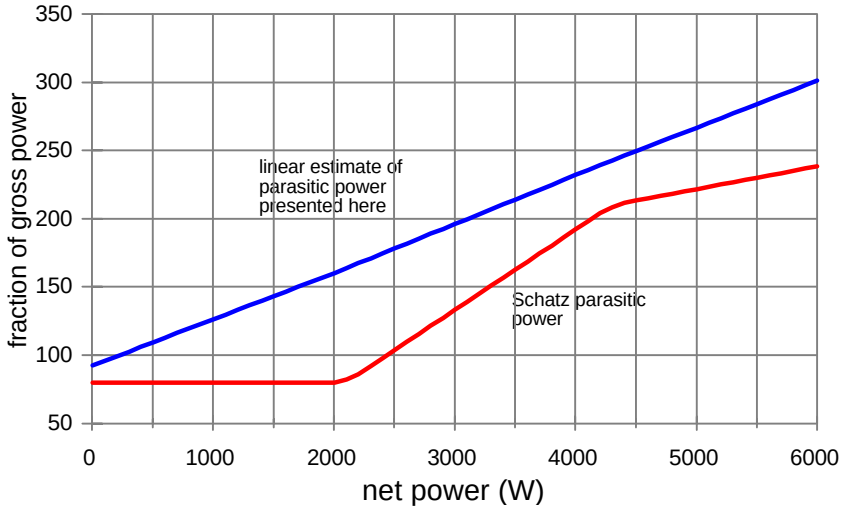

The next graph compares power usage as a percentage of gross power for both systems.

Figure 4.17 Parasitics as a percentage of power

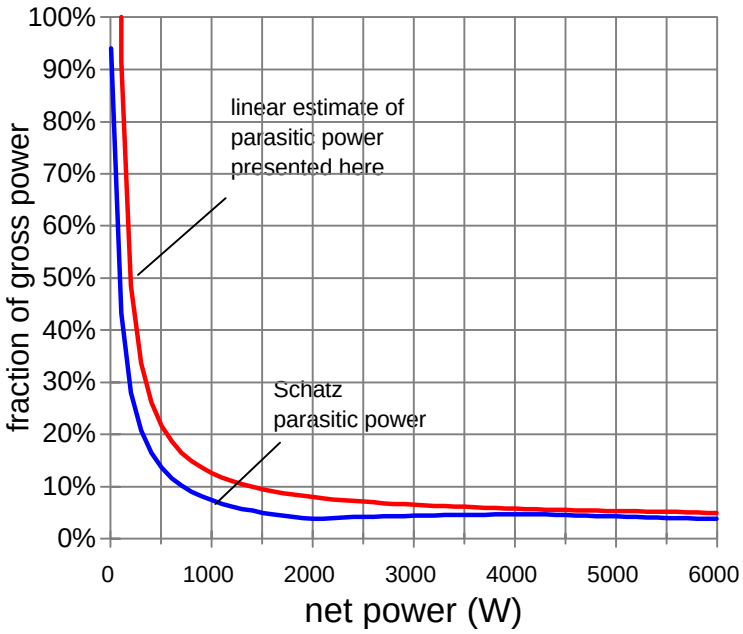

Finally, the parasitic power reduction is represented as a voltage reduction in the polarization curve. The result is a combined efficiency that has *net* electricity output as its numerator. The peak efficiency point is shifted to higher current densities and efficiency is reduced below 50% at all points.

Figure 4.18 Effect of parasitics on efficiency

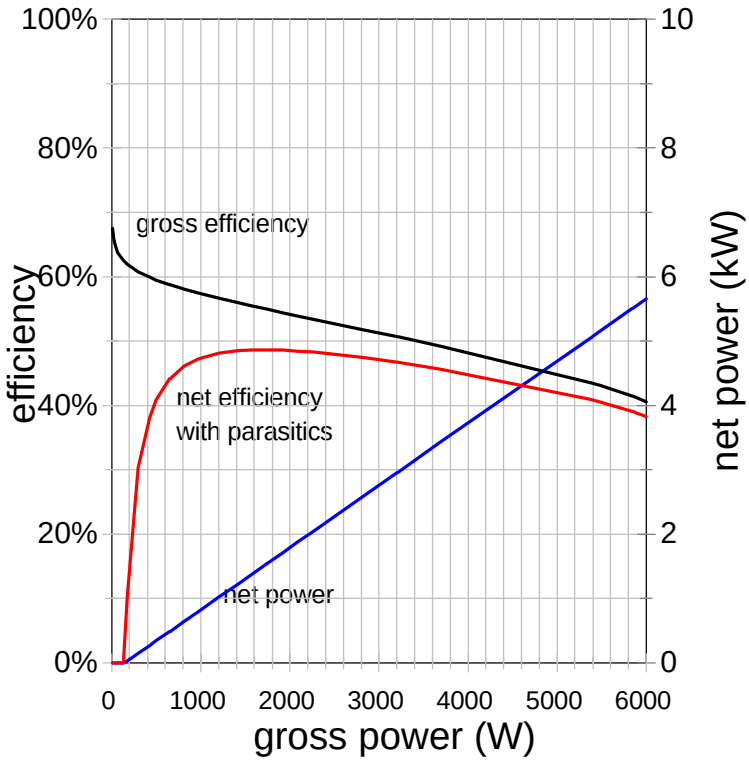

4.5 Integrated Model

4.5.1 System performance

The complete model takes the vehicle physical model described at the beginning of this chapter, and integrates the efficiency of the motor/controller subsystem, parasitic power demands, and the fuel cell polarization curve to determine overall efficiency: the amount of hydrogen consumed for a given travel distance under both the Taipei Motorcycle Driving Cycle and steady state 30 km/h driving conditions. The overall performance is used to identify the sizing of subcomponents like the fuel

storage supply and thus to determine the overall system weight and size.

Essentially, the driving cycle model is run, and at each discrete point in time, the power needed at the wheels is calculated and divided by the 77% drivetrain efficiency. An auxiliary power component of 60 W is added. Parasitic power is determined as a function of this total, and added. (This is an iterative process because the parasitic power is included in the total power, from which the parasitic power is calculated.)

Next, this total electrical output power is divided by the efficiency at that power demand; this efficiency is determined from the voltage on the polarization curve for the power required. The result is the amount of hydrogen consumed at the time interval, in terms of higher heating value energy units.

The results, over the driving cycle, are the maximum and average power (including parasitics); and the fuel economy in terms of hydrogen consumed per kilometer traveled. The latter is readily converted to miles per gallon of gasoline equivalent. An overall efficiency is calculated for the conversion process.

A battery-powered option is considered using the same basic model, but with no parasitic power to consider because fans, blowers, and pumps are not needed.

As before, the total scooter curb weight was set at 130 kg, and a 75 kg driver was added. Later results show that the vehicle weight is approximately the same as this assumption.

Table 4.13 System Performance under TMDC and at cruising speed

	TMDC	30 km/h cruise
Maximum power from fuel cell (includes drivetrain and parasitics)	5.91 kW	725 W
Average fuel cell output power	674 W	725 W
Overall efficiency	46.7%	58.5%
Fuel economy relative to hydrogen	0.527 km/g H_2	0.807 km/g
Equivalent "on-vehicle" fuel economy	344 mpge	522 mpge
Hydrogen storage for 200 km range	380 g	248 g
Average output power without parasitics (battery powered scooter)	566 W	614 W
Fuel economy of battery powered scooter	35.5 km/kWh	48.8 km/kWh
Battery energy storage for 200 km range	6.5 kWh	4.1 kWh

Note that these battery energies are given in terms of total energy output. The energy that must be put into these batteries is higher due to less-than-100% charging and discharging efficiency. However, this additional energy is not included here because price and performance figures for the zinc-air batteries are given in terms of energy output.

4.5.2 Size and weight of power system

The detailed analysis done in Appendix B and described in section 3.1.3.3 estimates a stack size and volume of 7.6 kg and 7.8 L respectively. This is a power density of 0.78 kW/kg and 0.76 kW/L for the stack alone, slightly less than 1996 Ballard stacks at 1 kW/L.

Assuming a factor of two extra for air and heat and water management subsystems gives power densities of 0.39 kW/kg and 0.38 kW/L. (The PNGV Technical Roadmap requirements are 0.4 kW/kg and 0.4 kW/L.[35]) That is a simple estimate;; the following paragraphs produce a more

detailed analysis of the subsystems. First, the heaviest and bulkiest subcomponents are analyzed and listed in Table 4.14. These are the blower that supplies air to the fuel cell stack, the pump that circulates cooling air, and the radiator. Prices are projected for mass production, with more details in section 5.1.3.

Table 4.14 Subcomponent summary

	Brand	Model	Dimensions (in cm)	Size	Weight	Cost (long term)
Fuel cell stack	–	–	–	7.8 L	7.6 kg	$220
Starter battery	Yuasa	GRT YT4L-BS	11 x 7 x 9	0.7 L	1.3 kg	$10
Coolant pump	generic	–	8 x 12 x 12	1.2 L	1 kg	$20
Radiator with fan	Lytron	M14-120		15.2 L	8.9 kg	$60
Blower	Ametek	116638-08	15 diameter x 17 length	2.9 L	2.7 kg	$110
plumbing, wiring, etc.	generic	–	–	2.0 L	3.0 kg	$50
coolant water	–	–	–	–	0.64 kg*	–
TOTAL STACK WITH AUXILIARIES	–	–	–	29.8 L	24.6 kg	$470

The "generic" pump has pressure requirements of 2.5 psi and a pumping flow rate of 1 gallon per minute. This is adequately supplied by an aquarium-type pump. Electric cabling, air manifolds, water plumbing were estimated to add 3 kg and 2 L and a cost of $100

*Note that the radiator holds 320 mL of water when full, and with an estimated total of twice that amount of water in the entire system, this adds an additional 0.64 kg of weight.

The total performance figures for the stack with auxiliaries are 0.24 kW/kg and 0.20 kW/L. The stack proper takes up 27% of the mass and 26% of the volume.

In comparison, the overall fuel cell stack weight of the Schatz 4 kW system described previously was 75 lbs or 34 kg; the entire power system weighed 200 lbs or 90 kg. Stack volume was 10" x

11" x 21", or 39 L.[36] With the greater room of a golf cart, engineering for minimum volume is not so critical, but these results still indicate that reduced size and weight have not yet been demonstrated

The sizes and weights with the hydrogen storage system included are listed in Table 4.15 below. Both a current Ergenics metal hydride system and predicted FeTi performance are included, along with a Dynetek cylinder and the ZES-2000 battery-powered scooter for comparison purposes.[37]

Table 4.15 Size of various storage designs

storage system	energy stored	range at 30 km/h (km)	range under TMDC (km)	energy storage (battery or H_2)		complete drive system	
				weight	volume	weight	volume
ZES-2000 lead-acid batteries	1.34 kWh	60	40*	44 kg	15 L	60 kg	24 L
DTI TiFe hydride	250 g H_2	200	132	21 kg	4 L	61 kg	43 L
Ergenics hydride (aluminum body)	204 g H_2	165	108	27 kg	14 L	67 kg	53 L
Dynetek cylinder (compressed gas)	350 g H2	282	184	11 kg	31 L	51 kg	70 L

"complete drive system" refers to the motor and controller from Table 2.2 (15.5 kg and 9.1 L together), the fuel cell stack, auxiliaries, and hydrogen storage.

* Note that the ZES-2000 can not actually sustain the TMDC, as it lacks the power necessary for the high-speed accelerations; its range is given as if it had could produce the required maximum *power* using its current batteries. For comparison, according to an unspecified pattern of "urban driving", it is listed at a range of approximately 30 km; reported data shows that it reaches 80 km on a single complete discharge at 30 km/h.[38]

Also, although the ZES-2000 does not actually use the Unique Mobility motor / controller system specified, these numbers are similar to those of other motor/controller systems and were used in calculating total size and weight for the battery-powered scooters.

This comparison has used the criteria of size and weight, but it should also be noted that cooling loads are higher for compressed gas hydrogen storage systems, due to the lack of desorption cooling. This results in larger cooling loads and higher parasitic demands from the cooling system, not shown here. The results of Table 4.15 are discussed in the subsection following.

4.5.3 Evaluation

Average two-stroke scooters weigh 70 kg and up, but the overall ZES-2000 prototype mass is 105 kg. A Honda CUV-ES electric scooter weighs 130 kg. Fuel cell powered scooters would weigh about as much as the CUV-ES; recall that one of the concerns in the consumer satisfaction survey was the extra weight of the electric scooter. While this might remain an item of difficulty in terms of handling while the system is off, the extra performance provided by the 6 kW fuel cell system partially compensates for the high mass.

The fuel cell vehicle offers more than three times the range of the ZES-2000, with roughly the same weight of drive system. The fuel cell systems requires 18 to 36 additional liters of storage space over that of the ZES-2000. There is a helmet storage chamber in the design that could be commandeered for additional fuel storage; this is approximately 10-15 L of space. Additional volume would have to come from a redesigning of the scooter body to make more room available, but note that current electric scooters already use redesigned large-capacity bodies.

Current laboratory-scale metal hydrides, as exhibited by the Ergenics system, are almost 30 L larger than the ZES-2000 power system, so progress must be made in improving metal hydride technology.

The following charts describe the breakdown of size and weight for the various subsystems, for a

FeTi hydrogen storage system

Figure 4.19 Weights of subsystems

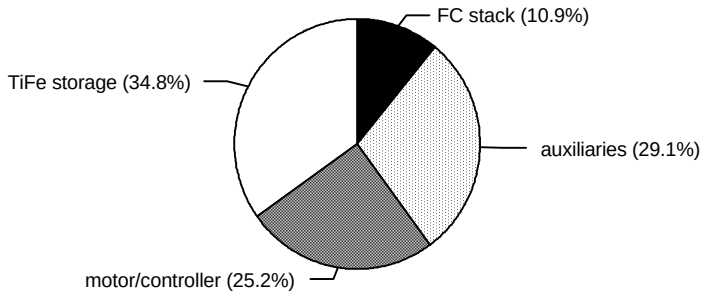

Figure 4.20 Volumes of subsystems

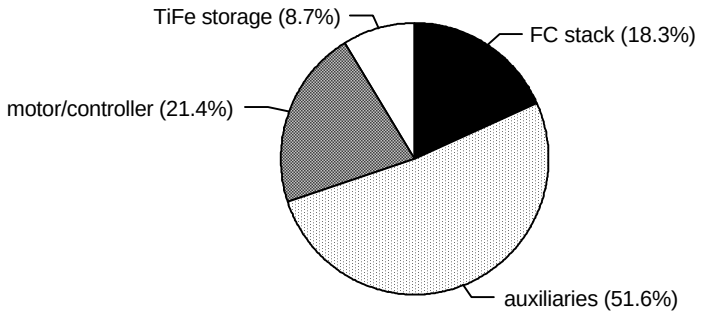

A subsequent chapter deals with the costs of the various systems, but the next section is a discussion of whether operating the fuel cell at higher pressures (with consequent greater efficiency) might improve performance and reduce the size of the fuel cell required.

4.6 Pressurized fuel cell option

One of the two options considered for improving the performance of the base design was to operate the fuel cell above atmospheric pressure. To quantify this benefit, the higher voltage output obtainable was compared to the additional power needed to drive the compressor. Also included was the fact that a turbine running of the fuel cell exhaust would reduce the compressor load. Calculations were based on a adiabatic, non-isentropic system with the 68% efficiency assumed previously.

Power out for an *adiabatic* expander (or compressor):

$$P_{adiabatic} = \dot{n}\int_{P_1}^{P_2} V\ dP = \dot{n}RT\,\frac{\gamma}{\gamma-1}\left(\left(\frac{P_1}{P_2}\right)^{\frac{\gamma}{\gamma-1}} - 1\right)$$

$\dot{n}$ is the flow rate in moles•s^{-1}; R is universal ideal gas constant, 8.314 J·mol^{-1}·K^{-1}. The specific heat ratio γ is the ratio of C_p to C_v for the working fluid. Assumptions: the intake air is an ideal gas consisting of nitrogen and 20.95% oxygen; the exhaust (mainly nitrogen, with some water vapour and unused hydrogen) is an ideal gas with the stoichiometric amount of oxygen removed by the fuel cell reaction, and no water vapour.

The benefit of compression is calculated using the two Energy Partners polarization curves discussed previously (3 atm and atmospheric). The atmospheric power is net of blower parasitic power, which is a linear function from 50 W to 250 W over the 5.9 kW operating range of the fuel cell stack. The pressurized stack power is net of compressor and expander powers, as calculated for a 68% efficiency expander and 68% efficient compressor. (same as the DOE's projected automotive

system). Note that this fails to capture the lowered efficiency expected at lower-than-nominal flow rates, while the blower's linear function does effectively reduce efficiency at low flow rates.

The mechanical power required by the compressor is always greater than the mechanical power recovered by the expander, and any supplement is calculated to be made up from the fuel cell at a 90% conversion efficiency from electricity to shaft power through an electric motor.

The figure below compares the power outputs at given current densities. Note that the powers, here, are proxies for efficiency because at a given current density both options are operating on the same amount of hydrogen per second.

Figure 4.21 Atmospheric power versus 3 atm power

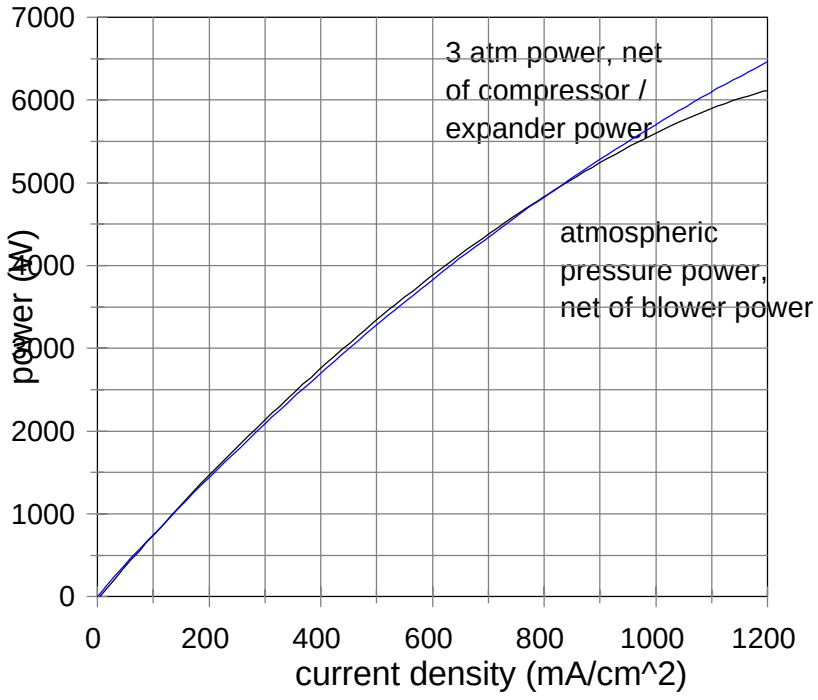

The difference expands to 350 W at 1200 A•cm^{-2}, so the pressurized fuel cell does have benefits at high pressure. However, at the maximum operating point of 1000 A•cm^{-2}, the advantage of the 3 atm fuel cell is only 105 W, or 1.8% of the gross power. Although there is an unquantified benefit for the pressurized fuel cell due to the lesser need for humidification and easier water removal, the gain is quite limited and the scooter cannot accept the additional cost and weight of an additional turbocompressor system. Also, unlike the case for automobiles, the fuel cell stack size would not be appreciably reduced by operating at 3 atm.

If the DOE goals of 3 kg and 4 L for a turbocompressor can be realized, and efficiency is good at the under-10 g/s flow rates required in scooters, then the slight performance benefit will be worth a small price premium.

4.7 Hybrid option design

A second optimizing option was considered. Due to the extremely irregular nature of scooter driving, with average power only 8% of maximum power, peaking power provided by a secondary power device might be an efficient way to reduce the fuel cell size. The fuel cell would provide baseload power and charge up the secondary (peaking) power source for later use. A peaking power device, which could be an advanced high-power battery, an ultracapacitor, or a flywheel, would also enable regenerative braking.

The targets of hybridization, for the scooter are to:

1. Reduce system cost by reducing fuel cell size; *peaking power* batteries are cheaper than additional fuel cell capacity, at least for the next several years.

2. Increase total fuel economy with regenerative braking and lower curb weight. For the same hydrogen storage, greater fuel economy means greater range.

3. Improve vehicle handling by reducing curb weight.

The major drawback is that hybrid systems require more complex controls and power conditioning systems. To optimize the system, a balance must be struck between secondary power source size and main power source size. An important consideration is whether weight and volume of auxiliaries will decrease significantly if a smaller fuel cell is used.

4.7.1. Types of hybrids

There are several types of hybrid vehicle designs. Most of these are defined for internal combustion engines and used for the purposes of (i) increasing engine efficiency, (ii) reducing emissions, and (iii) reducing cost if the main engine is expensive, like a fuel cell. Hybrids are divided into parallel and series systems.

For a combustion hybrid, a parallel system allows both the engine and the peaking battery (via electric motor) to drive the wheels using two separate systems. This system is more mechanically complex due to the two driveshaft attachments, but allows simultaneous use of the battery and the combustion engine.

In contrast, a series hybrid routes all power electrically. The combustion engine drives a generator (not required in the parallel version), which can supply energy to the wheels and the peaking battery. Output from the generator and the peaking battery go to the wheels. Generally, the engine can be set to operate only at its most efficient speed, recharging the battery as needed and avoiding transients which might produce more emissions.

The more specific operating policies listed below are from the DOE HEV program guidelines.[39] The word "battery" is used interchangeably with "secondary energy storage system," although this system could actually be a flywheel or ultracapacitor.

1. *Thermostat series*. The vehicle is run on battery power by default, with the primary power source activated (at the optimum power level) when the battery drops below a predefined minimum. The primary power source acts as a thermostat, turning on and off to maintain battery state of charge. This policy allows the primary power source to run at its peak efficiency point.

2. *Electric-assist parallel.* The primary source provides power by default, and the battery is discharged only in high-power situations. The battery is recharged by regenerative braking, but in the case of combustion engine hybrids, cannot be recharged by the engine because there is no generator. The primary power source can be sized below the maximum power required since it is assisted by the battery.

3. *Primary power-assist parallel.* Identical to the previous system, but with the battery providing power, and the internal combustion engine supplying peaking power. Very similar to a "range-extender" system in that the battery functions as the main energy storage device.

4. *Load-leveler series.* The average power is matched to the output of the primary power source, while logic attempts to maintain the state of charge of the battery at a predefined medium level. Peaking power is supplied by the battery, but the primary power source load is allowed to vary as well to maintain the state of charge of the battery. (This contrasts with the thermostat series option, where the combustion engine stays at its optimal point).

The different policies show that the design is motivated by a desire to keep the combustion engine at its optimum point (maximizing fuel economy and minimizing emissions) for the series options, and reducing the engine size in the parallel options.

A fuel cell hybrid is technically a series hybrid because there is a single drive system (electric). The fact that all power is electric means that, if designed properly, the control logic can allow both fuel cell and battery to drive the wheels (like an electric-assist parallel), or let the fuel cell recharge the battery (like a load-leveler series). Several axes of optimization remain - for example, how large to make the fuel cell, when to use the battery and when to recharge it, and how large to make the battery.

4.7.2. Fuel cell sizing

In order to calculate how to divide the power needs between the fuel cell and the battery, two criteria were specified. First, maximum power (5.6 kW net of parasitics) had be sustained for at least ten seconds. Users would be very disappointed to find that, after a few seconds of pushing their scooters to the maximum output, power started to fall off because the battery was used up. Second, the scooter had to sustain - indefinitely - the slope-climbing requirements. In other words, it had to generate enough power to climb a 12° slope at 18 km/h.

The physical model showed that these results can be obtained with a fuel cell stack with a maximum output of 3.2 kW gross power (3.0 kW net). Total cell active area was reduced by reducing the area of each cell to 110 cm^2, while the number of cells was kept the same in order to retain the 48 V motor voltage. To reach the maximum power *output* level thus required the addition of a 2.6 kW peaking battery. This is the first hybrid scooter case.

One other case was considered. This one is targets the short term where fuel cells are extremely expensive and the fuel cell size must be minimized at all costs: a fuel cell sized to output only 1.0 kW of net power (1.1 kW gross power), with a large battery for the remaining 4.6 kW.

This scooter would not be capable of indefinitely sustaining hill climbing as specified at the beginning of the chapter. The specified performances can only be achieved for under three minutes until the batteries drain down to their 20% limit, and the continuously sustained hill climbing speeds are lower than the requirements, as shown in the table below.

Table 4.16 Hybrid 1.1 kW scooter inadequacies

	15° slope	**12° slope**
Required performance	10 km/h	18 km/h
Limited amount of time at this speed as battery is drained	140 s	70 s
Limited distance at this speed	380 m	360 m
Sustainable maximum speed (after battery depleted; fuel cell only)	4.7 km/h	5.8 km/h

Cooling load is significant in hybrid vehicle design as well as in the original pure fuel cell design; again, the critical situation is hill climbing requiring 3.2 kW of continuous output. In the 5.9 kW full-sized fuel cell, continuous operation at 3.2 kW gross output takes place at 51% efficiency, and

heat production is consequently low. A 3.2 kW maximum power fuel cell, however, is only at 43% efficiency when it is continuously operated at 3.2 kW, producing more heat. The greater heat also necessitates higher pump and fan loads for the radiator, meaning greater parasitic loads.

Parasitic power loads were calculated with an iterative process. The first step was to estimate a parasitic load. Then the maximum gross output power including parasitics was calculated for hill climbing. A maximum heat output was then solved, and the parasitic power required to sustain this cooling load was calculated. The process was repeated until the results converged. In the example here, after the results had settled down to stable values, the following results were obtained:

For the first hybrid, the maximum load was 3020 W, with parasitic power costs of 66 W for pump and fan, and 50-250 W for the blower depending on load. The total fuel cell output was 3205 W at this net power output, for a waste heat load of 4240 W. With hydride cooling at 17.2% at this hydrogen flow rate, the remaining heat load was 3510 W, or 140 W/K at the pre-defined ΔT of 25°C, which was supplied by fans and pumps with the total of 66 W.

The 1.1 kW system was easier to solve because the output was simply capped at 1.0 kW of net output, because no attempt had to be made to find the total power at which the hill climbing requirements could be met. A smaller M10-080 radiator was used. Under maximum conditions of 1.1 kW gross power, heat generation was 1430 W, or 1180 W after metal hydride desorption, for a cooling load of 47 W/K.

Table 4.17 Hybrid fuel cell stack designs

	Pure FC	Hybrid 1	Hybrid 2
Maximum gross power	5.9 kW	3.2 kW	1.1 kW
Stack current at maximum power	172 A	89 A	31 A
Efficiency at maximum current density	41.2%	43.2%	43.6%
Total active area needed	9600 cm^2	5600 cm^2	2000 cm^2
Total number of fuel cells	56	56	56
Active area per cell	170 cm^2	100 cm^2	35 cm^2
Maximum fuel cell heat generation	8.4 kW	4.2 kW	1.4 kW
Maximum heat generation (after metal hydride cooling)	7.0 kW	3.5 kW	1.2 kW
Cooling factor needed at maximum power (ΔT=25°C)	280 W/K	140 W/K	47 W/K
Maximum net fuel cell power	5.9 kW	3.0 kW	1.0 kW
Battery power needed	–	2.6 kW	4.6 kW

4.7.3 Peaking battery and operating policy

The peaking power battery model is described in section 2.2.3.1 and has the following properties. Note that the specific power and power density are much higher for the battery than the fuel cells (see Table 4.24), so that hybridization makes sense in reducing total weight and volume.

Table 4.18 Peaking power battery characteristics

Specific power at 43 second discharge	836 W/kg
Specific energy	17 Wh/kg
Power density by volume	853 W/L
Energy density by volume	17 Wh/L

The heat generated by the battery is not included in the system modeling. It is on the order of 10%

of the output power, low compared to the fuel cell. At maximum output power (4.6 kW for the 1.1 kW stack hybrid) this could be almost 500 W in addition to the fuel cell, but this heat load is infrequently reached. The operating policy of the battery is defined as follows.

1. The state of charge of the battery is allowed to vary between 80% and 20% over the driving cycle. The state of charge is kept away from these "hard limits" in order to reduce the risk of large excusrions (overcharging or draining to zero), either of which could permanently damage the battery.

2. The state of charge is set at the beginning of the driving cycle is set to 50%

3. The battery is activated (discharged) whenever the fuel cell maximum power is not enough for the driving cycle power plus auxiliary and parasitic loads, and makes up the entire difference.

4. Regenerating always recharges the battery as long as the maximum charging current is not exceeded, up to the 80% limit

5. The battery is charged up from the fuel cell at a specified rate whenever (i) the state of charge dips below 55% and (ii) power demand at that instant is less than 400 W. The charging rate is equal to 400 W minus the instantaneous power demand from the wheels, auxiliaries, and parasitics.

4.7.4 Simulation results

First, fuel economy was determined under steady-state, 30 km/h driving conditions.

Table 4.19 Hybrid performance at 30 km/h

Parameters	5.9 kW pure FC	3.2 kW hybrid	1.1 kW hybrid
fuel cell conversion efficiency	58.5%	56.4%	50.0%
average fuel cell output power	725 W	751 W	710 W
fuel economy in terms of hydrogen	0.807 km/g	0.751 km/g	0.703 km/g
"on-vehicle" fuel economy	522 mpge	486 mpge	455 mpge
change from pure FC	–	-4%	-15%
hydrogen for 200 km	248 g	266 g	284 g

Efficiency decreased as the fuel cell size decreased, because the smaller fuel cells were operating closer to their maximum output. For the results below, the hydrogen storage system was scaled linearly to keep range at 200 km. The driving cycle was more interesting because its decelerations created the possibility of regenerative braking.

Table. 4.20 Hybrid performance under TMDC

Parameter	5.9 kW pure FC	3.2 kW hybrid	1.1 kW hybrid
Fuel cell maximum power	5.91 kW	3.24 kW	1.11 kW
Battery maximum power needed	–	2.61 kW	4.63 kW
Average total power output, battery + fuel cell	674 W	709 W	726 W
Average fuel cell power	674 W	698 W	577 W
Fuel economy (mpge)	344	316	343
Change in fuel economy	–	-8.2%	-0.3%
Overall conversion efficiency	56%	53%	47%
Braking energy absorbed	–	62 kJ	82 kJ
Average power absorbed	–	65 W	86 W
Braking energy recovered as a fraction of theoretical maximum braking losses	–	51%	68%

The 1.1 kW fuel cell puts out 100 watts less average power than the 5.9 kW fuel cell, because the 86 W (average) that is recovered from regenerative braking can supplement the peaks. However, conversion efficiency from hydrogen heating value to electricity is lower at 47%, because the fuel cell is operating more frequently near its maximum power (minimum efficiency). More hydrogen must be used to produce the 577 W of power than if the larger, pure fuel cell were used with the same batteries. The result is a net fuel economy that is the same as the pure fuel cell.

The 3.2 kW hybrid actually consumes more power in the TMDC due to the higher parasitic losses, and for the same reason of operation near maximum power given above.

The regenerated fractions of 51% and 68% are close to the 70% theoretical maximum that can be regenerated. The differences are due to the limiting maximum charging rate and the fact the at some points the battery is already full when regenerative braking is possible. In terms of total power, though, these figures are equivalent to 9% – 14% of the total fuel cell output.

Figure 4.22 Division of power between fuel cell and battery during TMDC, 3.2 kW stack

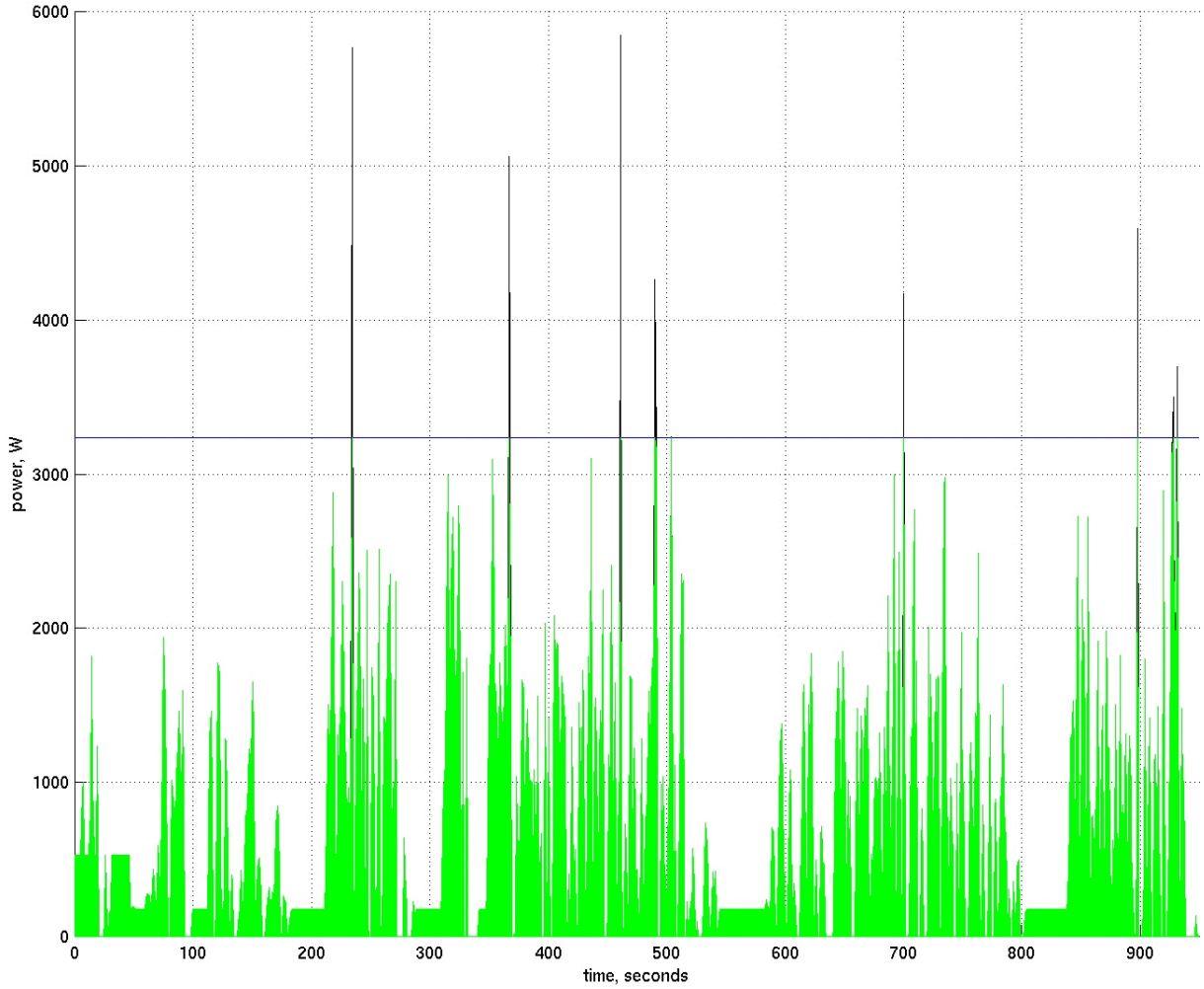

In this diagram, the dark area above the horizontal line represents the energy supplied by the peaking power battery, while the light gray area below the line is the energy supplied by the fuel cell. The same scheme is used in Figure 4.24.

Figure 4.23 State of charge of battery over TMDC, 3.2 kW stack

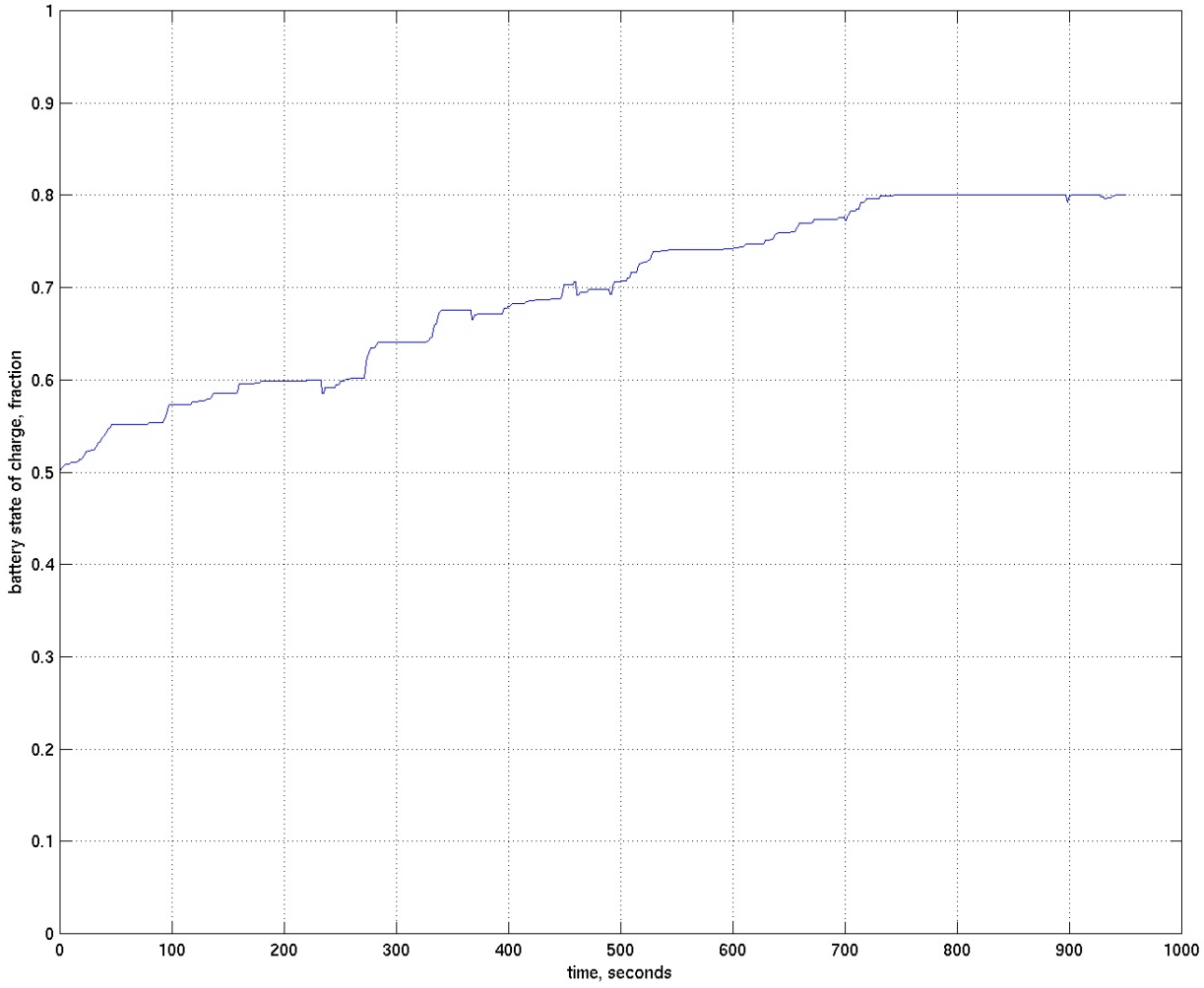

The careful observer will note that battery energy does not return to initial levels over the driving cycle - in fact, there is a net gain from regeneration of 58.3 kJ, or an average of 60 W over the 950 second cycle. There is a not insignificant amount of surplus energy that could be applied to the wheels, if the battery were employed using a more sophisticated policy (for example, using the battery even if power demand is *not* greater than the maximum fuel cell output), and fuel economy would be slightly improved.

Since the object was to minimize component cost and not necessarily produce the maximum mileage, the design of more efficient hybrid strategies will have to await future studies.

Figure 4.24 Division of power between fuel cell and battery during TMDC, 1.1 kW stack

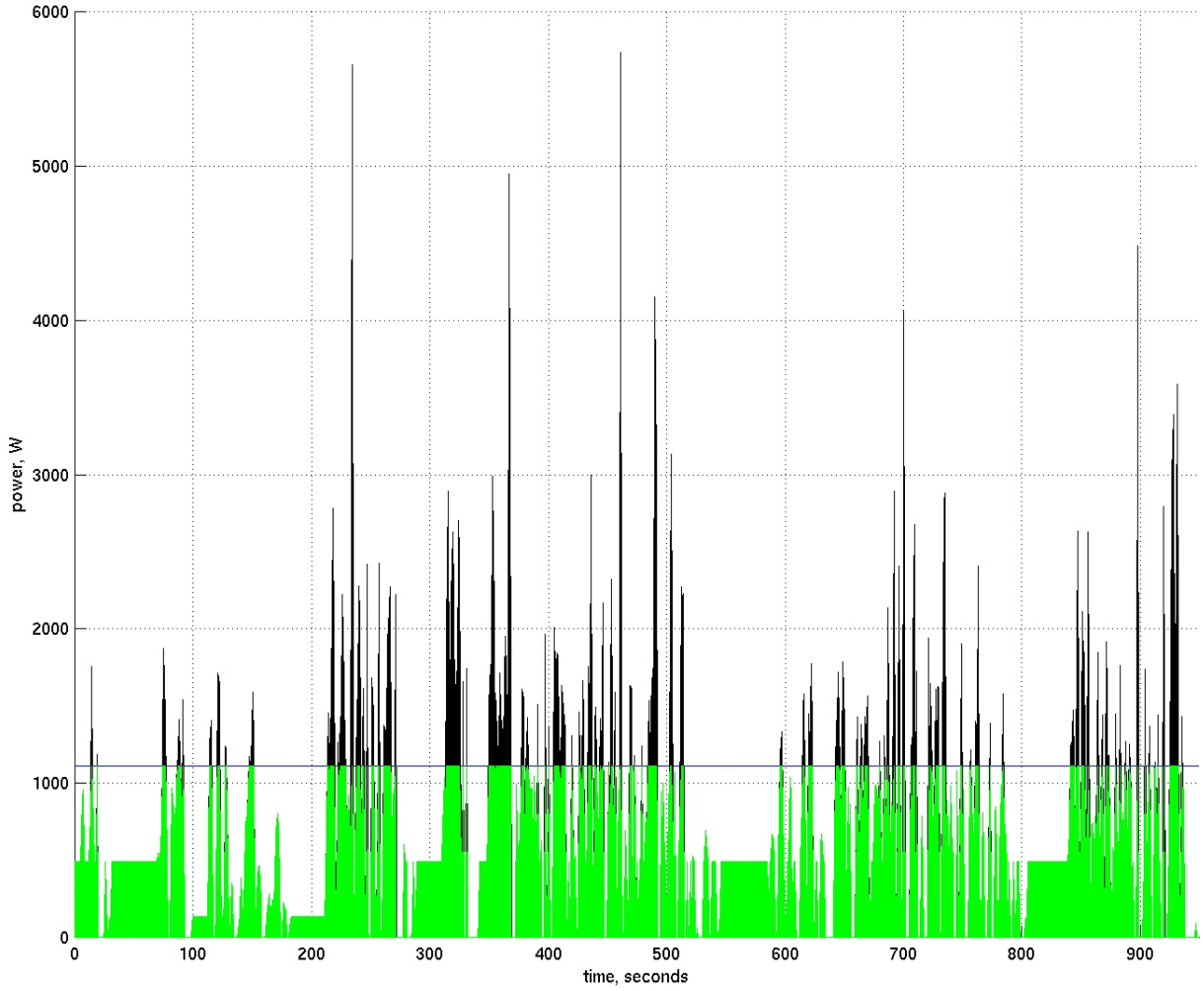

Figure 4.25 State of charge of battery over TMDC, 1.1 kW stack

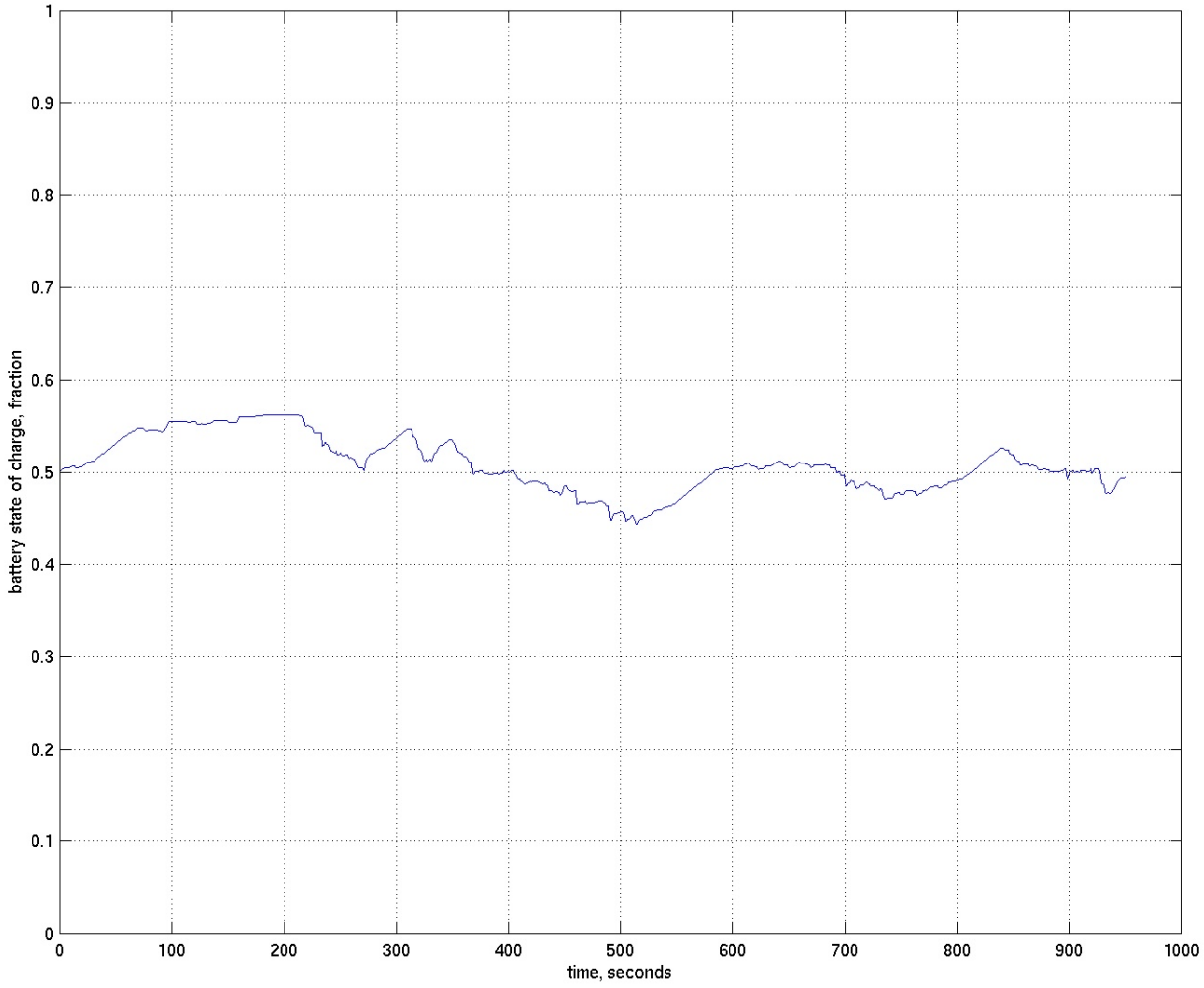

4.7.5 Hybrid power system designs

The subsystem performance requirements and sizes/weights are listed for the two hybrid designs, with the base pure fuel cell system for comparison.

Table 4.21 Hybrid system design

Parameter	5.9 kW pure FC	3.2 kW hybrid	1.1 kW hybrid
Maximum hydrogen flow rate	2.6 cfm	1.4 cfm	0.5 cfm
Maximum air flow rate	15.6 cfm	8.1 cfm	2.8 cfm
Worst-case cooling requirement	110 W/K	150 W/K	50 W/K
Cooling fan power requirement	14 W	28 W	4 W
Coolant pump power requirement	25 W	38 W	21 W
Fuel cell stack weight	6.7 kg	5.4 kg	4.1 kg
Fuel cell stack size	7.8 L	5.3 L	3.2 L
Fuel cell cost (manufacturing cost)	$220	$160	$140
Battery maximum power needed	–	2.6 kW	4.6 kW
Battery weight	–	3.1 kg	5.6 kg
Battery size	–	3.0 L	5.4 L
Battery cost (retail)	–	$195	$340

The same DTI model was used to calculate fuel cell stack sizes, weights, and costs. The designs are described in greater detail below.

4.7.5.1 Design for 3.2 kW fuel cell

For the 3.2 kW fuel cell, fuel economy actually goes down with hybridization. There are three reasons: (i) the cooling system parasitic load is larger (ii) the fuel cell is operating more frequently near its maximum load (iii) the battery is rarely used to output energy.

At maximum cooling load and 50% efficiency, the cooling fan runs at 500 cfm (0.24 inches of water pressure drop) and uses 28 W of power while the pump pushes coolant at 1 gpm (2.5 psi pressure drop) and uses 38 W. Thus, the base load power needed for the cooling system is 66 W.

The lower air intake flow requirements might make a smaller and cheaper blower feasible.

With auxiliaries the power system totals are 21.9 kg and 26.6 L, for power densities of 0.15 W/kg and 0.12 W/L.

Table 4.22 Component breakdown for 3.2 kW scooter

Component	Weight	Volume	Long-term cost
Fuel cell stack	5.4 kg	5.3 L	$165
Radiator and fan	8.9 kg	15.2 L	$60
Coolant pump	1.0 kg	1.2 L	$10
Blower	2.7 kg	2.9 L	$110
plumbing, wiring, etc.	2.0 kg	2.0 L	$50
coolant water	0.9 kg	–	–
peaking power battery	3.1 kg	3.0 L	$195
TOTAL STACK WITH AUXILIARIES	25.1 kg	29.6 L	$590
motor	11.4 kg	5.0 L	$125
controller	4.1 kg	4.1 L	$150
hydride for 266 grams H2	22.8 kg	4.0 L	$200
TOTAL DRIVE SYSTEM	63 kg	43 L	$1065

Due to the lower fuel economy of the 3.2 kW system at 30 km/h, slightly more metal hydride is needed: 266 grams for 200 km. This requires a 22.8 kg system taking up 4.0 L of space.

The total size and weight are very close to the original, 5.9 kW fuel cell. Mainly this is because the subsystem sizes remain the same even though the fuel cell proper becomes smaller. Smaller blowers and coolant pumps could be used, reducing weight slightly, but the largest subcomponent (the radiator) has to stay large in order to handle the higher cooling factor of 140 W/K.

4.7.5.2. Design for 1.1 kW fuel cell

In the second hybrid, the battery is used much more often and contributes frequently to the total power output. However, for the same reason, the battery must be frequently replenished, and due to the small size of the 1.1 kW fuel cell, the fuel cell often runs near its inefficient maximum output. The net fuel economy is almost identical to that of the pure fuel cell.

Cooling is different. The system is sized for cooling when it is running flat out at the maximum 1 kW of net output, rather than for sustained (3020 W) hill climbing. After metal hydride cooling, the worst-case cooling load is less than 50 W/K. This is achievable with a fan at 140 cfm with 0.125 inches of water air pressure drop (4 W of power), and a pump at 1 gallon per minute with 0.5 psi water pressure drop (21 W of power), for a total of 25 W. The lower cooling load of 50 W/K means that a smaller radiator can be used here – the Lytron M10-080.

With auxiliaries, the power system totals are 21.9 kg and 26.6 L, for power densities of 0.15 W/kg and 0.12 W/L.

Table 4.22 Component breakdown for 1.1 kW scooter

Component	Weight	Volume	Long-term cost
Fuel cell stack	4.1 kg	3.2 L	$135
Radiator and fan	3.1 kg	2.3 L	$30
Coolant pump	1.0 kg	1.2 L	$10
Blower	2.7 kg	2.9 L	$110
plumbing, wiring, etc.	2.0 kg	2.0 L	$50
coolant water	0.6 kg	–	–
peaking power battery	3.1 kg	3.0 L	$340
TOTAL STACK WITH AUXILIARIES	20.1 kg	17.0 L	$675
motor	11.4 kg	5.0 L	$125
controller	4.1 kg	4.1 L	$150
hydride for 285 grams H2	24.3 kg	4.3 L	$215
TOTAL DRIVE SYSTEM	60 kg	30 L	$1165

Due to the lower fuel economy of the 1.1 kW system at 30 km/h, slightly more metal hydride is needed: 284 grams for 200 km. This requires a 24.3 kg system taking up 4.2 L of space.

The extra battery size is compensated for by the smaller fuel cell, while the smaller radiator makes a large difference in reducing the total volume.

4.7.5.3 Hybrid zinc-air scooters

If fuel cells can be hybridized with peaking power batteries, why not battery powered scooters? Regenerative braking would extend the range of the vehicle, while separating the power and energy functions might allow a smaller, less expensive power system. In the fuel cell, energy and power are decoupled. The fuel cell engine is sized for a maximum power output, and the amount of hydrogen

carried can be varied to meet range requirements. With the battery, a larger power necessarily corresponds to a larger energy storage, and sizing for power may result in overdesigned energy (or vice versa). The hybrid battery system reduces this dependence by using batteries with two different power-to-energy relationships.

The hybrid battery design presented here uses zinc-air batteries (high energy density) for range, plus the peaking power lead-acid batteries (high power density) described above. The two sets of batteries operate in the same way as the fuel cell hybrid, so that the peaking power of the high power lead-acid batteries can be added to the zinc-air baseload battery's power, and the peaking batteries can be used to absorb regenerative braking energy.

The power and energy requirements are specified so that the scooter has enough power to sustain the maximum accelerations of the TMDC, and enough energy to drive 200 km at a constant speed of 30 km/h (or 145 km under the TMDC). 5.6 kW of output power and 4.1 kWh of energy storage are needed, and the following results are obtained:

Table 4.24: Hybrid battery configuration for Taiwan scooter model

Parameter	Zinc-Air baseload battery	Spiral lead-acid peaking battery	Total
Weight	20.5 kg	4.5 kg	25.0 kg
Energy Capacity	4.1 kWh	0.07 kWh	4.1 kWh
Peak Power	1.8 kW	3.8 kW	5.6 kW
Specific Energy	200 Wh/kg	17 Wh/kg	168 Wh/kg
Specific Power	90 W/kg	836 W/kg	210 W/kg
Volume	27.1 L	4.4 L	31.5 L
Long term mass-production price	80 $/kWh	75 $/kW	–
Total price	$330	$285	$615

The zinc-air volumetric energy density is calculated to be 150 Wh/L from published data; cost for high-power lead acid battery is estimated at 166 $/kW based on a scaled up version of Bolder batteries.[40] This is reduced to 75 $/kW in mass production (The Rebel battery's density is approximately 1 kg/L and the future goal is $150/kWh for long term USABC batteries and advanced lead-acid batteries. Somewhat arbitrarily, power systems are assumed to be half as expensive per kilowatt as base load batteries.[41])

Note that the continuous power output of 1.8 kW is not sufficient for the continuous hill climbing needs; rather, the baseload battery is sized for the 200 km range and 4.1 kWh required. Thus, the hybrid battery vehicle is more comparable to the 1.1 kW fuel cell system than the 3.2 kW system.

(The Electric Fuel company has its own, more conservative hybrid battery scooter theoretical design; it is specified for 4 kW maximum power and 3.0 kWh energy storage, for a claimed range of 200 km. This 3.0 kWh storage is underspecified, according to the calculations earlier in this chapter. Their power source consists of two 8 kg zinc-air batteries, each 9.9 L, 7.5 kg, and with an output of a maximum of 0.75 kW. The peaking power source must thus supply 2.5 kW, and is not described in the Electric Fuel report although it likely will be a NiCd battery.[42]

4.7.6 Hybrid results

The hybridization study reveals that peaking power batteries do not significantly reduce the mass and volume of the fuel cell system, because the auxiliary cooling and fluid management systems require a certain minimum space and mass which does not decrease rapidly with size.

Fuel economy did not improve significantly, due to the fact that with a 3.2 kW fuel cell, only a few

excursions required use of the battery and parasitic loads were higher than for the pure fuel cell. The 1.1 kW version produced fuel economies equal to the original pure fuel cell because of its lower efficiencies; on the other hand, it reduced the size of the fuel cell stack by a factor of more than five, which is important for the short term cost.

Table 4.25 Hybrid power system summary

	5.9 kW fuel cell	**3.2 kW hybrid**	**1.1 kW hybrid**	**1.8 kW battery hybrid**
ultimate stack cost	$244	$161	$124	–
stack cost/kW	$42	$47	$103	–
stack size	7.8 L	5.3 L	3.2 L	–
stack weight	7.6 kg	5.4 kg	4.0 kg	–
stack with auxiliaries, size (excl. peaking battery)	29.8 L	26.6 L	11.6 L	–
stack with auxiliaries, weight (excl. peaking battery)	24.6 kg	21.9 kg	14.6 kg	–
baseload battery (zinc-air) volume	–	–	–	27.1 L
baseload battery (zinc-air) weight	–	–	–	25.0 kg
power source power density	0.20 kW/L	0.12 kW/L	0.09 kW/L	0.07 kW/L
power source specific power	0.24 kW/kg	0.15 kW/kg	0.08 kW/kg	0.07 kW/kg

In terms of the useful performance measurements of fuel economy total power system size/weight (including fuel cell or baseload battery, peaking power battery, and hydrogen storage, but not motor and controller), the following results are obtained:

Table 4.26 Performance metrics

	5.9 kW fuel cell	3.2 kW hybrid	1.1 kW hybrid	1.8 kW battery hybrid
hydrogen storage (FeTi hydride) weight for 200 km range	21.4 kg	22.8 kg	24.3 kg	–
hydrogen storage (FeTi hydride) volume	3.7 L	4.0 L	4.3 L	–
peaking power battery weight	–	3.1 kg	5.6 kg	4.5 kg
peaking power battery size	–	3.0 L	5.5 L	4.4 L
total drive system weight	61 kg	63 kg	60 kg	45 kg
total drive system size	43 L	43 L	30 L	41 L
30 km/h fuel consumption	0.807 km/g	0.751 km/g	0.703 km/g	48.8 km/kWh
TMDC fuel consumption	0.527 km/g	0.484 km/g	0.525 km/g	36.2 km/kWh
30 km/h fuel economy	522 mpge	486 mpge	455 mpge	1053 mpge
TMDC fuel economy	344 mpge	320 mpge	363 mpge	780 mpge
Range at 30 km/h	200 km	200 km	200 km	200 km
Range under TMDC	131 km	129 km	149 km	148 km

"total drive system" includes fuel cell and hydrogen storage, or zinc-air battery; motor / controller; peaking power battery. Costs are discussed in the next chapter.

Note that the ZES drive system weight is 44 kg of lead-acid batteries plus 15.5 kg of motor and controller (assuming similar characteristics as the UQM motor/controller). This is about 60 kg, the same as the fuel cell systems.

System size does not decrease significantly with hybridization except in the case of the 1.1 kW hybrid where much lower cooling requirements mean a much smaller radiator. The smaller fuel cell weight is roughly compensated for by the added weight of the batteries, and the larger hydrogen storage tank. TMDC performance is better for the 1.1 kW hybrid because the frequent decelerations allow regenerative braking gains; the same is true for the 1.8 kW battery hybrid.

On the other hand, certain other factors decrease more or less linearly with fuel cell size, foremost among them membrane area and platinum cost. Significant cost reductions might be possible under such a system for the near future while fuel cells remain extremely expensive; unfortunately, these costs are not reflected in the price calculations above, which rely upon ultimate price estimates for mass-produced stacks.

More complex hybrid operation policies could be used to try to better predict power demands; these would optimize battery usage by controlling more cleverly when to recharge, how quickly to recharge, and the state of charge to maintain in the battery.

4.7.7 Near-term possibilities

To compare these designs with what is available today, portable stacks from H-Power and Ballard were inserted into the 1 kW fuel cell design. A single PS-250 fuel cell unit commercially available from H Power produces 250 W net power, weighs 10.3 kg, and has a volume of 16 L.[43] This does not include storage. (The system is air-cooled, and with the correct geometry this could be possible for a scooter version) The existing design can actually output 330 W; to be conservative, retail units are sold derated to 250 W. Using three units to supply the 1.0 kW net output desired produces a power system weight of 31 kg and volume of 48 L. Currently costs are on the order of $6,000 for a unit like the PS-250, with mass-production costs expected to drop to $1,000.[44] For the required three, then, the current cost would be on the order of $18,000 and $3,000 in the long run.

On the other hand, Ballard Power Systems has developed a 1 kW (net power) stack that weighs 18 kg and has a volume of 33 L including all packaging.[45]

Table 4.27: Near term 1 kW fuel cell hybrid designs

Parameter	as designed	Ballard stack	H-Power stack
fuel cell stack weight	4.1 kg	–	–
fuel cell stack volume	3.2 L	–	–
stack power density, gravimetric	95 W/kg	–	–
stack power density, volumetric	76 W/L	–	–
fuel cell system weight	14.6 kg	18 kg	31 kg
fuel cell system volume	11.6 L	33 L	48 L
fuel cell system power density, gravimetric	75 W/kg	61 W/kg	35 W/L
fuel cell system power density, volumetric	65 W/L	33 W/L	23 W/L

The fuel cell system size and weight exclude peaking power battery in all cases.

So in the short term, an unoptimized fuel cell hybrid based on Ballard performance figures would have a drive system at 63 kg and 51 L. This is 3 kg and 27 L more than the ZES-2000, which is technically feasible in a scooter.

The results here for the various types of hybrids show that they offer the opportunity to reduce fuel cell stack size and power, and thus save money, since peaking power batteries are currently cheaper (per kW) than additional fuel cell capacity. In the short term, hybrid scooters are overwhelmingly favoured. The first steps to take would be to reduce volume by optimizing the subcomponents for the scooter body.

However, in the long run, the decreasing cost of fuel cell stacks is expected to make hybrids less and less economical. A larger fuel cell also improves fuel economy at constant driving speeds, since the fuel cell is more frequently operating at its most efficient output levels.

A calculation of costs, both for the scooter and for the fuel it uses, is found in the next chapter.

Infrastructure and overall fuel economy are also discussed.

References for Chapter 4

1. Jet P. H. Shu, Wei-Li Chiang, Bing-Ming Lin, Ming-Chou Cheng. Mechanical Industry Research Laboratories, Industrial Technology Research Institute. "The Development of the Electric Propulsion System for the ZES2000 in Taiwan". (Date unknown; not the same as the SAE paper in reference 7, even though it appears to be written by the same authors. October 1997 or later.)

2. Yoshihiro Nakazawa, Chiaki Humagai, Mikio Kato. "Development of an electric scooter for practical use" in *JSAE Review* **15** (1994) 373-377

3. Chien-Tung Liu, Bing-Ming Lin, Jyh-Sheng Pan. "Design and development of a zero-emission scooter for Taiwan" in *Journal of Power Sources* **59** (1996) 185-187

4. Peter A. Lehman, Charles E. Chamberlin. "Design and Performance of SERC's Fuel Cell Powered Vehicle Fleet" in *Fuel Cell Seminar Abstracts 1998*. 714-717

5. Mowick Limited Golf & Leisure Vehicles. "E-Z Go 4Caddy" http://www.mowick.com/ezwhite.htm Accessed July 30, 1999

6. Chien-Tung Liu, C. C. Kuo, Jyh-Sheng Pan, Bing-Ming Lin. "Development of electric motor cycle technologies in Taiwan" *J. Power Sources* **48** (1994) p. 244

7. P. H. Jet Shu, Wei-Li Chiang, Bing-Ming Lin, Ming-Chou Cheng. "The Development of the Electric Propulsion System for the Zero Emission Scooter in Taiwan". (1997) SAE 972107

8. *ibid*

9. Highway Tire Committee, SAE. Revised by the Rolling Resistance Subcommittee. "Measurement of Passenger Car, Light truck and highway truck and bus tire rolling resistance" (March 1997) SAE Information Report J1270. Section 8.1

10. Frank Rowland Whitt, David Gordon Wilson. *Bicycling Science* (MIT Press: Cambridge, 1974) p. 93

11.Wei-Li Chiang, Power Machinery Division Director, ITRI-MIRL (Industrial Technology Research Institute, Mechanical Industry Research Laboratories. Personal communication, September 11 1998

12. CALSTART web site. "DARPA Consortia EV and Hybrid EV Technology Projects - (PNGV) Target Attributes" http://www.calstart.org/about/pngv/pngv-ta.html

13. Energy and Environment Analysis. "Analysis of Fuel Economy Boundary for 2010 and Comparison to Prototypes" (November 1990) Prepared for Martin Marietta Energy Systems, Contract No. 11X-SB0824.

p. 4-11.

14. M. Ross and W. Wu. “Fuel Economy Analysis for a Hybrid Concept Car Based on a Buffered Fuel-Engine Operating at a Single Point” SAE Paper 950958, presented at the SAE International Exposition, Detroit, MI, February 27 - March 2 1995

15. C. E. (Sandy) Thomas, Brian D. James, Frank Lomax, Ira F. Kuhn, Jr. Directed Technologies, Inc.“Integrated Analysis of Hydrogen Passenger Vehicle Transportation Pathways”, draft final report. For NREL, subcontract AXE-6-16685-01. March 1998. p. 61

16. Bernward E. Bayer, “Motorcycles”. Chapter 10 of *Aerodynamics of Road Vehicles*. Fourth Edition. Ed. Wolf-Heinrich Hucho. p. 502

17. Arne LaVen. “Driving Cycle Analysis of the Sun Com™ Battery Electric Scooter” (November 1998) Desert Research Institute. p. 26

18. Wei-Li Chiang, Power Machinery Division Director, ITRI-MIRL. Personal communication, September 11 1998

19. Owner’s manual for Honda CH250 Elite250 1986, (Honda Motor Company: 1985) p. 68

20. T. C. Pong, personal communication. October 29, 1998.

21. Arne LaVen. Energy and Environmental Engineering Center, Desert Research Institute. “Driving Cycle Analysis of the Sun Com™ Battery Electric Scooter” November 1998

22. Chien-Tung Liu, Bing-Ming Lin, Jyh-Sheng Pan. p. 186

23. Toshiharu Sawada, Minoru Wada, Masanori Noguchi, Buhei Kobayashi. Komatsu Zenoah Co. “Development of a Low Emission Two-Stroke Cycle Engine” SAE 980761 (1998)

24. C.T. Liu, C. C. Kuo, J. S. Pan, B. M. Lin.“Development of electric motor cycle technologies in Taiwan”

25. Christopher S. Weaver, Lit-Mian Chan.“Motorcycle Emission Standards and Emission Control Technology” Revised Final Report, submitted to The World Bank. (Engine, Fuel, and Emissions Engineering, Inc.: August 1994) page *v*.

26. Frano Barbir. Energy Partners. “Operating Pressure and Efficiency of Automotive Fuel Cell Systems” No date. 1997 or later.

27. Vicor product data sheet. “The MegaPAC family” http://www.vicr.com/pdf/ds_megapac.pdf Accessed July 9, 1999

28. Vicor sales representative. Personal communication. July 14 1999.

29. Lisa Fawcett, AMETEK. Personal communication. April 26 1999.

30. Charles Chamberlin, Schatz Energy Research Center, Personal communication. May 20 1999

31. Mazda Australia web page. “Mazda”. http://www.mazda.com.au/corpora/460.htm. Accessed June 17, 1999

32. If the entire 0.9 g/s were vaporized (with a latent heat of vaporization of 2.2 kJ/g for 100°C water) approximately 2 kW of cooling would be realized, or about 25% of the total heat generated.

33. Lytron product catalog, "Standard OEM Coils" at http://www.lytron.com/catalog/oemframe.htm. Last accessed April 11, 1999

34. Charles E. Chamberlin and Peter A. Lehman. "Design and Performance of SERC's Prototype Fuel Cell Powered Vehicle"

35. National Research Council. *Review of the Research Program of the Partnership for a New Generation of Vehicles.* Second Report (National Academy Press, Washington: 1996) p. 53

36.Susan Ornelas, Research Engineer, Schatz Energy Research Center. Personal communication February 17 1999.

37. No similar size and weight data was available for the CUV-ES scooter. Also, the Dynetek cylinder is one that holds about 40% more hydrogen than the DTI model, as no Dynetek cylinder currently exists for the designed 250 gram size.

38. Jet P. H. Shu *et al*, "The Development of the Electric Propulsion System for the ZES2000 in Taiwan"

39. Department of Energy Hybrid Electric Vehicle Program. "Energy Management and System Control". http://www.hev.doe.gov/components/energman.html. Accessed May 10, 1999.

40. Bolder "Rebel" battery pack product sheet; see specifications in section 2.2.3.1

41. ALABC [Advanced Lead-Acid Battery Consortium] web site. "About ALABC" http://www.alabc.org/about.html

42. Jonathan Whartman, Ian Brown. Electric Fuel, Ltd. "Zinc Air Battery-Battery Hybrid for Powering Electric Scooters and Electric Buses" November 1, 1998

43. Rene Dubois, H Power. Personal communication June 7 1999

44. Arthur Kaufman, H Power, personal communication May 21 1999

45. Ballard product data sheet. "1 kW fuel cell generator"

~

Chapter Five

Implementation and Conclusions

~

The main purpose of the thesis is to analyze the technical merits of the proposed fuel cell scooter. However, the scooter will never be practical unless it can be affordable as well. This chapter attempts to assess various issues contributing to the eventual adoption of commercial fuel cell scooters: price of the scooter itself; operating costs, in terms of fuel; and a brief survey of infrastructure and hydrogen distribution. The results of this chapter and the previous chapters is summarized in the final section.

5.1 Scooter cost

This first section of this chapter estimates costs of the fuel cell scooter after commercialization and mass production. This identifies the long term prospects of the hydrogen scooter, which are fair.

Three different types of prices must be defined. The cost-to-manufacture is the cost most often quoted by developers of new technology like zinc-air batteries. Estimated at double this manufacturing cost is the cost of the component as part of the vehicle – this is defined as the sale or retail vehicle price.[1] Finally, after-market replacement automotive components or those developed for separate purposes (like industrial blowers or radiators) are four times the manufacturing cost. Note that, depending on the part in question and the particulars of manufacturing and marketing and distribution, this factor of four may be quite different, so the cost totals should be taken with a grain of salt.

The method used here is to take existing scooter prices, remove the cost of the power system, and add back the new hydrogen fuel cell power system.

5.1.1 Base cost by subtraction

Current 50 cc two-stroke scooters retail for approximately $1,000 in Taiwan (1999), while the ZES-2000 has a target sale price of $1,850.[2] Costs for the major power system components are shown below and used to estimate a "base" cost for the vehicle body (with wheels and frame and controls and electronics) plus assembly.

Table 5.1 Internal combustion engine scooter parts

Part	Description	Cost
50 cc two-stroke engine	includes carburetor, transmission	$300
Exhaust system	Muffler, exhaust pipe	$60
Fuel tank	5 L of fuel	$40
Starting battery	Yuasa-Exide	$10
	TOTAL	$410

Prices are retail prices listed by an American parts dealer[3], and thus divided by two for cost as part of the complete vehicle sale price. The sole exception is the engine cost, which is based on a $150 manufacturing cost and a factor of two multiplier for the price it would cost as part of a vehicle's total sale price.[4]

Subtracting the total from a two-stroke's $1,000 sale price leaves a $590 base cost for the vehicle shell, assembly, internal electronics, controls, and assorted other ancillaries.

To verify this result by comparing with the cost of existing electric scooters, the most important electric scooter components – battery, motor, and controller – are added. With lead-acid batteries currently costing about $80/kWh retail, and a typical electric scooter having a stored energy of 1.2 kWh for 50 km of range at 30 km/h, a total battery cost of $96 is obtained. As previously quoted, Unique Mobility predicts motor and controller prices of $250 and $300 respectively for mass

production today, although this is expected to decrease over time.[5] This is assumed to be in-vehicle retail cost.

Table 5.2 Battery-powered electric scooter parts

Part	Description	Cost
DC motor	UQM brushless SR121/1.5 L	$250
Controller	UQM CD05-100A	$300
lead-acid batteries	1.2 kWh	$100
"base" cost	retail	$590
	TOTAL	$1,240

This electric scooter retail total is close to cost of the cheapest electric scooters, which now retail for about $1,500, and is lower than the $1,850 previously quoted for the ZES-2000. The difference is likely due to the current cost of electric motors.

5.1.2 Cost of hydrogen storage system

Metal hydride hydrogen systems are based on the calculations of Chapter 3. The long-term cost projection for the FeTi metal hydride was based on an $8.80/kg materials price, and an extra factor of 50% for systems and packaging.[6] This resulted in a storage cost of $0.75 per gram of hydrogen stored. The quantity of hydrogen, as previously discussed, was set to allow 200 km of travel at 30 km/h.

Table 5.3 Metal hydride storage costs

	5.9 kW	3.2 kW	1.1 kW
Hydrogen stored	248 g	266 g	285 g
Manufacturing cost of hydride	$187	$201	$215

5.1.3 Fuel cell system cost based on parts predictions

The cost estimate of Appendix B, first described in section 3.1.3, was repeated for the two other hybrid alternatives. For each of the three fuel cell options and the hybrid battery, a long term price prediction is made based on mass production of all parts – especially the fuel cell and metal hydride storage system. These cost predictions are difficult to make, given the uncertainty involved with this emerging technology and the several years before the mass produced prices can be realized, so should be treated as a rough estimate only.

Retail prices for industrial parts like blowers, radiators, starting batteries, and coolant pumps are divided by a factor of four to include them in the sum below. Other costs, like the fuel cell, zinc-air battery, and metal hydride, are already given as cost-to-manufacture. Peaking battery costs are assumed to decrease to 75 $/kW.

The fuel cell stack costs are for the ultimate long-term prices predicted by an automobile analysis done by Directed Technologies, Inc. These estimates are valid for the larger membrane sizes of 170 cm^2 and 100 cm^2 for the 5.9 kW and 3.2 kW stacks, but the 1.2 kW stack has membranes only 34 cm^2 in area, less than the minimum of 116 cm^2 employed in the DTI study, so the cost estimates are much less certain for this size. More details are in Appendix B. In contrast, the zinc-air battery cost was based on an 80 $/kWh projection for "large-scale production" made by Electric Fuel.[7]

The component parts are added to the base vehicle cost of $590 retail (or $295 to manufacture) in the chart below.

Table 5.4 Long-term scooter cost to manufacture

Part	Description	pure FC (5.9 kW)	hybrid (3.2 kW)	hybrid (1.2 kW)	zinc-air hybrid
FC stack	DTI model; long-term cost	$220	$165	$135	
Starter battery	Yuasa-Exide	$10			
Hydrogen storage	DTI metal hydride model; long-term cost	$190	$200	$215	
Storage batteries	Zn-air, 4.1 kWh				$330
Heat exchanger	Lytron M10-080			$30	
	Lytron M14-120	$60	$60		
Coolant pump	generic	$10	$10	$10	
Blower for 1-2 psi	Ametek 116628-E	$110	$110	$110	
Plumbing	Water, air pipes	$50	$50	$50	
DC brushless motor	UQM SR121/1.5L	$125	$125	$125	$125
Controller	UQM CD05-100A	$150	$150	$150	$150
Peaking battery	Bolder lead-acid	–	$195	$340	$285
Vehicle shell	body and misc. parts	$295	$295	$295	$295
	TOTAL	$1,220	$1,360	$1,455	$1,185

The hybrid battery appears to be a very competitive option in terms of capital cost, if Electric Fuel's predictions of long-term zinc-air battery cost are correct. Due to the low fuel cell prices predicted for the long run, the (relatively) high expense of peaking power batteries eradicate the benefit of smaller fuel cells. Right now this is certainly not the case, as peaking power batteries currently sell for approximately $166 per kW, while fuel cells are as high as $3000 per kW.

The greatest uncertainties in these cost estimates are in the most important components: the fuel cell stack itself, the metal hydride storage unit, and in the case of the electric hybrid, the zinc-air battery. The peaking power lead-acid battery is also relatively novel technology, although it has been demonstrated in prototype vehicles. The other components are all "off-the-shelf" industrial

parts and are not expected to decrease dramatically due to advancing technology. On the other hand, better engineering integration and design specific to the scooter application might reduce costs.

Doubling the costs gives a rough estimate of retail cost - the price for the consumer.

Table 5.5 Summary of cost estimates

type	price
pure FC (5.9 kW)	$2,440
hybrid (3.2 kW)	$2,720
hybrid (1.1 kW)	$2,910
hybrid battery	$2,370

There is some room for cost reductions in the motor and controller prices of $250 and $300, respectively. The peaking power battery price may also drop further, while there is great uncertainty in the zinc-air battery price. However, the fuel cell cost is quite low and it is unlikely that it could go much lower. In addition, the fuel cell stack itself makes up a relatively small portion of the total cost.

The results suggest that margins will be very low since the manufacturing cost is very close to the current prices for small scooters. The scooter as designed, with 5.9 kW of output, might be better targeted against the low end of the 125 cc scooter range, rather than the 50 cc two-stroke scooter. This would give more freedom in terms of higher sale price and larger size to store the various subcomponents. By the same token, resizing for smaller-power and lower-performance scooters (say 3 kW) would bring a fair cost reductions – a simple calculation shows that the 3.2 kW hybrid scooter stripped of its peaking power batteries would cost $1160 to make. While it would be able

to perform the basic performance criteria of acceleration and hill climbing, it would not be as quick to accelerate as comparable two-strokes.

5.1.3.1 The short term

In the short term, hybridization with peaking power batteries drastically reduces the price of the scooter. In the long run when fuel cells are less expensive, the added complexity of batteries (and their lack of performance advantage over comparably-sized fuel cells) make them unnecessary. However, there is an intermediate stage as the price of the fuel cell drops to meet the cost of the peaking power batteries, where at a rough estimate, fuel cells will cost about $500/kW and batteries are $100/kW. The hydrogen storage and Zn-air batteries might be twice as much as the ultimate costs.

Table 5.6 Short term bridging to the future

Part	**Description**	**pure FC (5.9 kW)**	**hybrid (3.2 kW)**	**hybrid (1.1 kW)**	**zinc-air hybrid**
FC stack	DTI model; long-term cost	$2950	$1600	$600	
Hydrogen storage	DTI metal hydride model; long-term cost	$380	$400	$430	
Storage batteries	Zn-air, 4.1 kWh				$660
Peaking battery	Bolder lead-acid		$260	$460	$380
	Rest of system	$810	$800	$770	$570
	TOTAL	$4140	$3060	$2260	$1610

The ordering of the costs is reversed for the fuel cell hybrids here, and illustrates how hybrids might be required for the next several years in order to bridge the gap to inexpensive fuel cells. Once again, hybrid batteries prove to be an able competitor, although it should be recalled that neither the 1.1 kW hybrid nor the zinc-air hybrid can sustain the original hill climbing

requirements. Whether the zinc-air hybrid scooter's lower capital cost is mirrored by lower operating costs is a subject for the next two sections, which deal with overall efficiency and fuel costs.

5.2 Wells-to-wheels efficiency

The on-vehicle fuel economy does not account for the entire story. To obtain complete cycle efficiencies, the inefficiencies in producing hydrogen or electricity, and in distributing the "fuel," must be considered. To be consistent with previous results and with the standard for large power plants in the United States, the higher heating value efficiency is considered here.

Steam reforming of natural gas in large plants is 84% efficient, with another 87% efficiency for distribution of hydrogen (including losses due to hydrogen compression). With a driving cycle fuel cell net conversion efficiency of 47.7% and 77% drivetrain efficiency, the final result is 27% from natural gas to road work.[8,9]

This should be compared to a scooter engine with gasoline distribution from the refinery to the filling station at 95% efficiency, a thermal efficiency of at most 20%, and transmission efficiency of 77%, for a total of 15%.[10]

In the case of the electric scooter, a factor of 40% is used to account for electricity production: the product of 90% electricity distribution efficiency and 45% electricity generation efficiency from a very good combined-cycle coal plant. The efficiency involved in electrowinning zinc from solution

and then discharging it again in the battery is the ratio of the electrowinning voltage (2.2 V) to the output voltage (1.16 V), or 52.7%. On the vehicle there is a 77% drivetrain efficiency, for a total efficiency of 16% from coal to road work.

(Admittedly, these three efficiencies of 27%, 15%, and 16% technically do not start from the same starting point. Hydrogen will almost certainly be produced from natural gas, scooter combustion engines will run on gasoline, and coal is the major source of electricity in Taiwan and would be used (indirectly) for battery powered scooters.)

The internal combustion engine performs its most wasteful conversion step onboard, and cannot take advantage of economies of scale to produce high efficiencies. On the other hand, the zinc-air battery converts coal to electricity at a large power plant and loses (relatively) little there, but the electrowinning process is energy-hungry. So the hydrogen fuel cell system is actually the most efficient in terms of converting chemical energy to road work. However, even if it is the most efficient, it may not be the cheapest.

5.3 Fuel cost and infrastructure

In addition to the cost of the scooter itself, the fuel cost must also be accounted for. This is the electricity in the case of the battery-powered scooter, the hydrogen for the fuel cell scooter, and the gasoline in the standard internal combustion engine scooter.

Energy prices for Taiwan and the United States (4^{th} quarter1997) are compared below. Note that

there is regional variation in American prices which is not reflected here.

Table 5.7 Taiwan vs. USA energy prices, 1997 USD

	Taiwan	U.S.A.
Unleaded premium gasoline	65.1 ¢/liter	36.9 ¢/liter
Natural gas (industrial price)	7.71 $/GJ GCV	3.53 $/GJ GCV
Natural gas (household price)	10.81 $/GJ GCV	6.26 $/GJ GCV
Coal (steam coal)	83.97 $/tonne	36.03 $/tonne
Electricity (industrial price)	6.69 ¢/kWh	4.07 ¢/kWh
Electricity (household price)	10.02 ¢/kWh	8.31 ¢/kWh

Data is from the International Energy Agency.[11] GCV stands for Gross Calorific Value, which is the same as higher heating value ("Net Calorific Value" is equivalent to lower heating value).

When converted to common units of GJ of thermal energy (higher heating value), this is:

Table 5.8 Fuel costs for Taiwan in $/GJ HHV

	Taiwan	U.S.A.
Gasoline (premium, at the pump)	16.7 $/GJ	9.5 $/GJ
Natural gas (industrial price)	7.7 $/GJ	3.5 $/GJ
Coal (industrial price)	2.6 $/GJ	1.1 $/GJ
Electricity (industrial price)	18.6 $/$GJ_{elec}$	11.3 $/$GJ_{elec}$

This calculation assumes that the coal energy content is 14,000 BTU/lb (HHV, and average for an American coal), gasoline is an average 140,000 BTU/gallon, and that the quoted price is industrial pricing.[12,13] The gasoline price "at the pump" includes a markup for retail which was not listed in the source data. All energy values are higher heating value.

Taiwan prices are about twice as high as American prices, due to the island's lack of natural resource. Also, the higher gasoline price may be due to a different taxation policy.

5.3.1 Zinc-air battery "fuel" costs

Traditional storage batteries are punished for their short lifetimes (on the order of 600 cycles, or approximately 2 years at the present); the need to purchase replacement batteries adds to the lifetime cost. The zinc-air case is different, though, since it is not electrically recharged. Instead, after the zinc anode is oxidized into ZnO, it is switched for a fresh zinc anode. The depleted anode is sent back to a factory where it is electrolyzed an converted back into zinc.

Electric Fuel's proposed zinc air infrastructure involves refilling stations (gas stations equivalents) where depleted anodes are exchanged for fresh zinc anodes, and "regeneration centers" which are centralized factories where the anodes are regenerated. The refilling stations essentially act as distributors and installers for the regeneration centers. The refilling stations could use automated machinery to switch the anodes in a short time (comparable to gasoline refilling) although capital costs might be high.

The regeneration centers are more complex. The "used up" zinc oxide is removed from the current collector plates, and dissolved in an alkaline (potassium hydroxide) solution. The solution is then electrolyzed ("electrowinning") to restore the original zinc, which collects on the cathode and is scraped off and allowed to sink to the bottom of the electrolyte solution. The resulting zinc and potassium hydroxide slurry is periodically drained off, strained, and pressed against a current collector frame to produce a new anode assembly.

First, the theoretical minimum cost from the energy required is calculated. The maximum efficiency of the process is 52.7%, based on the ratio between the 1.16 V discharge voltage and the 2.2 V for electrowinning. So a 4.1 kWh output from the batteries is equal to 7.8 kWh at the

electrowinning plant, and the electricity cost of 6.7 ¢/kWh gives a price of 52¢ for a single recharge. During daily driving, the Taipei Motorcycle Driving Cycle gives a fuel economy of 36.2 km/kWh. At 40 km/day (two hours of driving at TMDC speeds), and 300 days of travel per year, this is a total annual mileage of 12,000 km. The annual driving cost, taken from the 52¢ per recharge cost given previously for just the electricity needed to recreate the zinc anodes, is $42 per year. This is a net *electricity* cost of just 0.35 ¢/km.

A CSC (China Steel Corporation) study of costs for zinc-air battery replacement, however, calculated a total zinc-air driving cost over ten times higher, 4.3 ¢/km.[14] The assumptions are slightly different, with 4,300 km a year driving and a fuel economy of 40.3 km/kWh of output rather than 12,000 a year and 43.5 km/kWh:

Table 5.9 Comparison of assumptions for zinc-air electrowinning costs

	CSC study	**this study**
zinc-air battery size (output)	3.6 kWh	4.1 kWh
energy to recharge battery	4.9 kWh	7.8 kWh
single-charge mileage	145 km	200 km (at 30 km/h)
fuel economy (km/kWh-recharged)	29.6 km/kWh	25.7 km/kWh (at 30 km/h)
electricity cost	4.7 ¢/kWh	6.7 ¢/kWh
electricity cost per km	0.16 ¢/km	0.35 ¢/km

The electricity cost assumption is lower, but the energy price does not tell the whole story. The CSC study goes on to calculate costs for the complete refueling infrastructure: labour, periodic electrode and electrolyte replacement materials costs, spare batteries kept at the service station for exchange purposes, and land and building fees. Each station supplies approximately 2,400 scooters a day. This more comprehensive study results in annual fuel costs of $185 per year at 4,300 km

per year, or $516 per year at the 12,000 km per year assumed here – for a total "fuel" cost of 4.3 ¢/km. This is extremely high but it is possible that costs may come down with time.

(Note that the electricity cost is insignificant, only 3.6% of the total cost of refueling the vehicle.)

When converted to a cost per kWh for comparison to the hydrogen and gasoline cases, this is $2.1 per kWh of output. In other words, a full recharge of the 4.1 kWh battery costs $8.60. By taking the cost as a function of energy recovered, this allows the original assumptions about annual driving and fuel economy to be used.

Pilot regeneration plants currently exist in Italy and Israel to service fleets of zinc-air demonstration vehicles, but one major drawback for zinc-air scooters is that car makers are not considering this technology and that eliminates one of the major players in technology advancement and cost reduction. This is different from PEMFCs, which are seeing broad development for not only vehicles but also portable power and stationary generation.

5.3.2 Hydrogen costs and infrastructure

In comparison, the 5.9 kW pure fuel cell system with 250 g of storage has a fuel economy of 0.527 km per gram of hydrogen (344 mpge) under TMDC driving. Hydrogen in Taiwan would likely be produced by imported natural gas converted at local hydrogen filling stations using steam reformers.

A study by Ogden *et al*. calculated that hydrogen produced by on-site conventional steam reformers would cost 12-40 $/GJ based on a Los Angeles-area natural gas price of 2.8 $/GJ.[15] The

range of costs is a function of how large each reforming station is; a large reformer capable of producing 2 million standard cubic feet of hydrogen per day could handle 13,000 automobiles at a cost of 11.5 $/GJ, while a small 100,000 SCF/day station would handle 650 cars at 40 $/GJ. (Note that these calculations assume the existence of a natural gas distribution network, which may not be the case in Taipei.)

The same driving pattern that was calculated for the zinc-air version is assumed here: 45 km of travel per day. Taiwan prices for natural gas are 7.7 $/GJ, so prices for hydrogen increase by 5 $/GJ to 17-45 $/GJ. At the smallest station size (100,000 SCF/day), an area of 4,050 scooters running at 12,000 km per year could be serviced at a cost of 45 $/GJ. The fuel cost of operating a scooter turns out to be $145 a year or 1.21 ¢/km.[16] If a larger plant capable of servicing an area of 72,000 scooters was built, costs would drop to 17 $/GJ for a cost per vehicle per year of $55 and a driving cost of 0.46 ¢/km.

More advanced reformers would reduce the cost to 29 $/GJ for a 100,000 SCF/day 4,050-scooter plant, but larger stations would not be much cheaper. $29 $/GJ is the cost assumed here. Note that the raw natural gas cost is only 27% of the total delivered hydrogen cost; the rest is for labor, reformer construction, electricity, hydrogen storage and compressor.

While direct hydrogen is not currently being considered for first-generation fuel cell automobiles, buses are being demonstrated that store hydrogen in large compressed gas cylinders, and scooters could “piggyback” on a hydrogen distribution infrastructure for public transportation. In this case, there would not have to be 72,000 scooters within the operating area of a single refueling station plant.

Refueling metal hydrides essentially is a matter of filling at pressures of about 10 atm; the rate of adsorption is dependent on how quickly the excess heat of adsorption can be removed, and liquid coolants in the nozzle design can be used to effect this. The process could be done in just 5-15 minutes.[17]

5.3.3 Combustion scooter gasoline costs

The 100 mpg fuel economy of the gasoline-powered scooter is scaled down to 65 mpg for driving cycle performance (the same ratio as for the hydrogen powered scooter; note that actual performance will be different because of the efficiency-versus-power characteristics of the combustion engine).

Assuming the same travel distance of 12,000 km a year, and 65.1 ¢/liter for gasoline yields an annual fuel cost of $105, or 1.5¢ per kilometer.

5.3.4 Fuel cost summary

The advanced reformer for small service areas, at 24 $/GJ, was used for the hydrogen case; the China Steel Corporation cost analysis was used for the zinc-air battery to obtain a per-kWh price of $2.1, which was applied to driving 12,000 km per year under the lower mileage of the TMDC.

Table 5.10 Fuel cost summary

	zinc-air hybrid	**gasoline**	**5.9 kW pure FC**	**3.2 kW hybrid**	**1.1 kW hybrid**
refueling cost	583 $/GJ$_{elec}$ (2.1 $/kWh)	16.7 $/GJ$_{HHV}$ (65.1 ¢/L)	24 $/GJ$_{HHV}$ (0.34 ¢/g)	24 $/GJ$_{HHV}$ (0.34 ¢/g)	24 $/GJ$_{HHV}$ (0.34 ¢/g)
TMDC mileage	36.2 km/kWh	65 mpg	0.527 km/g	0.484 km/g	0.525 km/g
on-vehicle mileage	780 mpge	65 mpg	344 mpge	320 mpge	363 mpge
cost per distance under TMDC	5.8 ¢/km	1.5 ¢/km	0.65 ¢/km	0.70 ¢/km	0.65 ¢/km
annual cost	$696	$184	$78	$84	$78
present value of fuel over 10-year lifetime	$4,275	$1130	$480	$515	$480

Present value costs were calculated over a ten-year scooter lifetime, with a 10% discount rate (meaning future fuel costs are discounted heavily compared to the up-front capital cost)

The zinc-air battery's energy cost is actually very low, but infrastructure costs, spare battery expense, and depreciation of the stock of batteries all add up to a very expensive per-km cost. Over time, infrastructure costs must reduce drastically if zinc-air batteries are to be competitive.

The gasoline-powered scooter reflects current efficiencies, and improvements in air pollution technology like fuel injection will likely improve fuel economy by a small amount and reduce driving costs.

Hydrogen production at the infrastructure levels assumed here results in hydrogen costs that are less than half the price of gasoline, due to the high efficiency of the fuel cell scooter. Even with the extremely small-scale hydrogen reforming station assumed here, the cost is low enough to make hydrogen fuel cell scooters a cheaper option to drive than gasoline-powered scooters.

Under these assumptions, the fuel cost is roughly on the order of the vehicle cost for the gasoline vehicle, much more expensive for the zinc-air hybrid due to its low cost, and significantly cheaper for the hydrogen powered scooter due to its high efficiency. However, the comparison is uncertain due to the great uncertainties in the fuel cell and zinc-air technology costs. Also, maintenance and repair costs are not yet quantified for the advanced technologies. These two reasons explain why the capital and present value of fuel were not directly summed.

5.4 Final Conclusions

Advanced fuel cell powered scooters could produce more than three times the 100 mpg of current gasoline-powered scooters, with zero tailpipe pollution. In the long run, a rough cost estimate predicates that they would cost about $1,200 – $1,300 to produce, although prices for the consumer would be as much as twice this amount. In comparison, more advanced combustion-powered scooters (like four-stroke scooters) could offer pollution reduction of about 75% of hydrocarbons and 50% of carbon monoxide for an additional cost over two-stroke scooters of under $200. However, one methodology shows that there is significant health benefit to even removing that last stage of emissions, so if the proper dollar value were assigned to the air pollution reductions, a value of several hundred dollars would apply to the zero-emission scooters.

This study arrived at this conclusion through an analysis of current scooter performances and pollution trends, a general examination of the health benefits of zero-pollution scooters over four-stroke scooters, a discussion of electric vehicle technology including battery, fuel cell, and hydrogen storage options, and detailed modeling of scooter driving and fuel cell performance that had not been done before for this type of vehicle.

A fuel cell design was presented for the scooter that focused on simplicity on all fronts: pure hydrogen operation, low temperature. In addition, hybrid designs were examined in an effort to accelerate fuel cell scooter adoption by reducing the size of the fuel cell stack needed. Hybrids reduce price in the short term, but in the long run fuel cells should come down in price by enough to make peaking power batteries unnecessary.

Finally, another option, the zinc-air battery, was examined. This technology showed good technical performance, and a zinc-air drive system would be half the weight of a fuel cell system. Questions remain about the expense of developing an infrastructure for zinc anode regeneration and electrolyte / cathode replacement, which currently are projected to be very expensive. So low capital cost is traded for high fuel costs

The original work done and results obtained are summarized below.

5.4.1 Background

The focus was placed on Taiwan because of its extremely high vehicle density, the large number of scooters, and its pre-eminence as a scooter manufacturing center. High pollution levels, especially in cities, are a concern among the populace and government and one of the primary motivators for cleaning up cheap two-stroke scooters. Four-stroke scooters will likely expand to fill the role of these two-stroke scooters, and provide significant reductions in emissions.

A sketch of cost and benefits shows that hundreds to thousands of dollars of health benefit per vehicle could be realized by switching from four-stroke engines to zero-emission vehicles. The government’s chosen solution, the battery powered scooter, currently lacks adequate range.

Proton exchange membrane fuel cell systems offer greater range, with the same zero tailpipe emissions since they produce electricity electrochemically, with water as the only exhaust. As is the case with battery-powered scooters, pollution emissions would be shifted to central (in this case, hydrogen-generating) plants.

Hydrogen storage is best supplied with hydrogen stored onboard in cylinders or in the form of metal hydrides. The latter offers excellent synergy with the cooling system due to its endothermic hydrogen release, and greater safety due to the far lower pressures (1-10 atm), and is recommended here.

5.4.2 Modeling results

Modeling shows that maximum power required is just under 6 kW for performance comparable to combustion two-stroke scooters. Average power demands are a tenth, at 670 W for urban driving. The following performance specifications were required:

Table 5.11 Fuel cell scooter performance requirements

Specification	Fuel cell scooter
max motor power output	4-6 kW
range before refueling at 30 km/h cruising speed	200 km
fuel efficiency	> 100 mpge
acceleration	0-30 m in less than 5 seconds
sustained speed on 15° slope	10 km/h
sustained speed on 12° slope	18 km/h
maximum speed	60 km/h

5.4.3 Design

This thesis presents a fuel cell design for a scooter of approximately 5 or 6 kW, a niche that was previously unexplored. Size, weight, and cost restrictions force the design to be simple and to remove any unnecessary systems. Where data were not well known and assumptions were necessary, performances were assumed to be worse than expected to ensure a feasible design.

A compressor/expander system to provide 3 atm pressurized air at the cathode was rejected as the benefit did not outweigh the parasitic power losses and additional complexity, weight, and expense. The advantages of high pressure for water removal were not considered.

Cooling of the fuel cell system proved to be a significant problem. A radiator was chosen that could handle the maximum continuous cooling load (produced by slope climbing requiring 3020 W of power for an indefinite period). Benefits in cooling derived from “ram effect” air flowing over the radiator were not included so the system was somewhat overdesigned. Integration of a metal hydride hydrogen storage system provided a useful method of extracting 17% to 30% of surplus heat. The thermal mass of the system and the low *average* heat production meant that over the TMDC, cooling is not a problem

The complete drive system configuration (fuel cell, battery, motor, controller, hydrogen storage in DTI-modeled metal hydride) is summarized below.

Table 5.12 System design results

	today's ZES-2000	pure FC (5.9 kW)	hybrid (3.2 kW)	hybrid (1.1 kW)	zinc-air battery
Sustained net power	~ 3 kW	5.6 kW	3.0 kW	1.0 kW	1.8 kW
Range (30 km/h)	65 km	200 km	200 km	200 km	200 km
Range (TMDC)	< 35 km	131 km	129 km	149 km	148 km
Drive system (size)	24 L	43 L	43 L	30 L	41 L
Drive system (weight)	60 kg	61 kg	63 kg	60 kg	45 kg

The fuel cell auxiliary systems make the drive system heavy, even though the weight of the fuel cell itself is relatively low. To go from today's ZES-2000 to a 1.1 kW hybrid requires 6 L of additional space which is easily found in the current body frame, but the other systems will require a redesign of the body (although this is not be a "show-stopping" requirement).

The relatively poor energy density of the hybrid zinc-air battery causes the high volume requirements of that design, whereas the 5.9 kW and 3.2 kW fuel cells feature very large radiators that account for the high volume.

Hybrid power systems with a combined peaking power battery and hydrogen prime energy source offer significant reductions in cost because fuel cells are so expensive right now, although in the long run this situation is expected to reverse in favour of pure fuel cell scooters. The costs are detailed in the next section.

5.4.4 Costs and infrastructure

The following costs-to-manufacture are listed below for various cases.

Table 5.13 Long-term cost of hybrid fuel cell scooters

pure FC (5.9 kW)	hybrid (3.2 kW)	hybrid (1.1 kW)	hybrid battery
$1,220	$1,360	$1,455	$1,185

The sale cost may be as much as double this price, which would be significantly more than today's two-stroke internal combustion scooters at $1,000 and electric battery-powered scooters (albeit with only one third the range) at $1,500.

Assuming hydrogen costs of 24 $/GJ from small reforming stations running on pipelined natural gas obtains the following comparison:

Table 5.14 Fuel cost summary

	zinc-air hybrid	gasoline	5.9 kW pure FC	3.2 kW hybrid	1.1 kW hybrid
on-vehicle mileage	780 mpge	65 mpg	344 mpge	320 mpge	363 mpge
cost per distance under TMDC	5.8 ¢/km	1.5 ¢/km	0.65 ¢/km	0.70 ¢/km	0.65 ¢/km
annual cost	$696	$184	$78	$84	$78
present value of fuel over 10-year lifetime	$4,275	$1,130	$480	$515	$480

Fuel prices for the zinc-air hybrid battery scooter are incredibly high according to the one study cited in this study. Hydrogen fuel cell scooters have very good range and mileage, and can operate cheaply even if hydrogen is produced at the relatively small scales assumed here. It is not only the pollution benefits that make hydrogen scooters better than current gasoline-powered scooters; the fuel savings are also significant.

5.4.5 Parting words

Fuel cell scooters face many of the same problems as fuel cell automobiles: the technology is new, and thus expensive, and distribution infrastructure does not exist for hydrogen delivered to the end user. On the other hand, the Taiwan situation features somewhat high fuel prices, relatively high income levels, and extremely poor air quality, two drivers for more efficient and cleaner vehicles. The situation in China, Japan, and other Asian countries is similar, with varying degrees of pollution and wealth. Some European countries have high numbers of scooters as well and could be markets for this technology.

In the long run, the hydrogen fuel cell scooters could cost approximately $1,200 to manufacture. This is dependent upon significant reductions in metal hydride and fuel cell costs, and these reductions would occur most quickly if they piggybacked off other markets that called for large numbers of these two core components.

Ordinary electric battery scooters are not projected to have the energy densities required, and a recharging infrastructure is a problem in Taiwan where indoor vehicle storage off the street is not always guaranteed. Zinc-air scooters are likely to cost less than fuel cell scooters, but are projected to have, at least in the short term, extremely expensive refueling costs based on more complex battery exchanging stations. Hydrogen scooters would be cheaper to drive than combustion scooters.

Future work on this topic would move the conceptual design and feasibility test presented here to more applied design work and prototype construction. The performance presented here is unlikely to be far from actual results, and assumptions made here have always erred on the side of more

waste and worse performance. So building a prototype fuel cell scooter – or even only the fuel cell power system – and obtaining more detailed data on the parasitic power would be an excellent way to measure real-world performance, which for the reasons outlined above is expected to be higher than the conservative estimate here. System integration of the various heat flows and physical assembly of the variously-shaped parts also needs to be demonstrated.

Also, "smart" hybrid power management algorithms should be designed to optimize hybrid scooters that may be used in the next several years while fuel cells are still too expensive to be the sole power source for vehicles. Detailed research specific to Taiwan and other Asian locations is needed on the subject of hydrogen distribution. Finally, as reformer and direct methanol fuel cell technology advance, they may become feasible for this application and this must be kept in mind.

Recommendations: in the short run, getting rid of two-strokes and speeding a transition to four-stroke engines is an inexpensive path to deep reductions in emissions. The Taiwan government is following the right track in legislating emissions performance requirements rather than enforcing technology. A hydrogen fuel cell scooter offers additional air pollution reduction benefits over four-strokes that could justify its increased costs, however, and is worth investment in research and development. Peaking power batteries for upcoming scooters are highly recommended to allow the use of smaller and less expensive fuel cells without the performance compromises that would cause public rejection of advanced scooters, and metal hydride technology is the best fuel storage strategy.

FIN

References for Chapter 5

1. Mark DeLuchi. Institute of Transportation Studies, University of California, Davis. *Hydrogen Fuel-Cell Vehicles.* Research Report UCD-ITS-RR-92-14 September 1, 1992. p. 147

2. Jet P. H. Shu, Wei-Li Chiang, Bing-Ming Lin, Ming-Chou Cheng. Mechanical Industry Research Laboratories, Industrial Technology Research Institute. "The Development of the Electric Propulsion System for the ZES2000 in Taiwan" Internal paper, date unknown (October 1997 or later)

3. Randy Knudson, Scooter Therapy. Personal communication May 21, 1999

4. $150 estimate of cost from Dr. Philip G. Felton, Princeton University Department of Mechanical and Aerospace Engineering, personal communication July 26 1999

5. Jeffrey Ho. Deputy Director, Taiwan UQM. Personal communication May 24, 1999.

6. Brian D. James, George N. Baum, Franklin D. Lomax, Jr., C. E. (Sandy) Thomas, Ira F. Kuhn, Jr. Directed Technologies, Inc. "Comparison of Onboard Hydrogen Storage for Fuel Cell Vehicles" Task 4.2 Final Report. Prepared for Ford Motor Company under Prime Contract DE-AC02-94CE50389 "Direct Hydrogen Proton-Exchange-Membrane (PEM) Fuel Cell System for Transportation Applications" to the U. S. Department of Energy, pp. 4-56, 4-63, 4-52

7. Jonathan Goldstein, Ian Brown, Binyamin Koretz. "New developments in the Electric Fuel Ltd. zinc / air system" *Journal of Power Sources* **80** (1999) pp. 171-179

8. Joan M. Ogden, Margaret M. Steinbugler, Thomas G. Kreutz. "A comparison of hydrogen, methanol and gasoline as fuels for fuel cell vehicles: implications for vehicle design and infrastructure development" *Journal of Power Sources* **79** (Elsevier: 1999), pp. 143-168

9. Note that the overall conversion efficiency is actually 55.7% from hydrogen heating value to electricity. However, about 10% of that electricity is needed for parasitic purposes and is wasted in terms of useful output like road motion or auxiliary power. The efficiency net of parasitics is 46.7%

10. Matthew Brekken and Enoch Durbin. "An Analysis of the True Efficiency of Alternative Vehicle Powerplants and Alternative Fuels." Society of Automotive Engineers 981399, 1997.

11. International Energy Agency. "Key World Energy Statistics" http://www.iea.org/stats/files/keystats/stats_98.htm. Accessed May 8, 1999

12. World Bank. "World Bank - Typical Coals of the World" http://www.virtualglobe.com/html/fpd/em/power/sources/coal_tcw.htm Accessed August 19, 1999

13. World Bank. "World Bank - Typical Analyses and Properties of Fuel Oils*" http://www.virtualglobe.com/html/fpd/em/power/sources/oil_tapfo Accessed August 19, 1999

14. China Steel Corporation study for chemTEK. Received August 21, 1999 from chemTEK.

15. Joan Ogden, Margaret Steinbugler, Thomas Kreutz. "Hydrogen as a fuel for fuel cell vehicles: a technical and economic comparison"

16. *ibid*

17. Joan Ogden, Princeton University. Personal communication July 22 1999

Appendix A *current and prototype electric scooters*

Country	ROC	ROC	ROC	Japan	Japan	Japan	USA
maker	ITRI	Shangwei	ENTER	TOKYO R&D	HONDA	YAMAHA	DORAN [a]
model	ZES 2000	SWAP	City Bike II	ES-600	CUV-ES	MEST	ECO-SCOOT
maximum speed (km/h)	50	80	55	55	60	50	33
climb capability (tan θ)	16 km/h on 18° slope	30 km/h on 30° slope	15° [b]	18° [b]	12° [b]	10° [b]	12° [b]
range (km) at 30 km/h	60	80	75	60	60 (35 km in "urban mode")	30	40
dry weight, kg	105	130	95	117	130	80	89
motor	DC brushless, 48 V	DC brushless, 48V	DC brushless	DC brushless	DC brushless (3.25 kW), 48 V	DC brushless	DC brush
battery	four sealed lead-acid	sealed lead-acid	lead-acid	maintenance-free lead-acid	Ni-Cd	maintenance-free lead-acid	lead-acid
battery capacity (Ah/V)	28/12	40/12	52/24	30/48	20/86.4	17/48	46/24
charging time (hr)	no data	6~8	5~8	8	8	8	~10
transmission	CVT (?)	CVT	single-stage reduction	CVT	CVT	no data	single-stage reduction
acceleration	0-30 m, 4.5 s	no data	no data	no data	0-200 m, 17.3 s	no data	no data
price (US$)	no data	2000	1460	4750	8150	no data	1900
notes	demo only	750 W rated power	in development	limited fleet sales	limited fleet sales	introduction	on market

[a] The Doran vehicle was bought out by the Sun Cat Motor Company in 1995 and renamed the Sol Gato
[b] Speeds on these "climb capability" slopes were not given

The data were based on tables from the following sources:

P. H. Jet Shu, Wei-Li Chiang, Bing-Ming Lin, Ming-Chou Cheng. "The Development of the Electric Propulsion System for the Zero Emission Scooter in Taiwan" Japan Society of Automotive Engineers. 1997. JSAE 9734403, SAE 92107

Shang Wei web site. "Shang Wei SWAP vs. Other Electric Scooters". http://www.shangwei.com/compar-e.htm. Accessed August 30, 1999

Appendix B *detailed stack cost/size analysis*

The DTI model outlined in *Detailed Manufacturing Cost Estimates for Polymer Electrolyte Membrane (PEM) Fuel Cells for Light Duty Vehicles* (August 1998) was used to calculate size, weight, and cost of a scooter fuel cell stack. The ultimate purpose was to use the methodology described in that report to produce reasonable estimates of size, weight, and cost that were more accurate than simply linearly scaling down automotive fuel cells.

In their report, DTI studied several different sizes of fuel cells and calculated manufacturing costs for the various components of the cell stack (auxiliaries like compressors and cooling pumps were not examined). Two sets of analyses were done, and in each case the area of the membranes in each cell was varied between six different sizes ranging from 116 cm^2 to 697 cm^2. In the first set, "equal voltage," the number of cells was held constant at 420 cells and thus power varied with membrane area. In the second set, "equal power," the number of cells was varied to keep total power at 70 kW_{elec}. Options for the cell unit design include "unitized" bipolar metallic separator plates stamped with flow fields on both sides, three-piece unipolar metallic plates, carbon-polymer composite plates, and amorphous carbon plates. The more conservative three-piece metallic separator plates were chosen here (see section B.2 for details)

Note: A May 1999 DTI study has examined a range of small fuel cells (among them, 3-5 kW stacks) for electricity and heat for individual residences. For a production quantity of 10,000 units, this study found the installed cost per kW to be about $4,500.[1] These figures are based on top-down cost analyses, and other companies who are designing home fuel cell systems have quoted figures on the order of $3,500 to $5,000 for a residential fuel cell system of a few kilowatts using batteries for peak power.[2]

These high prices for this size of fuel cell would seem prohibitive for the scooter, except for the fact that stationary power fuel cells must be designed very differently from automotive fuel cells; they must operate 24 hours, unlike vehicle engines which are only run a few times daily. Also, vehicle engines rarely reach top output. All in all, stationary fuel cell lifetimes must be longer and they must be designed more robustly. Another factor cited in the DTI report was that the larger production quantities for vehicles would help to drive down costs. So despite these recent high projections of cost for stationary fuel cell systems of similar size as the scooter studied here, predictions of fuel cells for vehicles are still on target.

B.1 "Blind" curve-fitting

Curves were fit to the original DTI results for automotive fuel cell, based on an equal-voltage study with 420 cells and stack power varying with different membrane area. Each of the six different cell

---

1 C. E. (Sandy) Thomas, Jason P. Barbour, Brian D. James and Franklin D. Lomax, Jr. Directed Technologies, Inc. "Analysis of Utility Hydrogen Systems & Hydrogen Airport Ground Support Equipment". Prepared for the Proceedings of the U.S. DOE Annual Hydrogen Program Review. May 1999.

2 Plug Power and American Power Corporation. Quote is from Ronald J. Wolk. "Fuel Cells for Homes and Hospitals" *IEEE Spectrum* May 1999 p. 45

membrane areas is listed in Table B.1 below.

Table B.1 DTI automotive stack parameters

Membrane area (cm^2)	Stack power (kW)	Cost ($/gross kW_e)	Weight (kg)	Volume (L)
116	31.5	$36	22.0	23.7
181	49.0	$29	29.4	32.5
258	70.0	$26	38.5	42.7
348	94.5	$23	48.1	54.2
452	122.5	$22	59.5	67.1
568	154.0	$21	72.4	81.3
697	188.9	$20	86.4	96.9

Note: the total weight was not given in the study, and was summed in the same way the stack weights were calculated later in section B.3. Volumes were given in terms of stack dimensions and converted here to liters.

The DTI automotive stack costs per kilowatt were plotted against cell active membrane area in Figure B.1, and fit with a hyperbola of the form

$$y = A / (x-B) + C$$

for cost per kilowatt “y” and active membrane area “x”, and fitting parameters A, B, and C.

Figure B.1 Cost as a function of cell membrane area

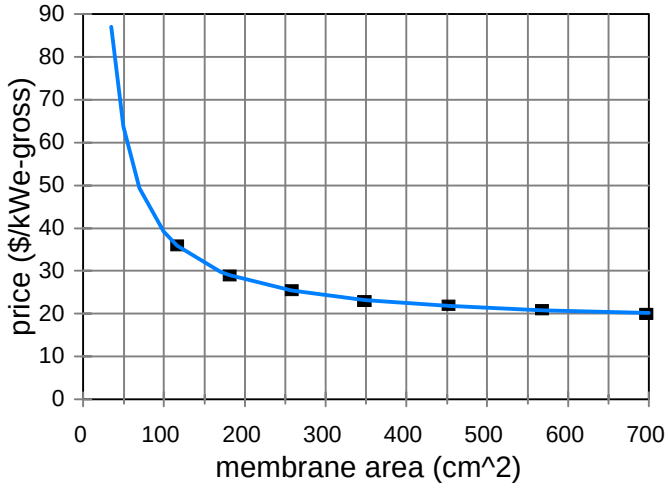

Similarly, per-kilowatt data for weight and volume were plotted and regressed against curves of the same form as for the cost in Figure B.2:

Figure B.2 Weight and volume as a function of cell membrane area

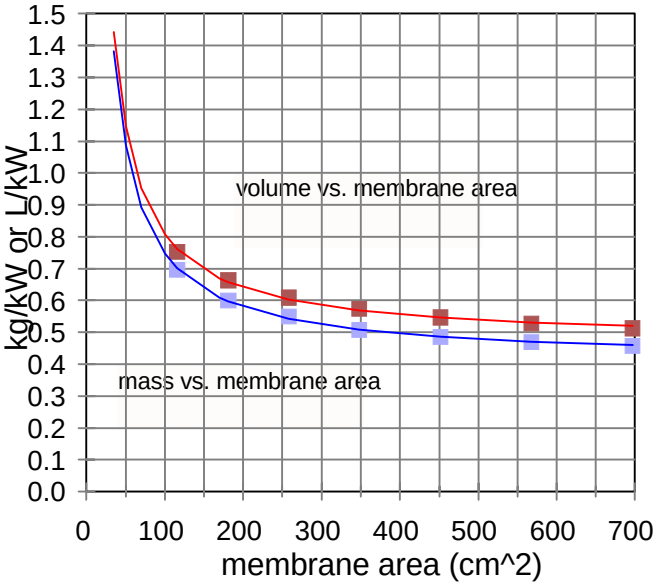

These results were extrapolated to the membrane areas required for the three fuel cell sizes studied here: 1.1 kW, 3.2 kW, and 5.9 kW (corresponding to stack membrane areas of 35 cm^2, 100 cm^2, and 170 cm^2 as discussed in Chapter 4). This produced the following results:

Table B.2 Curve-fitting versus bottoms-up model

	Stack power	Curve-fitting result
Stack cost	1.1 kW	$96
	3.2 kW	$125
	5.9 kW	$176
Stack weight	1.1 kW	1.5 kg
	3.2 kW	2.4 kg
	5.9 kW	3.6 kg
Stack volume	1.1 kW	1.6 L
	3.2 kW	2.6 L
	5.9 kW	4.0 L

B.2 Size and volume

To improve upon this estimate, bottom-up calculations of size, weight, and cost were made by following the DTI procedure. First, the total size of the three fuel cells were calculated by first calculating the sizes of three-piece stainless steel cooler cells and active cells, and assuming a 2:1 active-to-cooler cell ratio:

The active cell requires one metal separator plate and two separate, unipolar plates etched with flow fields and gaskets separating the flow fields from the MEA, for a total thickness of 2.27 mm per active cell:

51 µm separator plate

76 µm anode flow field

1000 µm anode gasket

70 µm MEA

76 µm cathode flow field

1000 µm cathode gasket

[repeat with next separator plate]

The cooler cells are thinner, at 1.13 mm each:

51 µm separator plate

76 µm coolant flow field

1000 µm gasket

[repeat with next separator plate]

With 56 active cells and 28 cooler cells, this produced a total thickness of 15.9 cm. The arrangement of cells is described in Figure B.3 following:

Figure B.3 Diagram of stack assembly

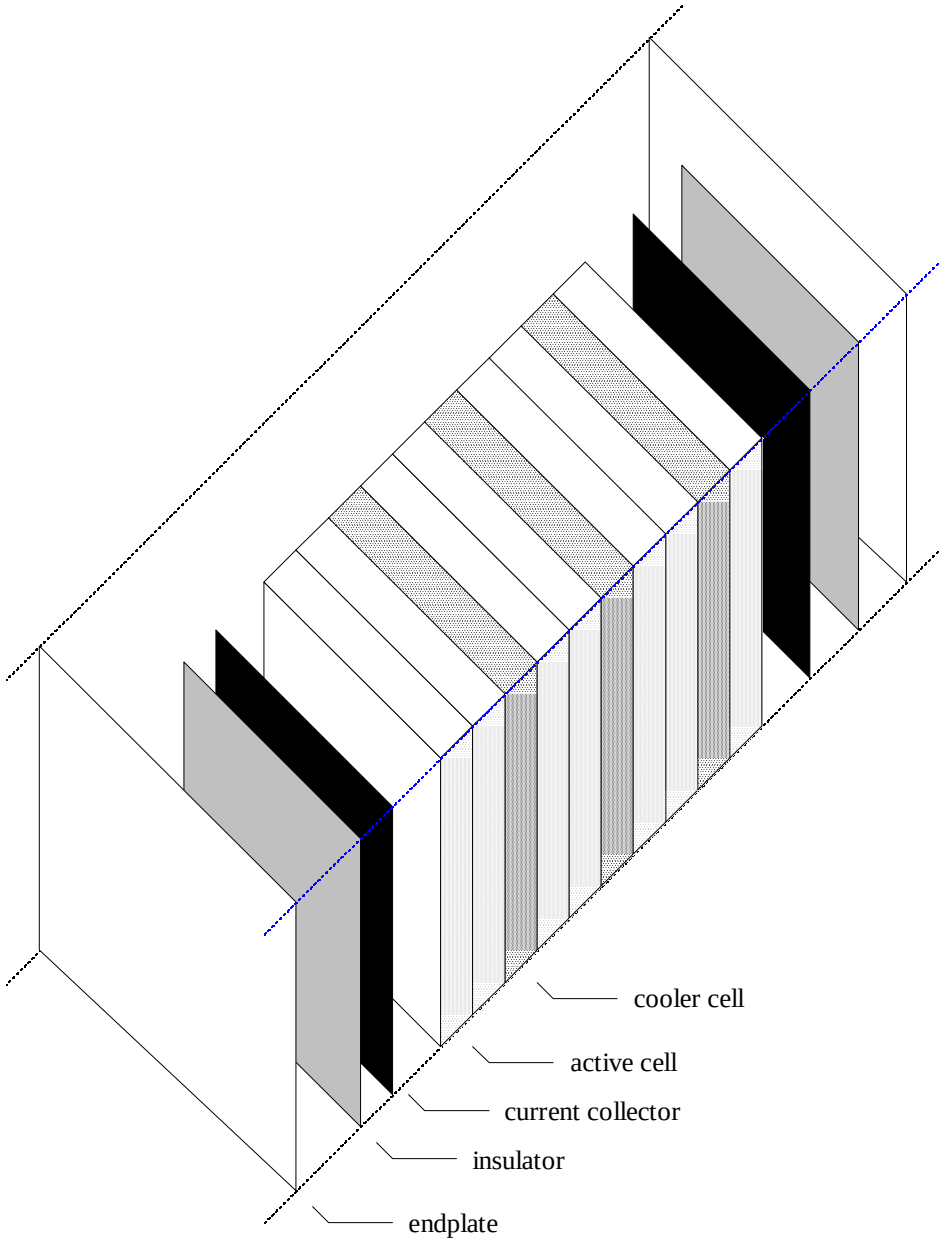

Following the DTI procedure, the dimensions of the repeat components were calculated by taking the active area needed per cell, selecting a height and width, and adding 2.54 cm of inactive membrane area to each dimension to obtain a total membrane area. Next, a 5.1 cm manifold space was added to the width of the membrane (including inactive margin) to obtain the total stack face area, and then 1.27 cm was added to each side of the stack to account for the thickness of the plastic housing and produce the fuel cell stack's overall dimensions as listed in Table B.3 below. (Note that the original DTI stack designs contained two parallel strings of 210 cells, while the design presented here uses a single 56-cell stack.)

Table B.3 Stack dimensions

	5.9 kW	**3.2 kW**	**1.1 kW**
membrane active area	170 cm^2	100 cm^2	35 cm^2
active membrane dimensions,	10.0 cm x 17.0 cm (170 cm^2)	10.0 cm x 10.0 cm (100 cm^2)	5.0 cm x 7.0 cm (35 cm^2)
total membrane dimensions, including inactive margin	12.5 cm x 19.5 cm (244 cm^2)	12.5 cm x 12.5 cm (156 cm^2)	7.5 cm x 9.5 cm (71 cm^2)
total dimensions of stack face -- includes manifolding	17.6 cm x 19.5 cm (340 cm^2)	17.6 cm x 12.5 cm (220 cm^2)	12.6 cm x 9.5 cm (120 cm^2)
overall dimensions with plastic housing	20.2 cm x 22.1 cm x 17.5 cm	20.2 cm x 15.1 cm x 17.5 cm	20.2 cm x 12.1 cm x 17.5 cm
total volume	7.8 L	5.3 L	3.2 L

B.3 Weight of stack

B.3.1 Weight of non-repeat components

The weights of the non-repeat components (plastic stack housing, two endplates, two insulators, two current collectors, sixteen tie-rods) were calculated based on their dimensions and

extrapolation from the DTI study.

The stack housing mass was based on previously calculated stack housing volume and a density of 0.576 g•cm^{-3} for the plastic housing material.

The sixteen tie-rods were estimated at 2.05 kg for DTI's default equal-voltage 52.5 cm stack. Since length is only 15.9 cm in this fuel cell, the tie-rod mass was pro-rated down to 0.6 kg.

The insulator and current collectors cap the ends of the array of cells and thus have an area equal to the total membrane area. They were regressed against total membrane area. The endplates, containing reactant and exhaust ports, tie rod holes, and serving as structural support for the stack, cover the entire face area of the stack. The endplate weights were regressed against stack face area. However, the regressions for the current collectors and endplates became negative at the low stack areas designed for the hybrid, so they were not used.

So, in the case of the 100 cm^2 and 35 cm^2 stacks, the current collector and endplate weights were simply taken to be the same as the weights for the DTI 116 cm^2 stack. For the 170 cm^2 stack, the current collector weight was interpolated between the weights for the collectors obtained for the DTI 116 cm^2 and 181 cm^2 stacks. The endplate, of area 344 cm^2, was set equal to the weight of the endplate for the DTI 116 cm^2 (452 cm^2 face area) stack.

The linear regression was retained for the insulator weights. The results for all of the parts were:

Table B.4 Non-repeat stack component weights

	5.9 kW	**3.2 kW**	**1.1 kW**
2 insulators	59 g	45 g	45 g
1 stack housing	1.32 kg	0.99 kg	0.66 kg
2 endplates	0.26 kg	0.26 kg	0.26 kg
2 current collectors	1.11 kg	0.71 kg	0.71 kg
16 tie rods	0.59 kg	0.59 kg	0.59 kg
total non-repeat weight	4.8 kg	3.6 kg	3.3 kg

B.3.2 Weight of repeat components

The repeat components were modeled as follows. First, the masses of the repeat units (separator plate, anode flowfield, cathode flowfield, gasket, MEA) were taken from DTI's values for the rubber gasket and MEA, and calculated from dimensions and densities for the separator plates and flowfields. A stainless steel density of 8 kg/L was used. This was done for each of the sizes studied in the DTI report; for example, the weights were 28.2 g for each active cell and 16.4 g for each cooling cell for a 116 cm^2 active area.

Then, the total weights of the repeat units were summed for all the 56 cooler cells and 28 active cells, and expressed as a function of total membrane area for the membrane sizes studied in the DTI study:

Figure B.4 Regression of total repeat unit weight

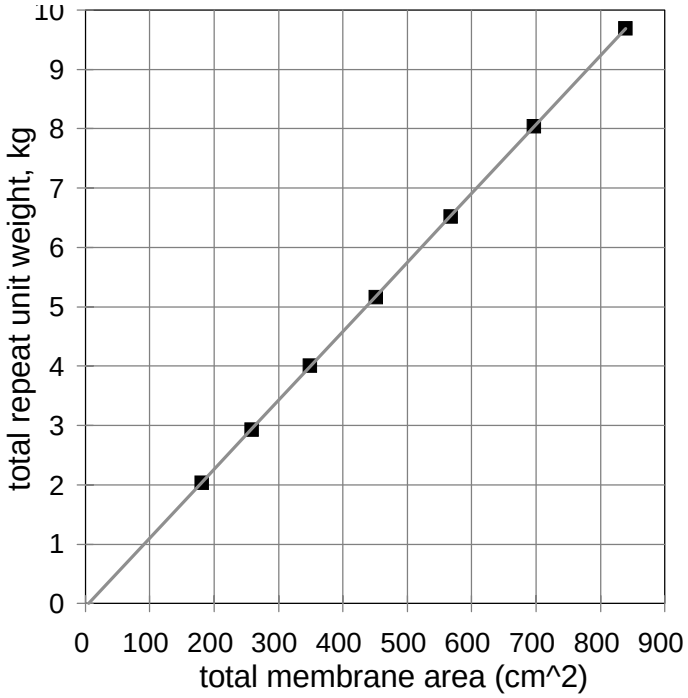

A straight line regression fit well to the repeat masses; because the majority of the weight comes from the stainless steel plates, and these plates' weights vary linearly with changing membrane area (because thickness is constant)

Table B.5 Total weight of stack repeat units

	5.9 kW	**3.2 kW**	**1.1 kW**
total membrane dimensions (including inactive)	12.5 cm x 19.5 cm	12.5 cm x 12.5 cm	7.5 cm x 9.5 cm
total membrane area	245.0 cm^2	157.3 cm^2	71.9 cm^2
total repeat unit weight	2.8 kg	1.8 kg	0.8 kg

B.4 Summary of stack weight and volume

The total stack weight and volume are summarized below with power densities.

Table B.6 Summary of size and weight results

	5.9 kW	**3.2 kW**	**1.1 kW**
membrane active area	170 cm^2	100 cm^2	35 cm^2
non-repeat mass	5.1 kg	3.6 kg	3.3 kg
repeat mass	2.8 kg	1.8 kg	0.8 kg
total mass	7.6 kg	5.4 kg	4.0 kg
volume	7.8 L	5.3 L	3.2 L
specific power	0.78 kW/kg	0.62 kW/kg	0.27 kW/kg
power density	0.76 kW/L	0.62 kW/L	0.34 kW/L

In comparison, Ballard reported in a 1995 press release a stack power density of 0.7 kW/L.

B.5 Cost

The costs were summed from minimum values of component costs as a function of cell membrane total area. In the case of this study, the total membrane areas were 244 cm^2, 156 cm^2, and 71 cm^2 for the 5.9 kW, 3.2 kW, and 1.1 kW hybrid scooters respectively. The insulators were the only parts actually regressed because the others became negative at the low membrane areas involved.

1. Again following DTI reported figures, stack housing prices were calculated at $1.16 per kg of material (based on the previous weight calculations) plus $15 assembly cost.

2. The insulators regressed to $0.24 each for the 5.9 kW stack, $0.20 each for the 3.2 kW stack, and $0.16 for the 1.1 kW stack.

3. The cost of the endplates became negative when regressed versus total membrane area, so the endplates were assumed to be the same cost ($4.02) as those for the smallest (116 cm^2) DTI case. For the same reason, "floor" values of $1.23 were chosen for the current collectors in the 100 cm^2 and 35 cm^2 stacks. The sixteen tie rods were calculated at $1.00 each.

MEA costs were simply the total membrane area multiplied by a cost of 52.3 $/$m^2$ predicted by DTI for mass-produced, low-cost technology. All subcomponents – MEA and cell hardware (gasket, separator plates, flow field plates) – were summed and then regressed against total membrane area for the repeat unit cost:

Figure B.6 Stack repeat unit regression

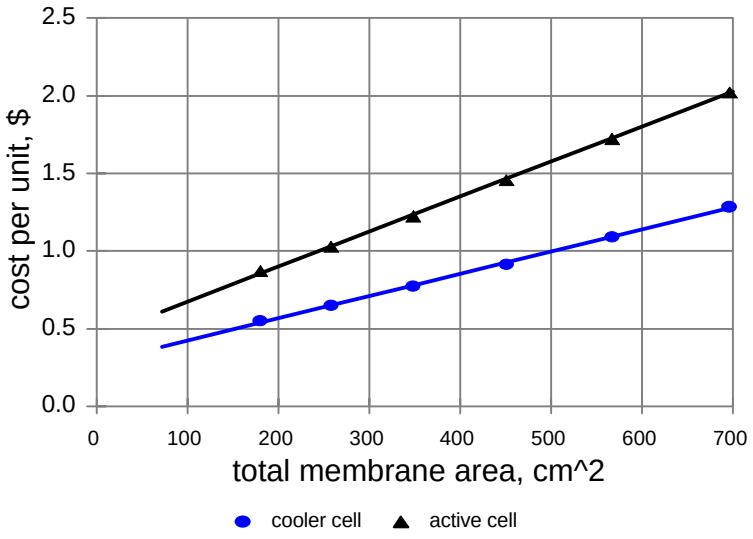

Finally, $10.00 was added for assembly, and a 10% contingency cost added at the end. The prices broke down as follows:

Table B.7 Cost summary

	price per component (number)	5.9 kW	3.2 kW	1.1 kW
REPEAT	**56 active cells**	56.04	37.75	29.55
	56 MEAs	83.56	34.10	11.94
	28 cooler cells	17.63	11.82	9.21
	assembly line machine cost per cell (total 84 cells)	8.40	8.40	8.40
	TOTAL	165.63	92.07	59.11
NON-REPEAT	**2 current collectors**	3.39	2.46	2.46
	16 tie rods	16.00	16.00	16.00
	2 insulators	0.47	0.40	0.33
	2 endplates	8.04	8.04	8.04
	1 stack housing	16.53	16.14	15.77
	TOTAL	44.44	43.04	42.59
SUMMARY	**final assembly and inspection**	10	10	10
	11% contingency cost	24.21	15.96	12.29
	total stack cost	$244	$161	$124

The costs per kilowatt for the stack are $103/kW for the 1.1 kW stack, $47/kW for the 3.2 kW stack, and $42/kW for the 5.9 kW stack.

These results were compared with the curve-fitting results listed in Table B.2:

Table B.8 Curve-fitting versus bottoms-up model

	Stack power	Curve-fitting result	Bottoms-up result
Stack cost	1.1 kW	$96	$124
	3.2 kW	$125	$176
	5.9 kW	$176	$244
Stack weight	1.1 kW	1.5 kg	4.0 kg
	3.2 kW	2.4 kg	5.4 kg
	5.9 kW	3.6 kg	7.4 kg
Stack volume	1.1 kW	1.6 L	3.2 L
	3.2 kW	2.6 L	5.3 L
	5.9 kW	4.0 L	7.8 L

The simplistic curve fits consistently overestimate stack performance (light weight, low cost, small volume). The more detailed model, which admittedly uses curve fitting in its numerous elements, more accurately captures the fact that parts not only increase in size, weight, and cost non-linearly as cell membrane size decreases, but that they increase more than expected from the initial fit.

Appendix C *radiator performance data*

The radiators used in the model are OEM coils produced by Lytron. The series has the following properties:

Table C.1 Lytron OEM coil weight and contained liquid volume

radiator model	dry (empty) weight	volume of coolant inside
M05-050	0.9 kg	115 mL
M05-100	1.8 kg	188 mL
M10-080	2.3 kg	320 mL
M10-160	3.6 kg	549 mL
M14-120	4.5 kg	606 mL
M14-240	7.3 kg	1090 mL

Figure C.1 shows performance curves of cooling factor (W/K) versus air flow rate (cfm) and coolant flow rate (gpm). Note that the M14-120 curve was accidentally printed twice on the data sheet from Lytron; the bottom figure is incorrect.

The source of the data in this appendix is the Lytron web site, “Lytron OEM Heat Exchangers (Radiators) Performance Curves” http://www.lytron.com/Catalog/oemperf.htm and “Lytron Manufacturers of Thermal Transfer Solutions”, http://www.lytron.com/Catalog/techwght.htm. Both sites were last accessed June 1999.

photocopy not included in PDF;

please see

http://www.lytron.com/Catalog/oemperf.htm

Appendix D *conversion factors*

1 gallon	3.785 L	
1 gallon per minute	0.06308 L/s	
1 cubic foot	28.32 L	
1 cubic foot per minute	0.472 L/s	
1 mole	22.5 L	(standard conditions)
1 atm	1.013 bar	
	760 mmHg	
	14.7 psi	
	101.3 kPa	
	407 in H_2O	
1 calorie	4.18 J	
1 BTU	1055 J	
1 horsepower	746 W	
1 ampere per ft^2 (“ASF”)	1.0764 $mA \cdot cm^{-2}$	
1 foot	30.48 cm	
1 pound	0.454 kg	
1 mile	1.609 km	

Appendix E *acronyms and abbreviations*

AIV	Aluminum Intensive Vehicle
BDC	Bottom Dead Center
CAFE	Corporate Average Fuel Economy
CFM	Cubic Feet per Minute
CSC	China Steel Corporation
DoD	Depth of Discharge
DFI	Direct Fuel Injection
DMFC	Direct Methanol Fuel Cell
ECE	Economic Commission for Europe
FHDS	Federal Highway Driving Schedule

FTP	Federal Test Procedure
FUDS	Federal Urban Driving Schedule
GCV	Gross Calorific Value (used in natural gas industry for HHV)
HHV	Higher Heating Value
ITRI	Industrial Technology Research Institute [Taiwan]
LHV	Lower Heating Value
LNG	Liquefied Natural Gas
MEA	Membrane Electrode Assembly
MIRL	Mechanical Industry Research Laboratory [ITRI]
MCFC	Molten Carbonate Fuel Cell
MPGE	Miles Per Gallon (Equivalent)
NCV	Net Calorific Value (lower heating value)
NGM	New Generation Motors
NiMH	Nickel Metal Hydride
NTD	New Taiwan Dollars
OEM	Original Equipment Manufacturer
PNGV	Partnership for a New Generation of Vehicles
PAFC	Phosphoric Acid Fuel Cell
PEMFC	Proton Exchange Membrane Fuel Cell (also Polymer Electrolyte Membrane Fuel Cell)
PM	Particulate Matter
PTFE	Polytetrafluoroethylene
ROC	Republic of China
SAE	Society of Automotive Engineers
SOC	State of Charge [of batteries]
SOFC	Solid Oxide Fuel Cell
TDC	Top Dead Center
THC	Total Hydrocarbons
TMDC	Taipei Motorcycle Driving Cycle
TSP	Total Suspended Particulates
UQM	Unique Mobility
USD	United States Dollars
VAC	Volts Alternating Current
VKT	Vehicle-Kilometers Traveled
VMT	Vehicle-Miles Traveled
ZES	Zero Emission Scooter

Appendix F *MATLAB simulation program listing*

This is a listing of the MATLAB m-file program used to simulate scooter performance over various driving cycles, `launch14.m`

```
% launch14.m
%
% Test bed to run various configurations through a specified driving cycle.
% Version 11 revises the efficiency calculation and changes baseparasitics
% Version 12 includes parasitic power in the final plot
% Version 13 refills the state of charge frequently - not just by regen
% Version 14 cleans up the code

more off; clear


%% STACK HEAT PARAMETERS
%
% stackmass is in kg, divided by two for the part in thermal contact
% with the cells; heatcapacity is in kJ/kg/C (water is 4.19,aluminum
% is 0.900, copper 0.386. We estimate 1.0 for stack) cooleff is in W/C
% and is different depending on which hybrid design is used

ambientTemp=40; initTemp=50;
stackmass=2.8; specheatcap=0.929;


%% CHOOSE TYPE OF HYBRIDIZATION (IF ANY)
%
% Select one of four configurations; adjust parameters accordingly
% The various hybrid versions reuqire different fuel cell areas,
% numbers of peaking power battery cells, and different parasitic power
% loads. "kickin" defines the power (watts) at which the battery kicks in.

disp(sprintf('Pick:\n  1 for pure FC\n  2 for 3.3 kW\n  3 for 1.1 kW\n  4 for
elec hybrid'));
hybridtype=input(' ?');
switch hybridtype
 case 1,
  cooleff=110; baseparasite=39.7; cellarea=170; numbolder=40;kickin=99000;
 case 2,
  cooleff=150; baseparasite=66.0; cellarea=100; numbolder=27; kickin=3020;
 case 3,
  cooleff=50; baseparasite=25.3; cellarea=35;  numbolder=47; kickin=1000;
 case 4,
  cooleff=35; baseparasite=0; cellarea=90;  numbolder=38; kickin=1830;
 otherwise,
  disp('Unknown option')
  keyboard
end


%% SET SCOOTER PHYSICAL PARAMETERS
%
% Crr     (coefficient of rolling resistance, dimensionless)
% Af      (frontal area, m^2)
% Cd      (drag coefficient, dimensionless)
% mass    (total mass of vehicle + driver)
% effd    (drive train efficiency - about 70%)
% paux    (auxiliary power, W)
```

```
g=9.81; rho=1.23;
Crr=0.014; mass=130+75;
Af=0.6; Cd=0.9;
effd=0.77; paux=60;


%% POLARIZATION CURVE
%
% Set number of cells in stack; area, in cm^2, of each stack. We define the
% polarization curve once, here, so we don't have to calculate efficiencies
% each time_inside_ the loop. Polarization curve is modeled with an
% analytic formula based on a least-squares fit to experimental data from
% Energy Partners (see reference in main body of thesis)
%
% power_for_density calculates gross power output for a given current
% density. vatmo is the voltage under atmospheric pressure for a given
% current density.

numcells = 56;
max_current_density=1800;
jaxis=[1:1:max_current_density];
for j=1:1:max_current_density,
 vatmo(j)=1.00-0.0260*log(j)-(2.015e-4)*j-(1.113e-5)*exp((6.00e-3)*j);
 power_for_density(j)=vatmo(j)*j*cellarea*numcells/1000;
end


%% DEFINE PEAKING BATTERY PARAMETERS
%
% We define efficiency and power here. The only reason we care about
% current is that we want to make sure the maximum charge/discharge
% current is not exceeded. Max current is in amps.
%
% numbolder   number of bolder peaking power cells
% capacity       maximum energy storable (J)
% batteryweight  weight of batteries (kg)
% effregen       fraction of kinetic energy available
% battenergy     current charge
% initSOC        initial state of charge (battenergy/capacity)
% currSOC        current state of charge
% regenerated    total energy regenerated so far (J)
% friction    total energy lost to friction in braking if no regen (J)

capacity=1*12*(numbolder/6)*60*60;
batteryweight=0.7173*(numbolder/6);
effregen=0.7;
initSOC=0.5; currSOC=initSOC;
battenergy=capacity*currSOC;
regenerated=0; friction=0;

%% DRIVING CYCLE DEFINITION
%
% Load in a driving cycle; uncomment to choose driving cycle.
% Note that FUDS must be converted to km/h as it is in mph.
% Timestep is defined here because different cycles have
% different time intervals.

%load ftp75.txt -ascii; vinput=ftp75; clear ftp75;
%timestep=1;

%load v2.txt -ascii; vinput=v2; clear v2;
%timestep=0.1;

%load v3.txt -ascii; vinput=v3; clear v3;
%timestep=1;

load realtmdc.txt -ascii; vinput=realtmdc; clear realtmdc;
```

```
timestep=1;

%load fuds.cycle -ascii; vinput=fuds; clear fuds;
%for i=1:1:size(vinput,1); vinput(i,1)=vinput(i,1)*1.609; end
%timestep=1;

%load j1082.txt -ascii
%vinput=j1082; clear j1082
%timestep=0.1;

%load ece40.txt -ascii; vinput=ece40; clear ece40;
%timestep=0.1;

v(1)=0; t(1)=0; cyclelength=size(vinput,1);

%% SMOOTH THE DRIVING CYCLE (BOX SMOOTH)
%
% (uncomment to use. Essentially we define temporary velocity vx
% and then overwrite the original vinput with vx when done smoothing)
%
% vx=vinput;
% vx(1,2)=vinput(1,2); vx(2,2)=vinput(2,2);
% vx(3,2)=vinput(1,2); vx(4,2)=vinput(2,2);
% vx(cyclelength,2)  =vinput(cyclelength,2);
% vx(cyclelength-1,2)=vinput(cyclelength-1,2);
% vx(cyclelength-2,2)=vinput(cyclelength-2,2);
% vx(cyclelength-3,2)=vinput(cyclelength-3,2);
% for i=3:1:cyclelength-1
%  vx(i,2) = ( 0.50*vinput(i,2) + ...
%              0.30*vinput(i-1,2)+0.20*vinput(i-2,2) );
% end
% vinput=vx;


%% CONVERT KM/H to M/S
for i=1:1:cyclelength
 t(i)=vinput(i,1)-timestep;
 v(i)=vinput(i,2)/3.6;
 if v(i)<0, v(i)=0; end
   %  Uncomment to clip if speed greater than 40 km/h
   %  if v(i)>(40/3.6), v(i)=40/3.6; end
 end

%% PAUSE TO ALLOW PLOTTING OF DRIVING CURVE
%
disp('plot your graph now')
keyboard

%% SMOOTH THE DRIVING CYCLE (LOW-PASS)
%
% note that the cutoff frequency - or rather cutoff period -
% occurs at To = 2pi/s0; periods below To are attenuated
% the smaller the To, the less smoothing. smaller s0 = more smoothing.
%
% If I wanted to close the loop I would use this
% [numc,denc]=feedback(num,den,gclose,1);

s0=1.5;  k=1; gclose=1;
num=k;
den=[1 s0];
v2=transpose(lsim(num,den,v,t))*s0;
v=v2; clear v2;


%% EXAMINE DRIVING CYCLE
%
% Evaluate driving cycle to calculate acceleration from finite
```

```
% differences of velocity; also, determine what fraction of the
% driving cycle is spent accelerating, decelerating, etc.
%
% plustime    if positive acceleration
% minustime   deceleration
% steadytime  steady velocity, no acceleration
%
% We also accumulate acceleration values to separate out
% average of positive accelerations and average of
% negative accelerations.

plustime=0; minustime=0; steadytime=0;
for i=2:1:cyclelength
 a(i)=(v(i)-v(i-1))/timestep;
 if a(i)>0,
  aplus(i)=a(i);
  aminus(i)=0;
  plustime=plustime+1;
 elseif a(i)<0,
  aminus(i)=a(i);
  aplus(i)=0;
  minustime=minustime+1;
 else
  aplus(i)=0;
  aminus(i)=0;
  steadytime=steadytime+1;
 end
end

clear vinput;
if ~((size(v) == size(a)) & (size(v) == size(t)))
 disp(sprintf('Error! Vectors v, a, and t are not the same size'));
 return
end

%% INITIALIZE OTHER VARIABLES
%
% bin is used to create a histogram of power consumption.
% fuelenergy accumulates the LHV of the fuel used
% distance is used to verify that the correct total distance is traveled

bin=zeros(1,30); fuelenergy=0; distance=0;


%% START THE MAIN LOOP

for i=1:1:cyclelength

 % p1 is the acceleration power
 % p2 is the rolling resistance power
 % p3 is the wind drag power
 % p4 is auxiliaries
 % p5 is parasitics
 % p6 is power supplied by FC to battery, if hybrid

 p1(i)=mass*a(i)*v(i);
 p2(i)=mass*g*v(i)*Crr;
 p3(i)=0.5*Cd*Af*rho*v(i)^3;
 p4(i)=paux;
 p5(i)=0; p6(i)=0;

 % We calculate output force in order to find torque needed.
 % Negative forces are discarded.
 % pwheels includes physical resistance power only, not aux. / para. / p6
 % p_no_parasitics is either equal to pwheels+auxiliary power+p6 recharge
 %  power, or if regenerative braking is taking place, it is equal to
 %  auxiliary power. Note that parasitic power p5 is not calculated until
```

```
%  later. p_no_parasitics includes output from the FC and

pwheels(i)=(p1(i)+p2(i)+p3(i))/effd;
if pwheels<0,
 p_no_parasitics(i)=p4(i);
else
 p_no_parasitics(i)=pwheels(i)+p4(i);
end


% we also record the instantaneous force in case we want to calculate
% torque. Here we discard values of force when v<0.

force(i)=mass*a(i) + mass*g*Crr + 0.5*Cd*Af*rho*v(i)^2;
if v(i)<0.01, force(i)=0; end


% Set up the histogram of pwheels by sorting each new data point
% into one of the bins. Bin(19) captures all powers greater
% than 9000 W.

if      (pwheels(i)<500),   bin(1)=bin(1)+1;
 elseif (pwheels(i)<1000),  bin(2)=bin(2)+1;
 elseif (pwheels(i)<1500),  bin(3)=bin(3)+1;
 elseif (pwheels(i)<2000),  bin(4)=bin(4)+1;
 elseif (pwheels(i)<2500),  bin(5)=bin(5)+1;
 elseif (pwheels(i)<3000),  bin(6)=bin(6)+1;
 elseif (pwheels(i)<3500),  bin(7)=bin(7)+1;
 elseif (pwheels(i)<4000),  bin(8)=bin(8)+1;
 elseif (pwheels(i)<4500),  bin(9)=bin(9)+1;
 elseif (pwheels(i)<5000),  bin(10)=bin(10)+1;
 elseif (pwheels(i)<5500),  bin(11)=bin(11)+1;
 elseif (pwheels(i)<6000),  bin(12)=bin(12)+1;
 elseif (pwheels(i)<6500),  bin(13)=bin(13)+1;
 elseif (pwheels(i)<7000),  bin(14)=bin(14)+1;
 elseif (pwheels(i)<7500),  bin(15)=bin(15)+1;
 elseif (pwheels(i)<8000),  bin(16)=bin(16)+1;
 elseif (pwheels(i)<8500),  bin(17)=bin(17)+1;
 elseif (pwheels(i)<9000),  bin(18)=bin(18)+1;
else bin(19)=bin(19)+1;
end


%% HYBRIDIZATION
% battenergy   current energy in battery (J)
% battery(i)   an array storing battery energy over time (J)
% pfc          power from the fuel cell
% pbatt        battery out of cell. pbatt<0 is charging
% SOC          state of charge over time (fraction)
% batt_V       current battery voltage (V)
% batt_R       instantaneous battery resistance (ohms)
% lid          maximum current battery can be charged at for given SOC (A)
% negpower     power regenerated into the batteries (net of eff.) (W)

battery(i)=battenergy; negpower(i)=0;
pfc(i)=0; pbatt(i)=0; SOC(i)=0;
batt_V = 1.88+0.375*currSOC-0.176*currSOC*currSOC;
batt_R = (2.09-1.28*currSOC+1.07*currSOC*currSOC)/1000;
lid(i) = 1*0.979*(currSOC^(-4.44)-1);

% "overflow" measures power over "kickin". if overflow>0, require
% energy from the battery. if overflow<0, allow recharge. We restrict
% the battery so it never depletes below 20% capacity (to avoid
% battery damage) and never discharges faster than 80 amps.

overflow=p_no_parasitics(i)-kickin;
if overflow>0,
```

```
    if (battenergy-overflow*timestep/.95) > 0.20*capacity;,
        powerneed=overflow;
    else
        powerneed=(battenergy-0.20*capacity)*.95/timestep;
    end

      % count up current until desired power is reached.
      % Ensure discharge current under maximum of 80 A

      battcurr=0;
      while (battcurr*numbolder*(batt_V+battcurr*batt_R)) < powerneed,
       battcurr=battcurr+0.1;
      end;

    % diagnostic: display battcurr
    % battcurr
    if battcurr>80,
     battcurr=80;

     % diagnostic: flag if max charging exceeded
     % disp(sprintf('max charging current exceeded at time %5.0f',i));
    end

      % update with new energy, state of charge, voltage ,resistance
      % efficiency is a function of instantaneous voltage and resistance

      effbatt(i) = sqrt(0.95)*batt_V/(batt_V+battcurr*batt_R);
      battenergy=battenergy-powerneed/effbatt(i)*timestep;
      SOC(i)=battenergy/capacity; pbatt(i)=powerneed;
      batt_V = 1.88+0.375*SOC(i)-0.176*SOC(i)*SOC(i);
      batt_R = (2.09-1.28*SOC(i)+1.07*SOC(i)*SOC(i))/1000;

elseif pwheels(i)<0,
      % If powerneed is positive, and deceleration "power" exceeds
      % drag and rolling resistances, then we can regenerate into
      % the battery. pbatt is negative when charging, and we make sure
      % not to charge over 80% of capacity, or faster than lid(i),
      % to avoid battery damage

     friction=friction+pwheels(i);

      if (battenergy+abs(pwheels(i))*effregen*timestep*.95) < 0.80*capacity,
       powerneed=abs(pwheels(i))*effregen;
      else
       powerneed=abs((0.80*capacity-battenergy)*effregen/timestep/.95);
      end

      % count up current until desired power is reached.
      % Ensure charging current under maximum of lid(i)

      battcurr=0;
      while (battcurr*numbolder*(batt_V+battcurr*batt_R)) < powerneed,
       battcurr=battcurr+0.1;
      end;
      if battcurr>lid(i), battcurr=lid(i);
      % diagnostic: flag if max charging exceeded
      % disp(sprintf('Exceed charging lid at %5.0f',i));
      end

      effbatt(i) = sqrt(0.95)*batt_V/(batt_V+battcurr*batt_R);
      negpower(i)=powerneed*effbatt(i);
      battenergy=battenergy+negpower(i)*timestep;
      regenerated=regenerated+negpower(i)*timestep;
      SOC(i)=battenergy/capacity; pbatt(i)=-powerneed;
      batt_V = 1.88+0.375*SOC(i)-0.176*SOC(i)*SOC(i);
      batt_R = 2.09-1.28*SOC(i)+1.07*SOC(i)*SOC(i);
else
```

```
      % i.e. if neither regenerating nor drawing from battery.
      % first check to see if SOC is low and we should refill battery
      % we refill at a rate 400 W minus current power demand, only if
      % this is a hybrid and if current power demand is less than 400 W.

    if currSOC<0.55,
     p6(i)= 400 - p_no_parasitics(i);
     if (p6(i)<0 | hybridtype == 1), p6(i)=0;  end

     battcurr=0;
     while (battcurr*numbolder*(batt_V+battcurr*batt_R)) < p6(i),
      battcurr=battcurr+0.1;
     end;

     if battcurr>lid(i), battcurr=lid(i);
      % diagnostic: flag if max charging exceeded
      % disp(sprintf('Exceed charging lid at %5.0f',i));
     end

     effbatt(i) = sqrt(0.95)*batt_V/(batt_V+battcurr*batt_R);
     negpower(i)=p6(i)*effbatt(i);
     battenergy=battenergy+negpower(i)*timestep;
     SOC(i)=battenergy/capacity; pbatt(i)=-p6(i);
     batt_V = 1.88+0.375*SOC(i)-0.176*SOC(i)*SOC(i);
     batt_R = 2.09-1.28*SOC(i)+1.07*SOC(i)*SOC(i);
     if (hybridtype ~= 1),
      p_no_parasitics(i)=p_no_parasitics(i)+p6(i);
     end

   else
      % currSOC>0.4 so no need to refill. Instead, set SOC from the
      % previous value, or if this is the first time through the loop,
      % set it to initSOC. (We need to do this manually here because the
      % other options calculate a new value of SOC at the end
      % automatically)

    p6(i)=0;
    if i==1,
     SOC(i)=initSOC;
    else
     SOC(i)=SOC(i-1);
    end
   end

end
currSOC=SOC(i);

% calculate how much fuel cell has to output, equal to
% p_no_parasitics-pbatt if pbatt>0 (discharge),
% equal to p_no_parasitics if pbatt<0 (charge)

pfc(i)=p_no_parasitics(i)-0.5*(abs(pbatt(i))+pbatt(i));


%% CALCULATE PARASITIC POWER
% note that no parasitic power is appropriate for the battery-only case
%
% p5         Parasitics. Base plus 50-200 W blower depending on power.
% pfc        Gross power from fuel cell (or zinc-air battery), no peaking
% poutput    Total system output including peaking power

p5(i)=baseparasite+50+200*pfc(i)/5900;
if (hybridtype == 4), p5(i)=0; end
pfc(i)=pfc(i)+p5(i);
poutput(i)=p_no_parasitics(i)+p5(i);
```

```
 % Calculate current density j (mA) at which desired power is
 % attained. Calculate efficiency from vatmo and accumulate LHV
 % of fuel used. effp is the fuel cell efficiency. 100% efficiency
 % for zinc-air battery, because energy in that case is measured in
 % terms of _output_.

 j=1; while (power_for_density(j)<pfc(i)), j=j+1; end;

 effp(i)=vatmo(j)/1.481; currentdensity(i)=j;
 if (hybridtype == 4), effp(i)=1; end
 fuelenergy=fuelenergy+pfc(i)*timestep/effp(i);


 % Include metal hydride cooling. heat1 is waste heat generated.
 % heat2 is heat1 minus hydridecool, which is 28 kJ/mol times the
 % number of molesH2 per second. This formula works if current density
 % j is given in mA.

 heat(i)=(pfc(i)/effp(i))*(1-effp(i));
 molesH2=currentdensity(i)/1000*cellarea/96485*numcells/2;
 hydridecool=28000*molesH2;
 heat2(i)=heat(i)-hydridecool;
 if heat2(i)<0, heat2(i)=0; end


 % "coolpower" is the amount of heat that can be removed (watts)
 % by the system with given cooling factor "cooleff" given the
 % instananeous difference between the stack temperature
 % and ambient temperature. "Temp" is the current stack temperature
 % If stack temperature is below the critical thermostat level of
 % 50 degrees C, no coolant is circulated and we assume only a
 % small, unintentional loss of 1 W/K.

 if i==1,
  coolpower=(initTemp-ambientTemp)*cooleff;
 else
  if Temp(i-1)<50,
   coolpower=(Temp(i-1)-ambientTemp)*1;
  else
   coolpower=(Temp(i-1)-ambientTemp)*cooleff;
  end
 end


 % We calculate how much the stack temperature changes in this
 % time step, based on maximum cooling and the heat generated
 % heat2.

 deltaT=(heat2(i)-coolpower)/1000/(stackmass*specheatcap)*timestep;
 if i==1,
  Temp(i)=initTemp;
 else
  Temp(i)=Temp(i-1)+deltaT;
 end
  coolpowerstore(i)=coolpower;

% this marks the end of the master loop
end


%% CALCULATE SUMMARY VARIABLES
%
% Note mpge fuel economy is calculated using 21.56 mpge ~ 1 km/kWh
% Also, overall conversion efficiency is electricity divided by enthalpy
%  of hydrogen - is not net of parasitics.

totaltime    = max(t);
```

```
avgspeed     = mean(v);
distance     = avgspeed*totaltime;
fueleconomy  = distance*21.56/(fuelenergy/3600);
fueleconomy2 = (distance/1000)/(fuelenergy/3600000);
avgeffp      = mean(effp);
[maxpower,i1]= max(poutput);
batteryecon  = avgspeed*3.6/(mean(pfc)/1000);

%% PRINT OUT NUMERIC RESULTS

disp(sprintf(' '))
disp(sprintf(' ------------ simulation results ---------- '))
disp(sprintf(' '))
disp(sprintf('avg speed (km/h) : %5.2f', avgspeed*3.6));
disp(sprintf('total dist. (m)  : %5.0f', distance));
disp(sprintf('Max power from the engine occurs at t=%5.1f and is %5.0f
W',t(i1),maxpower));
disp(sprintf('avg power from engine is (W) : %5.1f', mean(poutput)));
disp(sprintf('avg power, no parasitics (W) : %5.1f', mean(p_no_parasitics)));
disp(sprintf('avg power from FC is (W)     : %5.1f', mean(pfc)));
disp(sprintf('Overall Efficiency           : %5.1f
%%',mean(pfc)*100/(fuelenergy/max(t)) ))
disp(sprintf('Hydrogen LHV usage rate  (W) : %5.1f', fuelenergy/totaltime));
disp(sprintf('Equiv. fuel economy          : %5.1f mpge',fueleconomy))
if (hybridtype == 4),
 disp(sprintf('Fuel economy battery no para : %5.1f km/kWh
battery',batteryecon))
else
 disp(sprintf('Fuel economy 2               : %5.3f km/g
hydrogen',fueleconomy2*33/1000))
end

disp(sprintf(' '))
[y3,i3]=max(a);
[y4,i4]=min(a);
disp(sprintf('Max accel occurs at t=%5.1f and is %5.2f m/s^2',t(i3),y3));
disp(sprintf('Min accel occurs at t=%5.1f and is %5.2f m/s^2',t(i4),y4));
disp(sprintf('Std dev of acceleration is %5.2f', std(a)  ));
disp(sprintf('Max pwheels is %5.2f', max(pwheels)  ));
disp(sprintf(' '))

disp(sprintf('Max fuel cell power output is %5.2f W',max(pfc)     ));
disp(sprintf('Max battery   power output is %5.2f W',max(pbatt)   ));
disp(sprintf('Max battery   power in     is %5.2f W',-max(-pbatt) ));
disp(sprintf('Max battery energy         is %5.2f kJ',max(battery)/1000));
disp(sprintf('Min battery energy         is %5.2f kJ',min(battery)/1000));
disp(sprintf('Total kJ regenerated       is %5.2f kJ',(regenerated/1000)));
disp(sprintf('Area per cell at 614 mW/cm2 = %5.2f cm2',max(pfc)/.614/56));

% PLOT 1. BATTERY vs. FUEL CELL
subplot (311), plot (t,battery)
xlabel ('time, seconds')
ylabel ('battery energy, J')
grid on

subplot (312), plot (t,pfc)
xlabel ('time, seconds')
ylabel ('FC power, W')
grid on

subplot (313), plot (t,pbatt)
xlabel ('time, seconds')
ylabel ('battery power, W')
grid on


% avgposaccel is sum of positive accelerations divided by total cycle time
```

```
% avg acceleration is sum of positive and negative accelerations divided
%  by total cycle time

keyboard;
disp(sprintf(' '))
disp(sprintf('avg accel   power: %5.1f', mean(p1)));
avgposaccel=0;
for i=1:1:cyclelength,
 if p1(i)>0, avgposaccel=avgposaccel+p1(i); end
end
avgposaccel=avgposaccel/cyclelength;
disp(sprintf('avg pos accel    : %5.1f', avgposaccel ));
disp(sprintf('avg rolling power: %5.1f', mean(p2)));
disp(sprintf('avg drag    power: %5.1f', mean(p3)));
disp(sprintf('avg parasit power: %5.1f', mean(p5)));
disp(sprintf(' '))


% nonzerotime measures time spent in motion, i.e. not stationary
% "avg nonzero" refers to power when scooter is in motion
% plustime, calc'ed earlier, measures time when scooter is accelerating
% avg positive accel power is mean acceleration when scooter is accelerating

nonzerotime=cyclelength;posaccelpower=0;
for i=1:1:cyclelength
 if v(i)<0.001, nonzerotime=nonzerotime-1;end
 if p1(i)>0, posaccelpower=posaccelpower+p1(i); end
end
disp(sprintf('avg positive accel   power: %5.1f', posaccelpower/plustime));
disp(sprintf('avg nonzero  rolling power: %5.1f', sum(p2)/nonzerotime ));
disp(sprintf('avg nonzero  drag    power: %5.1f', sum(p3)/nonzerotime ));
disp(sprintf(' '))


% PLOT 2. plot velocity versus time, power versus time, parasitics

orient portrait
set(gcf,'paperposition',[0.8 3 7 5])

subplot (311), plot (t,v*3.6)
xlabel ('time, seconds')
ylabel ('speed, km/h')
orient landscape
grid on

subplot (312), plot (t,poutput/1000)
xlabel ('time, seconds')
ylabel ('power output, kW')
grid on

subplot (313), plot (t,p5)
xlabel ('time, seconds')
ylabel ('parasitic power, W')
grid on

keyboard
clf


% PLOT 3. plot heat characteristics versus time

subplot(311),plot(t,heat2)
title('heat generation after hydride')
ylabel('heat power, W')
xlabel('time ,s')
grid on
```

```
subplot(312),plot(t,Temp)
title('stack temperature')
ylabel('temperature, C')
xlabel('time ,s')
grid on

subplot(313),plot(t,coolpowerstore)
title('cooling power')
ylabel('cooling, W')
xlabel('time ,s')
grid on



%PLOT 4
% plot breakdown of various powers. include parasitics, regen'ed
% power. The zeroing is necessary to get the patch polygon filled in

keyboard
p1(cyclelength-1)=0;p2(cyclelength-1)=0;p3(cyclelength-1)=0;
p4(cyclelength-1)=0;p5(cyclelength-1)=0;
p1(cyclelength)=0;p2(cyclelength)=0;p3(cyclelength)=0;
p4(cyclelength)=0;p5(cyclelength)=0;

for i=1:1:cyclelength,
 if p1(i)>0,
  pospower(i)=p1(i);
 else
  pospower(i)=p1(i);
% COMMENT THIS SECTION OUT to show negative acceleration powers
  pospower(i)=0;
 end
end

clf; subplot(111); hold on

% plot (t,-negpower, 'k')
t(cyclelength)=0;

handle_accel=patch(t,p5+p4+(p2+p3+pospower)/effd,'r');
handle_drag =patch(t,p5+p4+(p2+p3)/effd,'b');
handle_roll =patch(t,p5+p4+p2/effd,'g');
handle_ppara =patch(t,p5+p4,'m');
handle_paux =patch(t,p4,'y');

set(handle_accel,'EdgeColor','r')
set(handle_drag, 'EdgeColor','b')
set(handle_roll, 'EdgeColor','g')
set(handle_ppara, 'EdgeColor','m')
set(handle_paux, 'EdgeColor','y')

patch( [570 570 980 980 570], [4600 5850 5850 4600 4600], 'w')

patch( [600 600 650 650 600], [5650 5800 5800 5650 5650], 'r')
patch( [600 600 650 650 600], [5450 5600 5600 5450 5450], 'b')
patch( [600 600 650 650 600], [5250 5400 5400 5250 5250], 'g')
patch( [600 600 650 650 600], [5050 5200 5200 5050 5050], 'm')
patch( [600 600 650 650 600], [4850 5000 5000 4850 4850], 'y')
patch( [600 600 650 650 600], [4650 4800 4800 4650 4650], 'w')

text (670,5750,'acceleration power')
text (670,5550,'aerodynamic drag')
text (670,5350,'rolling resistance')
text (670,5150,'parasitic power')
text (670,4950,'auxiliary power')
text (670,4750,'regenerated power')
```

```
grid on
xlabel ('time, seconds')
ylabel ('power, W')
keyboard



%PLOT 5 plot breakdown of powers _without_ parasitics
%the zeroing is necessary to get the patch polygon filled in

clf; subplot(111); hold on

handle_accel=patch(t,p4+(p2+p3+p1)/effd,'r');
handle_drag =patch(t,p4+(p2+p3)/effd,'b');
handle_roll =patch(t,p4+p2/effd,'g');
handle_paux =patch(t,p4,'y');

set(handle_accel,'EdgeColor','r')
set(handle_drag, 'EdgeColor','b')
set(handle_roll, 'EdgeColor','g')
set(handle_paux, 'EdgeColor','y')

patch( [570 570 980 980 570], [5000 5850 5850 5000 5000], 'w')

patch( [600 600 650 650 600], [5650 5800 5800 5650 5650], 'r')
patch( [600 600 650 650 600], [5450 5600 5600 5450 5450], 'b')
patch( [600 600 650 650 600], [5250 5400 5400 5250 5250], 'g')
patch( [600 600 650 650 600], [5050 5200 5200 5050 5050], 'y')

text (670,5750,'acceleration power')
text (670,5550,'aerodynamic drag')
text (670,5350,'rolling resistance')
text (670,5150,'auxiliary power')

grid on
xlabel ('time, seconds')
ylabel ('power, W')
keyboard


%PLOT 6 battery power versus total power
%the zeroing is necessary to get the patch polygon filled in

clf; subplot(111); hold on

plot (t,ones(1,cyclelength)*max(pfc),'b')
plot_total=poutput;
plot_fc=pfc;
t(cyclelength)=0;
plot_total(cyclelength)=0;
plot_fc(cyclelength)=0;
plot_total(cyclelength-1)=0;
plot_fc(cyclelength-1)=0;

handle_total=patch(t,plot_total,'k');
handle_pfc  =patch(t,plot_fc,'g');

set(handle_total,'EdgeColor','k')
set(handle_pfc,  'EdgeColor','g')

grid on
xlabel ('time, seconds')
ylabel ('power, W')
axis ([0 950 0 6000])

%UNUSED OPTIONS
%
```

```
%set(gca, 'YTickLabel', str2mat('0.0','0.1', '0.2', '0.3', '0.4', '0.5','0.6',
'0.7', '0.8', '0.9', '1.0'))
%set(gca, 'XTick', 0,50,100,150,200,250,300,350,400,450,500,550,
600,650,700,750, 800,850, 900, 950)
%set(gca, 'XTick', [0:50:950])
```

Appendix G *a prototype scooter*

The prototype scooter illustrated here is being constructed by graduate student Arne LaVen at the Desert Research Institute. Interested parties should contact him at arnel@dri.edu or the following address:

Arne LaVen

Energy and Environmental Engineering Center

Desert Research Institute

5625 Fox Ave.

Reno, NV 89506

The photographs below were from Arne LaVen in July of 1999.

Figure G.1 Fuel cell scooter prototype

This is the scooter frame without body. Note the blower attached to the front of the scooter, piping air to the fuel cell over the rear wheel. The power system is shown in more detail in Figure G.2:

Figure G.2 Closeup of scooter power system

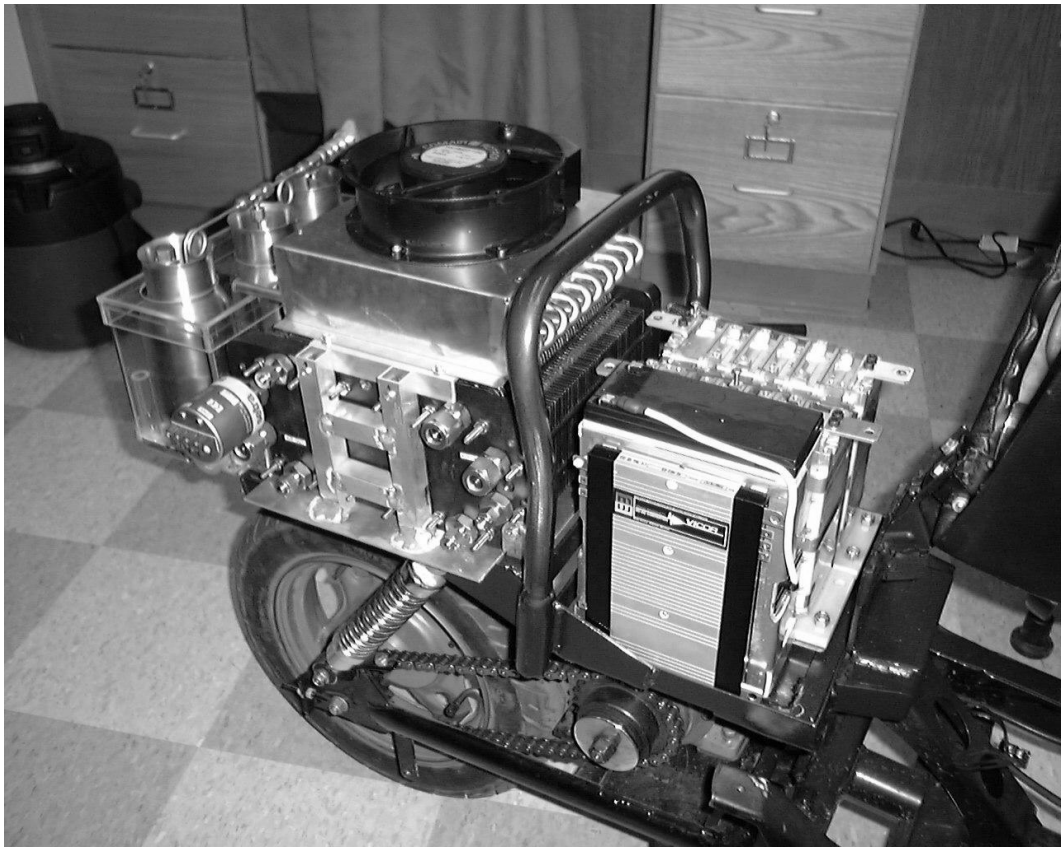

The seat has been removed and reveals the fuel cell, underneath a radiator and a fan. At the far back of the scooter are three metal hydride hydrogen canisters. The rear wheel is attached by a chain to the electric motor, which itself is below a DC-to-DC converter. Behind the converter are two ultracapacitors for peaking power.